Punching Shear Retrofit of Concrete Slab-Column Connections with GFRP Shear Bolts

by

Nicholas David Lawler

A thesis

presented to the University of Waterloo

in fulfillment of the

thesis requirement for the degree of

Master of Applied Science

in

Civil Engineering

Waterloo, Ontario, Canada, 2008

Author's Declaration

I hereby declare that I am the sole author of this thesis. This is a true copy of the thesis, including any required final revisions, as accepted by my examiners.

I understand that my thesis may be made electronically available to the public.

Abstract

Over the life span of a structure it may become necessary to retrofit, or strengthen certain components or elements. This may be due to construction errors, changes in use and occupancy, or changes due to material deterioration or damage. Slab-column connections in flat slab structures might need to be strengthened for punching shear.

Using steel shear bolts to strengthen connections for punching shear is a new technique used for retrofit that was developed at the University of Waterloo. If the retrofitted part of the structure is exposed to the atmosphere, or to chemicals such as deicing salts, the steel can corrode, thus furthering to damage the structure. Non-corrosive materials that can replace the steel shear bolts can be a good practical alternative to steel.

Reported in this thesis are the results of research on the development and use of non-corrosive shear bolts for reinforced concrete interior slab-column connections. Externally applied shear reinforcing bolts provide the punching shear reinforcement strength, while allowing the flexibility and ease of installation of an external application after construction. By providing a bearing area against both sides of the slab surface, the formation of punching shear cracks can be restrained, and the connection can become strengthened against punching shear failure. Three different types of non-corrosive shear bolts were developed and tested. The first was an off-the-shelf glass fiber reinforced polymer (GFRP) bolt / nut product. The two others used two different GFRP core rods with aluminum fittings crimped to their ends. A total of six specimens were tested, four were tested under an increasing static load, while two were tested with an unbalanced pseudo-dynamic lateral load. All six specimens were designed to fail in punching shear before reaching their flexural capacity. The results are compared against previous test results of specimens both unreinforced and reinforced with steel shear bolts to determine their effectiveness.

From the test results it was found that the GFRP shear bolts did strengthen the connections for punching shear. The GFRP nut and bolt did not strengthen the connection, and, in fact, decreased its overall strength when compared to the unreinforced specimen. The presence of the GFRP shear bolts also increased the connection ductility and the deflection capability. In the pseudo-dynamic tests the GFRP shear bolts significantly increased the amount of energy dissipated by the connection under reverse cyclic loading. The results of the testing appeared to be depended on the proper application of the crimping technique to place the bolts in the slab.

Acknowledgements

Table of Contents

List of Figures

List of Tables

Chapter 1

Introduction

1.1 Background

The primary function of a structural system is to transfer applied loads to the supports. Reinforced concrete slabs are thin, flat, structural elements that act to transfer loads applied perpendicular to their plane. These slabs are often used as floor or roof structures in buildings. Large foundation mats, and bridge decks can also be in the form of slabs.

Reinforced concrete slabs can take several forms. Some examples include solid, ribbed or waffle slabs. They can be reinforced with conventional reinforcing as well as they can be prestressed. Concrete slabs can also be constructed in-situ in a monolithic construction with the walls and other elements, precast and placed by crane, or composite construction, with the concrete slab supported by steel beams and steel deck.

This research will specifically look into what is known as 'flat plate' slabs. These are solid, conventionally reinforced, concrete slabs that are only supported by columns. Flat slabs contain no beams between the supports, and no drop capitals as shown in Figure 1.1.
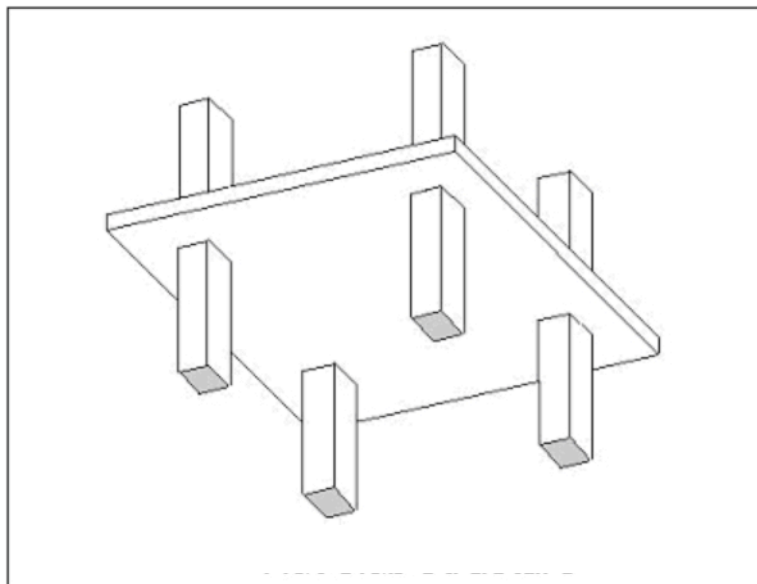
Figure 1.1 - Typical Flat Slab Construction

Flat plates are economical, as they speed up the rate of construction, and ease the installation of mechanical and architectural components. They are primarily used in structures with a light load, and short spans, mainly between 4.5m and 6m (Macgregor and Bartlett 2000). However, flat plates

experience high stresses forming at the column – slab connections. These high stresses can lead to the so-called punching shear failure.

1.2 Punching Shear

Punching shear (or sometimes called two-way shear) in flat plate reinforced concrete slabs is usually a critical design consideration. The failure can happen in a sudden and brittle manner, without any warning to the building occupants.   Punching shear failure involves the formation of a truncated cone (or pyramid shaped) of cracks forming around the base of the slab at the column connection, as shown in Figure 1.2.
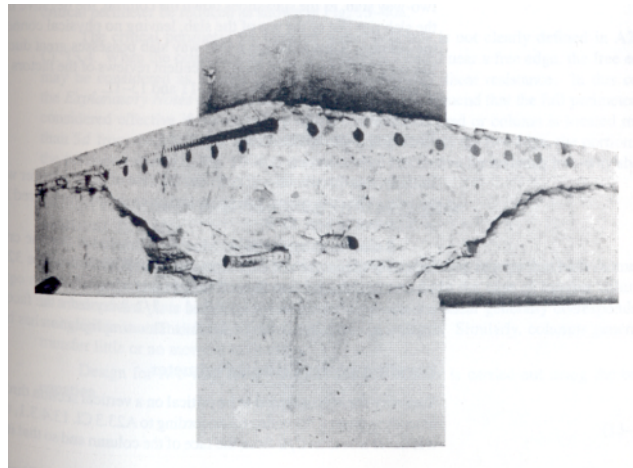
Figure 1.2 – Shear Cracks Forming the Punching Shear Cone

There have been many examples of punching shear failure in modern buildings since the development of the flat plate system. Built in 1989, in Seoul, South Korea, the Sampoong Mall collapsed, killing 501 and injuring nearly 1000. The mall was designed to be a residential condominium, but the owners changed the building to a shopping mall part way through construction. Punching shear failure of the support columns through the roof slab occurred on June 29, 1995. As a result of poor design decisions and corrupt government officials the building columns were sized under by 200mm.   The longitudinal reinforcing in the columns themselves was also wrong, as they contained half the number of bars needed for strength. The weight of the roof top air conditioner units was also not considered in the design of the roof slab (National Geographic 2005).

On January 21, 1971 a building under construction, at 2000 Commonwealth Avenue in Boston, Massachusetts, experienced a progressive collapse due to a punching shear failure. Four workers were killed when two-thirds of the 16-storey building collapsed. Upon multiple irregularities in administration and execution of the construction contract, the main cause of the collapse was contributed to inadequate shoring of newly placed concrete, overall weak concrete strength, and a failure to protect the freshly laid concrete against cold weather. Mechanical units and construction equipment were being stored on the

roof of the building during the construction phase. The roof slab was designed to resist 1.44kPa, but the presence of the mechanical units overloaded the slab to 6.22kPa. The structural drawings indicated that shoring was to be provided to increase the capacity of the roof slab, but none was ever installed. A commission investigated the failure and offered several recommendations for changes to the current building codes. These included changes to the way construction projects were supervised and inspected, and changes to detailing requirements in reinforced concrete structures to prevent progressive collapse. (King and Delatte 2004)

1.3 Corrosion of Steel in Structural Elements

In Canada, a significant amount of infrastructure is degrading due to the practice of combating ice and snow with deicing salts. Many bridges and parking garages are structurally deficient due to corrosion of reinforcement, and are in need of rehabilitation or strengthening. Also, with the introduction of more stringent design guidelines and increases in service loads, many structures are no longer considered functional, as they no longer meet current design standards.

While steel structural elements are widely used, they are not ideal in situations where they are exposed to high salt levels, as steel is very susceptible to corrosion. Steel reinforcing within concrete can become corroded after prolonged exposure to salt, with this process severely damaged the concrete elements for both strength and ascetics.

In recent years structural engineers have been able to use Fibre Reinforced Polymers (FRP's) to replace or protect reinforced concrete in some of these applications. The advantage of FRP is that it will not corrode under high salt levels like traditional steel. Research by the *ISIS Canada Research Network* has shown that FRP reinforcements are strong, reliable, and practical for use in many different types of structural applications and retrofits.

1.4 Punching Shear Reinforcing Elements and Shear Bolts

Bent-up bars, stirrups (either closed or U-shaped), shear heads, and shear studs are all currently accepted methods to reinforce new slab-column connections against punching shear failure. Dilger and Ghali in 1981 developed the shear stud concept at the University of Calgary. Vertical, headed stud elements are placed within a slab prior to casting, providing a tensile element to help resist the opening of the punching shear cone. However, if a connection needs to be reinforced after construction, to correct a construction error, introduce openings, or increase the connection capacity, a retrofit method is needed.

A retrofit method was developed at the University of Waterloo. This method requires the drilling of holes, and the mounting of steel shear bolts, externally, around the slab faces. As the punching cone is formed the face of the slab expands. By resisting this expansion, external steel shear bolts have been

shown to strengthen connections in punching shear in both static and seismic loadings. (El-Salakawy 1998, Adetifa 2003, Bu 2008). The retrofit method allows the punching shear strength of a connection to be improved after the structure has been built, and even while it is occupied.

1.5 Objectives of this Research

The ductility requirements for structures were introduced in the United Building Code of 1976. Buildings constructed in seismic zones before 1976 have shown to have substantial damage and cost to rehabilitate after a seismic event. It is therefore important to find an effective method to strengthen existing reinforced concrete flat plate structures, increase the punching shear capacity, ductility, and lateral drift capacity of the slab-column connections. Furthermore, due to construction errors, change in occupancy, or material degradation it is also desirable to increase the punching shear capacity of slab-column connections under gravity loadings.

The shear bolt developed at the University of Waterloo is one way that has been used to strengthen connections, both in gravity loading, and lateral cyclic loading. (El-Salakawy 1998, Adetifa 2003, Bu 2008) However the problem of steel corrosion has been a concern for structural engineers and thus GFRP bolts were to be developed in this research. Structures exposed to weather events, and road-deicing salts have started to degrade due to steel corrosion.

The main objective of this research was to develop FRP shear reinforcement elements for punching shear retrofit of slabs. Several options were investigated namely, an off-the-shelf glass fibre reinforced polymer (GFRP) threaded nut and rod product, and two different types of GFRP used with aluminum fittings. The comparisons with steel shear bolts slab testing results in terms of ductility and strength requirements are presented.

1.6 Contribution of this of Research

The present study involved the development of a new non-corrosive shear bolts for use as a retrofit for interior slab-column connections under both static and seismic loading. Previous research was undertaken by; El-Salakawy (1998) in strengthening edge slab connections under static load; Adetifa (2003) in strengthening interior connections under static load; and Bu (2008) in strengthening interior connections under pseudo-dynamic load.

A new shear bolt was designed for retrofit strengthening for punching shear. This new shear bolt is made of completely non-corrosive materials. The ability of this shear bolt to increase punching shear capacity of slab-column connections was investigated. A new anchorage technique for the retrofit technique was also developed. The hydro electrical industry utilizes a mechanical crimp to bond composite (GFRP) insulators to metal fittings. By crimping custom end fittings to GFRP rods, a solid connection between the

two materials can be developed. This strong bond was strong enough to resist the tensile forces imposed on it by the formation of the punching cone. This crimping technique is also very versatile and allows the retrofit method to be utilized in a variety of situations on construction sites.

Six isolated slab-column specimens were constructed, representing interior slab-column connections in a continuous flat plate slab system. They had various amounts and types of non-corrosive punching shear reinforcement elements. Two were tested under pseudo-dynamic load, similar to tests preformed by Bu (2008). The remaining four were tested under direct static load, similar to tests by Adetifa (2003). The two previous research studies provided the control specimens for this research. Loading, displacement, and strain data was recorded for each test, and is presented in this thesis. The conclusions made on the effectiveness and behaviour of the non-corrosive shear reinforcement is offered at the end of this thesis.

1.7 Contents of Thesis

This thesis is divided into 6 chapters; the data collected for each specimen is contained in the appendices.

Chapter 1 – contains background information on punching shear, and the objectives of the research.

Chapter 2 – provides further technical discussion on the topic, and presents research literature relevant to the scope and objectives of this thesis.

Chapter 3 – provides details on the test set-up, and specimen construction.

Chapter 4 – provides a description of the design, development, and construction of the non-corrosive shear reinforcement elements (GFRP shear bolts).

Chapter 5 – contains recorded observations and procedures from each of the tested slabs. Data such as crack width, deflections, and recorded strain are discussed.

Chapter 6 – discussed and reviews the results of the testing program. Comparisons are made between each of the tests, and the control specimens. The effectiveness of the non-corrosive shear bolts are discussed.

Chapter 7 – conclusions are drawn from the research and recommendations are presented for future study.

Chapter 2

Review of Literature

2.1 Punching Shear Models

Several researchers attempted modeling punching shear by mechanical models. The three best known models are presented in this section.

2.1.1 Rotational Model by Kinnunen / Nylander

The first mathematical model for punching shear was proposed by S. Kinnunen and H. Nylander in 1960 from the Royal Sweden Institute of Technology (Kinnunen and Nylander 1960). Their model was based on circular concrete slabs, loaded uniformly around their circumference. The test specimens were circular, polar-symmetric slabs supported by a central column. The slabs were 150 mm in nominal thickness, and 1710 mm in diameter. The derivation of their model was based on testing results of 61 slabs, not reinforced transversely.

The theoretical model proposed was based on the observed deflection measurements that showed that the deflection of the slab portion outside of the shear crack increased as a nearly linear function of the distance from the column. They concluded that the slab portion outside the shear crack, bounded by the shear crack, and by radial cracks, can be regarded as a rigid body, as far as the deformation in a radial plane is concerned.

A compressed conical shell that develops from the column to the bottom of the shear crack supports this rigid body, at the outer portion of the slab. The model below shows the proposed shape of this conical shell, as well as other parts of the mechanical model proposed (Figure 2.1).
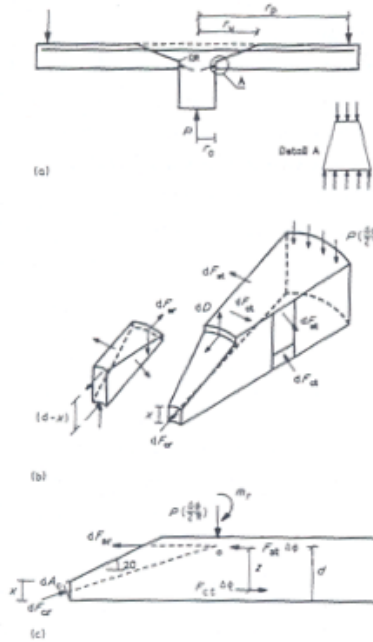
Figure 2.1 - Kinnunen / Nylander Conical Shell

Failure criteria were defined as the compressive stress in the inclined shell, or the tangential compressive strain at the shear crack. Equations 2.1 and 2.2 were developed as apart of an iteration procedure for calculating the ultimate punching load of slab with given dimensions, can sustain before failure.

$$P = \pi \frac{B}{d} d^2 \frac{y}{d} \cdot \frac{1 + 2\frac{y}{B}}{1 + \frac{y}{B}} \cdot \sigma_t f(\alpha) \quad [2.1]$$

Where,

α – inclination of the conical shell
B – column diameter
d – effective slab depth
y – distance from the bottom of the slab to the root of the shear crack at failure
σ_t – ultimate stress in the conical shell

$$P = 2f_y \cdot \frac{r_s}{d} \left[2\pi \cdot \rho \cdot d^2 \ln\left(\frac{c}{2c_0}\right) + A_{sc} \frac{d}{c_0} \right] \frac{d - \frac{y}{3}}{c - B} \quad [2.2]$$

Where,

f_y – yield stress of the reinforcement
ρ – the reinforcement ratio
r_s – the radius of the slab area in which the yield point stress, f_y, is reached.
A_{sc} – cross-sectional area of the column reinforcing steel

7

d – effective slab depth
c – Diameter of the circle concentric with a column in a flat slab, along where the bending moment is zero at failure
c_0 – Radius of the conical shell

The value of *y* is iterated until Eqn. 2.1 and 2.2 are found to be equal. Although a good first step, the Kinnunen / Nylander model is very simplistic and several modifications have been made over the years.

2.1.2 Modifications to the Kinnunen / Nylander Model by Broms

Broms (1990) introduced two modifications. First he adopted standard values of concrete properties, rather then the calibrated ones from test results that Kinnunen and Nylander used. He also calculated different heights of the compression zone, as opposed to the iterative approach used previously. He also introduced accounting for unsymmetrical punching and size effects. Again, two failure mechanisms were proposed for failure in punching. A limiting value of ε_{cpu} was proposed for the case of high tangential compressive strain, for which a critical punching load, P_ε could be calculated.

$$\varepsilon_{cpu} = 0.0008 \left(\frac{150}{\alpha \cdot h_{pu}} \cdot \frac{25}{f_c'} \right)^{1/3} \quad [2.3]$$

Where,
h_{pu} – is the height of the compression zone at flexure in the tangential direction when punching occurs.
$\alpha \cdot h_{pu}$ – height of the equivalent rectangular stress block with the stress f_c'

The radial concrete compressive stress failure mechanism occurs when the conical shell reached a critical value of $1.1 f_c'$ at the bottom of the shear crack. As such Brooms described the punching load as,

$$P_\sigma = 0.46(B + 3.6y)y \cdot f_c' \left(\frac{300}{y} \right)^{1/3} \quad [2.4]$$

Where,
B – diameter of the column
y – approximate thickness of the conical shell
f_c' – compressive strength of concrete

The critical punching load is taken as the lesser of P_ε and P_σ

2.1.3 Truss Model by Alexander and Simmons

Alexander and Simmonds (1992) developed a model for punching shear using the truss analogy for cracked concrete. Their model consisted of a three-dimensional space truss, composed of concrete compression struts and steel tension ties. These are further broken down into individual bar-strut units, there are two types of compression struts:

8

1. Those parallel to the plane of the slab (anchoring struts)
2. Those at some angle, α, to the plane of the slab (shear struts)

Shear struts oppose the movement of the slab relative to the column, and are further broken down into:

Gravity Struts: oppose downward movement; they are tied by top mat steel.

Uplift Struts: oppose upward movement; they are tied by bottom mat steel.

Two perpendicular reinforcing bars equilibrate each anchoring strut. One bar passes through the column, parallel to the axis about which the unbalanced moment is acting, and the other is at a proximal distance from the column. The proximal distant bars are able to exert moment on the connection by flexure. The compression struts meet the column face at the front corner of the column, and equilibrium of the entire system can be satisfied by summation of moments of the bar forces at this point.
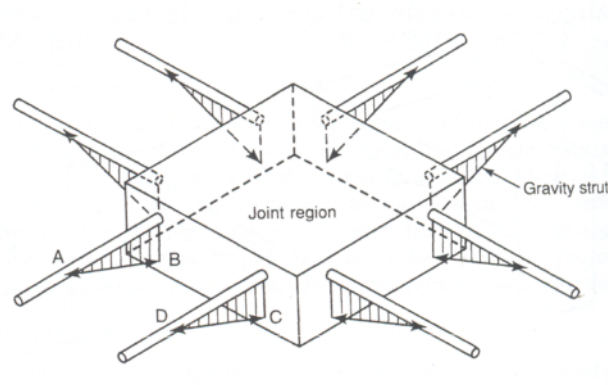
Figure 2.2 - Alexander / Simmons Strut and Tie Model

Failure criteria have been established to find the ultimate capacity of a bar-strut combination. Three failure modes have been identified, the failure of the tension tie, failure of the compression strut, or shear strut failure, which may occur when the out of plane force component of the compression strut exceeds the confining strength of the slab. It is assumed that the steel strut (tension tie) will always reach yield, therefore a compression failure of the compression strut will never govern. This is based on the fact that most testing data shows that steel in the immediate vicinity of the column yields prior to failure. As well, predicting compression failure of concrete would rely on assumptions, to define both critical concrete stress and to estimate the axial stresses within the struts. Therefore, the ultimate capacity of the anchoring bar-strut unit is limited only by the yielding of the participating reinforcing bars.

Prior to the formation of cracking, the shear is transferred by shear stresses. Once the cracks have formed, shear cannot be transferred across the cracks, which is then carried by the inclined shear struts. The horizontal component of the force in the strut causes a change in the force in the reinforcement. For

9

a gravity strut, the force in the top bar changes, for an uplift strut the force in the bottom bar changes. The vertical component however pushes against the bar, which is turn pushes against the face of the slab. This force is resisted by the tensile strength of the concrete, assumed to be $\sqrt{f_c'}$. Eventually the forces cause the bond between the bar and the concrete to be lost, and the struts are no longer anchored. With no shear stress transfer (lost when cracking occurred), and no shear struts (without anchorage the struts become ineffective), a punching shear failure results.

2.2 Shear Design Procedures for Reinforced Concrete Slabs

The various design codes examined herein are all based on limit states design. The requirement for shear design, is that the strength of the connection must be greater then the load or stress that is applied on it, as follows:

$$V_u \leq V_r \qquad V_s = \frac{\phi_s A_{vs} f_{yv}}{b_o s}$$
$$V_u = \frac{V}{b_0 d}$$
$$V_r = V_c + V_s \qquad V_c = 0.19 \lambda \phi_c \sqrt{f_c'}$$

Where,
V_u - ultimate applied shear stress [MPa]
V_r - nominal shear stress capacity of the critical section [MPa]
V_c - contribution of concrete to shear stress resistance [MPa]
V_s - contribution of steel to shear stress resistance [MPa]
b_o – A critical perimeter taken at some distance from the face of the column [mm]
d – the effective depth of the slab [mm]
A_{vs} – cross section area of shear reinforcement [mm^2]
f_{yv} – yield stress of shear reinforcement [MPa]
s – peripheral spacing of shear reinforcement [mm]
ϕ - material safety factors for the prescribed code

2.2.1 American Concrete Institute, ACI 318-05 (United States of America) and Canadian Portland Cement Association, CSA A23.3-04 (Canada)

Since both CSA A23.3-04 and ACI 318-05 derive their design equations from the same source, they are presented together. ACI equations have been converted so that the variables are in metric units, and the CSA are presented in their original metric units. Both codes specify that the shear capacity be calculated on the minimum perimeter located at a distance $d/2$ from the column face or concentrated load. The nominal shear stress of the concrete shall be the smallest of:

$$v_c = \left(1 + \frac{2}{\beta_c}\right) 0.17 \lambda \phi \sqrt{f_c'} \qquad \text{[ACI 318-05 Eqn. 11-33] [2.5]}$$

10

$$v_c = \left(1 + \frac{2}{\beta_c}\right) 0.19\lambda\phi_c\sqrt{f_c'} \qquad \text{[CSA A23.3-04 Eqn. 13-5] [2.6]}$$

Where, β_c is the ratio of long side to short side of the column. Tests have shown that shear resistance decreases with increasing rectangularity of the loaded area, β_c takes this into account. As β_c becomes very large and approaches infinity (in the case of a wall support) the equations become the shear resistance for one-way slabs (Pillai, Kirk and Erki 1999).

$$v_c = 0.083\left(\frac{\alpha_s d}{b_0} + 2\right)\sqrt{f_c'} \qquad \text{[ACI 318-05 Eqn. 11-34] [2.7]}$$

$$v_c = \left(\frac{\alpha_s d}{b_0} + 0.19\right)\lambda\phi_c\sqrt{f_c'} \qquad \text{[CSA A23.3-04 Eqn. 13-6] [2.8]}$$

Where, α_s = 4 for interior, 3 for edge, and 2 for corner columns. The factor $d\alpha_s/b_o$ accounts for the size of the loaded area. For example, a square column having a size greater then $4d$ makes these equations critical for two-way shear resistance (Pillai, Kirk and Erki 1999).

$$v_c = 0.33\lambda\phi\sqrt{f_c'} \qquad \text{[ACI 318-05 Eqn. 11-35] [2.9]}$$

$$v_c = 0.38\lambda\phi_c\sqrt{f_c'} \qquad \text{[CSA A23.3-04 Eqn. 13-7] [2.10]}$$

In general, Eqn. 13-7 (or Eqn. 11-35) govern two-way shear design; with Eqn. 13-5 and Eqn. 13-6 taking into account uncommon situations that effect shear resistance. Eqn. 13-7 and Eqn. 11-35 are twice the value given for one-way shear (beam) resistance in A23.3-04 and ACI 318-05. Changes were made to the material safety factors in A23.3 in 2004, as such the equations were adjusted to allow calculation by the ACI equations, to be the same as for A23.3.

In CSA A23.3-04 the value of $\sqrt{f_c'}$ is limited to 8MPa, or $\sqrt{f_c'} \leq 64$MPa, in an effort to compensate in the inaccuracy of determining the square root of high strength concrete compressive strength. As well, if d is greater than 300mm, the values of v_c are factored by $1300/(1000+d)$ to account for size effect. The factored shear stress, v_f, is given by $v_f = \dfrac{V_f}{b_0 d}$ where b_o is the perimeter of the critical section at d/2 from the column.

Unbalanced moments also contribute to the factored shear stress, with unbalanced moments acting both in the x and y direction:

$$v_f = \frac{V_f}{b_0 d} + \left(\frac{\gamma_v M_f e}{J}\right)_x + \left(\frac{\gamma_v M_f e}{J}\right)_y \qquad \text{[CSA A23.3-04 Eqn. 13-9]}$$

Where, e the eccentricity is calculated from the centrodial axis of the critical section, to the respected face of the critical perimeter. J is taken as the polar moment of inertia of the critical section, about its centroidal axis.

$$\gamma_v = 1 - \frac{1}{1 + \frac{2}{3}\sqrt{\frac{b_1}{b_2}}} \qquad \text{[CSA A23.3-04 Eqn. 13-8]}$$

Where, b_1 is the length of the critical perimeter parallel to the axis of bending, with b_2 being the other length. This factor is one of contention, and comes from empirical results compiled by Hanson and Hanson (1968), who arbitrarily set $\gamma_v = 0.4$ (when $b_1 = b_2$). It also assumes that shear stresses caused by V_f can be added directly to shear stresses caused by moment transfer. The assumption ignores the effect of cracking, the uneven distribution of shear stresses around the column, and strut and tie action after cracking (Macgregor and Bartlett 2000). For interior columns, some of the unbalanced moment must also be transferred to the flexural reinforcement placed within a width $b_b = 1.5h$, CSA A23.3-04 gives $\gamma_f = 1 - \gamma_v$ (Eqn. 13-25).

2.2.2 British Standard, BS 8110-97 (United Kingdom)

The British Standard takes a critical squared perimeter $1.5d$ from the loaded area, for both circular and rectangular loaded areas. The resistance of the concrete to punching is given as,

$$\frac{V_f}{ud} < v_r = 0.79(100\rho)^{1/3}\left(\frac{400}{d}\right)^{1/4} < 0.8\sqrt{f_{cu}} \qquad [2.11]$$

Where,
f_{cu} – the characteristic concrete cube strength [MPa]
$u = 4(c+3d)$ for circular columns [mm]
$u = 4(b+3d)$ for square columns [mm]
$\rho = (\rho_x + \rho_y)/2 < 0.03$ [%]
ρ – flexural steel ratio calculated for a width equal to u [%]
d - effective slab depth [mm]

British code provides two methods to account for the effect of combined shear and unbalanced moment of interior columns; either eccentric shear expression equation, or simple shear force multipliers.

$$v_f = \frac{V_f}{A_c}\left(1 + \frac{1.5 A_c M_{fx}}{V_f x}\right) \qquad [2.12]$$

Where,

V_f and M_f are factored shear force [kN] and unbalanced moments [kN-m] determined at the centroidal axis of the critical section.

A_c - is the concrete area of the assumed critical section [mm²]

x – the length of the side of the control perimeter parallel to the axis of bending [mm]

Alternatively, the nominal shear force can be multiplied by 15% to account for unbalanced moments at an interior column.

2.2.3 Deutsches Insitut für Normung (German Institute for Standardization), DIN 1045-1:2001 (Germany)

The critical section taken for DIN 1045-1 is a critical perimeter, with rounded corners, 1.5d away from the face of the column. The provisions are similar to CEB-FIP MC90, as well as Eurocode 2, for the sake of consistency. The applied stress at the critical section is taken as,

$$v_f = \beta \frac{V_f}{ud} \qquad [2.13]$$

Where,

$u = \pi(c + 3d)$ (interior circular columns) [mm]

$u = 2a + 2b + 3\pi d$ (interior rect. columns) [mm]

when $a/b > 2$

$u = 2a_1 + 2b_1 + 3\pi d$ [mm]

$a_1 < \begin{cases} a \\ 2b \\ 5.6d - b_1 \end{cases} [mm]$

$b_1 < \begin{cases} b \\ 2.8d \end{cases} [mm]$

$\beta = 1.05$ for interior, 1.4 for edge, and 1.5 for corner columns.

Shear strength is given by,

$$v_r = 0.14\gamma_v \eta_1 (1 + (200/d)^{1/2})(\rho_1 f_{ck})^{1/3} - 0.12\sigma_{cd} \qquad [2.14]$$

Where,

f_{ck} – characteristic concrete cylinder strength [MPa]

η_1 – factor to account for concrete density

$\rho_1 = (\rho_x + \rho_y)/2 < 0.40 f_{cd}/f_y < 0.02$ [%]

$f_{cd} = 0.85 f_{ck}/\gamma_c$ with $\gamma_c = 1.5$

d – effective slab depth [mm]

$$\sigma_{cd} = \frac{N_x + N_y}{2A_c} = \text{average in-plane stress [MPa], due to horizontal loads or prestress } (N_x \text{ or } N_y).$$

2.2.4 Eurocode 2: Design of Concrete Structures, EN 1992-1-1:2004 (Europe)

Eurocode 2 has been introduced to provide design guidance across the European Union design codes. Eurocode method for punching shear calculations will eventually supersede both BS 8110-1:1997 and DIN 1045-1:2001. The punching shear stress is to be calculated at a critical perimeter $2d$ from the face of the column, with rounded corners, the applied stress can be calculated as follows;

$$v_f = \beta \frac{V_f}{u_1 d} \qquad [2.15]$$

Where,

$$\beta = 1 + k \frac{M_{Ed}}{V_{Ed}} \cdot \frac{u_1}{W_1}$$

k depends on the ratio c_1 / c_2 the side lengths of the column under loading.

$$W_1 = \int_0^{u_1} |e| dl$$

dl – elementary length of the perimeter [mm]
u_l – perimeter of the critical area [mm]
e – distance of dl from the moment M_f axis [mm]

This β factor is further detailed in the standard for special cases of different column dimensions, and eccentricities of the loading. If the loading is concentric, and no unbalanced moments are present, the resistance stress can be calculated as follows;

$$V_{Rd,c} = C_{Rd,c} k (100 \rho_1 f_{ck})^{1/3} + k_1 \sigma_{cp} \geq (V_{min} + k_1 \sigma_{cp}) \qquad [2.16]$$

Where,

14

$$k = 1 + \sqrt{\frac{200}{d}} \leq 2$$

$$\rho_1 = \sqrt{\rho_{lz} + \rho_{ly}} \leq 0.02 \ [\%]$$

$$\sigma_{cp} = (\sigma_{cy} + \sigma_{cz})/2 \ [\text{MPa}]$$

$$C_{Rd} = \frac{0.18}{\gamma_c}$$

$$V_{\min} = 0.035 k^{3/2} f_{ck}^{1/2} \ [\text{MPa}]$$

$$k_1 = 0.18$$

$$\gamma_c = 1.5 \ (\text{Safety Factor})$$

ρ_{lz} and ρ_{ly} are related to the bonded tension steel in both the z and y directions, and should be calculated as mean values taking into account an assumed slab with of $3d$.

σ_{cy} and σ_{cz} are the concrete stresses in the critical section, in each direction given by,

$$\sigma_{cy} = \frac{N_{Ed,y}}{A_{cy}}, \sigma_{cz} = \frac{N_{Ed,z}}{A_{cz}}$$ where N_{ed} are due to horizontal loads or prestress.

2.3 Selected Experimental Studies on Punching Shear

2.3.1 Punching Shear Reinforcement

2.3.1.1 Dilger and Ghali: Shear Reinforcement for Concrete Slabs

Dilger and Ghali (Dilger and Ghali 1981) investigated four different types of shear reinforcement at the University of Calgary. Figure 2.3 shows the three types that were studied. They tested 40 slab-column connections with various types of shear reinforcements, which they developed. The specimens were subject to pure concentric load, and had a flexural reinforcement ratio of approximately 1.1%, and concrete design strength of 28 MPa. From their tests, Dilger and Ghali concluded that after full yield of the flexural reinforcement was reached, the steel reinforcement need only resist shear stress in excess of $0.33\sqrt{f_c'}$. Currently, CSA and ACI require that stresses over $0.2\sqrt{f_c'}$ be resisted by shear steel. They suggested from their experiments that the upper limit of shear steel resistance could be as high as $0.67\sqrt{f_c'}$. They also found the v'_c decreases as the distance of the critical section from the column face increases. As such, they suggested rules for punching shear at the critical section at $d/2$ away from the face of the column face.
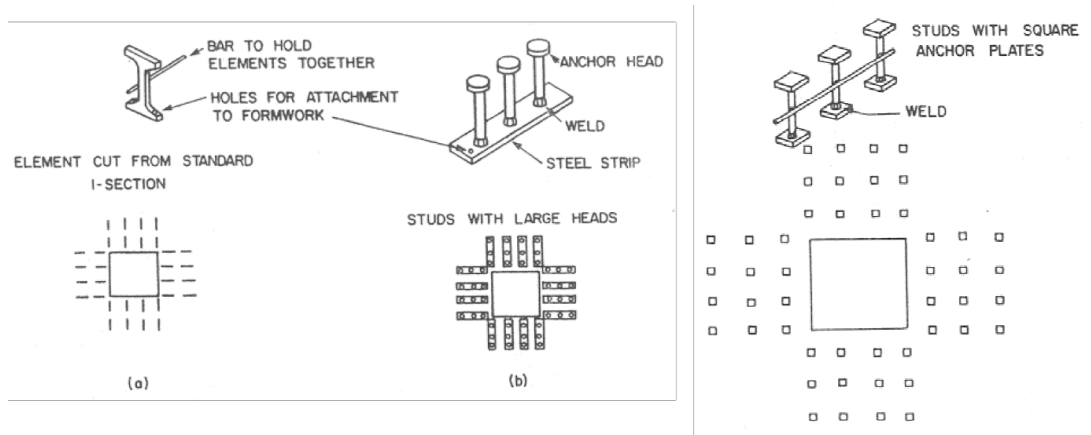
Figure 2.3 - Types of Reinforcement Studies by Dilger / Ghali

2.3.1.2 Elgabry and Ghali

Elgabry and Ghali (1990) presented design and detailing rules for shear stud punching shear reinforcement, based on data acquired from previous experiments. They recommended the following design points, and suggested the reinforcement design as shown in Figure 2.4. Their conclusions and studies would become the basis for the current shear stud design provisions found in CSA A23.3-04.

- Bottom anchors should be in the form of steel strips, with a width greater than 2.5D.

- Top anchors could be in the form of circular or square plates with the limitations that the areas be at least 10 times the area of the stem.

- In the direction parallel to a column face, the distance between anchor strips should not exceed *2d*, where *d* is the effective depth of the slab.

- Bottom anchor strips should be aligned parallel to column faces.

- Minimum distance of the first peripheral line from the column should be *d*/4. They suggested that upper limits for the spacing based on the value of the factored shear stress.
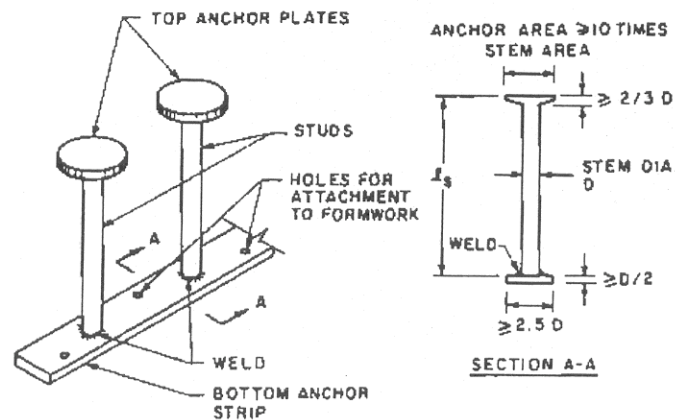
Figure 2.4 - Reinforcement Design Proposed by Elgabry / Ghali

2.3.1.3 El-Salakawy, Polak and Soudki: New Shear Strengthening Technique for Concrete Slab-Column Connections

El-Salakawy et. al (1998) at the University of Waterloo carried out an investigation into using shear bolts as an external retro-fit method to strengthen connections for punching shear. The objective of the study was to determine the feasibility of using shear bolts on edge-connections, under both concentric and eccentric loading. This research was the first to introduce the concept of a shear bolt as a retrofit technique. The bolt that was developed is shown in Figure 2.5.

Figure 2.5 - Shear Bolt Developed by El-Salakawy (1998)

Test slabs were 1540 x 1020 x 120 mm in dimension; monolithically cast with a column 250 mm square, Figure 2.5 shows the shear bolt reinforcement arrangement. The shear bolts were similar to shear studs

17

(Dilger and Ghali) but one end was threaded as to be fitted with a nut as shown in Figure 2.5. El-Salakawy et. al (1998) reported measured maximum deflections at ultimate load of between 54% and 162% larger than for the control specimens. They also reported an enhancement of ultimate strength of 12% to 13% for the reinforced specimens. They concluded that the bolts were an effective transverse reinforcement for punching shear, and can effectively be used as strengthening retrofit of existing slabs.
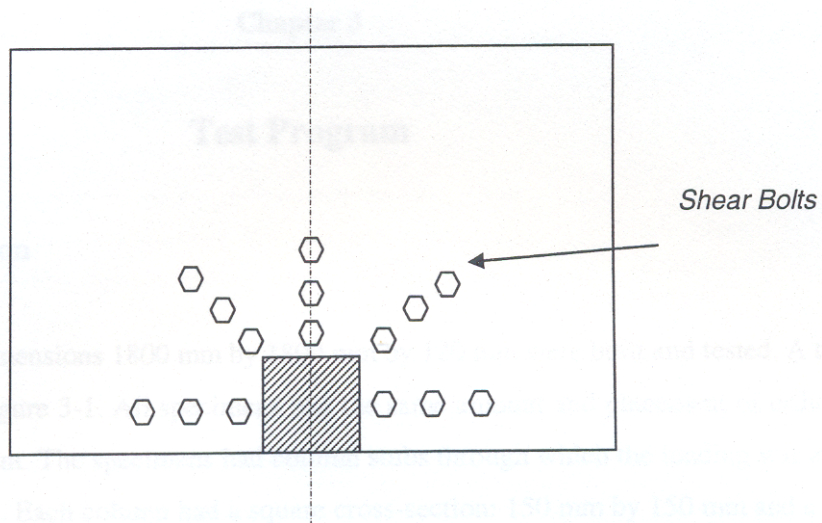
Figure 2.6 - Shear Bolt Arrangement by El-Salakawy et al.

2.3.1.4 Adetifa and Polak: A New Punching Shear Strengthening Technique for Reinforced Concrete Slabs at Interior Slab-Column Connections

Adetifa and Polak (2003) continued the work of El-Salakawy et. al (1998), this time focusing the study on interior connections under a concentric load. Six specimens were prepared, with dimensions of 1800 x 1800 x 120 mm. In order to determine different effects of loading, two specimens were built with openings (70 x 70 mm) around the columns, and one specimen was used as a control.

Figure 2.7 shows the shear bolts placed within the slab before testing. The basic design of the shear bolt remained the same as designed by El-Salakawy (1998) as shown above in Figure 2.5. Thicker washers were added on both sides of the slab to aid in the transfer of stresses from the concrete.

Head of a Shear Bolt   Washer with a Nut
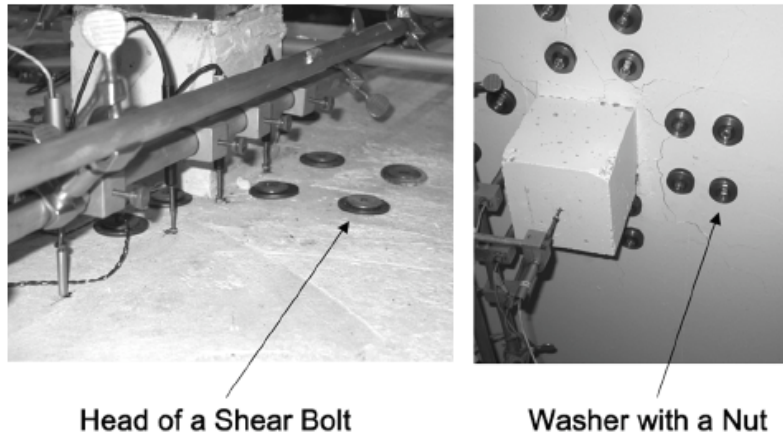
Figure 2.7 - Shear Bolts by Adetifa (2005)

Adetifa and Polak (2003) reported that they were able to increase both the strength and ductility of the reinforced interior connections over the unreinforced specimen. The specimens were reinforced to such an extent that they experienced flexural failure, as opposed to the brittle punching failure of the control specimen. Connection strength increased as much as 48%, and ductility of the connection was increased by 275%. They concluded that the shear bolt retrofit method is effective, and practical for interior connections. They also concluded that the shear bolt method is also effective for enhancing the strength of connections after openings have been added around the column for ductwork or other applications.

The work by Adetifa (2005) and El-Salakawy (1998) formed the basis for continuing work at the University of Waterloo in retrofit for punching shear. The contributions they made into understanding the behaviour and mechanics of shear bolt retrofit allowed research to continue.

2.3.1.5 Bu and Polak: Punching Shear Retrofit Method Using Shear Bolts for Reinforced Concrete Slabs under Seismic Loading

Bu (2008) tested nine full-scale reinforced concrete slab-column connection specimens under vertical service and cyclic loads. The vertical load for each specimen was kept at a constant value throughout the testing. The cyclic lateral drift with increasing intensity was applied to the columns. Bu reinforced the specimens with the steel shear bolts as designed by Adetifa (2005) and El-Salakawy (1998). The pattern, vertical load and amount of shear bolts were varied over the nine tests. The testing results showed that shear bolts could increase lateral peak load resisting capacity, lateral drift capacity at peak load, and ductility of the slab-column connections. Shear bolts also change the failure mode of the slab-column connections and increase the energy dissipation capacity.

Bu was able to increase the drift ductility of the slab-column connection at peak load point and post peak substantially (26% - 84%). The specimens with shear bolts also could undergo more lateral drift cycles at

19

larger deformation, showing a significant increase in energy dissipation capacity. The testing method for the reverse lateral loading by Bu was used in this research to test the new GFRP shear bolts under pseudo-dynamic loading, to determine their effectiveness under seismic loading.

2.3.2 Punching Shear Reinforcement Using Fiber Reinforced Polymer Bands

2.3.2.1 Binici and Bayrak: Punching Shear Strengthen of Reinforced Concrete Flat Plates Using Carbon Fiber Reinforced Polymers

Binici and Bayrak (2005) worked at the University of Texas used a new method to reinforce connections for punching shear, using FRPs. The slabs had dimensions of 2135 x 2135 x 152 mm. Vertical holes were arranged around the specimen columns by using PVC pipe prior to pouring. Strips of Carbon Fibre Reinforced Polymer (CFRP) cut to 25 mm in width and an appropriate length were passed through the holes, and wrapped to form external stirrups. A diagram of the strengthening technique follows in Figure 2.8.
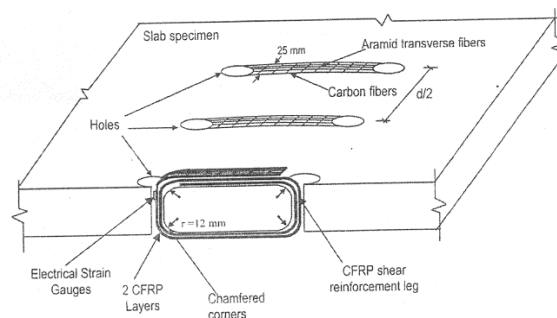
Figure 2.8 - CFRP Sheet Stirrups by Binici / Bayrak

Various hole patters and wrapping techniques were investigated. After the wrapping was complete additional CFRP sheets were bonded to the bottom of the slab to act as closures for the holes, so that they may be filled with epoxy. They were not used to strengthen the connection in flexure.

They reported an increase in punching capacity of 20% to 58% against the controls. In all cases a punching failure was observed, in most cases it was outside of the reinforced perimeter. They also reported a 30% to 145% increase in the displacement capacity of the reinforced specimens over the control.

2.3.2.2 Sissakis and Sheikh: Strengthening Concrete Slabs for Punching Shear with Carbon Fiber-Reinforced Polymer Laminates

A study was done at the University of Toronto by Sissakis and Sheikh (2007). This study used a similar reinforcement technique as Binici and Bayrak. The slab specimens had dimensions of 1500 x 1500 x 150

mm. A total of 32 slabs were tested, with four being controls, all slabs were placed under concentric monotonically increasing load until failure.

Holes were cast into the slabs using PVC pipe, 25 mm in diameter. Commercially available CFRP was used. The strands were made as long as possible, and stitched between the various holes made in the slabs, after being soaked in epoxy resin. This continuous loop of CFRP formed a solid ring of reinforcement, confining the concrete. The holes were later filled with epoxy resin.

The difference between this method, and the one by Binici and Bayrak (2005) is that a continuous CFRP sheet was used. By not separating the sheets into singular stirrups, Sissakis and Sheikh (2007) were able to achieve more ductility in the connection, however anchorage becomes critical, as any slip along the sheet weakens the entire stitch. They reported that the slab specimens reinforced with CFRP laminates had increased punching strength by 80%, and increased ductility by more then 700%.

Chapter 3
Testing Program

3.1 General Description

A total of six slabs (SN1, SN2, SN3, SN4, SN5, and SN6) of dimensions 1800 x 1800 x 120 mm were built and tested. The specimens were designed to ensure punching failure, before application of the shear bolt strengthening reinforcement. Simple supports were applied at the in-plane distances of 1500 x 1500 mm. A general diagram of the test specimen can be seen below in Figure 3.1.
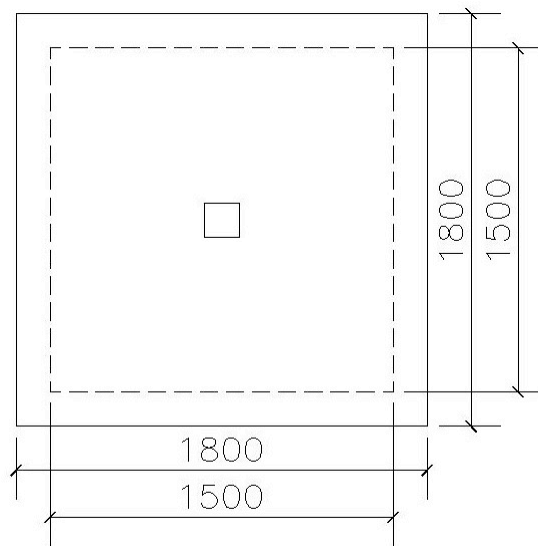
Figure 3.1 - General diagram of testing specimen

Two methods of inducing a punching shear failure were investigated, concentric punching (SN1 through SN4) and punching from pseudo-dynamic loading which included constant gravity load and lateral reversed loading to simulate earthquakes (SN5 and SN6). The pseudo-dynamic specimens had larger and longer columns, due to the way that the unbalanced moment was applied to the specimens. All specimens had the same amount and placement of orthogonal longitudinal reinforcement. For the tension mat, 10M bars at 100 and 90 mm centers were used for the bottom and top tension layers (two orthotropic directions), respectively. The slabs had almost identical moment capacities in both orthogonal directions. 10M bars at 200 mm, both layers, were used for the compression mat. The concrete cover in both tension and compression zones was 20 mm. Due to the experimental set-up design, the slabs were tested in the "upside down" position, when compared with the real slab-column system. The tension reinforcement was therefore placed on the bottom of the specimens.

22

The specimens had column stubs through which the loading was applied to the slab during testing. For the concentric punching specimens, each column had a square cross-section of 150 x 150 mm and a height of 150 mm extending beyond the top and bottom faces of the slab. The column stubs were reinforced with four 20M bars enclosed in four 8 mm ties. Specimens SN5 and SN6, the pseudo-dynamic loaded specimens, were built with 200 x 200 mm columns extending 700 mm beyond the top and bottom faces of the slab. These columns were reinforced with six 25M bars enclosed with eight 10M ties. Stronger columns were needed for the pseudo-dynamic testing to avoid failure of the column due to the applied loading. Since the control specimens for this research were from previous work by Adetifa (2003) and Bu (2008) the slab details were identical to previous experiments. Specimen SN5 was built with 2 openings placed next to columns. Openings (150 x 150 mm) were to simulate reinforced concrete construction in which openings are made in floors to allow wells or ducts for ventilation, electrical, and other services. Table 3.1 outlines the details for each tested specimen.

Table 3.1 - Testing Specimen Details

Specimen	Test Type	Column Size	Column Reinf.	Openings?	Control
SN1	Static	150x150x150h	4-20M 4-8mm stirrups	No	SB1
SN2	Static	150x150x150h	4-20M 4-8mm stirrups	No	SB1
SN3	Static	150x150x150h	4-20M 4-8mm stirrups	No	SB1
SN4	Static	150x150x150h	4-20M 4-8mm stirrups	No	SB1
SN5	Pseudo-dynamic	200x200x700h	6-25M 8-10M stirrups	No	SW5
SN6	Pseudo-dynamic	200x200x700h	6-25M 8-10M stirrups	Yes (150x150)	SW6

SB1 (Adetifia and Polak, 2003), SW5 and SW6 (Bu, 2008)

3.2 Material Properties

3.2.1 Ready-Mix Concrete

Specimens were cast with concrete made with normal Portland cement. Ready-mix concrete was donated by Hogg Read-Mix Concrete, with a specified compressive strength of 25MPa. To improve workability, a superplastisier was added at discharge, to achieve a slump of approximately 200mm. A total of six 150 x 300 mm control cylinders were cast with each specimen. Standard material properties of concrete were determined from these cylinder tests. The cylinders were made, compacted and tested according to Canadian Standard A23.3.2-9C and A23.3.2-13C, testing for the compressive and splitting tensile strength of the cylinders, respectively. The control cylinders were stored in the same conditions as the test specimens, and tested for compression and splitting tensile strength at the time of the punching shear

tests. Table 3.2 summarizes the material properties of the concrete. The first batch was cast on May 20, 2007, and consisted of SN1, SN5, and SN6, and had an average compressive strength of f_c' of 47.0 MPa. The second batch was cast on November 20, 2007 and consisted of SN2, SN3, and SN4, and had an average f_c' 36.0 MPa at the time of testing.

Table 3.2 - Tested Concrete Material Properties

Specimen	Compressive Strength			Test Avg. f'_c	Batch Avg. f'_c	Tension Strength			Avg. f'_t	Age at Testing
	(MPa)	(MPa)	(MPa)	(MPa)	(MPa)	(MPa)	(MPa)	(MPa)	(MPa)	
SN1	54.1	46.7	51.5	50.8	**47.0**	4.1	4.3	4.0	**4.1**	362 days
SN2	35.2	32.4	37.3	35.0	**36.0**	3.7	3.3	3.9	**3.6**	192 days
SN3	33.2	37.6	36.3	35.7	**36.0**	3.6	3.5	3.7	**3.6**	194 days
SN4	36.2	34.0	38.2	36.2	**36.0**	3.8	3.8	--	**3.8**	237 days
SN5	47.1	52.0	46.2	48.4	**47.0**	3.4	3.4	4.4	**3.7**	321 days
SN6	45.4	36.8	42.4	41.5	**47.0**	3.8	3.7	3.8	**3.8**	330 days

3.2.2 Longitudinal Reinforcing Steel

Steel used for longitudinal reinforcement was supplied, pre-bent, by Albrecht Steel Ltd of Kitchener, Ontario. The top and bottom reinforcing bars consist of 10M bars. Full reinforcement details can be seen in Figure 3.5 through Figure 3.8.

Reinforcing steel was found to have yield strength of 413 MPa, and a yield strain of 2000με, a stress-strain curve for one of the samples follows, as Figure 3.2.
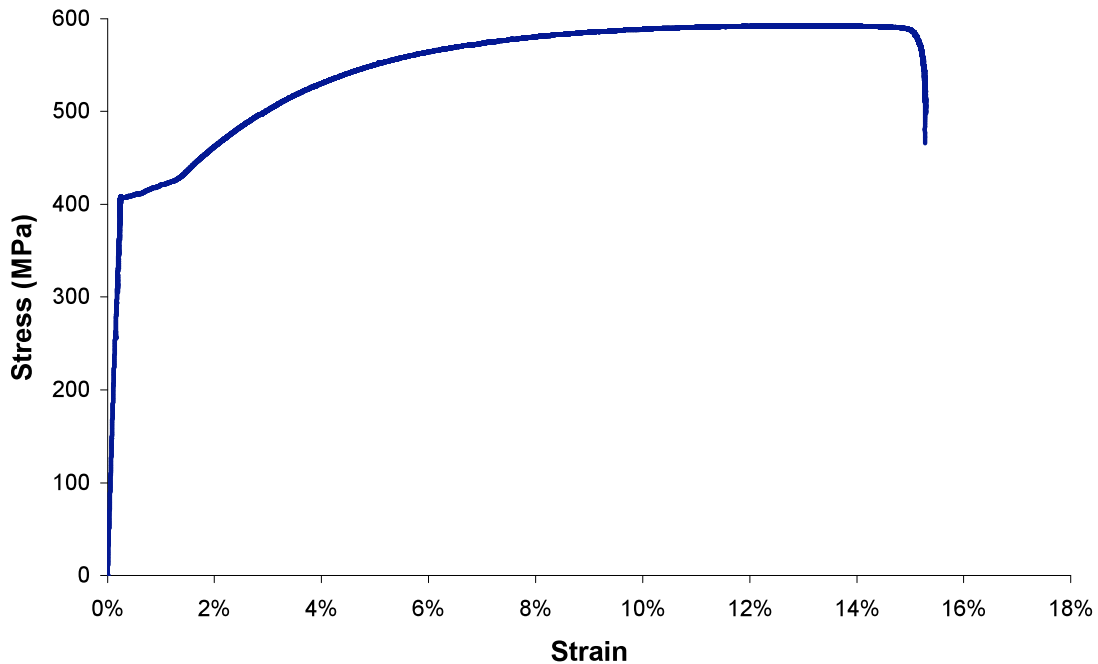
Figure 3.2 - Stress-strain curve of steel reinforcement tension test

24

3.3 Experimental Program

3.3.1 Equivalent Continuous Slab System

The test specimens are large-scale models equivalent to a slab-column connection in a continuous slab system, consisting of at least five 3.75 m spans in one direction, and an infinite amount of bays in the other direction. All previous research on punching shear at the University of Waterloo under the supervision of Dr. Polak used the same continuous slab system as a basis for specimen dimensions (Figure 3.3).
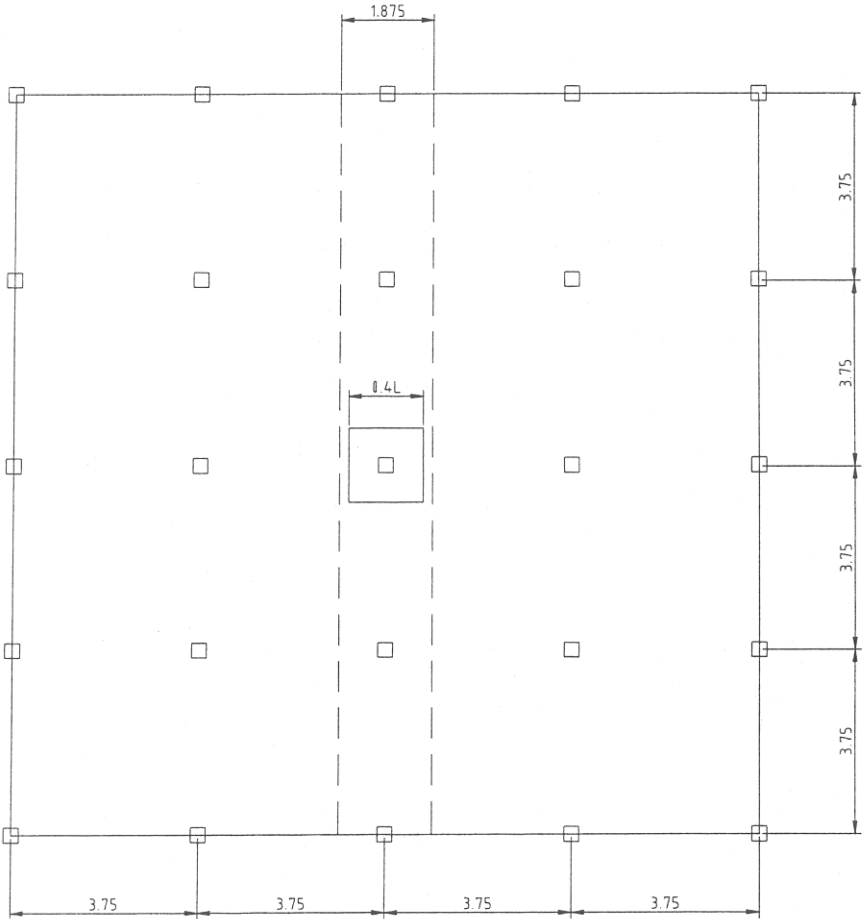
Figure 3.3 – Continuous Slab System (Adetifa 2003)

3.3.2 Test Specimens

The dimensions of the specimens were determined by boundaries representing the lines of contraflexure (approximately 0.4 times the span, equal to 1500 mm). The typical specimen in Figure 3.1 shows the outward boundaries of the slabs and the support lines at 1500 mm. The simple support system is assumed to have the same effect as the lines of contraflexure (no moment) in the parent system. The overhang at

the supports, equal to 150mm, was to ensure that adequate development is achieved, and to prevent anchorage or bond failure.

The simple support system was achieved by the use of 1500mm long flat solid bars, with dimensions of 1500mm x 40mm x 25mm thick. Neoprene pads, 25mm thick were adhered to the surface of the flat bars to ensure uniformity of contact during testing and to allow rotations.

3.3.3 Slab Flexural Reinforcement

The flexural reinforcement in the slabs was designed according to CSA A23.3-04. In order to allow comparison to previous research, the design was the same as previous studies by Bu (2008) and Adetifa (2003). The specimens were designed to ensure that failure occurs in punching before the flexural capacity in reached for the specimen without shear reinforcing.

All six specimens were reinforced with top and bottom layers running orthogonally. The tension layer was designed so that the slab was close as possible to being orthotropic. This was achieved by varying slightly the spacing of the tension layer. The average main tension reinforcement ratio is 1.2%.

The reinforcement used is as follows:

- The bottom mat lower layer was 10M bars at 100 mm on center. The upper layer was 10M bars at 90 mm centers.
- The top mat had 10M bars, spaced at 200 mm on center.

The clear cover at the top and bottom was taken to be 20 mm. Due to experimental set-up the slabs were tested in the "upside down" position, in that the tension reinforcement layer was on the bottom, and the compression steel layer on the top. The reinforcement layout for all specimens was the same. With the introduction of openings in one specimen, the layout was altered slightly, to account for the added stresses at the openings. Reinforcement layout diagrams for all six specimens follow as Figure 3.5 through Figure 3.7. As required by A23.3-04 integrity steel was included as two bars running through the column cross-section, each way. All of the bars were hooked at their ends to provide adequate anchorage. Details of the hooks follow in Figure 3.4.
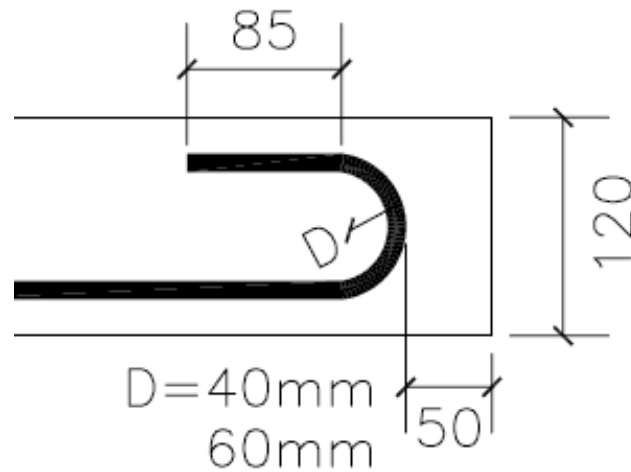
Figure 3.4 - Hook Detail of Flexural Reinforcement

3.3.4 Column Reinforcement

Since two different columns were used in the testing program, two different column designs were required. The columns on SN1 through SN4 were 150 x 150 x 150 mm in dimension, and contained four 20M bars, running from the top to the bottom of the column, through the slab, and enclosed by 8 mm ties placed at 100 mm on center. The columns on SN5 and SN6 were slightly larger, due to the applied lateral load. They had dimensions of 200 x 200 x 700 mm, and were reinforced with six 20M bars, running top to bottom, tied with 10M stirrups at 100 mm on center. (Adetifa 2003), (Bu 2008)

A-A

1:25

Specimen in Plan

1:25

B-B

1:25

10−10M @ 200x200
BAR DETAIL 'A'

T&B END BARS DETAIL 'C'.
THIS DIRECTION ONLY.

20−10M @ 90
BAR DETAIL 'B'

18−10M @ 100
BAR DETAIL 'B'

4−20M

8mm STIRRUPS
@ 100

DENOTES LINE OF
SIMPLE SUPPORTS
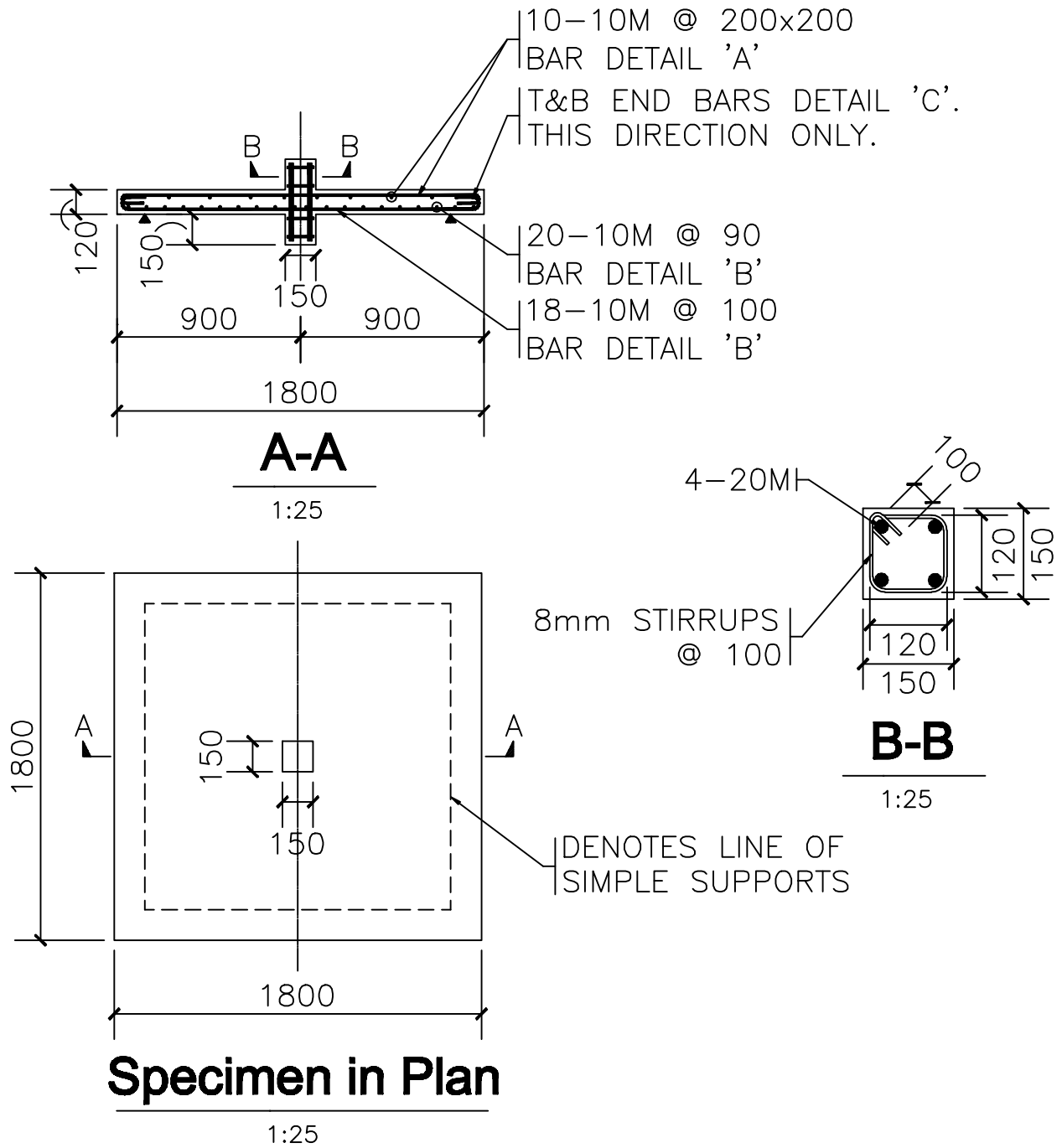
Figure 3.5 - Plan and Section Details for Statically Loaded Specimens (SN1, SN2, SN3, SN4)

28

A-A
1:25

B-B
1:25

Specimen in Plan
1:25
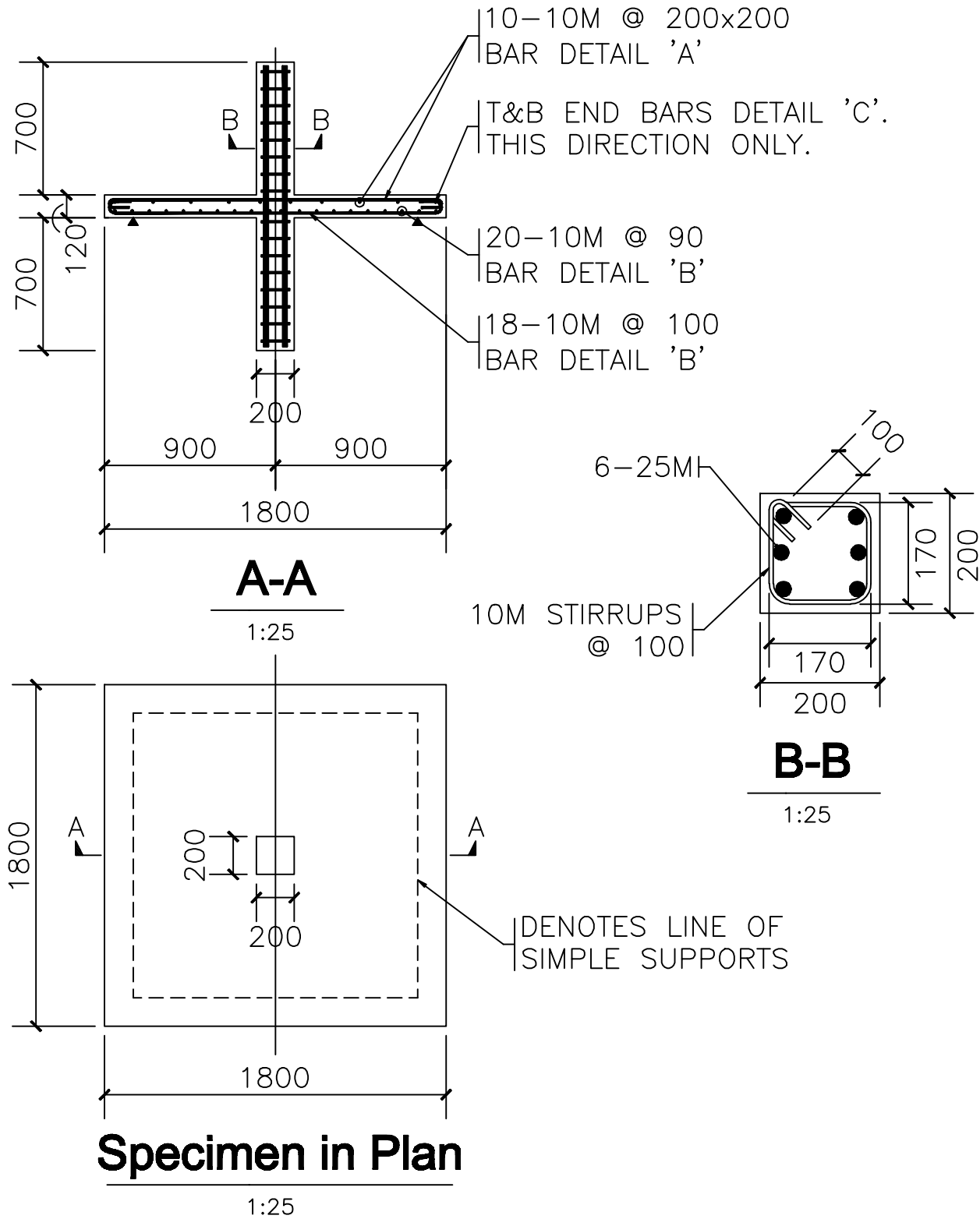
Figure 3.6 - Plan and Section Details for Specimens Loaded under Pseudo-Dynamic Load (SN5 & SN6)
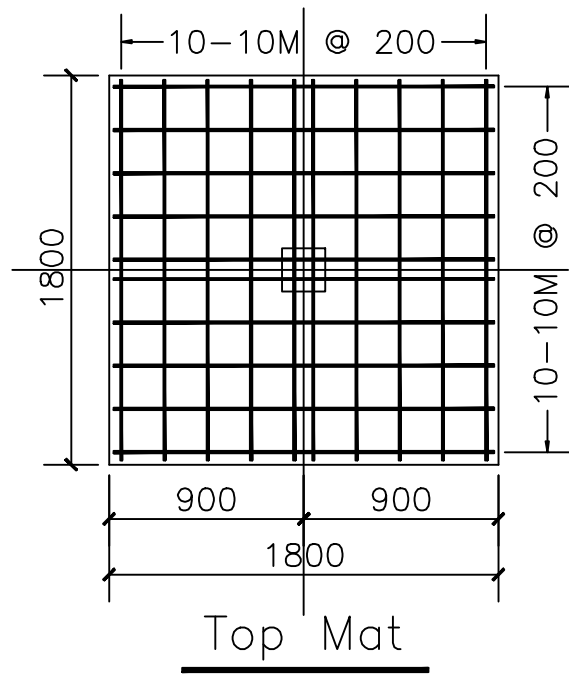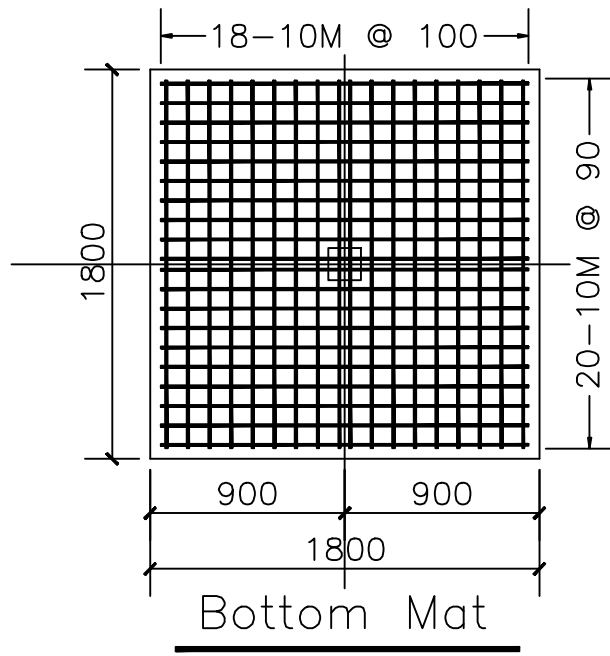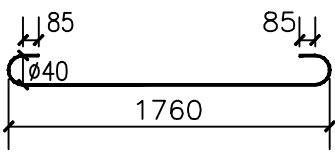
Figure 3.7 - Top and Bottom Reinforcing Mats in Plan (same for all specimens)
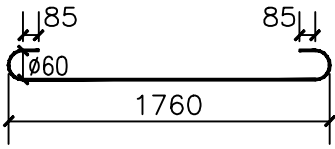
Detail 'A'
Bar Type: 10M

85 ⌐   ⌐ 85
◯ø40
         1760
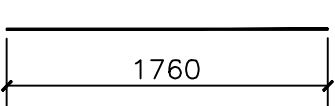
Quantity of bars: 26*6 = 156
Size: 10M
Length(each):   2060

Detail 'B'
Bar Type: 10M

85 ⌐   ⌐ 85
◯ø60
         1760

Quantity of bars: 28*6 = 168
Size: 10M
Length(each):   2110

Detail 'C'
Bar Type: 10M

         1760

Quantity of bars: 4*6 = 24
Size: 10M
Length(each):   1760
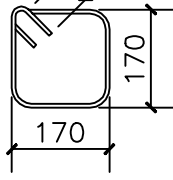
Stirrup Bars

Static Specimens:
Bar Type: 8mm

680

100

170

170

Quantity of bars: 4*4 = 16
Size: 8mm
Length(each):   680

Dynamic Specimens:
Bar Type: 10M

Quantity of bars: 16*2 = 32
Size: 10M
Length(each):   880
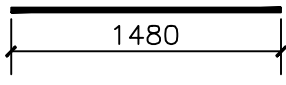
Column Bars

Static Specimens:
Bar Type: 20M

380

Quantity of bars: 4*4 = 16
Size: 20M
Length(each):   380

Dynamic Specimens:
Bar Type: 25M

1480

Quantity of bars: 6*2 = 12
Size: 25M
Length(each):   1480

Tie Wires:
             Size: 8 in.
             Quanity: 1 bundles

Material for
Testing:
             Size: 10M
             Quantity: 5
             Length: 1000mm

*Note: All dimentions are in milimeters.

Figure 3.8 - Reinforcement Details and Schedule

31

3.4 Preparation of the Test Specimens

3.4.1 Form-work Building

Forms were designed and built using plywood and lumber. Rigidity of the formwork was achieved using bracing, and at some points, double-ply construction. Connections were done using screws, nails, and glue. Form oil was applied prior to pouring, to ensure easy removal of the specimens after curing.

3.4.2 Caging

Caging was done in the laboratory, using pre-bend reinforcement from the supplier. Rigs were constructed to hold the reinforcement prior to tying. This ensured uniformity throughout all of the specimens, and helped construction. Tying was done manually, using 6" standard reinforcement ties. The cages were hoisted into place, using a crane, where they were set and tied into the formwork.

Figure 3.9 - Reinforcement Cages Prior to Casting

3.4.3 Casting

Casting took place in two batches of three slabs each. The concrete was transferred from the delivery truck to the formwork in the laboratory by use of a bucket and crane. Several rod vibrators were used to ensure uniformity and consolidation of the concrete in the formwork. A superplastisiser was also added to improve workability. To allow the slabs to be moved around the laboratory after curing, anchors were cast into the concrete. A 8x21/2" Grade 5 anchor bolt was tapped and screwed into the formwork in a upside down position. A 1-8" couple nut was then screwed onto the anchor bolt until the distance from the bolt head to the couple nut end was 120 mm. To stop movement during casting the couple nuts were

spot-welded onto the bolts when the desired height was met. A diagram and picture of these anchors prior and post to casting is shown in Figure 3.10.

Figure 3.10 - Lifting anchor bolt prior to casting

3.4.4 Curing

For at least 72 hours after casting the slabs were kept moist, and covered with burlap and plastic sheets. The side forms, and upper column forms were removed after 48 hours, and the slabs were continually wetted and kept covered for a total of 7 days, when the remaining formwork was removed. The specimens were stored at room temperature conditions in the structures lab at the University of Waterloo, until the time of testing.

3.5 Test Set-Up and Experimental Apparatus

3.5.1 Frame Supports

While two different tests were preformed, the same test frame was used for all testing. Since the results from this research were compared directly against results from previous research, testing set-ups were replicated as much as possible. The frame was designed according to CSA S16-94 (Canadian Steel Design Code) to ensure that no excessive deflections would occur (Bu 2008).

3.5.2 Test Set-up for Pseudo-dynamic Testing

The pseudo-dynamic loading tests were compared with results by Bu (2008). A picture of the experimental setup is shown in Figure 3.11. The steel frame includes two parts: the main frame and the supporting frame. The main frame consists of four vertical steel columns (W310x86), the crosshead (two

deep channels, MC460x86), and stiffeners for the crosshead. Three hydraulic actuators are installed on the main frame to apply load to the concrete slab-column specimen: two of them are horizontal to apply cyclic lateral drifts (50 kips); the third is a vertical actuator (150 kips) to apply the vertical constant load to the column of the specimen. The height difference between the two horizontal hydraulic actuators was 1250 mm.
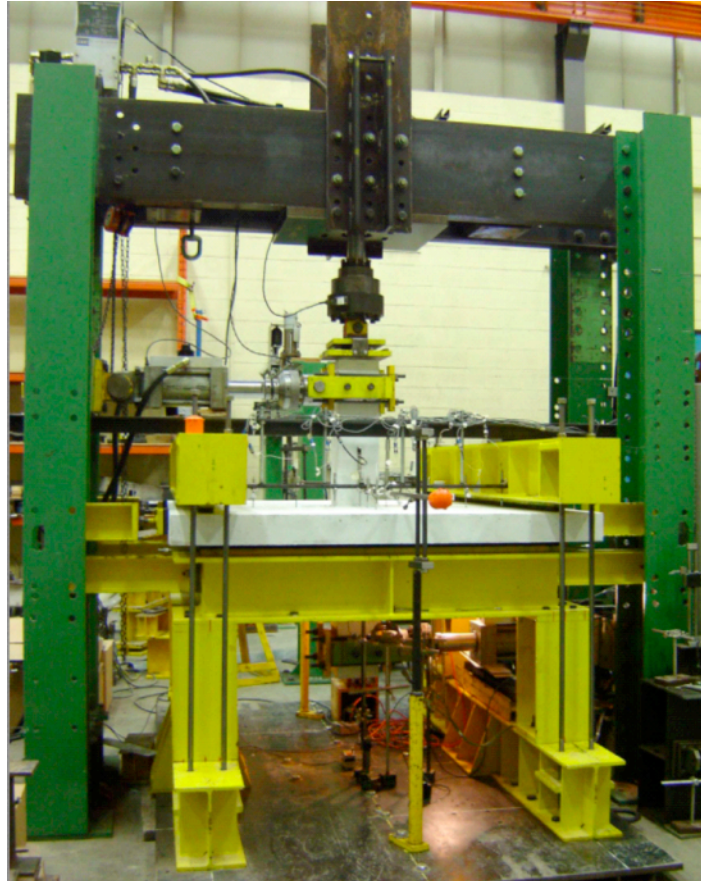
Figure 3.11 - Pseudo-dynamic Experimental Set-up

The second part of the experimental setup, the specimen support frame, is shown in Figure 3.12. This frame was designed to support a concrete slab-column specimen. The concrete slab was supported on its bottom from four sides by the square ring beam. To restrain overturning of the specimen due to cyclic lateral loading, two top reaction beams were installed in the direction perpendicular to the axis of cyclic loading. On each end of this beam, two vertical steel rods, attached to the bottom beam, were used to hold the top reaction beam.

Neoprene pads of 25 mm thickness were inserted between the concrete slab and the support beams and also between the slab and the top restrain beam along the support lines. The neoprene was used to simulate a simply supported condition at the point of contraflexure. The 25 mm thick neoprene flat pads

were glued to 25 mm thick steel flat bars of the same dimensions with the neoprene. This provided sufficient space for rotation between the concrete slab and the support ring beam or the top reaction beam.

| Elevation 'A' Testing Setup | Elevation 'B' Testing Setup |
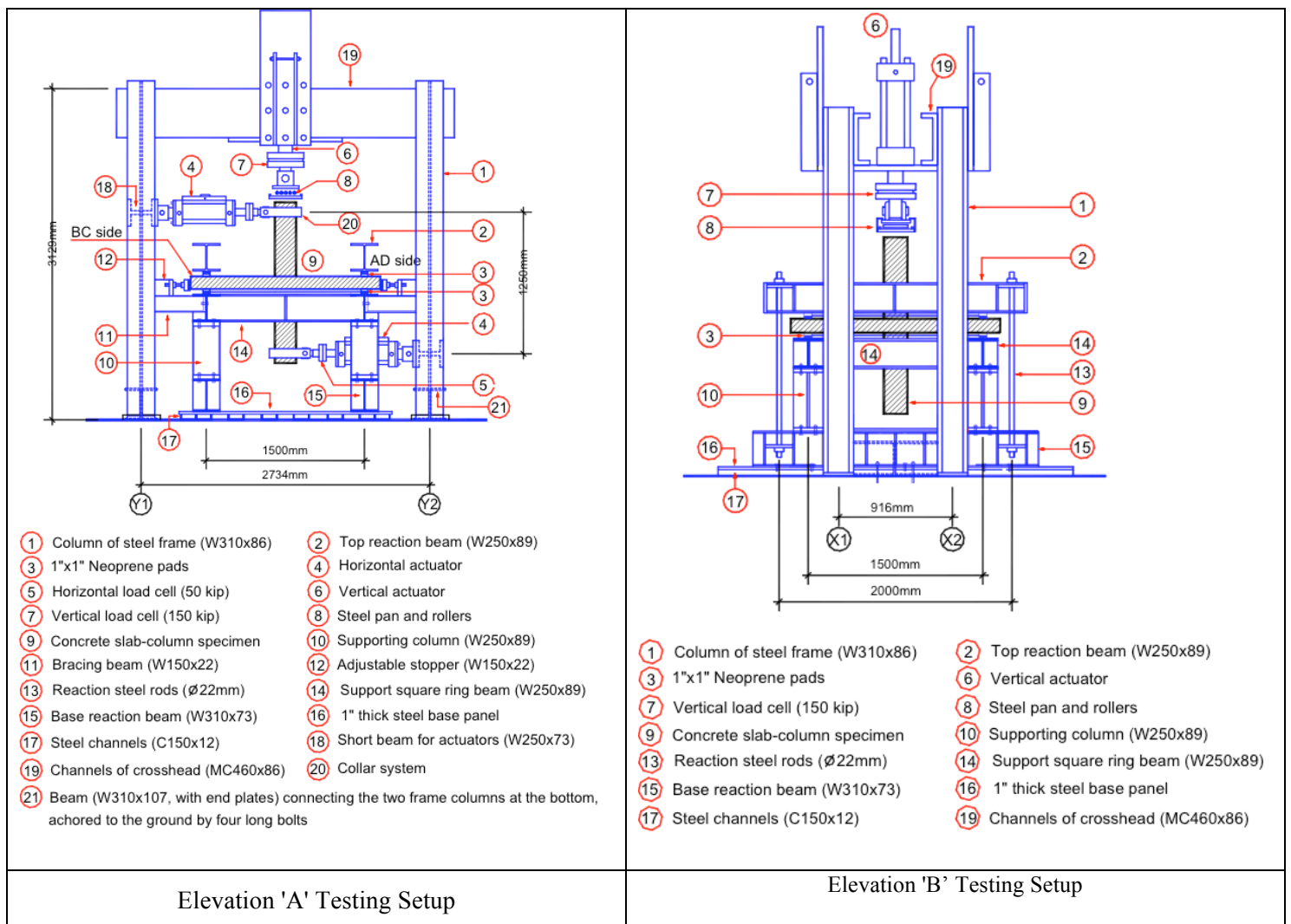
Figure 3.12 - Elevations of testing setup (Bu 2008)

To restrain the lateral sway of the supporting frame, four horizontal bracing beams (W150x22) were installed between the square ring beam and the four columns of the main frame. In order to restrain any possible excessive horizontal movement of the concrete slab due to horizontal lateral force difference, four adjustable stoppers were installed horizontally on the four-mainframe columns, at the concrete slab level.

The vertical load was first applied by the vertical hydraulic actuator, which would keep the constant load on top of the upper concrete column. The vertical actuator was connected to a 150 kip load cell and a threaded stud with a pinhole. Through a round steel pin (diameter 49mm), a flat square steel plate was connected to the actuator. The upper and lower concrete columns were also connected to horizontal

35

actuators through steel collars to apply horizontal cyclic loading, Figure 3.14. In order to reduce the friction between the top concrete column and the steel plate, steel rollers were used. A steel pan with five steel rollers, shown in Figure 3.13 was inserted between the plate and top surface of the concrete column.
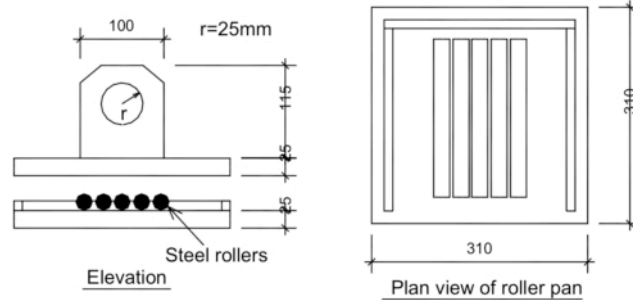
Figure 3.13 - Mechanism to apply vertical loads
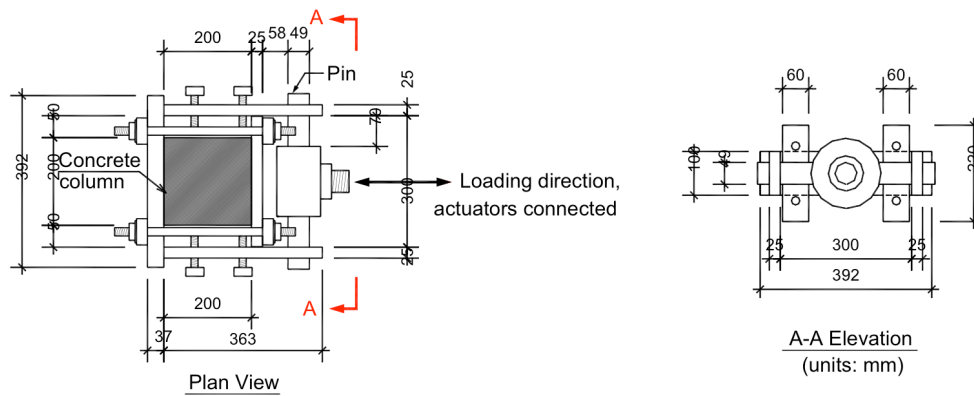
Figure 3.14 - Collar detail for application of horizontal loads

3.5.3 Test set-up for Statically Loaded Specimens

The method used in the statically loaded specimens was similar to the previous research by Adetifa (2003). The loading and support frame used for the static specimens was exactly the same as the frame described above, used by Bu (2008) in his research. The only exception is that the horizontal actuators were not used, and the vertical actuator was used to apply a vertically increasing load. Also according to Adetifa's experiments, and to simulate continuous slab construction and to avoid the slab edges from lifting during testing, each of the four corners of the slab was held in place by four tubular sections, cut from HSS 3x3x1/4 sections. The restraint was achieved by anchoring the sections to the base plate of the testing frame. In order to even the load over the slab face, neoprene pads (1/4" thick) were adhered to the bottom on the HSS. The following figure shows the testing frame set up during one of the static punching shear tests. The test results indicate that the test set-up provided more rotations at the supports then the

36

setup used by Adetifa (2003). This is probably due to the increased thickness of neoprene pads that provided simple supports.
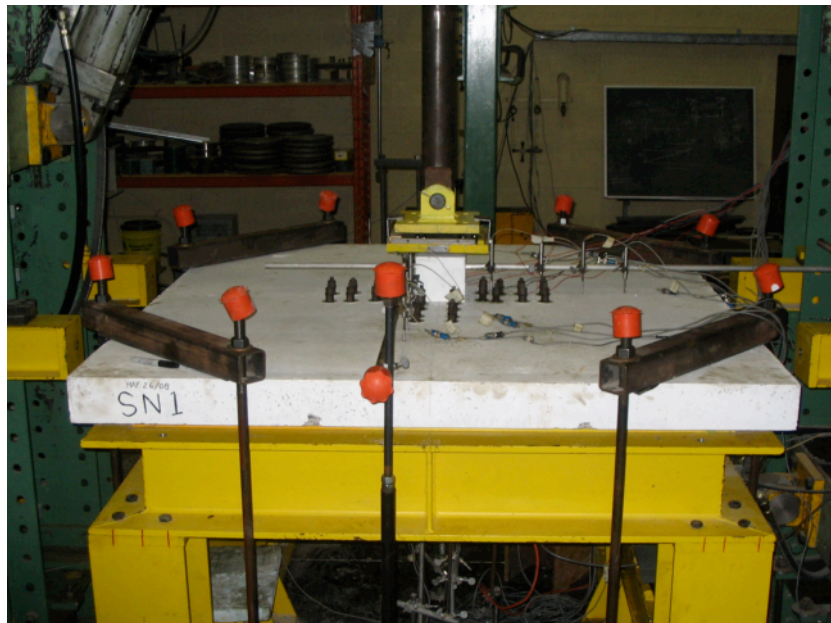
Figure 3.15 - Test Frame Set-up to Test Static Loaded Specimen

3.6 Instrumentation

3.6.1 Strain Gauges

Strain gauges were placed on the flexural reinforcement prior to casting the specimens. An average of 16 gauges were placed on the positive and negative reinforcement to measure steel strains during testing. All strain gauges were made by TML, Tokyo Sokki Kenkyujo Co. The type was FLA-5-11, for steel and composites. The Gauge length was 5mm, and resistance was measured to 120 ± 0.3 ohms. The strain gauges were bonded to the steel with an acrylate based strain gauge adhesive. The reinforcement was prepared by grinding a flat spot on the face of the reinforcement, and treating the steel with alcohol to achieve maximum adhesion by the gauges. The strain gauges were connected to electrical wires by the way of terminal strips so that the gauges could be connected to the data acquisition system. As much as possible the position of strain gauges was replicated from the previous research. Several figures follow as Figure 3.19 through Figure 3.21, which outline the position of the gauges in each specimen.

3.6.2 Displacement Transducers

To measure the deflection of the slab during testing, an array of Linear Displacement Transformers (LVDT), and Direct Current Displacement Transformers (DCDT) was set up on the top and bottom of the slabs. This was done to monitor the opening of the internal inclined crack during testing. Differential

displacement readings from the top and bottom, gave an estimate of the vertical width of the inclined shear cracks. A diagram of the position of displacement transducers is shown as Figure 3.16 and Figure 3.17. For the case of the statically loaded specimens an additional string-pot was placed on the bottom of the column, to measure the vertical displacement of the column during testing. String-pots were also placed at mid-slab depth on each side of the slab to measure any movement of the slab during testing.
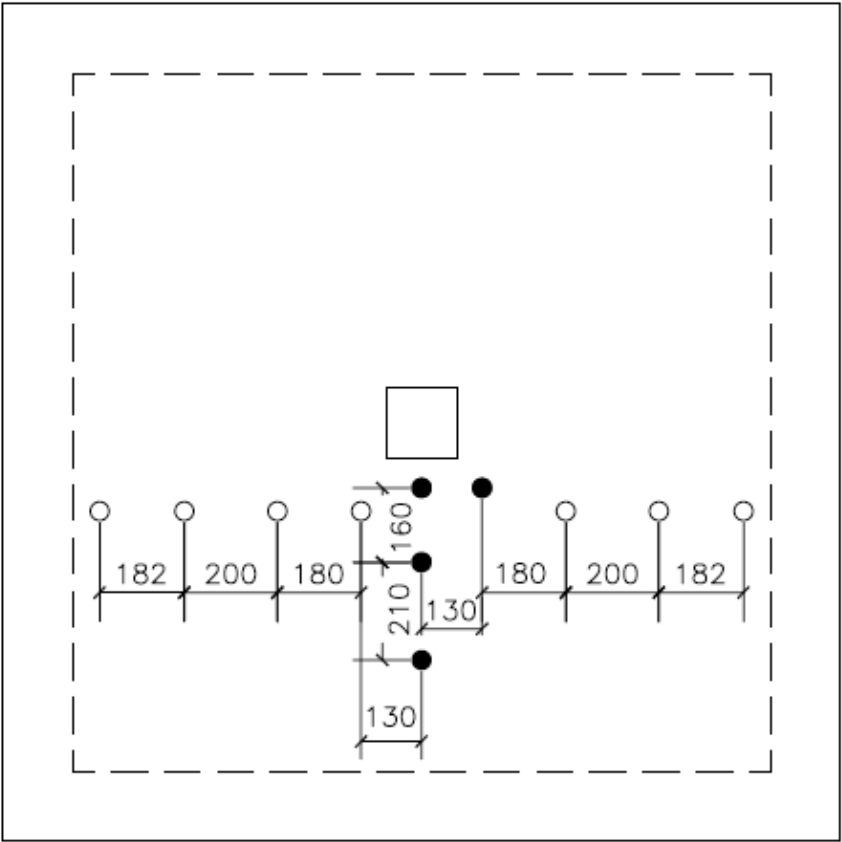
(Solid circles indicate locations where displacement gauges were placed on top and bottom of slab)

Figure 3.16 - Position of LVDTs on Pseudo-dynamic Loaded Specimens (SN5 and SN6)
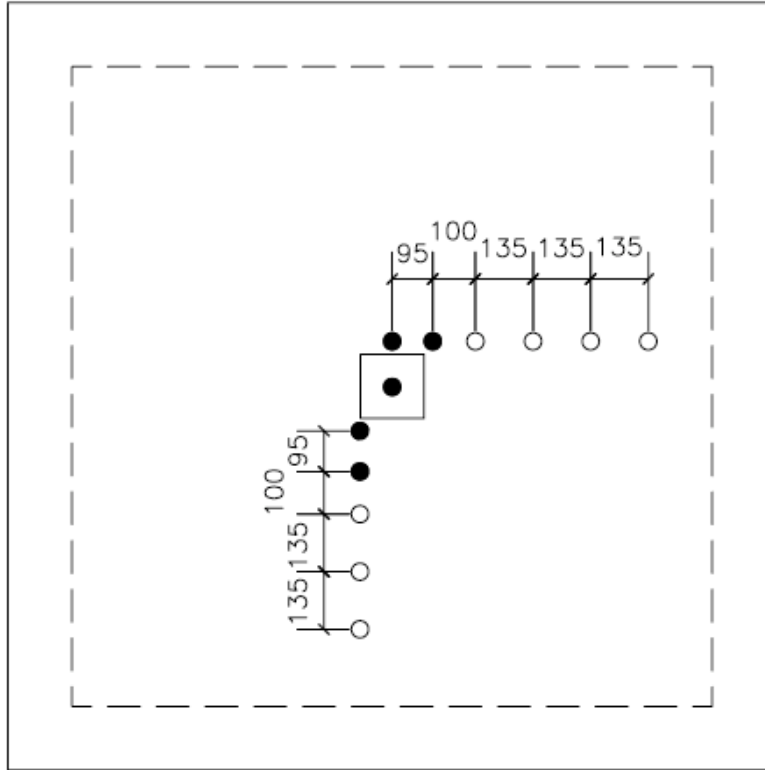
(Solid circles indicate locations where displacement gauges were placed on top and bottom of slab)

Figure 3.17 - Position of LVDTs on Statically Loaded Specimens (SN1 through SN4)

3.6.3 Headed Shear Reinforcement Patterns

Both ACI (ACI 318, 2005) and CSA (CSA A23.3, 2004) recommend that the shear reinforcement be located along concentric lines, which are parallel the perimeter of the column cross section (CSA A23.3-04 Cl.13.3.8.4). ACI and CSA also give guidelines for spacing of the reinforcement. The first line of reinforcement must be located at a distance of $s/2$ from the face of the column, where s is based on the value of v_f at a critical section $d/2$ from the column face, and is given as,

$$s \leq 0.75d \text{ when } v_f \leq 0.6\lambda\phi_c\sqrt{f_c'}$$
$$s \leq 0.5d \text{ when } v_f > 0.6\lambda\phi_c\sqrt{f_c'}$$

[CSA A23.3-04 13.4.8.6]

In Europe, particularly Germany, other shear reinforcement patterns have been suggested for headed punching shear reinforcement. A radial pattern is often used, which has been outlined in Figure 3.18. Slab SN3 has been reinforced with a radial reinforcement pattern, while the other specimens had orthogonal patterns consistent with ACI / CSA guidelines, Figure 3.18 outlines the patterns used on each specimen tested.

39

SN1:

SN2:

1800

1500

1800

1500

SN3:

SN4:

SN5:

SN6:

Figure 3.18 - Shear Bolt Hole Details

40
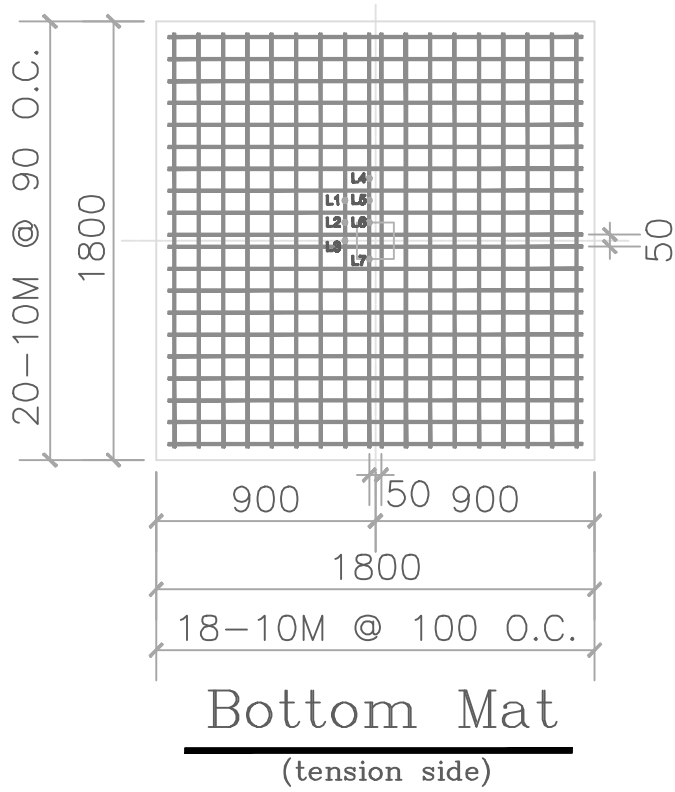
Figure 3.19 - Strain Gage Locations Statically Loaded Specimens (SN1, SN2, SN3, SN4)
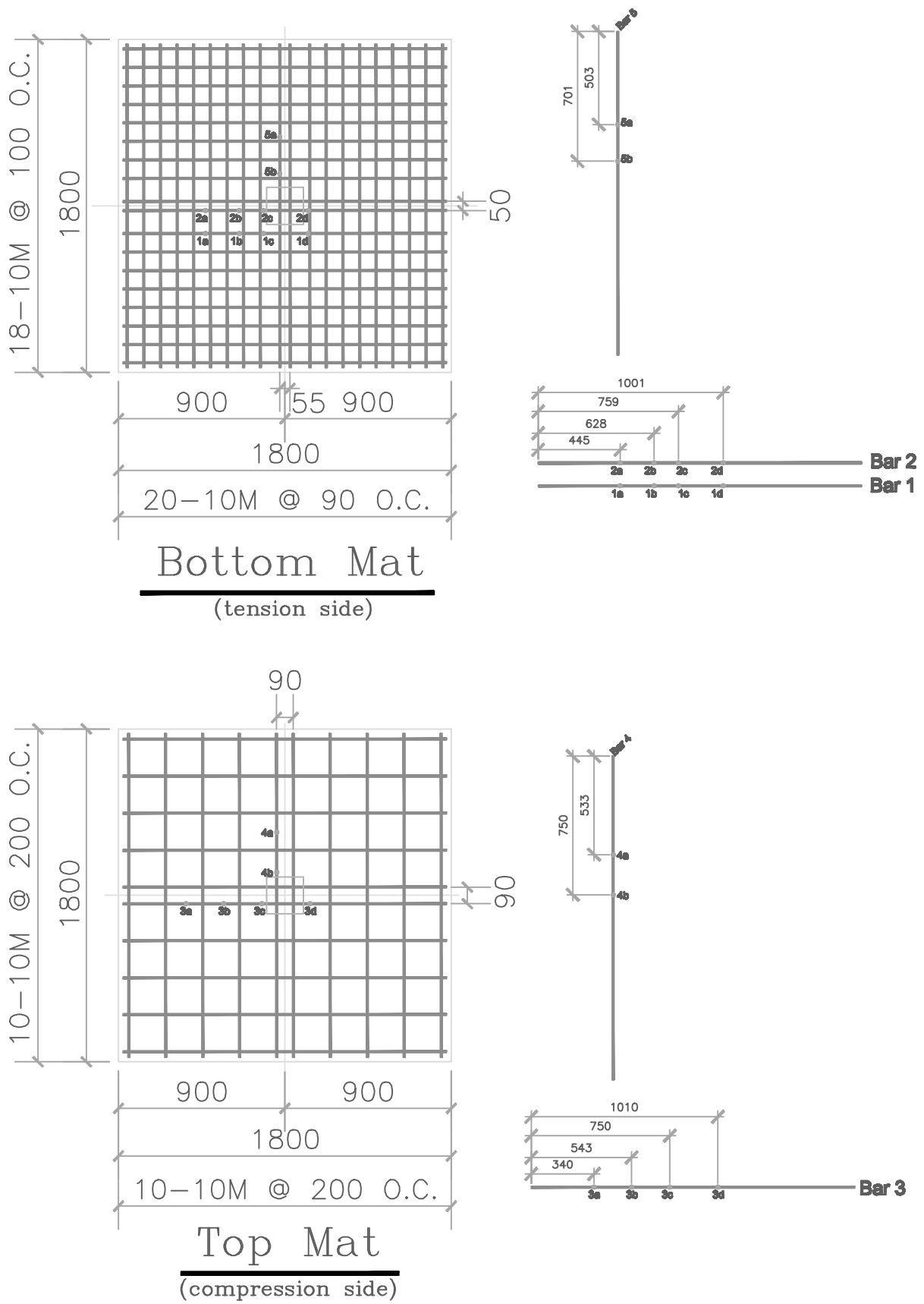
Figure 3.20 - Strain Gage Locations Quasi-Static Loaded Specimen without Openings (SN5)

42
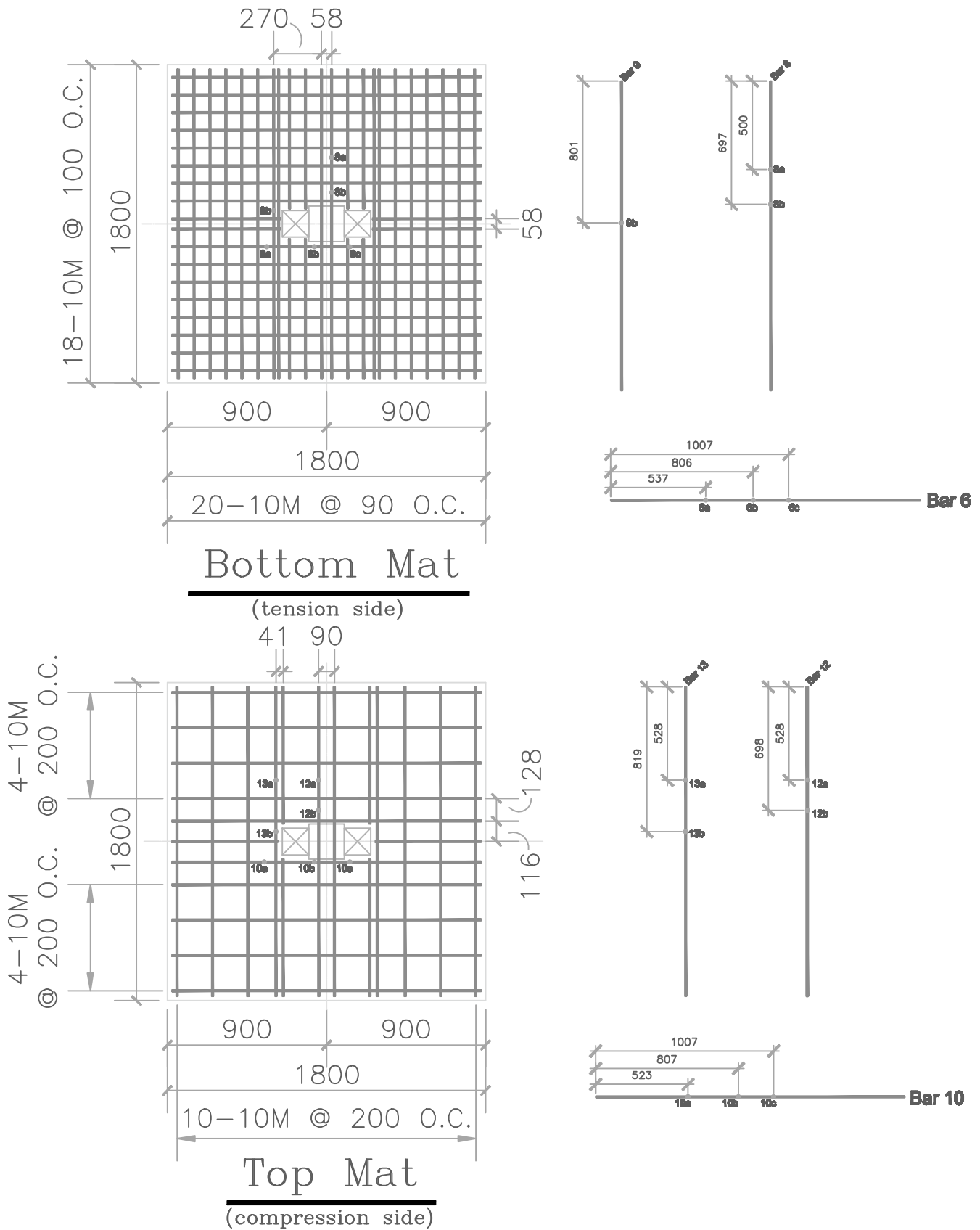
Figure 3.21 - Strain Gage Locations, Quasi-Static Loaded Specimen with Openings (SN6)
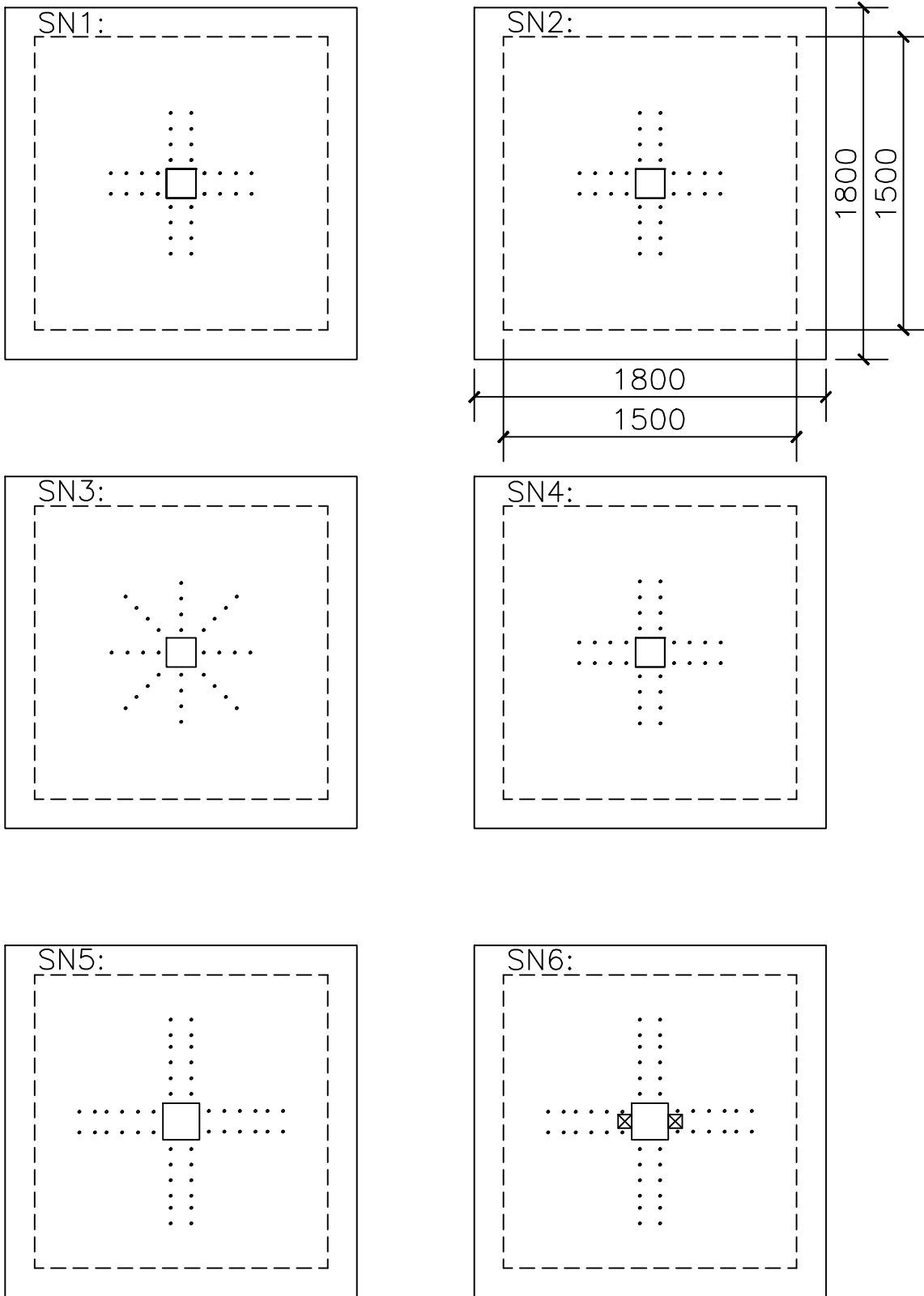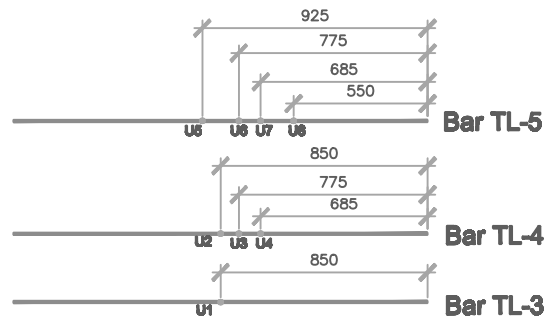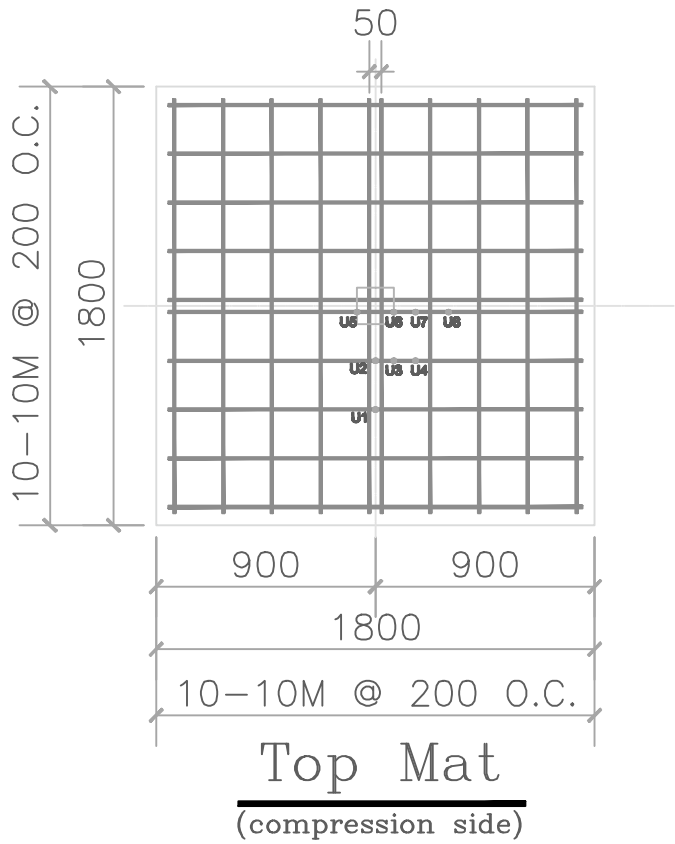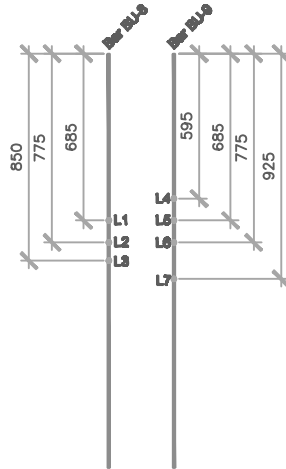
43

Chapter 4
Punching Shear Reinforcement

Previous research at the University of Waterloo involved the design and testing of externally applied steel shear reinforcement as a retrofit technique. This research involves the development of a shear bolt made of glass fibre-reinforced polymer (GFRP). Section 2.3.1 of this thesis details the work by previous researchers and their results. Development of a custom GFRP bolt is not a simple task. Steel can be easily formed, drilled, tapped and fit to meet almost every custom purpose. Two characteristics were critical. First, the product had to be able to resist the required tensile force, and second, in order to develop this force through the product, it must be correctly anchored at the slab's surface. The second point provides some difficulty. There is a severe strength reduction of strength when GFRP rods are threaded in the same manner of steel; this eliminates the possibility of the traditional nut and bolt approach previously undertaken (Bu, 2008). Another approach to anchorage, undertaken for this research, was adopted from the production of transmission line insulators. Three different products were developed and tested; they are detailed as follows.

4.1 Design of Punching Shear Reinforcement

Sample calculations were performed, in order to establish what loads the shear bolts need to resist. Adetifa (2003) used yield line theory when designing the slabs; and determined a vertical load of 362kN to be the load that causes flexural failure of the connection. The specimens were designed to fail in punching shear first, if unreinforced for shear, the reinforced specimens should fail in flexure and this consideration was used in designing FRP shear bolts.

Using the Canadian concrete code, (CSA A23.3-05) one can calculate how much load the shear bolts must resist to allow a flexural failure of the specimen. The calculations below assume 8 bolts, spaced at 70 mm rows concentrically placed around the slab column connection, with a concrete strength of 35 MPa.

$$v_f = v_r = v_c + v_s = \frac{362kN}{b_0 d} = 4.21 MPa \qquad [4.1]$$

$$v_c = 0.28\sqrt{f_c'} = 0.28\sqrt{35MPa} = 1.66 MPa \qquad [4.2]$$

$$v_s = v_f - v_c = 2.55 MPa \qquad [4.3]$$

$$v_s = \frac{8 \cdot F_b}{b_0 s} \Rightarrow F_b = \frac{v_s b_0 s}{8} = \frac{(2.55MPa)(955mm)(70mm)}{8} = 21.3 kN \qquad [4.4]$$

From this calculation, it is found that the bolt in the present tests must be able to resist a load of 21.3kN in order to strengthen the slab column connection to fail in flexure.

4.1.1 K-Line GFRP Shear Bolts

K-Line Insulators from Toronto are a manufacturer of composite transmission line insulators. Transmission line insulators act as a non-conductive bridge between the active power lines, and the structures that support them. Traditionally, these insulators have been made of ceramics, however a modern approach is to manufacture them with a composite (GFRP) core. In order to attach the insulating material to the power lines, or the structure, fittings must be attached to the composite rod. These end-fittings are typically metal; and when a GFRP core rod is used, the end-fittings are mechanically crimped. By compressing the end fitting, the residual stress is transmitted through the metal to the GFRP providing a frictional bond between the two materials. Using this approach, fairly large loads can be resisted by the end-fittings. With some limitations, the larger crimp load applied to the end fitting, the larger tensile force the connection can resist. It was proposed to use these GFRP rods, with aluminum end fittings, to resist punching shear loads. Some material properties of the rods used by K-Line are provided below (Table 4.1).

Table 4.1 - Properties of K-Line GFRP Rods (by Glasforms Inc.)

Glass weight (by percent)	75%
Tensile modulus, E_t (GPa)	414
Tensile Strength, MPa	827

A major component of the shear bolt design is the design of the restraint method to hold the bolt in place under loading. In order for the shear bolts to work, they must be able to resist the tensile loading induced when the concrete begins to expand in the formation of the punching cone. The critical point of the shear bolt assembly is the connection between the end fitting and the GFRP rod. K-Line's, traditional insulators, can achieve loadings of 20,000 to 40,000 lbs of force (90kN – 180kN). These forces are achieved using an industrial press to crimp the aluminum to the GFRP.

4.1.1.1 Installation Procedure for K-Line (and Schöck) GFRP Shear Bolts

The developed retrofit method must be practical for use on construction sites, within existing buildings, and on existing structures. As such, a method needed to be developed so that the end fittings could be attached on site. The hydro electrical industry produces hand held, portable devices that can be used to exert large crimping forces in the servicing and construction of larger power lines. It was proposed that one of these portable hand-crimping devices be used to crimp end fittings onto the GFRP in the field. The most powerful compression tool, that could be used on-site, allowed 15 tons of pressure. The portable crimping tool was provided by Huskie Tools; a REC-3610 Robo*Crimp. Appendix G includes the

technical data sheet of this product. Figure 4.4, shows the proposed shear bolt design and dimensions. One end (the so called "factory end") was crimped using the industrial machines at K-Line. Once the rod is crimped on one end, it is inserted through the slab, in a predrilled hole detailed in Figure 3.18. If the fittings are not tightly secured against the slab face, shear cracks may be allowed to propagate, and punching failure would result. A hydraulic hand jack is used to jack the bottom "factory" fitting against the bottom of the slab (Figure 4.3). This jack is able to slightly compress the aluminum end fitting, and hold the assembly tightly in place. The "field end" fitting is placed over the rod and crimped. Tests done at K-Line indicate that three crimps of 15 tons are required to give an ultimate tensile load of 20.1kN. After the field fitting has been installed, the hydraulic jack is removed, as the bottom fitting relaxes, a slight stress remains on the bolt assembly. This finished assembly creates the shear reinforcement necessary to resist the punching shear load. Pictures of the step-by-step installation process are shown in Figure 4.3.

This procedure was continuously developed and improved during the testing program. SN5 and SN6 were the first slabs to be crimped, followed by SN2 through SN4, respectively. As the author became more familiar with the behaviour of the crimping process, significant improvements were made with regards to the effectiveness of the crimping procedure. Several points are outlined below which highlight important items when crimping:

- Restraint of the bottom fitting to the slab with the hydraulic jack is imperative. The jack will slightly compress the bottom aluminum fitting, and move the GFRP rod upwards. After crimping of the top fitting, and release of the jack, some prestress will remain in the rod.

- When the top "field" fitting is being crimped, the fitting should be held tight against the slab, as not to allow the fitting to move upwards during the crimping process.

- When moving the hydraulic ram to compress the fitting, the ram should be stopped, and slowly induce the crimp on the fitting. If the ram is allowed to push into the fitting with some force, bending can be induced, and the fittings will not be tight against the slab face.

- When manufactured, most GFRP rods are coated to protect against fiberglass getting stuck into the users hands. This coating should be removed with sandpaper to allow for a better crimping surface.

- Great care should be taken to ensure that no bending is induced on the rod during the crimping process. The crimp must be applied perfectly perpendicular to the rod. Bending creates elongation of the rod, causing a space between the fitting and slab after crimping.
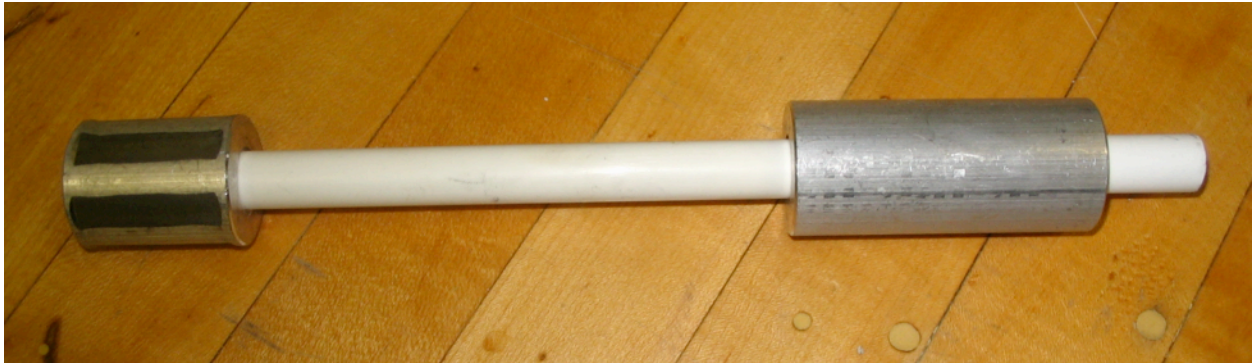
Figure 4.1 - K-Line Style Shear Bolt

Figure 4.2 - K-Line Shear Bolts Installed in Slab During Testing

1. A hand jack is placed beneath the slab and jacked up to press the "factory side" of the bolt to the slab face.	2. The bolt is now held in place, and the "field side" can now be seen extending out of the top face of the slab.
3. The FRP washer and aluminum fitting are placed over the rod. This fitting is held down during crimping.	4. The jaws of the crimping tool are placed over the fitting.
5. The crimping tool applies 15tons of pressure to the outside of the fitting, attaching it to the GFRP rod.	6. The fitting is now attached to the GFRP rod, the tool marks from the crimping tool can be seen.

Figure 4.3 - Installation Process for Crimping Aluminum Fitting to GFRP rod.

THIS FITTING IS TO BE CRIMPED IN THE FIELD WITH A 15ton HAND CRIMP TOOL.

"FIELD END"

68mm

FRP WASHER BY BOKER'S. 50mm O.D. 12mm I.D. 3mm THICK.

120mm

38mm

THIS FITTING IS TO BE CRIMPED AT K-LINE.

"FACTORY END"

240mm

12mm

GFRP Rod
(by K-Line)

40mm

5mm

ØR1mm

28mm

Ø22mm   Ø12mm

**Aluminium "Factory"
End-Fitting**
(by K-Line)

55mm

5mm

ØR1mm

28mm

Ø22mm   Ø12mm

**Aluminium "Field"
End-Fitting**
(by K-Line)

Figure 4.4 - Bolt Design for K-Line Bolt

49

4.1.2 Schöck GFRP Shear Bolts

Recently, a new producer of composite reinforcement for concrete has entered the Canadian market. Schöck, a major supplier of the construction industry in Europe from Baden-Baden, Germany has been granted approval from the Canadian Standards Association to distribute composite reinforcement for concrete in Can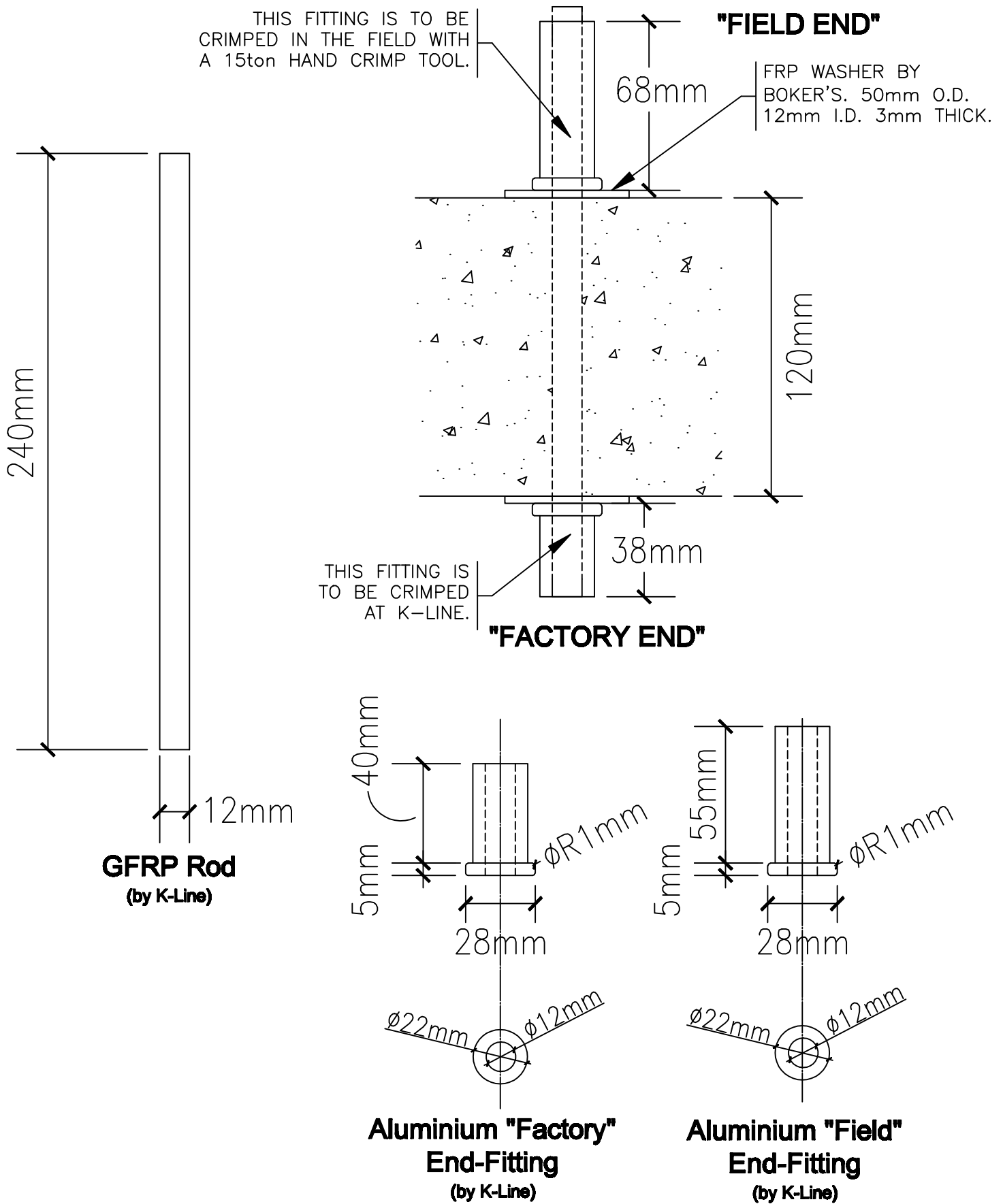ada, as well they have been granted membership in the American Composites Manufacturers Association. Their main reinforcement product is known as ComBAR, which is glass fibre reinforced polymer reinforcement. ComBAR is useful for this research, as it is GFRP reinforcement, approved for construction use in Canada. As the crimping methodology used in this research works well with glass composites, it was proposed that these bars should also be able to sustain the crimping force. ComBAR are also threaded along the bar. These threads are used for bond in the cast-in-place method of reinforcing, however they can also be of some assistance to this research. Furthermore, Schöck also make a ComBAR with a head, which possibly could work as an anchor in the shear bolt system.

Ideally, the best shear bolt system designed using Schöck products would be a bolt where one end is anchored to the slab with the unique ComBAR head, while the other end would be anchored using the crimped aluminum fitting from K-Line. For the purposes of this research the largest diameter bars that should be used are 12.5mm (0.5 inch). While 12mm headed ComBAR are currently under development, it is not ready to be used in practice. However, a study was undertaken with Schöck 16mm bar to determine the strength of the head. The study involved loading of the headed ComBAR to determine its resistance.

4.1.2.1 Study of Schöck GFRP ComBAR

Schöck has designed the headed ComBAR to be cast in place. The heads are intended to be developed in tension, in a similar way to hooks in conventional black steel reinforcement. According to Schöck, a 16mm headed ComBAR cast in place should be able to resist 27kN under direct tension (Schöck Bauteile GmbH 2006). However this is the design load and, without safety factors, the ultimate load can be assumed to be much higher. The loading scenario in the case of ComBAR cast in the concrete is very different then shear bolts application used in this thesis. With the entire head being cast in concrete, the tensile stresses are spread along the entire member. In the case of the testing that was performed at UW (in a retrofit scenario), the load was applied directly to the head of the ComBAR, as a radial point load over the underside of the head, and it was not surprising that the 27kN design tensile strength could not be achieved. Based on this testing, it was determined that a crimping of the ComBAR should be investigated, as a solution for current research needs.

The crimped Schöck ComBAR was used in punching shear slab test. The anchorage method used here is similar to the one used for the K-Line system, except the ribbing on the ComBAR had to be removed by manually grinding the surface of the rod. This needed to be done, as the aluminum fittings could not be made to fit over the ComBAR's ribbed surface. In the future, it is desired that a process could be developed to allow the inside surface of the fittings to directly match the ribbing pattern on the ComBAR. Figure 4.7 shows the punching shear retrofit bolt that was used to strengthen test specimen SN4.

The Schöck bars used in the full-scale tests were designed to resist 21kN in tension. It is expected that the controlling factor on this resistance will be the connection between the aluminum fittings and the GFRP rod. As shown above in Section 4.1, a resistance of 21kN should reinforce the slab to the point where it fails by flexure, at a punching load of 362kN.

Figure 4.5 - ComBAR GFRP rod prior to fittings being attached

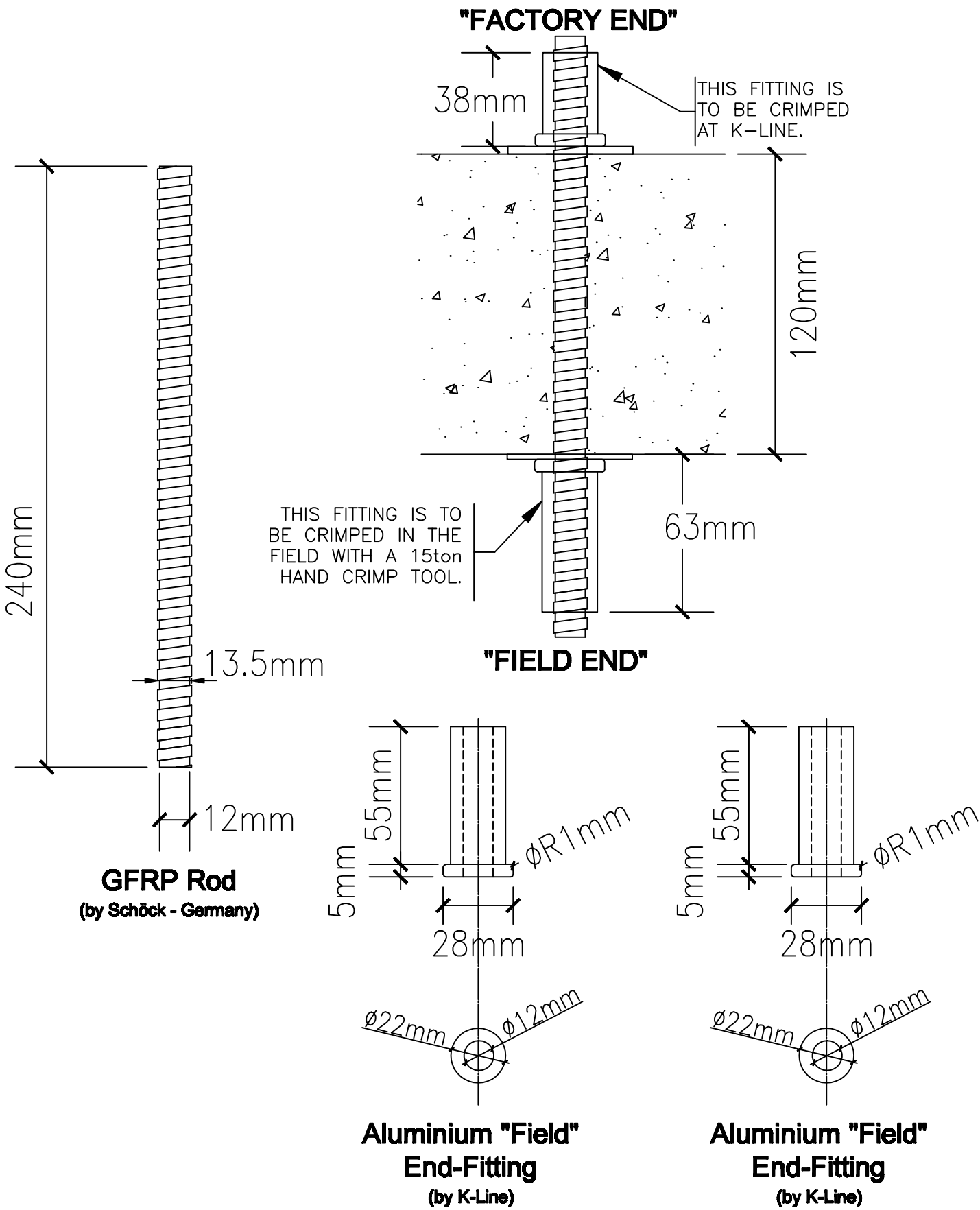Figure 4.6 - ComBAR Type Shear Bolts during testing

"FACTORY END"

38mm

THIS FITTING IS TO BE CRIMPED AT K-LINE.

120mm

THIS FITTING IS TO BE CRIMPED IN THE FIELD WITH A 15ton HAND CRIMP TOOL.

63mm

"FIELD END"

240mm

13.5mm

12mm

GFRP Rod
(by Schöck - Germany)

55mm

5mm

φR1mm

28mm

φ22mm   φ12mm

Aluminium "Field" End-Fitting
(by K-Line)

55mm

5mm

φR1mm

28mm

φ22mm   φ12mm

Aluminium "Field" End-Fitting
(by K-Line)

Figure 4.7 - Bolt Design for Shoeck Bolt

4.1.3 Strongwell GFRP Shear Bolts

Strongwell is a producer of fibre reinforced polymer composites. Out of several product lines they produce, one is of particular interest in this research. An off-the-shelf product, known as a Fibrebolt, is a fiberglass stud and a nut system. A picture of a standard 12.5mm (0.5 inch) diameter Fibrebolt is in Figure 4.8. It should be noted that Fiberbolts were not developed as structural elements, but rather for use for fastening non-structural lightweight fixtures.

Figure 4.8 - A Fibrebolt from Strongwell

The bolts are threaded over their entire length, and also have fiberglass nuts that are used in conjunction with the threaded rods. The manufacturer outlines installation techniques that must be followed when using Fibrebolts, and are mostly concerned with applying the correct torque to the nuts. A torque wrench was used according to the manufacturers specifications. For the purposes of this research, the 12.5mm (0.5 inch) diameter bolt was investigated and used as a reinforcing for punching shear. Strongwell provides several material properties and strengths in their published literature, however these values contain safety factors. Therefore the strength of the Fibrebolts was tested in the laboratory at the University of Waterloo. Table 4.2 outlines the recorded data.

Table 4.2 - Results from Lab Tensile Testing on Fibrebolts

Specimen Label	Bolt Type (0.5")	Measured Tensile Strength (kN)	Deformation (mm)	Failure Type
Bolt 1	1 nut	11.43	2.29	- delamination of the threads from the FRP core.
Bolt 2	2 nuts	13.55	2.47	- slip of the threads along the FRP core.
Bolt 4	2 nuts	14.70	2.50	- slip of the threads along the FRP core.
Bolt 5	2 nuts	15.87	2.22	- slip of the threads along the FRP core.
Bolt 3	3 nuts	14.02	2.33	- slip of the threads along the FRP core.

In order to accurately and correctly measure the ultimate tensile strength capability of the Strongwell product, the design codes were referenced for the accepted method of tensile testing. As composite materials are variable, the CSA has outlined specifically how composites should be tested, prior to their use as structural components in construction. CSA S806-02, "Design and Construction of Building Composites with Fibre-Reinforced Polymers" was recently introduced as the accepted design specification for building with composites. Annex C from CSA S806-02 outlines a test method for tensile testing, and was used in this research.

The testing machine must conform to ASTM Standard E-4; the machine used for this testing was an MTE-810 in the Structures Lab at the University of Waterloo. The test was performed using stroke (or displacement) control. The rate of loading for all the specimens was approximately 1 mm / minute.

In all cases the failure mode was the same. In all of the bolts tested the threaded part failed, first in tension at the point where the nut was attached to the rod, and then by slipping off the FRP core. The best visible example was during the test of only one nut, where the threading completely slipped off the end of the FRP core, a picture taken at the time of the test is shown in Figure 4.9.

Figure 4.9 - Slip Failure of the Fiberbolt Under Direct Tension

In each test the following was observed; the threading fractured, then the slippage of the thread over the surface of the FRP core occurred. From this it can be concluded that the tensile strength of the Strongwell bolt does not depend on the strength of the FRP core, but the adhesive strength that attaches the threading to the FRP core. The failure observed was sudden and brittle.

In order to increase the tensile strength of the bolts, additional nuts were added on each side of the bolt. Bolt #1, Bolt #2, and Bolt #3 had 1, 2, and 3 nuts respectively. These nuts were tightened on the bolts until approximately 10mm of the bolt could be seen exposed past the top nut. On these specimens, the amount of threading effective during loading would therefore be just the amount engaged by the nut, plus the approximate 10mm or so at the top of the bolt. Using this method, by adding three nuts to each side of the bolt, an ultimate tensile strength of 14 kN was achieved, on Bolt #3.

However after seeing the failure mode of the bolts, it was concluded that by increasing the amount of threading effective to sustain the load (the portion above the nut), the strength of the bolt would increase independent of the amount of nuts. Two more bolts were tested, with two nuts on each end, and 25mm of the threading sticking past the top nut. These two specimens had an average tensile strength of 15.3kN. The stress vs. strain diagram of all the bolts tested appears below, as Figure 4.10.
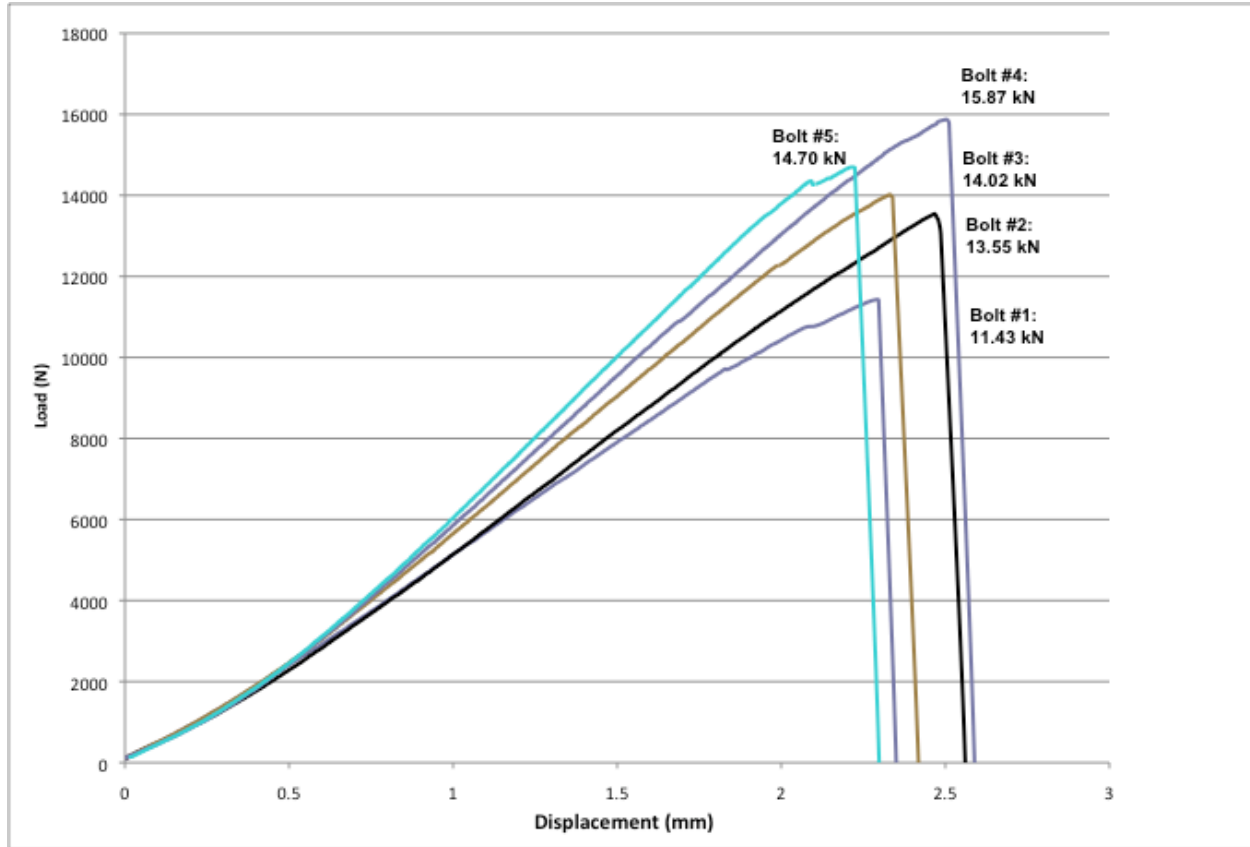
55

Figure 4.10 - Force vs. Displacement, Tension Test on Fibrebolts

Figure 4.10 illustrates the high stiffness of the bolts, and the sudden failure they experience at ultimate loading. The ultimate strength that is required for this research is 21kN. The Strongwell bolts were used in the testing of slab SN1, and details of this application follows in Figure 4.11. The following calculation shows the total punching load that the reinforced slab can resist, assuming an ultimate load as observed can be achieved by the Fibrebolts.

$$v_c = 0.28\sqrt{f_c'} = 0.28\sqrt{35MPa} = 1.66MPa \qquad [4.5]$$

$$v_s = \frac{A_{vs}f_{vy}}{b_0 s} = \frac{\#\,Bolts\cdot T_u}{b_0 s} = \frac{8\cdot 15kN}{(955mm)(70mm)} = 1.79MPa \qquad [4.6]$$

$$v_f = v_r = v_c + v_s = \frac{P}{b_0 d} \qquad [4.7]$$

$$P = (v_c + v_s)b_0 d = (1.66MPa + 1.79MPa)(955mm\cdot 90mm) = 296.5kN \quad [4.8]$$

Where,

f'_c = 35 MPa $\qquad\qquad$ b_o = 955 mm $\qquad\qquad$ T_u = 15kN $\qquad\qquad$ d = 90 mm

FRP WASHER
BY BOKER'S.
50mm O.D.
12mm I.D.
3mm THICK.

12mm

45mm

240mm

120mm

45mm

12mm

13mm

NUTS PROVIDED
BY STRONGWELL,
INSTALLED TO A
RECOMMENDED
MAXIMUM TORQUE
OF 8 ft−lbs.

**Threaded "Fiberbolt"
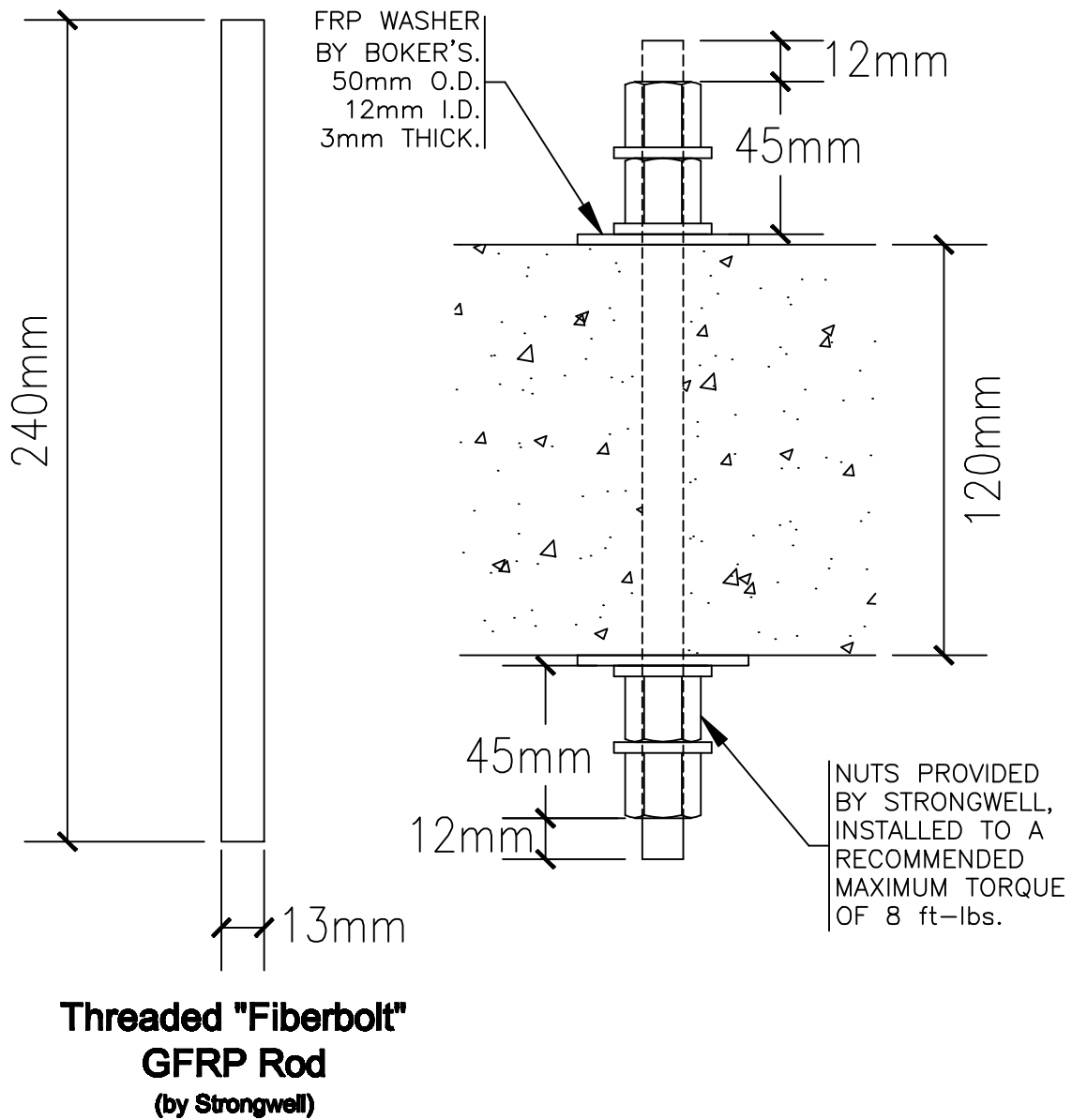GFRP Rod
(by Strongwell)**

Figure 4.11 - Shear Bolt Design for Strongwell "Fibrebolt"

With the Fibrebolts reinforcing the specimens, according to the CSA / ACI guidelines on punching shear, the specimens should be able to resist a punching load of about 296.5kN. This is an increase of the punching resistance, as an unreinforced specimen should only be able to resist 242 kN. This method however, does not predict that the Fibrebolt product will change the failure mode into the desirable flexural failure. By this method SN1 should fail in punching, with a punching cone forming outside of the shear bolt perimeter, at a vertical load of about 300 kN.

4.1.4 Summary of Expected Punching Resistances

A summary table has been created to outline the expected punching resistance of each specimen. All of these values were calculated using the CSA (2005) recommended procedure for punching resistance. The assumed strength of the punching shear reinforcement (F_s) was found from the tensile tests that were described in this chapter.

Table 4.3 - Calculated Punching Shear Load Summary, Statically Loaded Specimens

Specimen	Reinforcement Layout	Reinforcement Method (12.5mm diameter)	Assumed Strength F_s (kN)	Calculated Punching Capacity (kN)
SN1	4 rows, orthogonal	Strongwell Fibrebolts	15	297
SN2	4 rows, orthogonal	K-Line core shear bolts	20	348
SN3	4 rows, radial	K-Line core shear bolts	20	348
SN4	4 rows, orthogonal	Schöck ComBAR core shear bolts	20	348

Table 4.4 - Calculated Punching Shear Load Summary, Pseudo-dynamically Loaded Specimens

Specimen	Reinforcement Layout	Reinforcement Method (12.5mm diameter)	Assumed Bolt Strength F_b (kN)	Calculated Moment Capacity (kN-m)
SN5	6 rows, orthogonal	K-Line core shear bolts	20	46.2
SN6	6 rows, orthogonal, 2 openings	K-Line core shear bolts	20	46.2

The moment capacity of SN5 and SN6 was calculated as follows, according to CAN/CSA A23.3-04

$$v_r = \frac{V_n}{b_0 d} + \frac{\gamma_v M_n e}{J_x}$$

$$v_r = v_s + v_c = \frac{n \cdot F_b}{b_0 s} + 0.3\sqrt{f_c'}$$

$$M_n = \frac{J_x}{\gamma_v e}\left[\frac{n \cdot F_b}{b_0 s} + 0.3\sqrt{f_c'} - \frac{V_n}{b_0 d} \right]$$

J_x – polar moment of inertia of the critical section about the centrodial axis

e – distance from the centroid of the critical section where the moment is calculated.

γ_v – fraction of the moment transferred by shear.

$V_n = 160$kN	$d = 90$mm	$n = 8$ bolts
$b_0 = 1160$mm	$f_c' = 35$MPa	$s = 70$mm

Chapter 5

Experimental Procedures and Observations

The following chapter describes each test in detail. The two testing procedures are presented first, and then observations for the six specimens follow. The observations are presented in terms of deflections, cracking and reinforcement response. As discussed previously, six specimens were tested, namely: SN1, SN2, SN3, SN4, SN5, and SN6. Each specimen is described with respect to configuration and transverse reinforcement in Figure 3.7

5.1 Testing Procedures

5.1.1 Specimens SN1, SN2, SN3, SN4

Slabs SN1, SN2, SN3, and SN4 were loaded under pure vertical load. All of the specimens loaded in this manner are the same. All slabs are without openings. As control specimens are from previously conducted research, an attempt was made to use similar testing procedures as Adetifa (2003). All slabs were tested in displacement control. The displacement rate was chosen to approximately follow the required rate of 1 – 2 mm/min.

SN1 was reinforced transversely with 4 peripheral rows of 12.5mm diameter GFRP bolts by Strongwell Industries. The expected strength of the Strongwell GFRP bolts was 16kN, and the corresponding expecting punching load was 297kN. Based on Strongwell recommendations, the bolts were tightened with a torque wrench to a capacity of 8 ft-lb. At a load of approximately 160kN the slab had to be unloaded, then reloaded, as the ramp generator controlling the displacement of the vertical actuator had to be reset. It is not expected that this had any effect on the test. The test time for SN1 was 103 minutes.

Slab SN2 was reinforced transversely with 4 peripheral rows of 12mm diameter GFRP shear bolts with a composite core by K-Line. The anticipated bolt strength for the shear bolts with a K-Line core was 20kN. Expected punching load of SN2 was 348kN. The slab was unloaded and reloaded at a vertical load of approximate 225kN; the stiffness degradation and strength of the specimen does not appear to be affected. A change was made to the test setup so that this was not required in future tests. Test time was 101 minutes.

Slab SN3 was reinforced transversely with 4 peripheral rows of 12mm diameter GFRP shear bolts with a composite core by K-Line, this time in a pattern recommended by Eurocode 2. Instead of being orthogonal with the flexural reinforcement, the shear bolts are placed in a "radial star pattern" on diagonals surrounding the column. Shear reinforcement details for this slab can be found in Figure 3.18.

The anticipated punching load for SN3 was 523kN (according to Eurocode 2). Again, loading was typical for this entire testing series. Test time was 63 minutes.

Slab SN4 was reinforced transversely with 4 peripheral rows of GFRP shear bolts with a composite core of Schöck ComBAR. The reinforcement layout was consistent with SN1 and SN2. The anticipated bolt strength for the shear bolts with an Schöck core was 20.1kN, and the expected punching load of SN4 was 348kN. Test time was 52 minutes.

5.1.2 Specimens SN5 and SN6

Slabs SN5 and SN6 were subjected to constant vertical load and increasing lateral load, applied in a cyclic manner. Slab SN5 was without openings, while SN6 contained two 150x150 mm pre-built openings in the direction of the applied moment, against the column face. As control specimens are from previously conducted research, an attempt was made to use the same testing procedures as Bu (2007). All slabs were tested in displacement control mode. Bu (2007) tested specimens with both a vertical load of 110kN and 160kN, for the current tests a vertical load of 160kN was used. The pseudo-dynamic lateral displacement path was predetermined by Bu (2007), and is in Figure 5.1. The path is a function of drift ratio, that is, the ratio of horizontal displacement, to the distance from the mid-slab depth to the applied horizontal load. The moment capacity of each connection was calculated by CAN/CSA A23.3-04, and found to be 46.2kN-m. Given that the moment arm of the test setup was 1.25m, this moment capacity would translate to a maximum horizontal load of 36.9kN.

SN5 was reinforced transversely with 5 peripheral rows of GFRP K-Line type shear bolts. The shear bolts were installed and crimped according to the installation procedure discussed above in Figure 4.3. Only 5 rows were installed, as opposed to the desired 6 as the dimensions of the crimping tool would not allow the 1st row to be installed. During the test, the hydraulic system in the structures lab experienced a sudden loss of power. While restarting the system, the specimen was exposed to an unwanted drift ratio of 4%. The data collected unto this point, and after indicates that the stiffness of the connection was compromised; consequences of this are discussed later. The test time for SN5 was 216.7 minutes.

Slab SN6 was reinforced transversely with 6 peripheral rows of GFRP shear bolts with a composite core by K-Line. This specimen contained two openings, as discussed above. The test time for SN6 was 223 minutes.
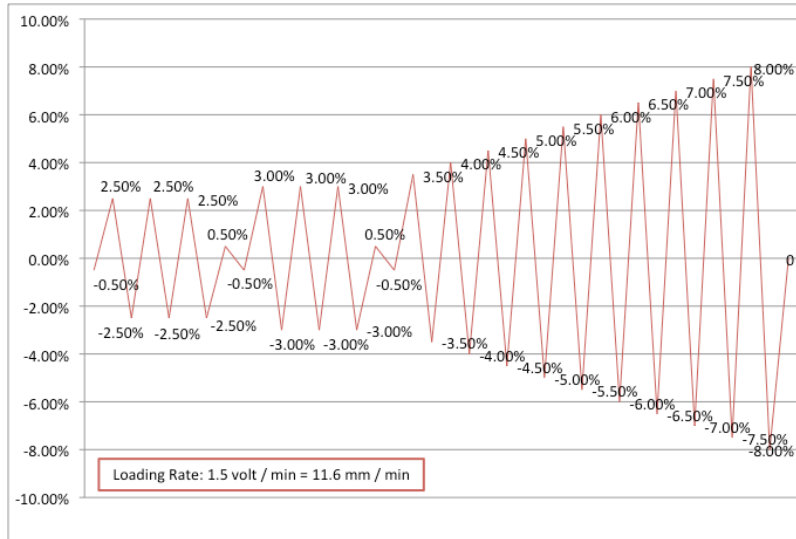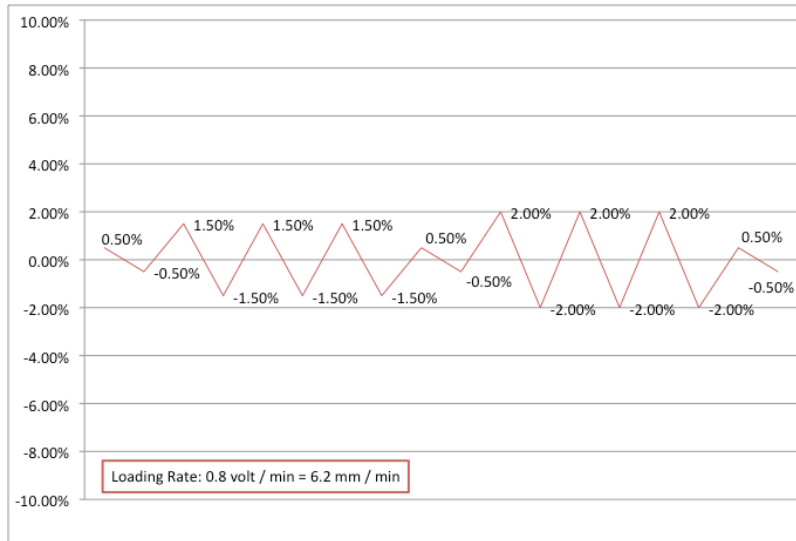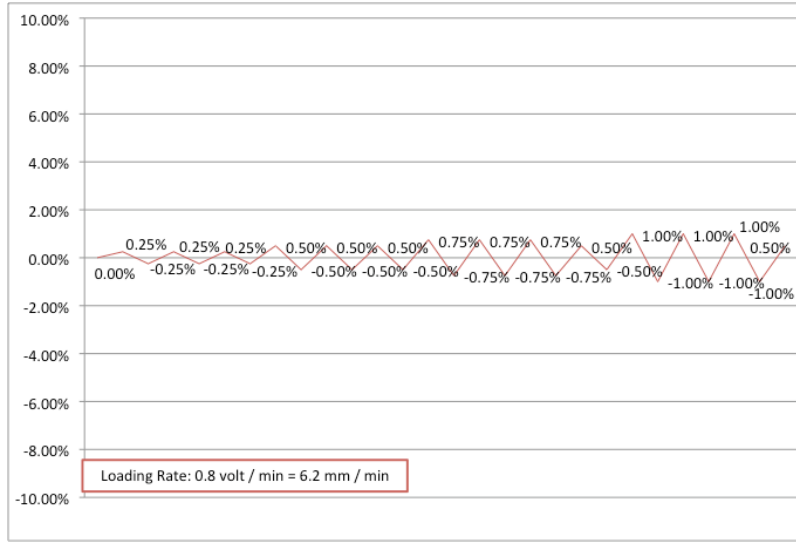
Figure 5.1 - Drift Ratio Displacement Path (SN5 and SN6)

5.2 Test Observations

5.2.1 Slab SN1

Slab SN1 failed in a sudden punching mode at a maximum load of 199kN. The load-displacement graph (Figure 5.2), and post-test cracking pattern, and strain measured on longitudinal reinforcement, all confirm this mode of failure. While under loading, the specimen experienced a sudden, and rapid drop of stiffness at the maximum load, which was accompanied by failure of the shear bolts in tension. Loud "popping" noises were heard, followed by complete stiffness loss, and punching failure of the slab specimen. All of the data collected from slab SN1 is presented in Appendix A.

Cracks were first noticed at a vertical load of about 100kN on the tension (bottom) side of the slab. The first cracks started from the corners of the column, and moved outward toward the supports. Further along in the test, cracks parallel to the column formed between the first and second rows of shear bolts forming the punching cone. Crushing cracks were observed around the column on the compression (top) side of the slab at failure. These cracks were inside the first row of shear bolts, between the connection of the slab to the column face.

Displacements were measured at several locations during the test. By measuring displacements at the top and bottom of the slab at some locations, internal crack widths could be estimated. Central column deflection was measured in two ways. The vertical load cell contained an internal LVDT, which measured the deflection at maximum vertical load as 23.6 mm. A displacement string pot was attached to the bottom column by drilling a small hole, and using a concrete anchor. This maximum displacement was measured to be 21.2 mm. Both of these values contain uncertain variables, such as support movement (compressing the neoprene pad), and flexing of the testing frame. Estimated crack width was plotted against the vertical load; these figures also indicate where the crack was measured on the slab surface. Crack width was estimated at four locations during the test, two in each direction. The crack width at location 1-1 could not be estimated due to failure of one of the LVDT's early on in the test. Near the end of the test, the deflection of the specimen exceeded the maximum stroke available on the external LVDT's placed to measure deflection. As such, crack width had only been estimated until a vertical load of 160kN, or 80% of maximum vertical load.

The estimated crack at location 2-2 was constrained to no more then 2.5mm during the test. Estimated crack width at location 3-3 was measured for only a short period of time, as rapid crack growth at this location overran the stroke on the LVDT's here, and the data becomes irrelevant. Data was collected until a vertical load of 118kN, or 60% of total load. Until this point the crack appears to be rapidly increasing, up to a value of 6.5mm. It is expected that the punching cone formed in and around this

location, and the crack width was very large at failure. At the location 4-4 the estimated crack width was about 0.5mm. It is expected that this location was outside of the punching cone, and no significant shear cracks formed at this location.

Data was collected from the strain gauges placed on the longitudinal reinforcement. First yielding of longitudinal reinforcement was observed at 110 kN (55% of maximum load) at L2, L3, L6, and L10. First yielding was followed by yielding at gauge locations L5 at 59% of ultimate load, and L1 at 62% of ultimate. At maximum load the remainder of the strain gauges indicated that the bars had yielded, at locations L4, L9, U5, U6, U7, and U8. The strain at ultimate load in each gauge is presented in Table 5.1 below. The location of each gauge with respect to the longitudinal reinforcement can be found in Figure 3.19.

Table 5.1 - Strain on Longitudinal Reinforcement at Max. Load (199kN) and First Yield (91kN), SN1

Gauge	Load	L1	L2	L3	L4	L5	L6	L8	L9	L10
Bar #		BU-8	BU-8	BU-8	BU-9	BU-9	BU-9	BL-8	BL-8	BL-8
$\mu\epsilon$	91kN	1233	1997	1553	1052	1273	1465	737	785	1549
$\mu\epsilon$	199kN	2230	10055	3200	1941	2023	3738	1840	2130	2450

Gauge	Load	U2	U5	U6	U7	U8
Bar #		TL-4	TL-5	TL-5	TL-5	TL-5
$\mu\epsilon$	91kN	-168	-227	-242	-77	-11.3
$\mu\epsilon$	199kN	-1140	3792	-336	340	268

Strain gauges were also placed on some of the shear bolts. One perpendicular row, in each direction was fitted with strain gauges, for a total of 8 bolts.   The lead wire connecting the strain gauge on Bolt #3 to the data acquisition system was damaged during the test setup, and therefore no information was collected. The gauges were located on the stem of the Fibrebolt, after the threads had been removed with a grinder. The data collected indicates how active the Fibrebolt was during loading, as it measures stretch of the Fibrebolt at mid-length. All bolts experienced strange behaviour at a vertical load of 54.5kN. At this point, the strain gauge data jumped from approximately 0 to about 6500$\mu\epsilon$. It appears the data acquisition system was not recording strain data until this point. As such, it is difficult to determine what the actual strains were in the shear bolts, but an effort has been made to correct the data, so that reasonable information could be collected. When the strains started to be recoded at a vertical load of 54.4kN, the strain appears to have been in error to a value of 6500$\mu\epsilon$. To correct this, the difference in strain just before and after this point was used to remove the erroneous data. All data for SN1 shear bolt strain presented in this thesis had been corrected to reflect this.

Table 5.2 - Strain in Shear Bolts at Maximum Load (199kN), SN1

	Bolt #1	Bolt #2	Bolt #4	Bolt #5	Bolt #6	Bolt #7	Bolt #8
με	2708	2112	182	2475	2657	1366	195
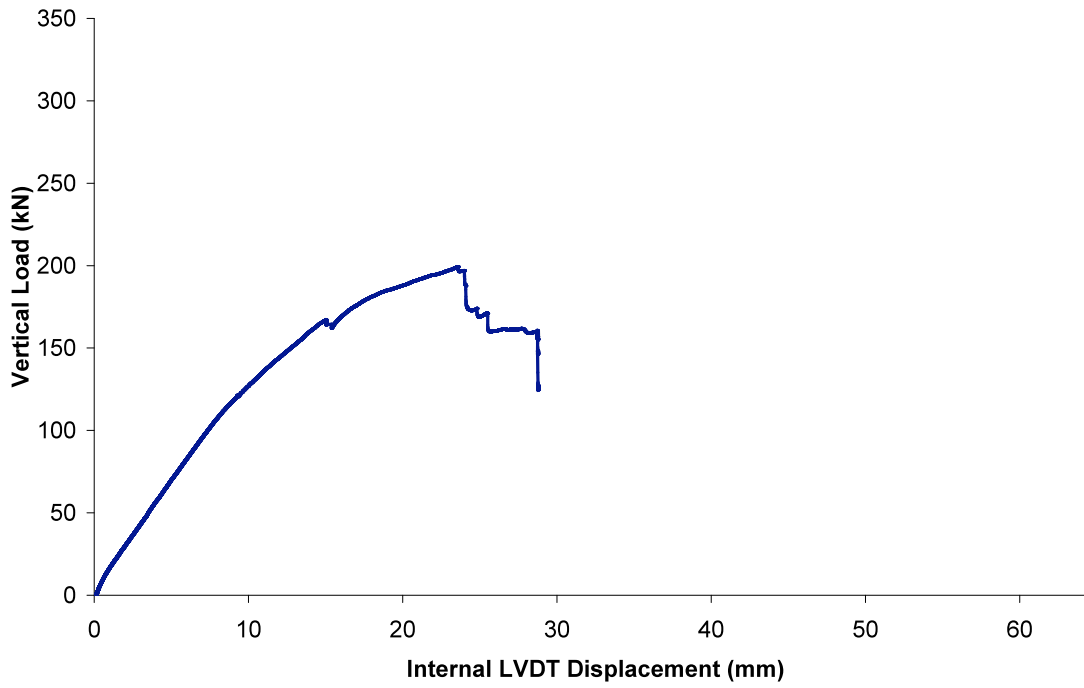
Figure 5.2 - Load vs. Internal LVDT Displacement, Slab SN1

64

5.2.2 Slab SN2

Slab SN2 failed in punching shear at a maximum load of 280kN. The load-displacement graph, and post-test cracking pattern, and strain, measured on longitudinal reinforcement, all confirm this mode of failure. After reaching a peak load, the specimen experienced several small increases in strength and stiffness, as can be seen on Figure 5.3. The test was stopped after no more increases in post-peak load were observed. All of the data collected from slab SN2 is contained in Appendix B.

Cracks were first noticed at a vertical load of approximately 60kN on the tension (bottom) side of the slab. The first cracks started from the corners of the column, and moved outward toward the supports. These radial cracks, were joined by more cracks of the same nature for the rest of the test. Crushing was observed around the column on the compression (top) side of the slab at failure. This crushing was between the first and second row of shear bolts. More cracks were concentrated on one side of the column, this may be evidence that the vertical load was slightly offset, and not exactly perpendicular to the face of the slab. As such, the punching cone may have been slightly rotated.

Displacements were measured at several locations during the test. By measuring displacements at the top and bottom of the slab at some locations, internal crack widths could be estimated. Central column deflections were measured in two ways. The vertical load cell contained an internal LVDT, which measured the maximum vertical deflection as 35.9mm. A displacement string pot was attached to the bottom column by drilling a small hole, and using a concrete anchor. This displacement was measured to be 32.2 mm. Estimated crack width was plotted against the vertical load. Crack width was estimated at four locations during the test, two in each parallel direction. Near the end of the test, the deflection of the specimen exceeded the maximum stroke available on the external LVDT's placed to measure deflection. As such, crack width had only been estimated until a vertical load of 256kN, or about 91% of maximum load.

Crack width was estimated to be approximately 12.1mm at location 1-1. Maximum crack width at location 2-2 was estimated to be 3.2mm. Significantly larger crack widths were estimated at locations 3-3 and 4-4. Since the punching cone was slightly rotated, it is expected that the punching cone intercepted these two locations more then the first two locations. The crack width was estimated to be 27.3mm and 25.4mm at 3-3 and 4-4 respectively.

Data was collected from the strain gauges placed on the longitudinal reinforcement. First yielding of longitudinal reinforcement was observed at 70.5kN (25% of maximum load) at L2. First yielding was followed by yielding at gauge locations U1 and U2 at 27% of maximum load, L3 (at 31%), L6 (at 34%), L1 (at 47%), L4 (at 54%). At approximately 77% of maximum load strain gauges indicated that the bars

had yielded, at locations U3, U4, U5, U6, U7, U8. Gauge location L5 did not indicate that yielding had occurred. Gauge location L7 did not give any readings as it was damaged during the construction process. The strain at ultimate load in each gauge is presented in Table 5.3 below. Some gauges had failed at the point of maximum load, and did not provide a reasonable value for strain, they have been omitted below, but the strain versus load plots in the appendix show the full load history. The location of each gauge with respect to the longitudinal reinforcement can be found in Figure 3.19.

Table 5.3 - Strain on Longitudinal Reinforcement at Max. Load (280kN) and First Yield (71kN), SN2

Gauge	Load	L1	L2	L3	L4	L5	L6
Bar #		BU-8	BU-8	BU-8	BU-9	BU-9	BU-9
$\mu\varepsilon$	71kN	1238	2035	1612	849	75	1375
$\mu\varepsilon$	280kN	3070	6600	n/a	3005	1172	8000

Gauge	Load	U1	U2	U8
Bar #		TL-3	TL-4	TL-5
$\mu\varepsilon$	71kN	1856	1900	222
$\mu\varepsilon$	280kN	8000	14000	4549

Strain gauges were placed on some of the shear bolts. One perpendicular row, in each direction was fitted with strain gauges, for a total of 8 bolts. Figure B15 through Figure B22 contain the data collected, as well as indicate the locations for each bolt. Below, in Table 5.4 the strain data collected at the maximum load are summarized. The gauges were located on the stem of the GFRP rod, after the protective coating had been removed with sandpaper. The data collected indicates how active the rod was during loading, as it measures stretch of the rod at mid-length. An obvious trend can be seen, as the bolt location increases further from the face of the column, the amount of peak strain decreases. Bolt #1 and #5 were located in the first row next to the column, and consequently had high strain at maximum load. This confirms the assumed mechanical behaviour of the formation of the punching cone.

Table 5.4 - Strain in Shear Bolts at Maximum Load (280kN), SN2

	Bolt #1	Bolt #2	Bolt #3	Bolt #4	Bolt #5	Bolt #6	Bolt #7	Bolt #8
$\mu\varepsilon$	2227	3031	789	77	5782	3795	194	106
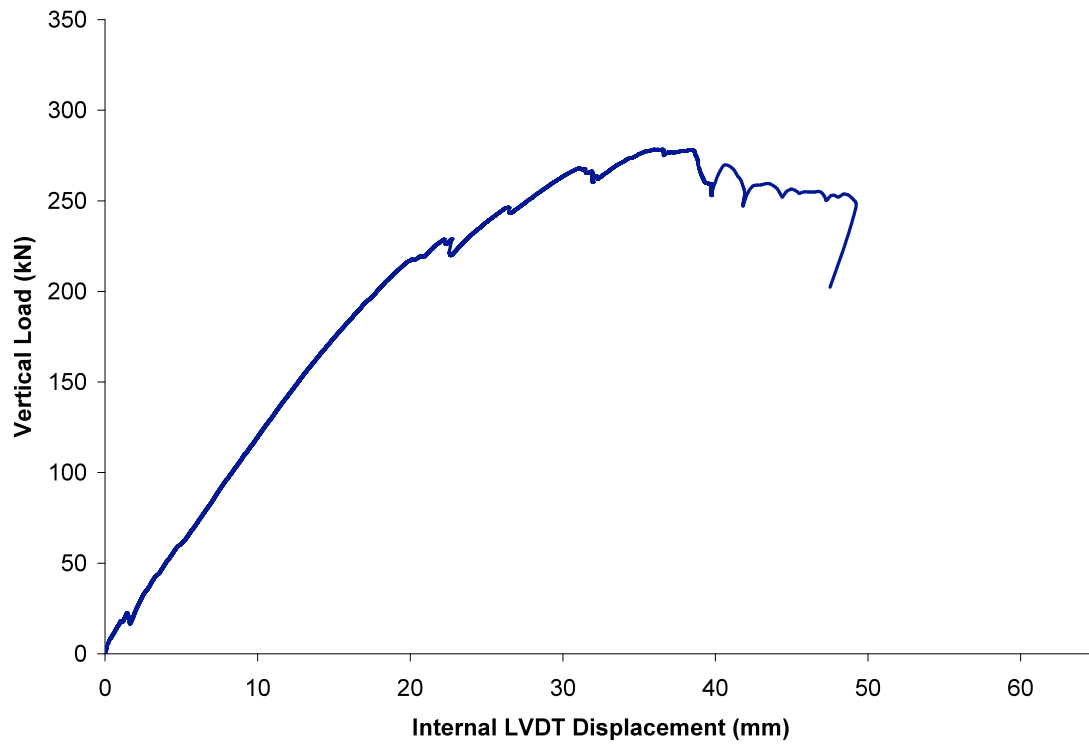
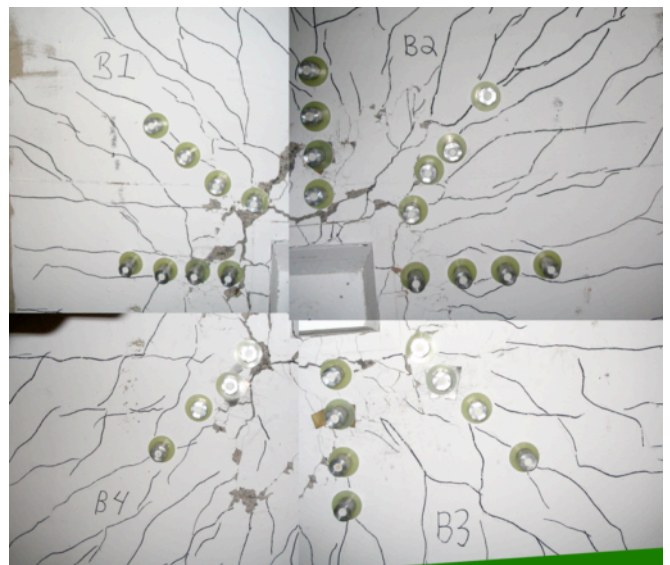Figure 5.3 - Load vs. Internal LVDT Displacement, Slab SN2
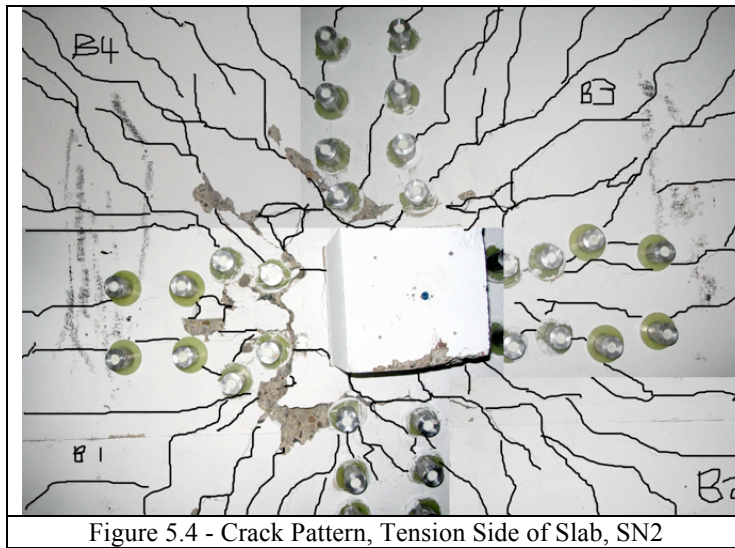
Figure 5.4 - Crack Pattern, Tension Side of Slab, SN2

5.2.3 Slab SN3

Slab SN3 failed in flexural / punching shear at a maximum load of 310kN. The load-displacement graph, and post-test cracking pattern, and strain measured on longitudinal reinforcement, all confirm this mode of failure. After reaching a peak load, the specimen experienced several small increases in strength and stiffness, as can be seen on Figure 5.5. Unlike the two previous static tests, no significant reduction of strength could be achieved during the test. In this manner, this connection behaved very ductile, and the test had to be stopped as the deformation had reached the limit of the testing apparatus. All of the data collected from slab SN3 is contained in Appendix C.

Cracks were first observed at a vertical load of approximately 70kN on the tension (bottom) side of the slab. The first cracks started from the corners of the column, and moved outward toward the supports. These radial cracks, were joined by more cracks of the same nature for the bulk of the test. Crushing cracks were observed around the column on the compression (top) side of the slab at failure. These cracks were between the second and third row of shear bolts, or about 170mm from the face of the column. On the compression side of the slab at approximately 570mm from the face of the column a radial cracking pattern can be seen. This may be evidence that a punching cone was forming at the extreme edges of the testing area.

Displacements were measured at several locations during the test. By measuring displacements at the top and bottom of the slab at some locations, internal crack widths could be estimated. Central column deflections were measured in two ways. The vertical load cell contained an internal LVDT, which measured the maximum vertical deflection as 42.6mm. A displacement string pot was attached to the bottom column by drilling a small hole, and using a concrete anchor. This displacement was measured to be 38.5mm. Both of these values contain uncertain variables, such as support settlement, and flexing of the testing frame. Estimated crack width was plotted against the vertical load. Crack width was estimated at four locations during the test, two in each parallel direction. Failure of a LVDT caused no data to be collected at location 3-3.

Crack width was estimated to be approximately 13mm at location 1-1. Maximum crack width at location 2-2 was also estimated to be 11mm. Maximum crack width at location 4-4 was also estimated to be about 14mm. Some error had to be taken out of the crack width data, as it appeared the bottom LVDT frame was shifted during testing. Large, sudden, reductions in crack width were recorded at three points during the test. It was assumed this was due to setup error, and these reductions were removed manually after the test. The data presented in Appendix C is the corrected data.

First yielding of longitudinal reinforcement was observed at 230kN (74% of maximum load) at L6 and L7. First yielding was followed by yielding at gauge locations L1 and L3 at 79% of maximum load. At approximately 93% of maximum load strain gauges indicated that the remaining bars had yielded, at locations L4, L5, U2, U7, and U8. Gauge location U3 did not indicate that yielding had occurred. Gauge locations U1, U4, U5, U6, U7, L2, did not give any readings as it was damaged during the construction process. The strain at ultimate load in each gauge is presented in Table 5.3 below. Some gauges had failed at the point of maximum load, and did not provide a reasonable value for strain, they have been omitted below, but the strain versus load plots in the appendix show the full load history.   The location of each gauge with respect to the longitudinal reinforcement can be found in Figure 3.19.

Table 5.5 - Strain on Longitudinal Reinforcement at Max. Load (310kN) and First Yield (122kN), SN3

Gauge	Load	L1	L3	L4	L5	L6	L7	U2	U3	U7	U8
Bar #		BU-8	BU-8	BU-9	BU-9	BU-9	BU-9	TL-4	TL-4	TL-5	TL-5
$\mu\varepsilon$	122kN	1388	2009	1181	1399	2016	2083	26	-162	-58	-87
$\mu\varepsilon$	310kN	--	--	-3330	6398	-4141	--	1275	1275	133	1689

Strain gauges were placed on some of the shear bolts. One perpendicular row, in each direction was fitted with strain gauges, for a total of 8 bolts. Table 5.4 outlines the strain data collected at the maximum load are summarized. The gauges were located on the stem of the GFRP rod, after the protective coating had been removed with sandpaper. The data collected indicates how active the rod was during loading, as it measures stretch of the rod at mid-length. An obvious trend can be seen, as the bolt location increases in distance from the face of the column, the amount of peak strain decreases. Bolt #1 and #5 were located in the first row next to the column, and consequently had high strain at maximum load. This confirms the assumed mechanical behaviour of the formation of the punching cone.

Table 5.6 - Strain in Shear Bolts at Maximum Load (310kN), SN3

|	Bolt #1	Bolt #2	Bolt #3	Bolt #4	Bolt #5	Bolt #6	Bolt #7	Bolt #8
$\mu\varepsilon$	2227	3031	789	77	5782	3795	194	106
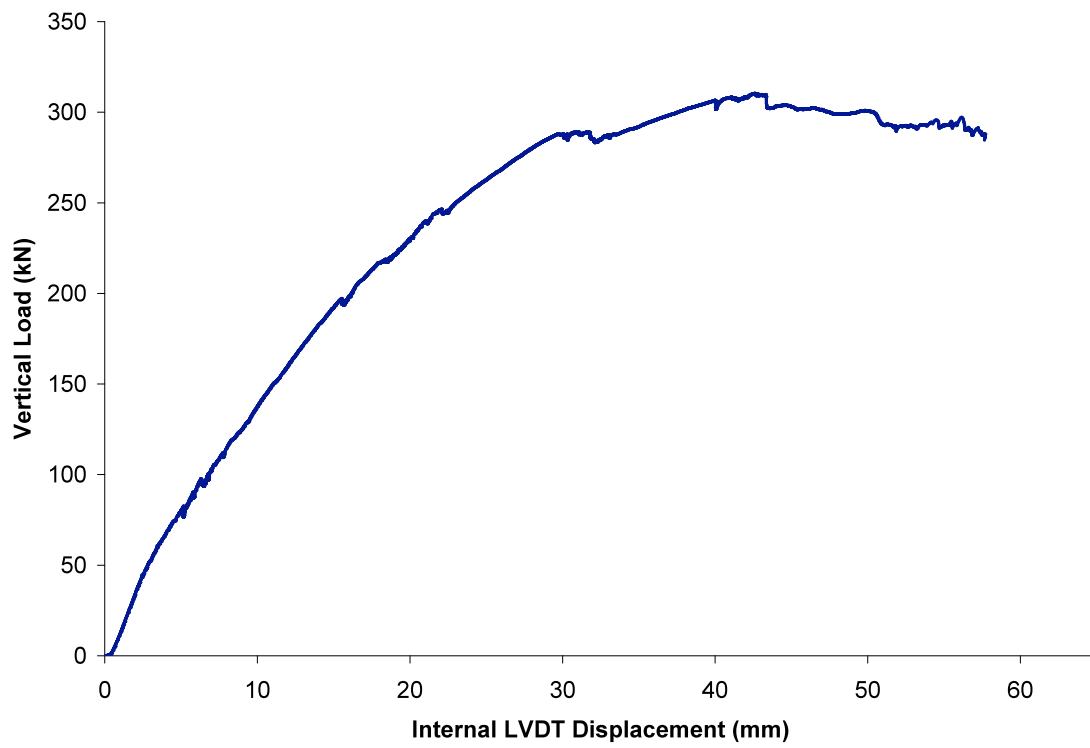
Figure 5.5 - Load vs. Internal LVDT Displacement, Slab SN3
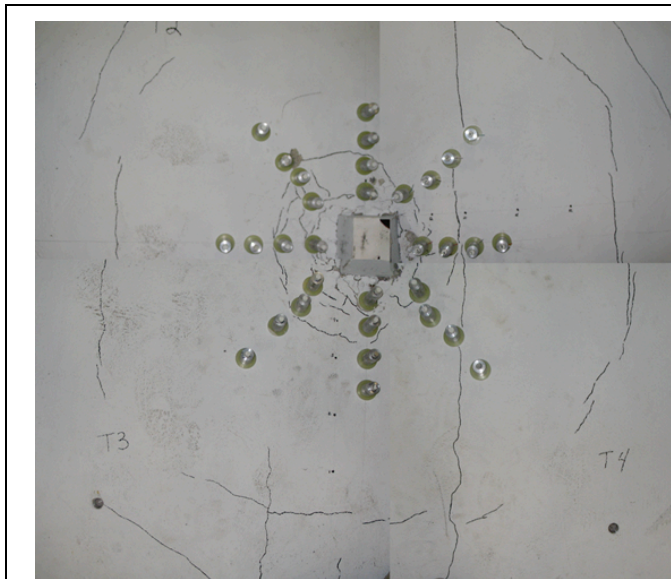
| Figure 5.6 - Crack Pattern, Compression Side of Slab, SN3 | Figure 5.7 - Crack Pattern, Tension Side of Slab, SN3 |

5.2.4 Slab SN4

Slab SN4 failed in flexural / punching shear at a maximum load of 332 kN. The load-displacement graph, and post-test cracking pattern, and strain measured on longitudinal reinforcement, all confirm this mode of failure. After reaching a peak load, the strength that the specimen could resist reduced, but maintained at a constant load until no more additional load could be added, as can be seen on Figure 5.8. At the end of the test the specimen was at the limit of the testing apparatus. All of the data collected from slab SN4 is contained in Appendix D.

Cracks were first noticed at a vertical load of approximately 80kN on the tension (bottom) side of the slab. The initial cracks started from the corners of the column, and moved outward toward the supports. These radial cracks, were joined by more cracks of the same nature for the bulk of the test. Crushing cracks were observed around the column on the compression (top) side of the slab at failure. These cracks were between the second and third row of shear bolts, or about 170mm from the face of the column. On the compression side of the slab at approximately 570mm from the face of the column a radial cracking pattern can be seen. This may be evidence that a punching cone was forming at the extreme edges of the testing area, before the connection punched in the perimeter of the shear bolts.

Displacements were measured at several locations during the test. By measuring displacements at the top and bottom of the slab at several locations, internal crack widths could be estimated. Central column deflections were measured in two ways. The vertical load cell contained an internal LVDT, which measured the maximum vertical deflection as 36.3mm. A displacement string pot was attached to the bottom column by drilling a small hole, and using a concrete anchor. This displacement was measured to be 31.5mm. Both of these values contain uncertain variables, such as support settlement, and flexing of the testing frame. Estimated crack width was plotted against the vertical load. Crack width was estimated at two locations during the test, two in each parallel direction.

The maximum crack width was estimated to be approximately 35mm at location 1-1, with the maximum estimated crack width to be 25mm at location 2-2. At location 1-1 the crack growth appears to have continued without much impact from the presence of shear bolts. This is an indication that the punching shear cone formed near this location. This is confirmed by the presence of a punching failure in and around the column. At location 2-2 the crack appears to have be restrained by the shear bolts, before rapid growth around a vertical load of about 280kN.

First yielding of longitudinal reinforcement was observed at 98kN (29% of maximum load) at L3 and L7. First yielding was followed closely by yielding at gauge locations L2 and L6 at 33% of maximum load (110kN). Gauge locations U8 and U6 did not indicate that yielding had occurred. Gauge locations U2,

U3, U4 did not provide any readings as they were damaged during the construction process. The strain at ultimate load in each gauge is presented in Table 5.7 below. Some gauges had failed at the point of maximum load, and did not provide a reasonable value for strain, they have been omitted below, but the strain versus load plots in the appendix show the full load history. The location of each gauge with respect to the longitudinal reinforcement can be found in Figure 3.19.

Table 5.7 - Strain on Longitudinal Reinforcement at Max. Load (332kN) and First Yield (96kN), SN4

Gauge	Load	L1	L2	L3	L4	L5	L6	L7	U5	U6	U7	U8
Bar #		BU-8	BU-8	BU-8	BU-9	BU-9	BU-9	BU-9	TL-5	TL-5	TL-5	TL-5
$\mu\varepsilon$	96kN	376	1458	1897	304	487	1606	1976	38	58	-27	-16
$\mu\varepsilon$	332kN	20390	10912	23644	2893	4763	8078	9058	-1969	-997	4202	1610

Strain gauges were placed on several of the shear bolts. One perpendicular row, in each direction was fitted with strain gauges, for a total of 8 bolts. Table 5.8 summarizes the strain data collected at the maximum load. The gauges were located on the stem of the GFRP rod, after the protective coating and unique Schöck ribbing had been removed with sandpaper. The data collected indicates how active the rod was during loading, as it measures stretch of the rod at mid-length. An obvious trend can be seen, as the bolt location gets further from the face of the column, the amount of peak strain decreases. The gauge on Bolt #1 appears to have been in error during the peak loading of the test, as the data collected does not make any sense. Bolt #1 and #5 were located in the first row next to the column, and consequently had higher strains at loading of the specimen.

Table 5.8 - Strain in Shear Bolts at Maximum Load (332 kN), SN4

	Bolt #1	Bolt #2	Bolt #3	Bolt #4	Bolt #5	Bolt #6	Bolt #7	Bolt #8
$\mu\varepsilon$	330	1792	188	9	1660	217	997	92
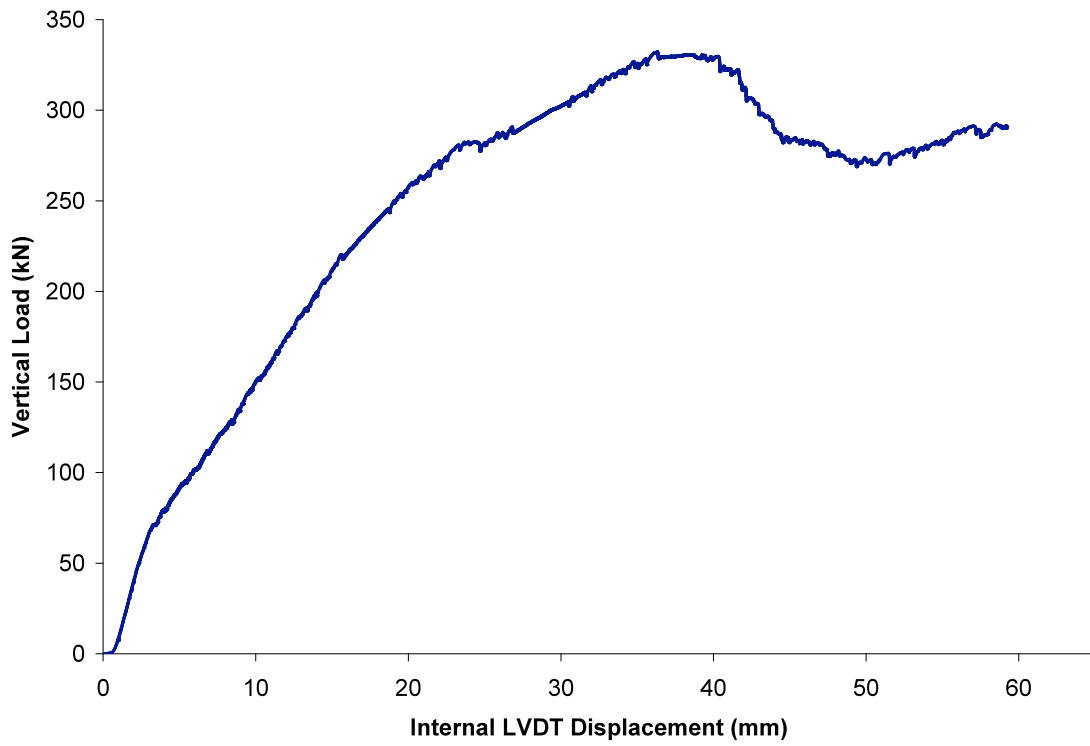
Figure 5.8 – Load vs. Internal LVDT Displacement, SN4
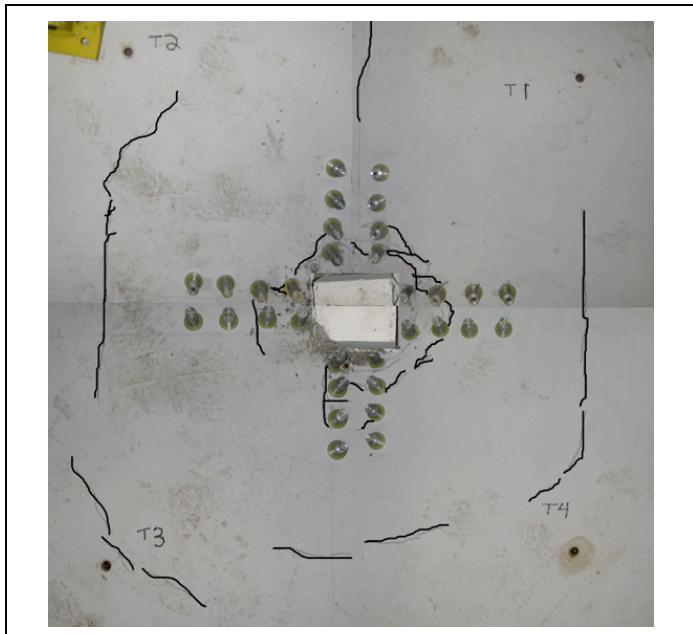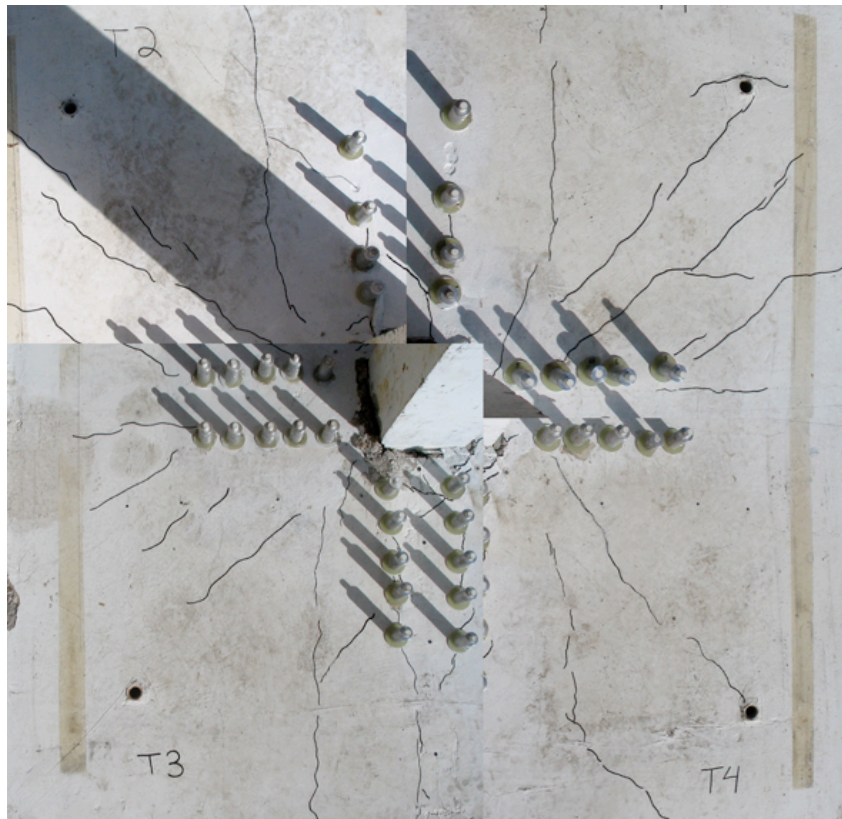
Figure 5.9 - Crack Pattern, Compression Side of Slab, SN4	Figure 5.10 - Crack Pattern, Tension Side of Slab, SN4
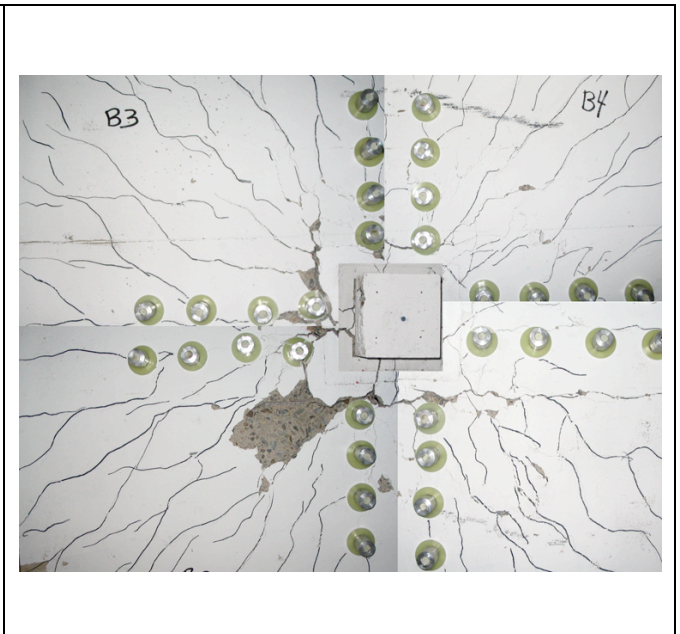
5.2.5 Slab SN5

Slab SN5 was reinforced with five rows of K-Line style GFRP shear bolts. The number of bolts were reduced, as the crimping technique did not allow the first row of the bolts to be installed. The specimen was tested according to the displacement path as previously discussed. Slab SN5 failed in punching at an approximate drift of 3.5%. Crack patterns observed during the test, and after, on the bottom of the slab confirm this mode of failure.

At approximately 1.5% drift, cracking was noticed on the bottom of the slab, in the area of the column. These cracks propagated outward, and formed a punching shear cone in between the first and second rows of shear bolts. At approximately 2.5% drift, the hydraulic system in the structures lab experienced a sudden loss of power. In the effort to restart the system, and reload the slab, the slab was over loaded in the horizontal direction by 4% drift, after this point, the stiffness of the section was reduced. The experimental data must be analyzed considering this event.

Displacement transducers were used for measuring deflections and estimating crack width, of the included shear cracks. Figure 3.16 shows the arrangement for this specimen. As well, displacement string pots were attached to the slab columns and base, to measure the sideways movement of the slab during testing. The actuators all included internal LVDTs, and this data was recorded along with the other displacement transducers. All data recorded for specimen SN5 has been included in Appendix E. As indicated in Figure 3.16, some displacements were measured in pairs. The difference in these displacements enabled the monitoring of the growth of the shear crack. There were four locations where the crack width was estimated. At location 1-1 the LVDT appears to have been damaged, and no usable data was recorded for the majority of the test. Location 4-4 was perpendicular to the line of applied moment, and at this location the estimated crack width was about 4mm. The two other locations, in the direction of the applied moment had higher estimated crack widths, as theses were under direct influence from the applied moment. Location 2-2 had a maximum crack width of about 8mm; Location 3-3 had a maximum of about 6mm. A larger crack opening at location 2-2, versus Location 3-3 is indication that the punching cone formed closer to the column then Location 3-3. This confirms the observed punching cone formation between the first and second row of shear bolts.

Strain measurements on longitudinal reinforcement were recorded at different locations, as shown in Figure 3.20. During the casting process, some of the strain gauges were damaged and did not collect any data, gage numbers 3b, 4a, 5a, and 5b did not collect any useful data. Due to accidentally overloading the specimen, the strain gauge data is presented in two shades on the plots. The lighter plot lines being before the hydraulic failure, and the darker lines indicating the strain after the failure. Some of the reinforcement bars yielded as a result of this failure. The plots for reinforcement strain versus horizontal load are

contained in Appendix E. The strains at the point of maximum horizontal load are reported below, locations can be found in Figure 3.20.

Strains were also recorded from a select amount of shear bolts. Five bolts in the same perpendicular row, in each direction were gauged. Bolts #1 through #5 were in the direction of the applied load, #6 through #10 were in the other direction. The plots for shear bolt strain versus horizontal load are contained in Appendix E. The same convention applies as above, with respect to the line types before and after the hydraulic failure. Maximum strains are also summarized below.

Table 5.9 - Strain of Reinforcement Bars, at Max. Horizontal Load (53kN) and First Yield (27kN), SN5

	Load	1,2a	1,2b	1,2c	1,2d	3a	4b	1,2a(col)	1,2b(col)	1,2c(col)	1,2d(col)
με	53kN	8511	9737	7712	9028	7761	7137	9270	11649	4729	2481
με	27kN	-391	-534	996	-570	6.7	61	-636	-1213	-986	1224

Table 5.10 - Strain on Shear Bolts at Maximum Horizontal Load (Tension and Compression), SN5

Load	Bolt #1	Bolt #2	Bolt #3	Bolt#4	Bolt #5	Bolt#6	Bolt#7	Bolt#8	Bolt#10
-43kN	522	75	49	14	1138	9	16	17	63
53kN	196	37	5	5	2470	796	919	15	2744

Figure 5.11 - Crack Pattern, Compression Side of Slab, SN5

Figure 5.12 - Crack Pattern, Tension Side of Slab, SN5

5.2.6 Slab SN6

Slab SN6 was reinforced with six rows of K-Line style GFRP shear bolts. The specimen contained two 150x150mm openings, on each side of the column in the direction of the moment. The specimen was tested according to the displacement path as previously discussed. Slab SN6 failed in punching at an approximate drift of 5.5%. At approximately 0.5% drift, cracking was noticed on the bottom of the slab, in the area of the column. These cracks propagated outward, and formed a punching shear cone in between the first and second rows of shear bolts.

Displacement transducers were used for measuring deflections and estimating crack width, at few locations. Figure 3.16 shows the arrangement of transducers. As well, displacement string pots were attached to the slab columns and base, to measure the sideways movement of the slab during testing. The actuators all included internal LVDTs, and this data was also recorded. All data recorded for specimen SN6 is included in Appendix F. As indicated on Figure 3.16, some displacements were measured in pairs. The difference in these displacements enabled the monitoring of the growth of the shear crack. Location 1-1 and 4-4 were in the direction perpendicular to the applied moment. Location 1-1 had a maximum estimated crack of approximately 1.5mm, from this it can be assumed that the punching cone formed outside of this point on the slab. Further away from the column is Location 4-4, perpendicular to

the applied moment. The maximum crack width at this point was found to be nearly 18mm. This point indicates that the punching cone was forming at this location. The crack appears to be restrained, until at approximately 3.5% drift, where the crack opening quickly. Locations 2-2 and 3-3 were in the direction of the applied moment. Location 2-2 had a crack width of 5mm, while Location 3-3 had an estimated maximum crack width of about 3mm.

Strain measurements on longitudinal reinforcement were recorded at different locations, as shown in Figure 3.20. During the casting process, some of the strain gauges were damaged and did not collect any data, gauge numbers 10a, 10b, 10c, and 13b did not collect any useful data. The plots for reinforcement strain versus horizontal load are contained in Appendix F.

Strains were also recorded from a select amount of shear bolts. Six bolts in the same perpendicular row, in each direction were gauged. Bolts #1 through #6 were in the direction of the applied load, #7 through #12 were in the other direction. The plots for shear bolt strain versus horizontal load are contained in Appendix F. Maximum strains are also summarized below.

Table 5.11 - Strain of Reinforcement Bars, at Max. Horiz. Load (-35.5 kN) and First Yield (23kN), SN6

	Load	6a	6b	6c	8a	8b	9b	12a	12b	12c
$\mu\varepsilon$	23kN	989	670	-1620	-1206	-617	73	-237	334	19
$\mu\varepsilon$	-35.5kN	856	-1593	-1305	-1329	614	-132	-472	508	-175

Table 5.12 - Strain on Shear Bolts at Maximum Horizontal Load (Tension and Compression), SN6

Load	Bolt #1	Bolt #3	Bolt#6	Bolt #7	Bolt#8	Bolt#10	Bolt#11
26.6kN	1192	-136	18	-924	-10	1483	127
-35.5kN	2945	3035	33	1379	0	2229	76

77

Figure 5.13 - Crack Pattern, Compression Side of Slab, SN6

Figure 5.14 - Crack Pattern, Tension Side of Slab, SN6

Chapter 6

Analysis of Experimental Results

6.1 Specimens Tested Under Static Loading

Slabs, SN1, SN2, SN3, and SN4 were all tested under static load, according to the procedure outlined in Section 5.1.1, and as discussed in the preceding chapter. This chapter summarizes and analyzes the relevant data collected in the experimental program. The data is analyzed based on the crack pattern, stiffness, ductility and strain. Crack patterns for each slab can be found in Chapter 5.

6.1.1 Maximum Observed Load and Predicted Punching Load

A summary table (Table 6.1) has been created to illustrate and compare the maximum observed loads during the testing program, and the predicted punching values expected by the design codes.

Table 6.1 - Summary of Predicted and Observed Maximum Vertical Load

Specimen	Shear Reinforcement	Maximum Observed Load (P_{TEST})	Percentage of Strengthening		Mode of Failure	Assumed Shear Bolt Strength
			$\dfrac{P_{TEST}}{P_{SB1}}$	$\dfrac{P_{TEST}}{P_{SN1}}$		
		(kN)				(kN)
SB1	none	253	100%	127%	Punching	N/A
SN1	Fibrebolts (Ortho. Pattern)	199.3	78.7%	100%	Punching	15
SN2	K-Line Type (Ortho. Pattern)	278.4	110%	140%	Punching	20
SN3	K-Line Type (Radial Pattern)	310.4	123%	156%	Flexural / Punching	20
SN4	Schöck Type (Ortho. Pattern)	332.4	131%	167%	Flexural / Punching	20
SB4	Steel Type (Ortho. Pattern)	360	142%	181%	Flexural	27

The previously tested specimen by Adetifa (2003) SB1 is used as a control specimen for the current studies. SB1 was identical to current specimens, however the boundary conditions were slightly different, namely the neoprene pads used for SB1 were 3mm thick, as opposed to 25mm used in the current study. Two comparisons have been done to determine how much strength the shear bolts added to the connection. Since the support conditions between the test performed on SB1 and the current round of testing had been changed, caution was taken before directly comparing results. The load/displacement curve for SB1 is also plotted in Figure 6.2, and shows a decrease in stiffness of the current tests, as compared to SB1. Thicker neoprene pads are contributing to the decrease in specimen stiffness. The P_{TEST}/P_{SB1} shows how the slabs reinforced with GFRP shear bolts compare to the maximum vertical load

found for a similar slab with no shear reinforcement. The last test, SN4, reinforced with 4 peripheral rows of Schöck Type GFRP shear bolts had an increase in strength of 131%. SN1 actually had a decrease in strength, as it was only able to achieve at strength of 79% that of SB1. The Fibrebolts used to reinforce SN1 did not appear to activate upon loading. The presence of reinforcing elements can therefore be disregarded when it comes to SN1; SN1 behaved as if no shear bolts were present at all. The drilling of 32-16mm holes around the slab-column connection most likely weakened the specimen further. SN1 can be considered a control slab for the current round of testing.   By using SN1 as a control, the three remaining specimens experienced a strength increase of between 140% and 167%.

The final comparison is done with the strength achieved by 4 peripheral rows of steel shear bolts, as tested by Adetifa (2003). The results from Adetifa for specimen SB4 are compared to both SB1 and SN1. SB4 was strengthened to 142% of SB1, and 181% of SN1. SB4 was tested on thinner neoprene pads; thus it shows also stiffer behaviour. Comparing results from similar testing frames, SB1 to SB4 (increase of 142%) and SN1 to SN4 (increase of 167%) the GFRP shear bolts performed equally as steel bolts while in strengthening the connection. It is hoped that as the crimping process gets more refined, and GFRP shear bolt manufacturing more consistent, the GFRP system will be able to match the strength increases found with the steel shear bolt retrofit technique.

6.1.2 Stiffness and Ductility

Ductility in a slab-column connection can be defined as the ratio of the ultimate deflection, to the deflection at first yielding of the flexural reinforcement (Marzouk and Hussein, 1991). Stiffness is the slope of the load / displacement curve during testing up to 20% of the maximum load. The following table, Table 6.2, lists the ductility of the various specimens tested, as well as the control specimen SB1 from previous research. The table also includes a calculation to show how much increase in ductility was achieved by reinforcing the connection with shear bolts. Two results are presented, one comparing the test results to the ductility found by Adetifa (2003), the other comparing the test results to SN1.

Table 6.2 - Calculated Ductility

	Calculated Stiffness (kN/mm)	Ultimate Vertical Displacement (mm)	Yield Displacement (mm)	Calculated Ductility (mm/mm)	Test Ductility SB1 Ductility (%)	Test Ductility SN1 Ductility (%)
SB1	19.1	10.4	7.7	1.4	100%	50%
SN1	11.4	23.6	8.2	2.9	213%	100%
SN2	12.6	35.9	6.3	5.7	422%	198%
SN3	17.2	42.6	8.5	5.0	371%	174%
SN4	22.1	36.3	5.6	6.5	480%	225%

The inclusion of shear reinforcement increased the connection ductility. It also stiffened the connection. Since SN1 contained shear bolts, it did experience a slight increase in ductility over SB1 a maximum increase of ductility when compared to SN1, was 225. When making comparison to SB1, a maximum increase of 480% was found. Adetifa (2003) found a maximum ductility increase of 280% between the slab reinforced with 4 rows of steel shear bolts (SB4) and the control slab, SB1. Thus, the GFRP shear bolts increased connection ductility more than the steel shear bolts. The small movement due to the aluminum fittings being not tight may have allowed small cracks to form, allowing more yielding of the reinforcement, and more ductility in the connection.

6.1.3 Deflections

As shown in Table 6.2, the ultimate deflections were significantly increased with the inclusion of shear bolts. Within the current testing program, the lowest ultimate deflection was that of SN1. Since the control SB1 had slightly different support conditions, a better comparison for deflection can be made amongst the current testing program. Larger deflections were observed in the three slabs reinforced, SN2, SN3, SN4, then in SN1 indicating how effective the 'K-Line or Schöck type bolts were. Two figures follow; Figure 6.1 shows the vertical load versus the deflection data collected by the internal LVDT on the load cell. Figure 6.2 plots the vertical load versus the deflection data gathered by an external string pot placed on the bottom of the column during testing. The differences in these two recorded deflections can be caused by the flexing of the testing frame, and settlement of the support. The differences in ultimate deflection in all four tests was approximately 2-3mm.
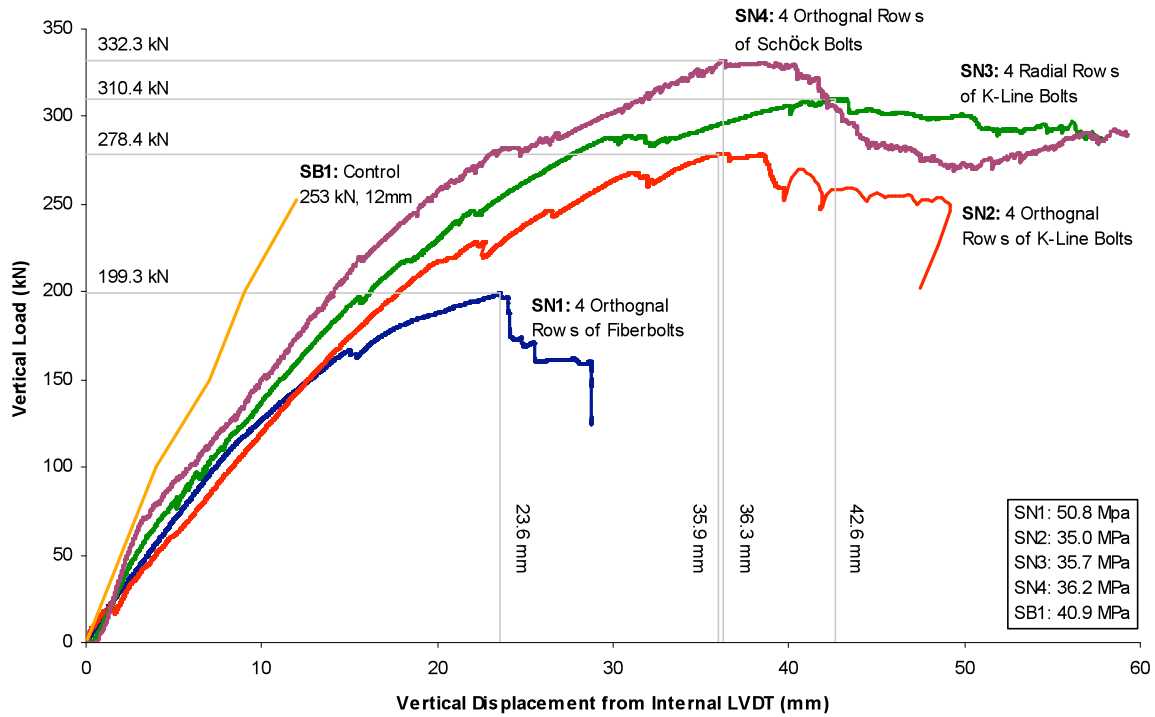
Figure 6.1 - Summary of Vertical Load vs. Internal LVDT Displacement
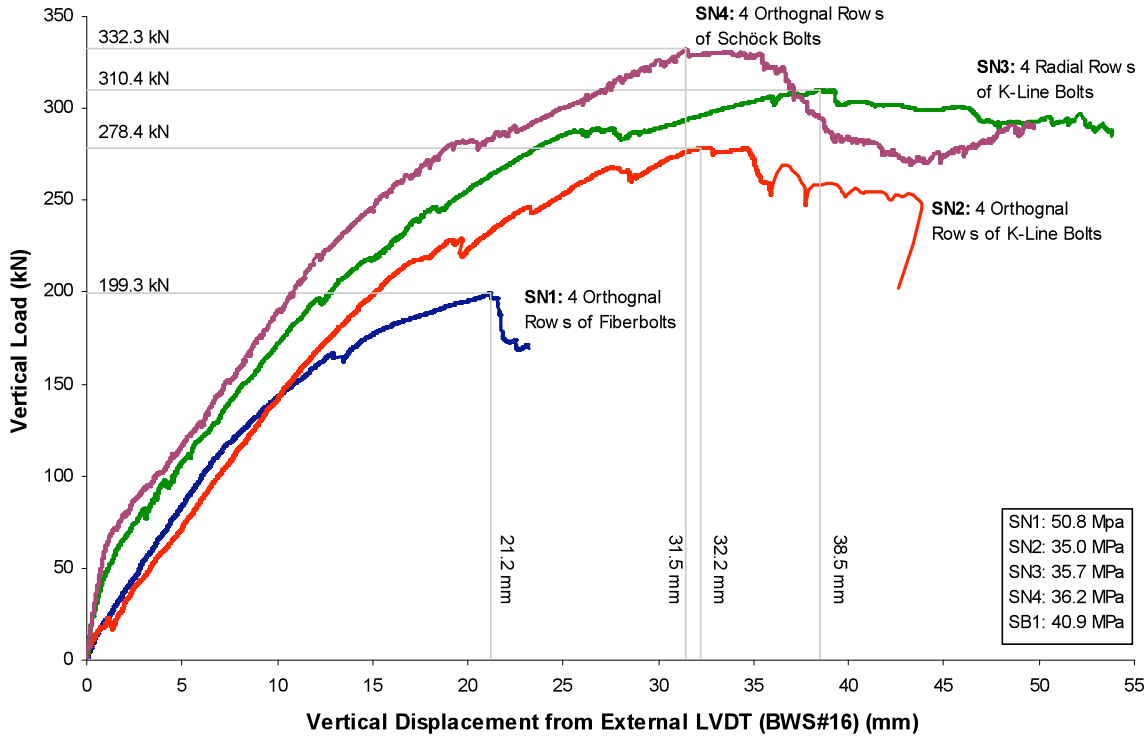
Figure 6.2 - Summary of Vertical Load vs. External LVDT Displacement

6.1.4 Strains in Longitudinal Reinforcement

Strain data was recorded on the internal longitudinal reinforcement. Table 6.3 lists the location and value at which first yield occurred, with respect to the layouts given in Figure 3.19. Also, the locations where yielding occurred at ultimate load are also given.

Table 6.3 - Yielding of Flexural Reinforcement

	Maximum Load (kN)	Load at 1st Yield (kN)	Location at 1st Yield	Locations Yielding at Maximum Load
SB1	253	204	L7	U6, U7
SN1	199	91	L2	L1, L2, L3, L5, L6, L7, L9, L10, U5, U6, U7
SN2	278	70.5	L2	L1, L2, L3, L4, L6, U1, U2, U3, U4, U5, U6, U7, U8
SN3	310	122	L3, L6, L7	L1, L3, L4, L5, L6, L7, U2, U8
SN4	332	96.2	L3, L7	L1, L2, L3, L4, L5, L6, L7, U5, U7

Comparison are done between the strains recorded at location L4 and L6 in the tested specimens. Strain gauge L4 and L6 were located on the steel bar that passes directly through the column. L4 was at some distance down the bar, while L6 was located directly beside the column reinforcement (Figure 3.19). Two figures follow, summarizing the strain on L4 and L6 for all four slabs, with respect to the vertical load (Figure 6.3 and Figure 6.4).
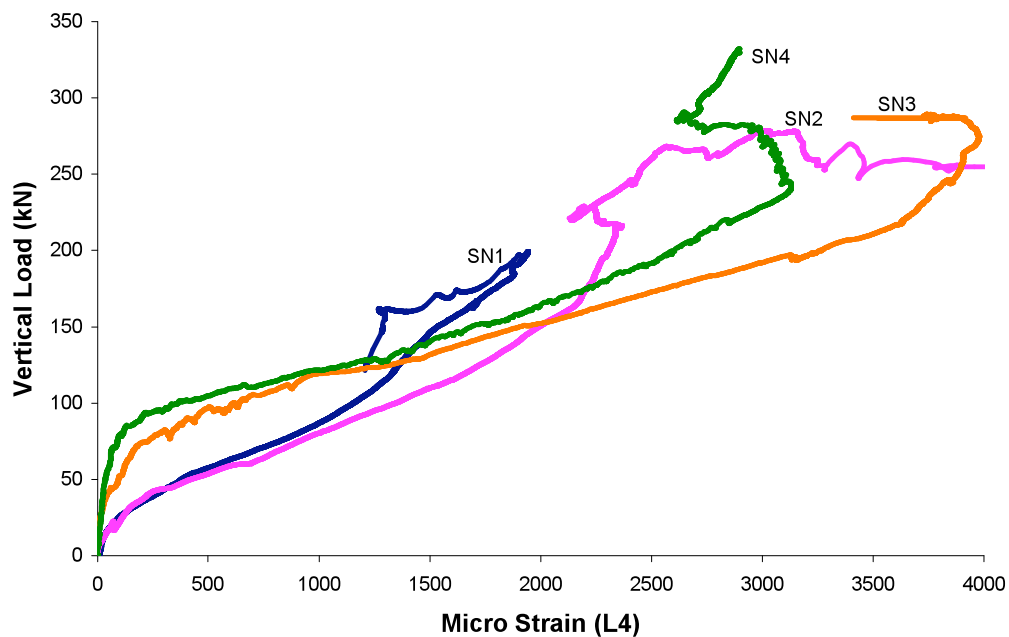
Figure 6.3 - Vertical Load vs. Micro Strain at Gauge L4

83
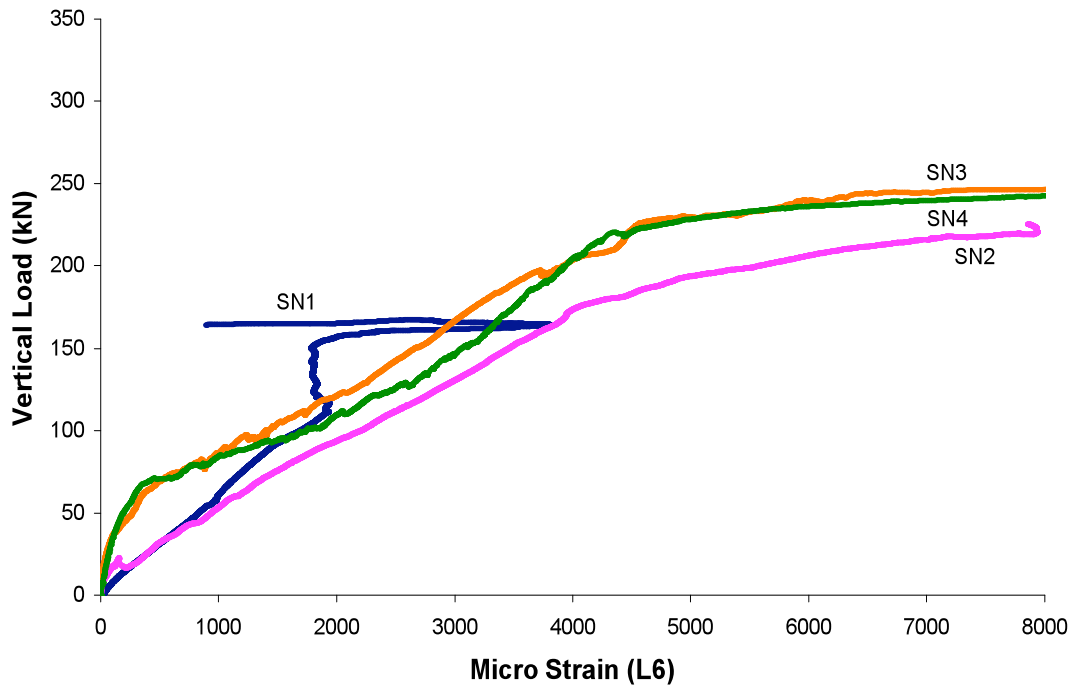
Figure 6.4 - Vertical Load vs. Micro Strain at Gauge L6

Figure 6.3 shows the results at gauge location L4. SN1 did not yield at this location. Since L4 is placed at a distance from the column, this may indicate that the shear bolts did not strengthen the connection enough to transfer shear stresses to the longitudinal reinforcement. The yield strain of the longitudinal reinforcement was found to be about 2000με. At this point, both SN2 and SN3 appear to yield at the same load, approximately 153kN. SN4 reaches this yield point at a slightly higher (but relatively similar) load of 167kN. This is a very interesting result, as it shows that regardless of the shear reinforcement placed within the slab, the longitudinal reinforcement was behaving in a similar manner. Furthermore, this indicates that both the K-Line and Schöck bolt systems, in both radial and orthogonal layout patterns were equally effective. The curves created by the strain / load behavior can also be compared. Early on in the loading of the specimens, SN1 and SN2 behave similarly, with SN2 eventually yielding, behaving plastically. Also, in the early stages of loading, SN3 and SN4 behaved in a similar manner. The linear portions of the curves for SN3 and SN4 are stiffer then SN1 & SN2. The crimping technique was applied with more effectiveness in tests for SN3 and SN4, as these occurred later in the testing program.

Figure 6.4 compares the results at gauge location L6. The yielding of the reinforcement was found to occur at about 2000με. Some unexpected behavior can be seen in SN1, again leading to the conclusion that the shear bolts in SN1 were not effective as punching shear reinforcement elements. When the

specimen punched at approximately 200kN, the strain gauge could have been damaged, and thus resulting in data erroneous. The behavior of SN1 and SN2 are similar in the early stages of the loading. The results from SN3 and SN4 are similar for most of the loading path. This is a good indication of how effective the shear bolts were in their task of strengthening against punching.   In the cases of SN2, SN3, and SN4 yielding occurred within a relatively narrow range of the loading (96kN – 121kN).

6.1.5 Strains on the Shear Bolts

6.1.5.1 Strains in the Bolts at Various Points in the Loading History

Several plots have been created to show the relationship between the strains recorded in each of the shear bolts. The shear bolts were fitted with strain gauges in two perpendicular directions (on the slab surface). Bolt #1 and Bolt #5 are the bolts that were placed closest to the column. The highest amount of strain was recorded in these bolts. Figure 6.5 through Figure 6.8 follow. The strain in each bolt was calculated at 25%, 50%, 75%, and 100% of maximum load sustained by the specimen.
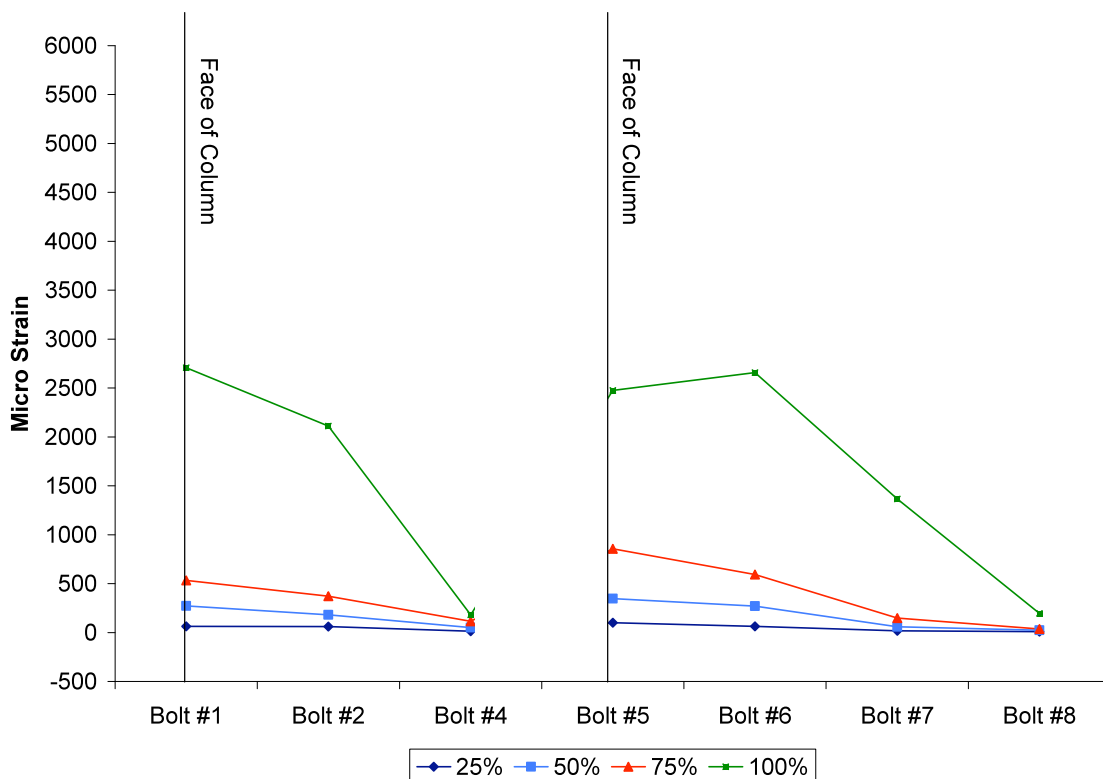
Figure 6.5 - Strain in Shear Bolts, SN1
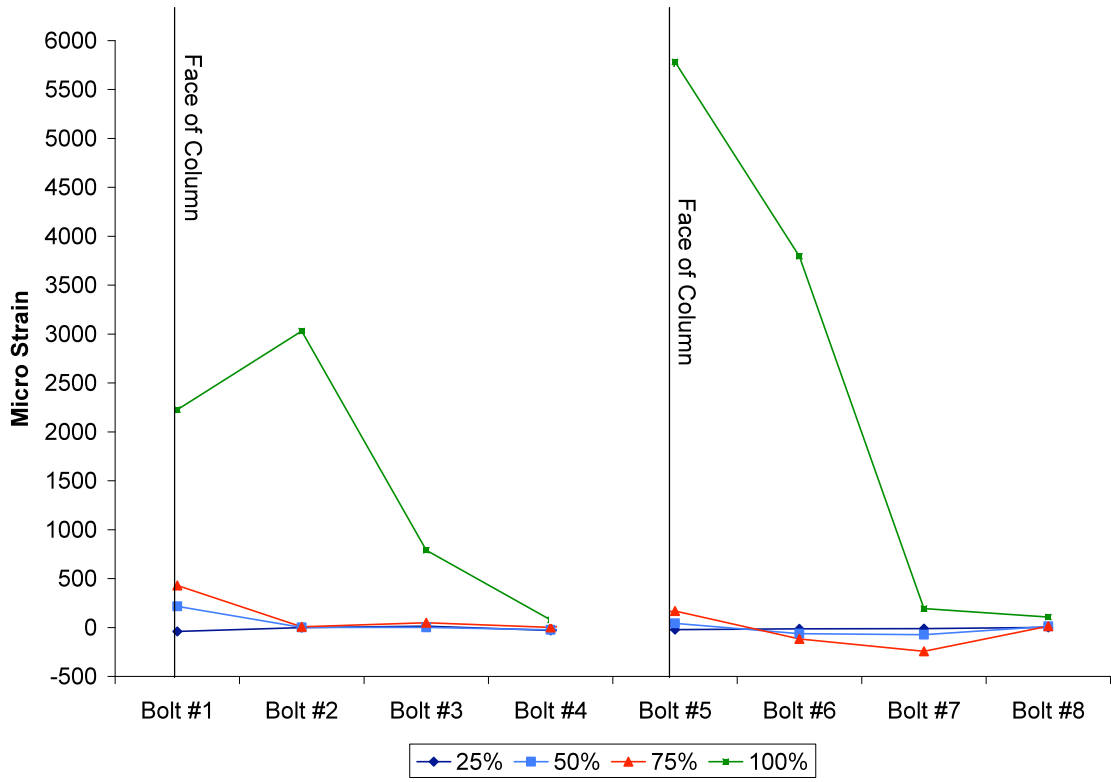
Figure 6.6 - Strain in Shear Bolts, SN2
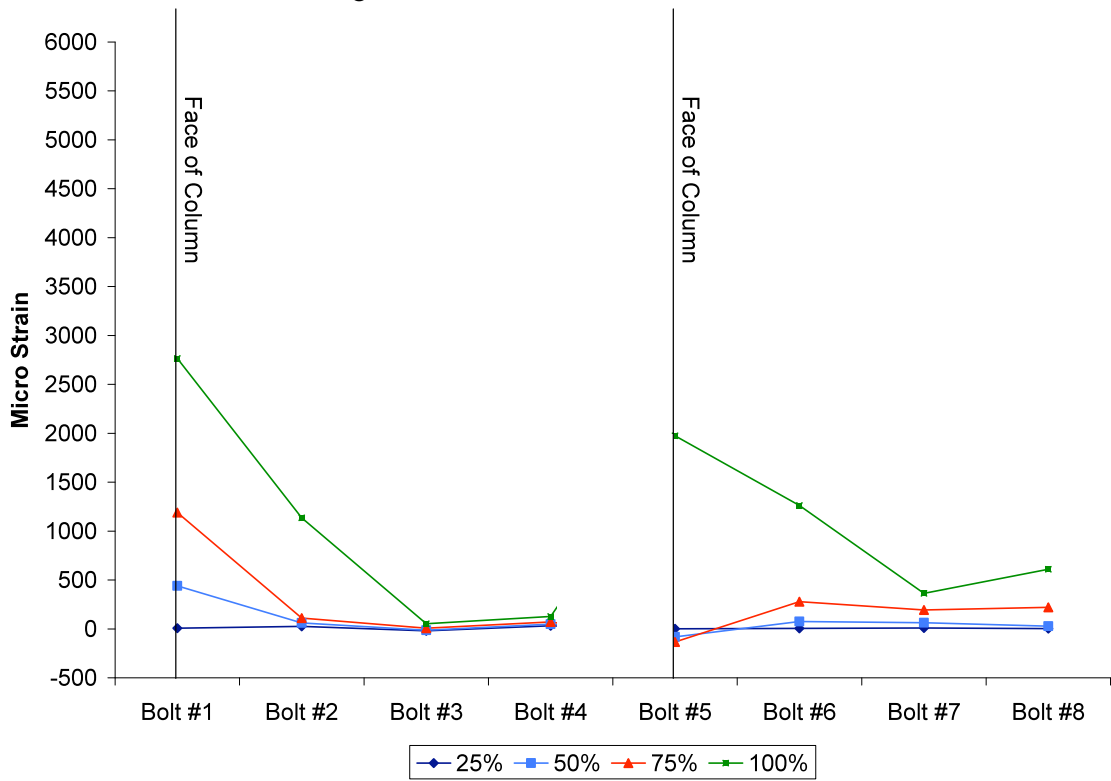
Figure 6.7 - Strain in Shear Bolts, SN3
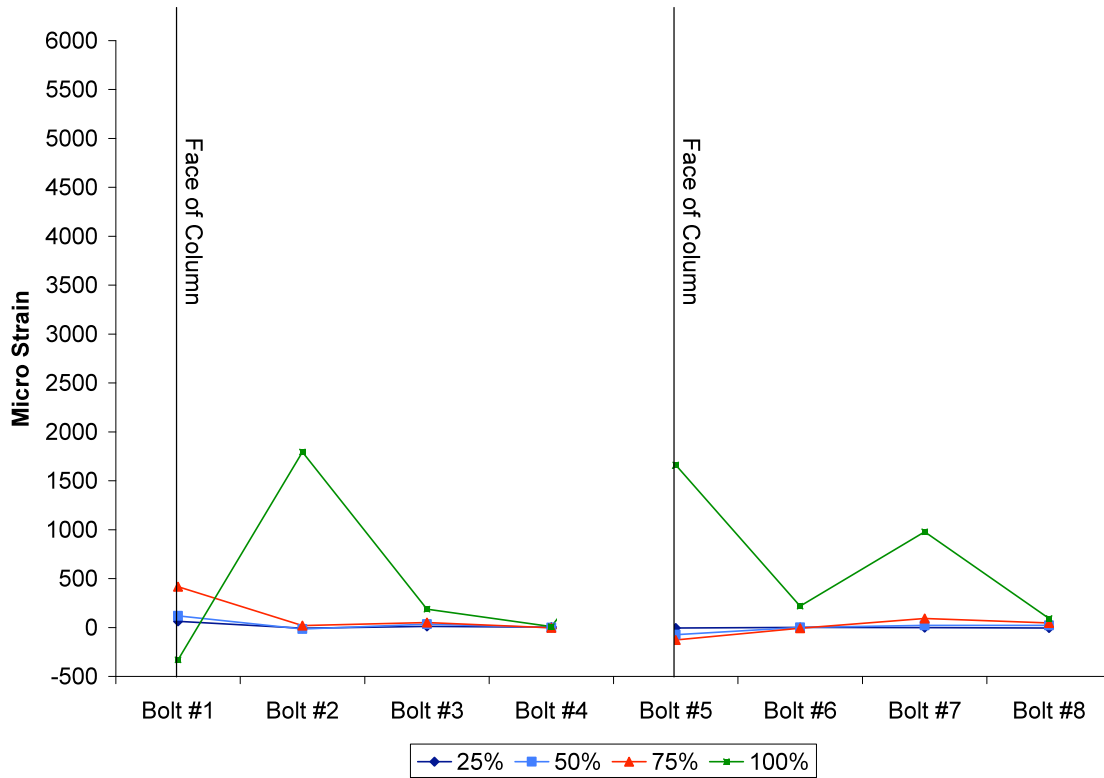
Figure 6.8 - Strain in Shear Bolts, SN4

In all three plots, very little strain can be observed in the bolts at 25% of the load. Indicating that the bolts were not yet active and the punching cone was not formed, or spread wide enough to activate the bolts. In all cases the strain in the bolts at the column face was the highest. This is to be expected, as research by Dilger and Ghali (1981) has shown that the shear stress in a slab-column connection is highest near the column. Even though the specimens were reinforced with different types of shear bolt systems, all four specimens had the same strain performance. As the loading increased, the recorded strain increased, and as the distance from the column increased, the strain decreased.

SN2, SN3 behaved in a similar manner. At 25%, 50%, and 75% the bolts were mostly inactive, experiencing almost no strain. Somewhere between the value of peak load, and 75% of peak load the bolts have become active, and are indeed acting as tensile resistance elements. For the most part SN4 follows this behaviour as well, however the gauge at Bolt #1 appears to have failed during the test, as it registered negative strain at peak load. However, the plots do show that the bolts are more active at peak load, and are indeed under tension.

6.1.5.2 Summary of Strains in the Bolts over Entire Loading History

Plots have been created that show the strain history in each of Bolt #1, Bolt #2, Bolt #5, and Bolt #6 in each specimen, over the entire loading path. Bolt #1 and Bolt #2 were in orthogonal directions then Bolt

87

#5 and Bolt #6. Bolt #1 and Bolt #5 were in the perpendicular row closest to the columns, while Bolt #2 and Bolt #5 were in the next row away from the column. Figure 6.9 follows, and illustrates the strain history at Bolt #1.
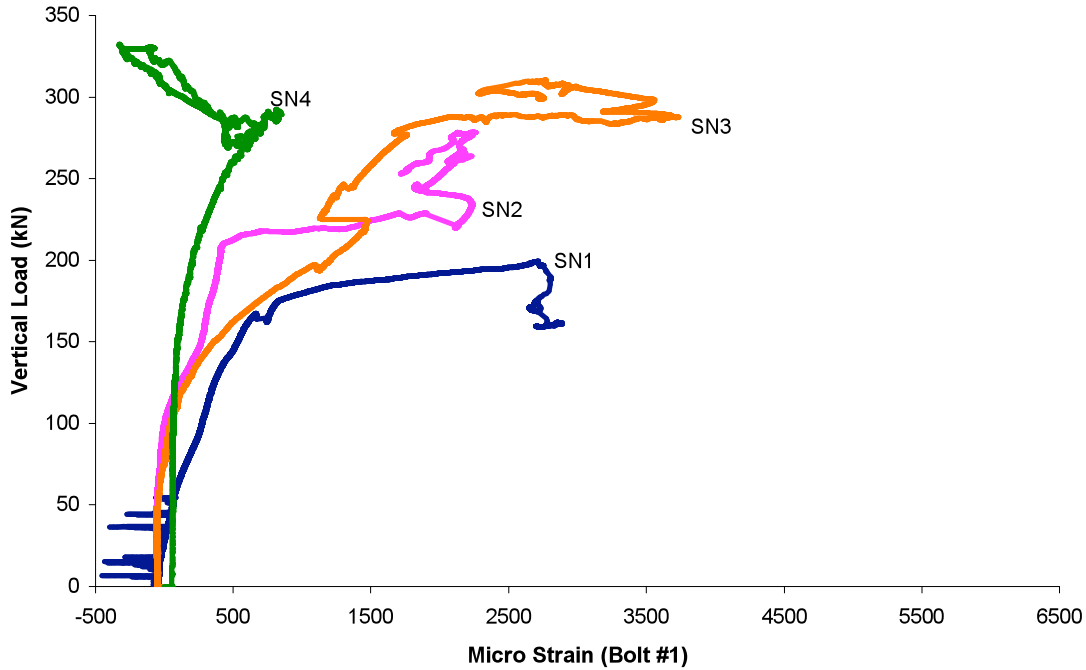
Figure 6.9 - Strain vs. Vertical Load in Bolt #1

The strain gauge on Bolt #1 in SN4 appears to have been recording erroneous strain, and will be discounted in the following analysis. In SN2 and SN3 the two K-Line bolts behaved in almost the same manner until approximately 150kN into the loading. At this point, SN2 experiences a drastic increase in load, with little strain increase. At this point, either the fitting is slipping, or cracks are forming within the concrete. A large increase in strain can be observed in SN2 at approximately 220kN, this is when the bolt became active, and started to restrain the formation of the punching cone. This indicates that Bolt #1 in SN2 was behaving as a shear resisting element. Bolt #1 in SN3 sustains a greater load and more strain then SN2. Slip of the connection is visible on the plot, however the crimp is able to further sustain more load before experiencing a large increase in strain near the peak load of 300kN.
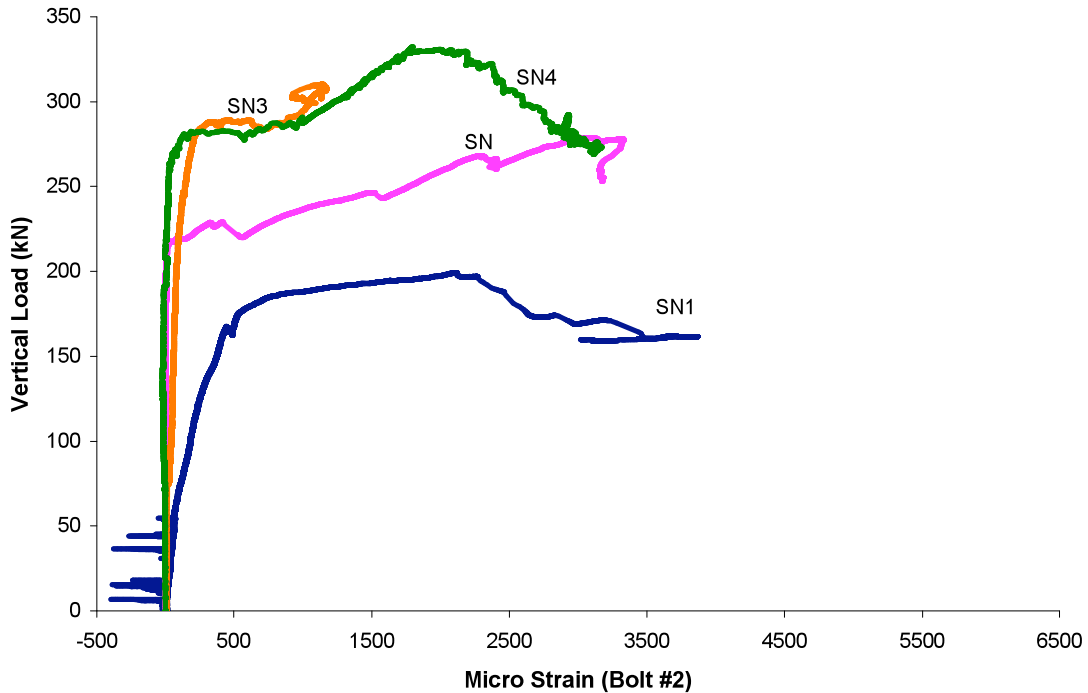
Figure 6.10 - Vertical Load vs. Strain for Bolt #2

The strains in SN3 and SN4 at Bolt #2 behaved very similar (Figure 6.10). Both did not become active until about 270kN, at which point they both had an increase in strain, followed by peak loading of the specimen. SN2 also responded with similar stiffness, but experienced a strain increase at the lower load of approximately 230kN. As the crimping process was being improved upon each test, the crimps were likely not as strong in SN2 versus the last two tests. In conclusion, the punching cone in SN2 formed at a lower load, and as a result activated the shear bolts. By allowing the punching cone to form at a lower load (comparatively to the last two specimens) the peak load was lower in SN2. SN1 experienced a sudden increase in strain at the lowest load, after an initial slip and cracking of approximately 170kN, the strain history shows increase of strain prior to failure of the specimen, which is probably due to slippage of the nut / bolt connection.
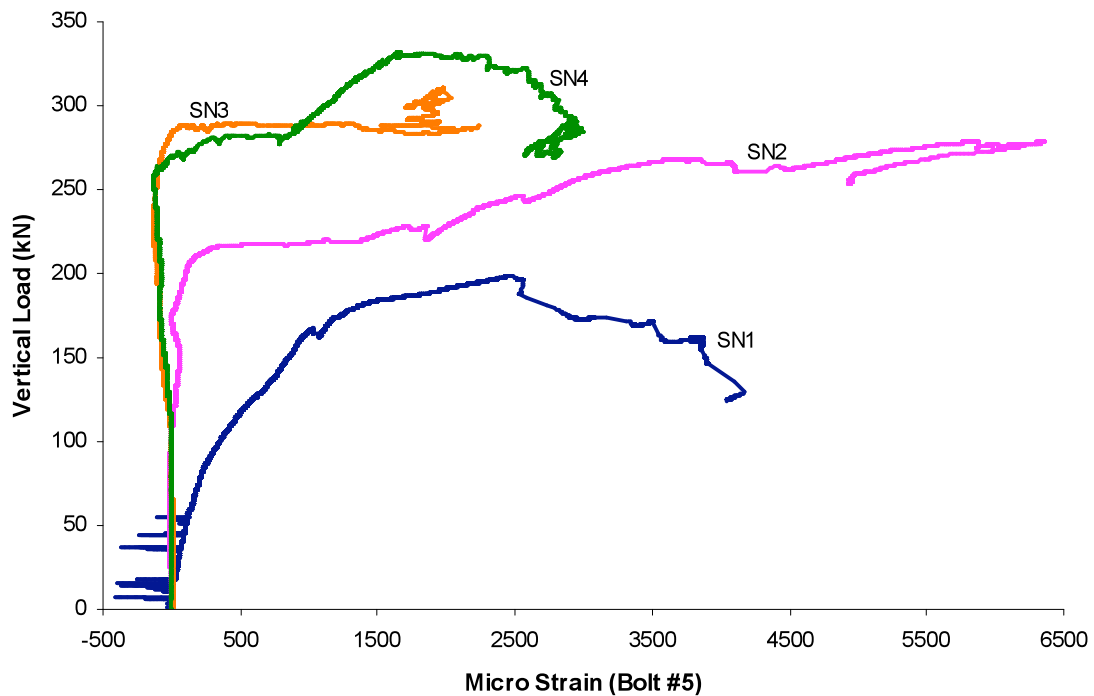
Figure 6.11 - Vertical Load vs. Strain for Bolt #5

The strains in SN3 and SN4 at Bolts #5 behave in a very similar fashion. With similar stiffness, and an increase in strain at a similar load, it can be concluded that the bolts in SN3 and SN4 were behaving in a similar manner. Bolt #5 in SN2 experiences a large increase in strain over the loading history, indication of the formation of the punching cone near to Bolt #5's location. As with Bolt #2, Bolt #5 in SN2 experienced strain increase at a lower point then SN3 and SN4, which can be contributed to the crimping process. SN1's Bolt #5 did not behave as Bolt #2, however, a sudden failure is observed at approximately 2500$\mu\epsilon$. The results from Bolt #6 are illustrated in Figure 6.12.
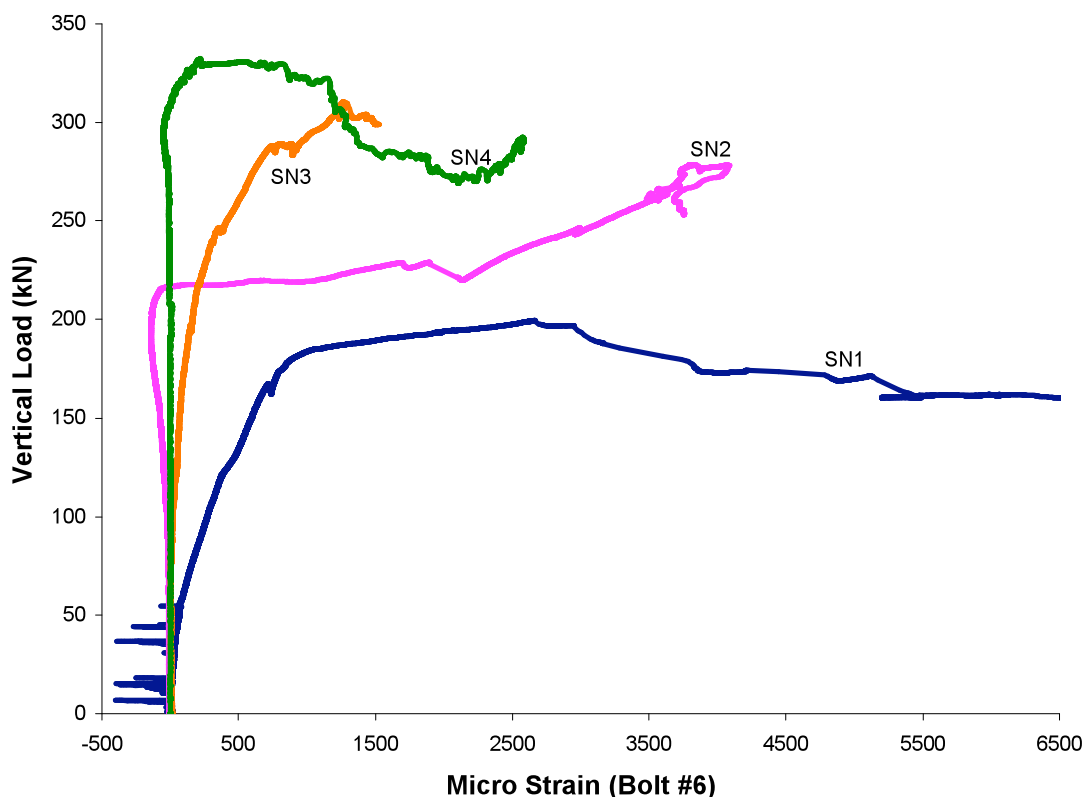
Figure 6.12 - Vertical Load vs. Strain for Bolt #6

Figure 6.12 (Bolt #6) demonstrates that the behaviour of each slab was consistent in each perpendicular shear bolt row. The trends discussed above, for the most part, again occur in Bolt #6. In SN1 the bolt experiences more strain, and no sudden failure. It is expected that Bolt #6 in this case did not fully intercept a shear crack. The punching cone was observed to be located between the first row of bolts and the column face in SN1. With SN6 being located in the second row from the column, the punching shear cone probably did not reach this point in the slab. As such, Bolt #6 did not receive enough loading to fracture, but did however become elongated under such loading.

6.2 Specimens Tested Under Pseudo-dynamic Loading

Slabs SN5 and SN6 were tested under pseudo-dynamic load, according to the procedure outlined in Section 5.1.2. This chapter summarizes and analyzes the relevant data collected in the experimental program. The data is analyzed based on the crack pattern, stiffness, ductility and strain. Crack patterns for each slab tested can be found in Chapter 5.

91

6.2.1 Lateral Load versus Drift Ductility

A summary table has been created to compare the two control specimens from Bu (2008) to the tested specimens. The two control specimens are SW5 and SW6. SW5 was loaded with a vertical load of 160kN, and contains no shear reinforcement or openings. SW6 contains no shear reinforcement, was also loaded with a dead load of 160kN, and contains two 150x150mm openings against the column in the direction of the applied moment. The loading path was identical for all specimens.

The peak moment was calculated from the data collected during the testing. The distance from each horizontal actuator was 1.25m (the moment arm). Lateral drift ratio is the ratio of horizontal displacement to vertical distance from mid-depth of the slab. The yield drift ratio was equated to the drift ratio at the point of the first yielding of flexural reinforcement under each moment direction (negative and positive).

The method used to calculate drift ductility of a connection is the ratio of the yield drift ratio to the peak drift ratio. It can be defined as:

$$\mu_{peak} = \frac{\delta_{peak}}{\delta_y}$$

Bu (2008) used two methods to calculate this value, where the difference in these two methods is the definition of the value of δ_y. Pan and Moehle (1989) define two points on the backbone curve, as shown in Figure 6.17, these points correspond to $(2/3)P_{max}$ and P_{max}. A line between the origin, the point of $(2/3)P_{max}$, and crossing the horizontal line corresponding to P_{max} defines the assumed yield drift ratio, δ_y.

The second method used by Bu (2008), and the method used in this thesis for comparison, identifies δ_y from experimental observations, as the drift ratio when the flexural reinforcement first yields.

Table 6.4 - Peak Moment and Drift Ductility

Slab Name	$\dfrac{V}{V_0}$	Peak Moment (kN-m)		Lateral Drift Ratio at Peak Moment, δ_{peak} (%)		Yield Drift Ratio, δ_y (%)	Drift Ductility at Peak Moment, μ_{peak}	
		-	+	-	+		-	+
SN5	0.68	-62.25	66.28	1.66	4.00	1.30	1.28	3.08
SW5	0.68	-52.04	59.86	2.74	2.61	1.04	2.63	2.51
SN6	0.74	-44.38	33.25	2.59	2.49	1.40	1.85	1.78
SW6	0.74	65.05	74.83	1.31	1.71	1.07	1.23	1.60

In the case of SN5 and SN6, the drift ductility was increased with the inclusion of shear bolts in the specimen. The connection in SN5 was also able to sustain a slightly higher peak moment. SN6, was able to sustain a much higher lateral drift at peak moment, showing an improvement of 197% and 146% on

each side of the moment. The inclusion of shear bolts has also increased the yield drift ratio of the specimens.

6.2.2 Hysteresis and Energy Dissipation

Cyclic load versus displacement plots were prepared for each specimen. When loading under reverse moment cyclic load, a hysteresis plot can be created. These plots indicate permanent deformation of the connection, stiffness degradation, and also the energy dissipated over the loading history.
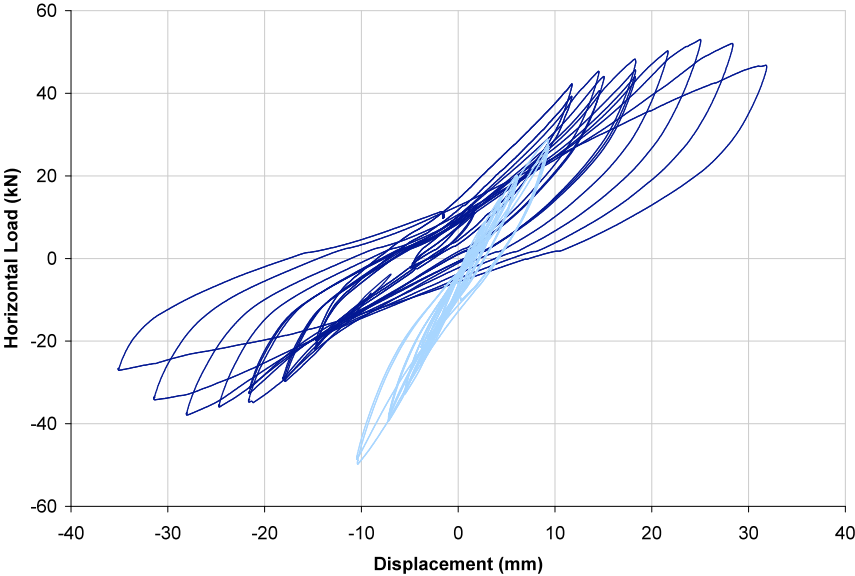
Figure 6.13 - Lateral Load vs. Drift Ratio, SN5 (GFRP Bolts)
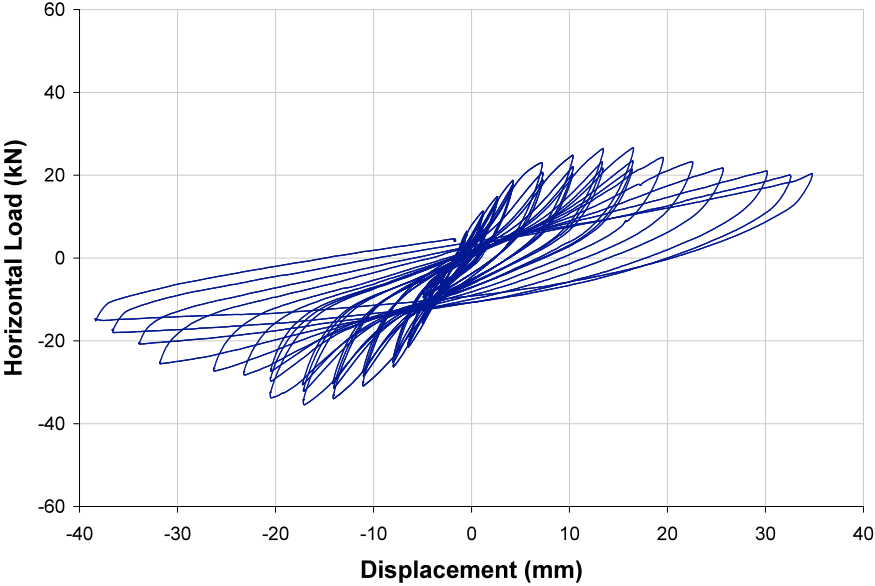
Figure 6.14 - Lateral Load vs. Drift Ratio, SN6 (GFRP Bolts, 2 openings)

Figure 6.13 shows the hysteresis for SN5. There are two plots here, as the test was restarted after the overload due to the hydraulic failure, and subsequent overloading of the specimen as mentioned previously. It is quite obvious that the stiffness of the connection decreased after the overload event, and continued to degrade over the period of the loading. The test was finally stopped when the connection could not sustain any further increases in loading. In seismic events the amount of energy dissipated through a structural connection is an important factor. Energy dissipation causes damage, ideally this damage should be isolated to load paths where the loads can be redistributed, and absorbed by other structural elements. The current design philosophy in steel structures calls on building sacrificial connections into the structure, which can be replaced after a seismic event, without damage to the overall structure (Chopra 2001). If damages (energy dissipation) can be isolated, or concentrated to the sacrificial connection, overall cost to repair the structure can be decreased. On a hysteresis plot the amount of energy dissipated is indicated by the area under the curve as it passes through the origin. When a material or connection always passes through the origin, independent of loading history, the curve is said to be "pinched", and little energy is being dissipated. As it can be seen above in Figure 6.13 and Figure 6.14 a large amount of energy appears to be dissipated. For comparison a hysteresis plot of the control, SW5 is shown in Figure 6.15.
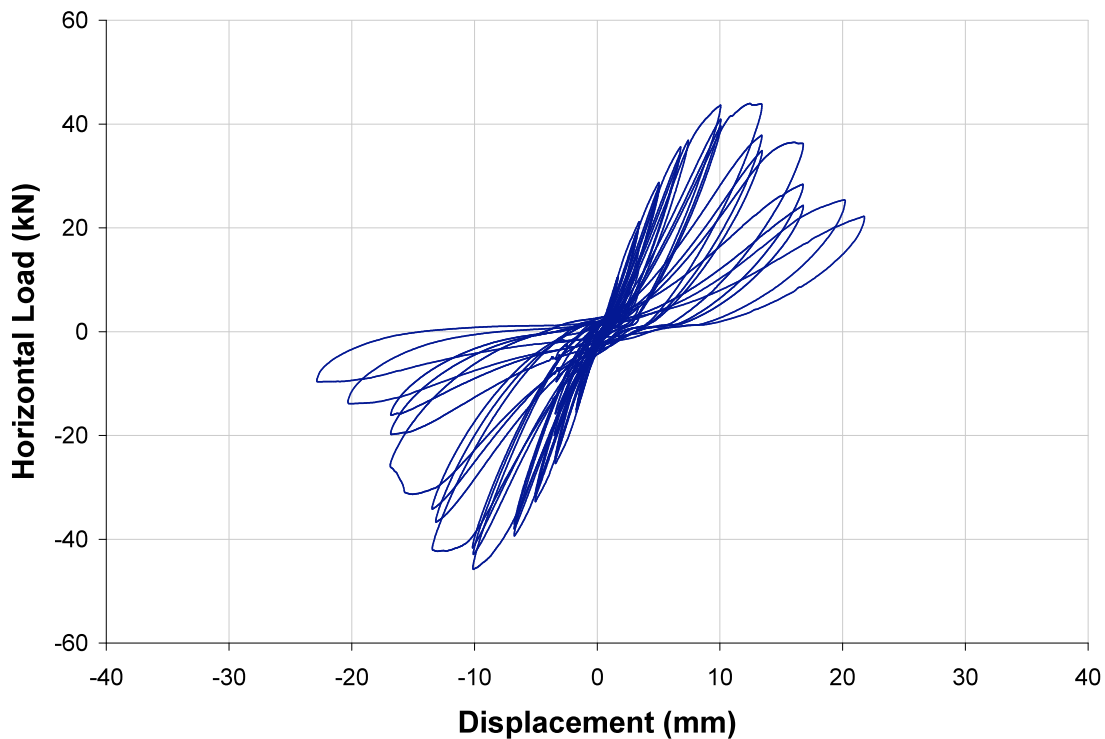
Figure 6.15 - Lateral Load vs. Drift Ratio, SW5 (control)

94

By comparing Figure 6.13 and Figure 6.15, it can be seen that the inclusion of GFRP shear bolts had an effect on the amount of energy dissipated. However, this was the case unique only to the GFRP system, Figure 6.16 follows which contains a hysteresis plot for SW8, a specimen from Bu (2008) which was reinforced with 6 rows of steel shear bolts.
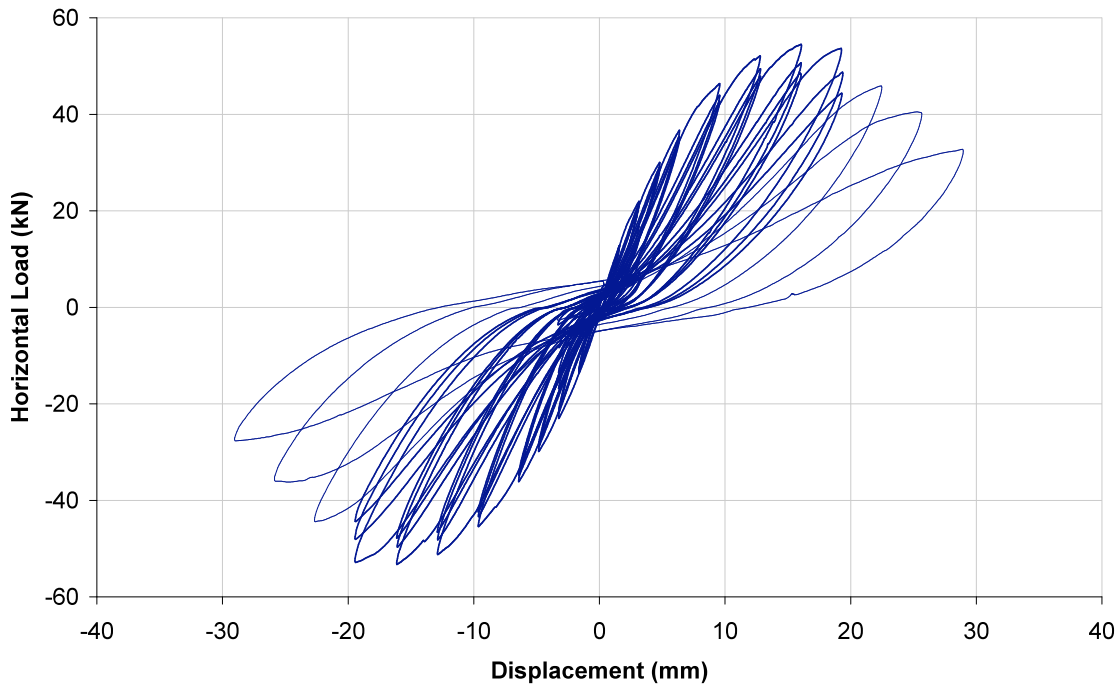
Figure 6.16 - Lateral Load vs. Drift Ratio, SW8 (Steel Bolts)

Pinching is clearly evident in Figure 6.16, and clearly a greater amount of energy is being dissipated in the connection that has been reinforced with GFRP shear bolts. The steel shear bolts were tightened against the slab by way of a torque wrench, to a load of 10% of the yield strength of the steel bolt. The GFRP system had no such tightening technique, as the GFRP rods were not threaded. Furthermore, the connection of the fittings to the GFRP rod was not perfectly tight, and allowed more movement under reverse loading then the rigid head of the steel shear bolt would. These two factors allowed more movement within the concrete slab under loading. As shear cracks opened and closed, they were allowed to rub and move with the drifting of the specimen, and this movement likely contributed to dissipation of energy. Energy dissipation in concrete connections is not common, and is highly desirable in seismic zones where a lot of reinforced concrete is used as a building material (e.g. Turkey).

For comparison purposes, a backbone curve for each tested specimen was created. This curve represents the maximum load and displacement experienced under testing at each loading step. Backbones were prepared for SN5 and SN6, as well as for the two control specimens SW5 and SW6.
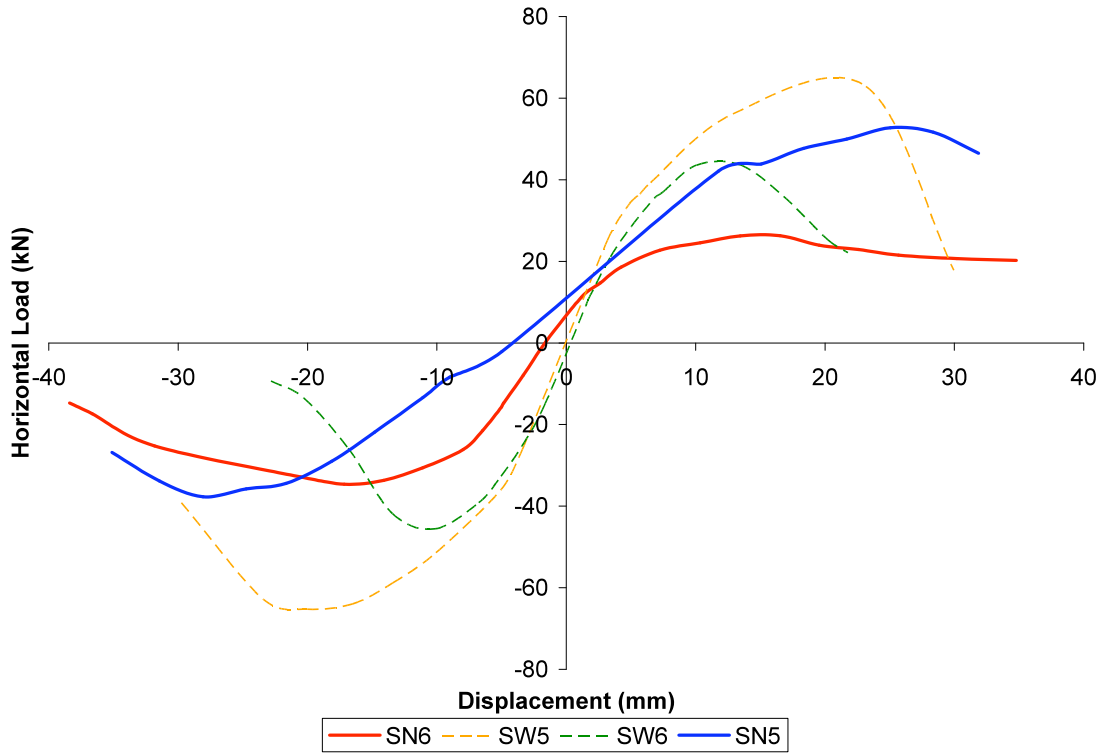
Figure 6.17 - Backbone Curves for SN5, SN6, SW5, and SW6

6.2.3 Strains in Shear Bolts

In each specimen 12 shear bolts were fitted with strain gauges. The data recorded is in Appendix E for SN5, and Appendix F for SN6. One radial row in each direction was fitted with gauges. A general trend was observed in both SN6 and SN5 that the shear bolts placed further away from the column, experienced less strain than the bolts placed in the first two rows. The strain data recorded showed that the bolts in the last two rows experienced almost no strain at all. This is an indication that the punching cone formed inside of this perimeter. For comparison purposes the data recorded in Bolt #1 for both SN5 and SN6 is presented in Figure 6.18 and Figure 6.19 respectively.
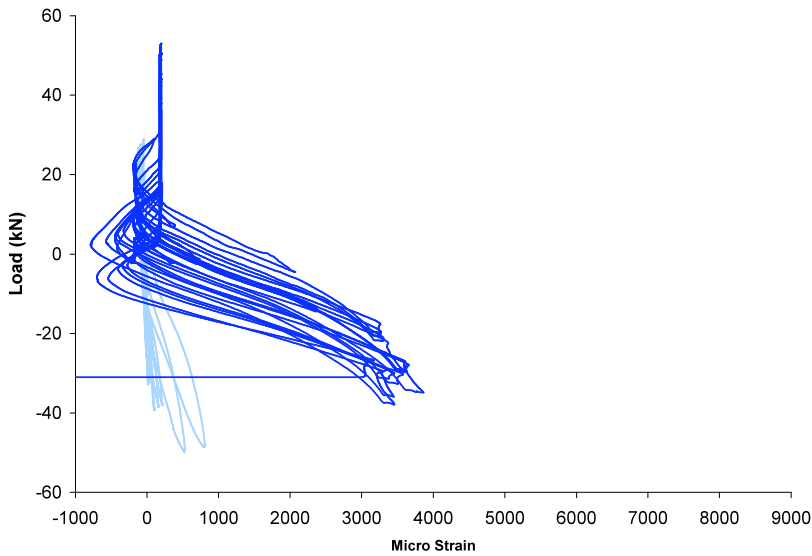
Figure 6.18 - Shear Bolt Strain Data, Bolt #1, SN5
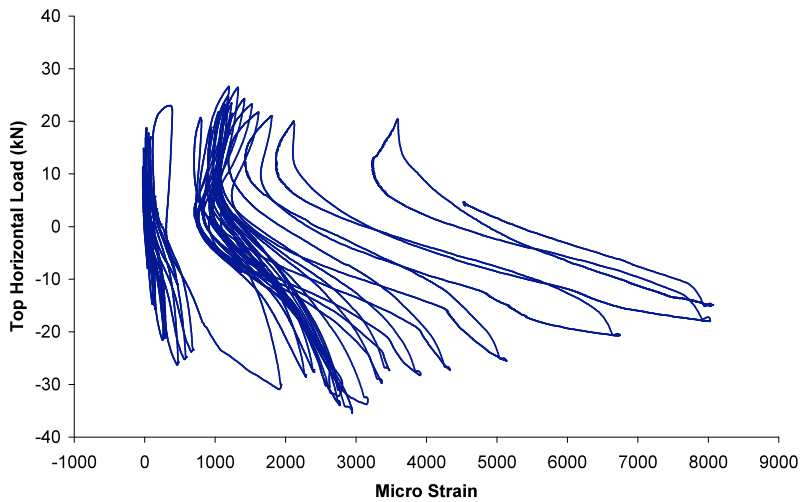
Figure 6.19 - Shear Bolt Strain Data, Bolt #1, SN6

Figure 6.18 illustrates that the bolt only experienced strain when the drift ratio was in the negative direction. The strain data goes to nearly zero when the drift ratio is positive. During the testing it was observed that the column had failed in bending partly through the loading path (Figure 6.21). This may have been due to the overloading event, although this cannot be confirmed. With the column failing, the stresses from the imposed drift may not have been transferring to this side of the specimen. As such, this behavior should not be contributed to the shear reinforcement but experimental error. Figure 6.19 shows the strain data from SN6. This data indicates that the bolt was experiencing strain in both the positive and negative drifts. An obvious adjustment in strain can also be observed at around the first positive 1% drift ratio. This is when the bolts have become active in restraining a punching shear crack, and indicates the

97

start of the formation of the punching cone. Bolt #1 in SN6 was placed near the opening and at the end of the test a shear crack could be seen in the opening near the location of Bolt #1, this follows as Figure 6.20.

Figure 6.20 - Shear Crack Through Opening, SN6

Figure 6.21 – Column Failure, SN5

6.2.4 Strains in Flexural Reinforcement

A number of strain gages were attached to the flexural reinforcement, and embedded in the concrete specimens. A full layout pattern for SN5 and SN6 is illustrated in Figure 3.20 and Figure 3.21 respectively. The data recorded can be found in Appendix E and Appendix F. Table 6.5 summarizes the initial yielding point of the flexural reinforcement for the two specimens.

Table 6.5 - Flexural reinforcement yielding during test

Slab Name	Peak Lateral Load (kN)		Lateral Drift Ratio at 1st Yield (%)	1st Yield Gage	Gages that yielded during testing.
	+	-			
SN5	53.02	49.77	+1.4%	1.2a, 1.2b, 1.2c, 1.2d, 3a	1.2a, 1.2b, 1.2c, 1.2d, 3a, 4b, 1.2a(col), 1.2b(col), 1.2c(col), 1.2d(col)
SN6	26.61	35.46	+1.3%	6c	6b, 6c, 8b

SN6 had significantly less bars yielded over the entire test, however the bars that did yield did so at almost the same point as the bars from SN5. Since openings were made in the specimen, some of the flexural reinforcement had to be cut to allow the opening to be placed in the slab. This would have resulted in the decrease of development length on these bars. Also with the inclusion of openings, the integrity steel in the applied moment direction (1.2 and 1.2(col) bars) was not placed in the specimen. In SN5 these comprise the bulk of the bars that yielded during testing. This demonstrates how critical openings are in a slab with concerns for punching shear failure, and shows how care must be taken when designing such openings.

6.3 Effect of the Crimping Process on Test Results

Over the course of the testing program, a method was developed to allow aluminum fittings to be mechanically crimped to GFRP rods. The procedure developed, and suggestions for its future use can be found in Section 4.1.1.1. Some of the improvement in maximum loads and deflections that was observed between SN2, SN3 and SN4 can be contributed to the improvement of the crimping procedure over the testing program. As the author became more familiar with the procedure, the crimp, and tightness of the fitting to the slab face was improved. Since external shear bolts are a passive reinforcement, their ability to restrain cracks and slab expansion at a very early stage in the loading is very important. As the fittings became tighter against the slab, the results should be expected to improve.

The impact of the crimping procedure on test results is most evident in SN5 and SN6. These were the very first two slabs tested, and were the first slabs to use the crimping technique. The fittings on SN5 were not as tight as on subsequent tests, or that of SN6. This had an effect on the test results in several ways. With the bolts not tight against the slab, cracks were allowed to form unrestrained, causing expansion of the slab. The bolts later restrained this expansion, when the slab expanded enough to engage the looser bolts. This helps to explain the lower moment capacity of the specimens, then that of the controls, but higher ductility. By not having shear bolts effective at the start of the test, punching shear cracks were allowed to form, as well, the presence of holes where the bolts were installed further weakened the slab for punching shear capacity. Both of these factors contributed to the lower moment capacity of the connection, despite the presence of shear bolts. Being a passive reinforcement, the loose shear bolts did not become active until later on in the test. By not being loaded until some time into the test, the bolts increased the ductility of the connection by only starting to restrain movement after the concrete was cracked and expanded. This decreased the overall stiffness of the connection, and increased ductility.

The testing has shown that by making small improvements to the crimping procedure and process, significant gains can be made in the ultimate strength and reinforcement of the connection.

Chapter 7
Conclusions and Recommendations

7.1 Conclusions

It can be concluded that FRP can be used as an effective reinforcement material for the retrofit of slab-column connections against punching shear failure in both static and seismic loadings. Some more detailed conclusions follow, regarding specific areas of the research and testing.

- The anchorage and tightening of this element to the slab face is critical. In order to sustain the necessary loads, and develop the necessary tension, no (or little) movement can be allowed between the slab face and the end fitting.

- The process of crimping the GFRP shear bolts in the field was found to be a feasible way to provide anchorage for this type of application.

- By utilizing the transfer of stresses through an aluminum fitting to a GFRP rod (crimping) structural type loads can be sustained, and brittle failures of the bolt system were not found.

- The crimping process had an impact on the placement and location of shear bolts with respect to the patterns dictated by current design codes. Installers must be diligent so that no space or area is allowed so that punching shear cracks are allowed to form inside the area reinforced for punching shear.

- The GFRP bolts provide some internal movement during the formation of the punching cone. This allows for a significant amount of energy to be dissipated under reverse cyclic loading. The presence of GFRP shear bolts allows more energy to be dissipated over the specimens without any shear reinforcement and the specimens retrofitted with steel shear bolts.

- GFRP shear bolts provide connection ductility in both static and pseudo-dynamic loadings.

- A completely non-corrosive retrofit method has been developed that will allow the strengthening and retro fit of slab-column connections against punching shear.

- Openings around the slab-column connection impact the strength of the connection. GFRP shear bolts were effective in providing increased strength and ductility in a connection with openings

- The GFRP shear bolts behaved as a pure tensile element. The tensile load was developed due to expansion of the slab during in the formation of the punching cone. Transfer of this stress to the shear bolt it critical, as is maintaining this stress over the loading history.

7.2 Recommendations and Future Work

This research provides a good first step in developing GFRP shear bolts as a retrofit method for slab-column connections. With action and insight into some of the following items the system can be improved upon to a point where it could be used in existing structures.

- The crimping technique should be further studied to make it more efficient. An optimum point between crimping pressure and fitting size could be found, where the amount of tensile resistance could be maximized.

- While the loads sustained by the crimping process were able to increase the punching capacity of the specimens, more detailed work could be done to increase the amount of strength of the crimp. In particular this could include added more pre-stress to the GFRP rod to aid in the constraint of shear stresses.

- Placement with respect to the layout patterns dictated by design codes were hindered by the crimping tool. Further study should be made so that a crimping tool can be manufactured or found that will minimize the need to alter the layout pattern.

- The size of the "field end" of the GFRP shear bolt is too large for practical purposes. Further studies should be done to examine reducing the size of this head, as well as investigating retrofit methods where the headed portions of the bolt are partially buried in the concrete cover or topping.

- The increase in energy dissipation under reverse cyclic loading shows great promise, further research should be done into how to control and predict the amount of energy that can be dissipated.

- The impact of filling wrongly drilled holes with cementious grout should be investigated with respect to the effect on overall punching shear strength of the connection. While care must be taken not to cut reinforcement steel when drilling holes for reinforcement, a procedure should be developed to maximize the effectiveness of the patching and repair when steel reinforcement is contacted with the drilling machine.

References

Adetifa, Bamidele. *A New Punching Shear Strengthening Technique for Reinforced Concrete Slabs at Interior Slab-Column Connections.* MASc Thesis, Department of Civil Engineering, University of Waterloo, Waterloo: University of Waterloo, 2003, 134.

Alexander, Scott D.B., and Sidney H. Simmonds. "Bond Model for Concentric Punching Shear." *ACI Structural Journal* (American Concrete Insitute) 89, no. 3 (March-April 1992): 325-335.

Broms, C. E. "Punching of Flat Plates - A Question of Concrete Properties in Biaxial Compression and Size Effect." *ACI Structural Journal* (American Concrete Insitute) 87, no. 3 (May-June 1990): 292-304.

Bu, Wensheng. *Punching Shear Retrofit Method Using Shear Bolts for Reinforced Concrete Slabs Under Seismic Loading.* PhD Thesis, Department of Civil and Envionmental Engineering, University of Waterloo, Waterloo: University of Waterloo, 2008.

Canadian Standards Association. *CAN/CSA-S806-02 Design and Construction of Building Components with Fibre-Reinforced Polymers.* National Standard, Canadian Standards Association, 2004.

Canadian Standards Association. *CAN/CSA-S806-02 Design and Construction of Building Components with Fibre-Reinforced Polymers.* Design Standard, Canadian Standards Association, 2002.

Cement Association of Canada. *A23.3-94, Design of Concrete Structures.* Design Code, Canadian Standards Association, 1994.

Dilger, W. H., and A. Ghali. "Shear Reinfocement for Concrete Slabs." *Journal of the Structural Division* (American Society of Civil Engineering) 107, no. 12 (December 1981): 2403-2420.

Elgabry, Adel A., and Amin Ghali. "Design of Stud-Shear Reinforcement for Slabs." *ACI Structural Journal* (American Concrete Insitute) 87, no. 3 (May 1990): 350-361.

El-Salakawy, Ehab Fathy. *Shear behaviour of Reinforced Concrete Flat Slab Edge Connections with Openings.* PhD Thesis, Faculty of Engineering, Menoufia University, Shebin El-Koum: Menoufia University, 1998, 209.

Ghali, Amin, and Sami Megally. "Design for Punching Shear in Concrete: Critical Review of Canadian Standard CSA-A23.3-94." *Canadian Journal of Civil Engineering* (Canadian Society of Civil Engineers) 23, no. 2 (Feb. 1996): 444-456.

Harajli, M. H., and K. Soudki. "Shear Strengthening of Interior Slab-Column Connections Using Carbon Fiber-Reinforced Polymer Sheets." *Journal of Composites for Construction* (American Society of Civil Engineers) 7, no. 2 (May 2003): 145-153.

King, Suzanne, and Norbert J. Delatte. "Collapse of 2000 Commonwealth Avenue: Punching Shear Case Study." *Journal of Performance of Constructed Facilities* (ASCE) 18, no. 1 (Feburary 2004): 54-61.

Kinnunen, S., and H. Nylander. "Punching of Concrete Slabs without Shear Reinforcement." *Transactions of the Royal Insitute of Technology* (Royal Insitute of Technology), no. 158 (1960).

MacGregor, James G., and F. Michael Bartlett. *Reinforced Concrete, Mechanics and Design.* 1st Canadian Edition. Toronto, Ontario: Prentice Hall, 2000.

National Geographic. "Explorer: Collapse." Sepember 2005.

Pan, A.D., Moehle, J.P., "Lateral Displacement Ductility of Reinforced Concrete Flat Plates." *ACI Structural Journal,* 86, no. 3 (March 1989): 250-258.

Pillai, S. U., D. W. Kirk, and M. A. Erki. *Reinforced Concrete Design.* 3rd Edition. Toronto, Ontario: McGraw Hill, 1999.

Schöck Bauteile GmbH. "Technical Information Schöck ComBAR." Technical Manual, 2006.

Sissakis, Kyriakos, and Shamim A. Sheikh. "Strengthening Concrete Slabs for Punching Shear with Carbon Fiber-Reinforced Polymer Laminates." *ACI Structural Journal* (American Concrete Insitute) 104, no. 1 (January-Feburary 2007): 49-59.

Stark, Andrew, Baris Binici, and Oguzhan Bayrak. "Seismic Upgrade of Reinforced Concrete Slab-Column Connections Using Carbon Fibre-Reinforced Polymers." *ACI Structural Journal* (American Concrete Insitute) 102, no. 2 (march-April 2005).

Strongwell Corporation. *Section 11 - Fibrebolt Studs and Nuts.* Product Guide, Bristol: Strongwell Corporation, 2002, 1-11.

Appendices

Appendix A – Data from SN1
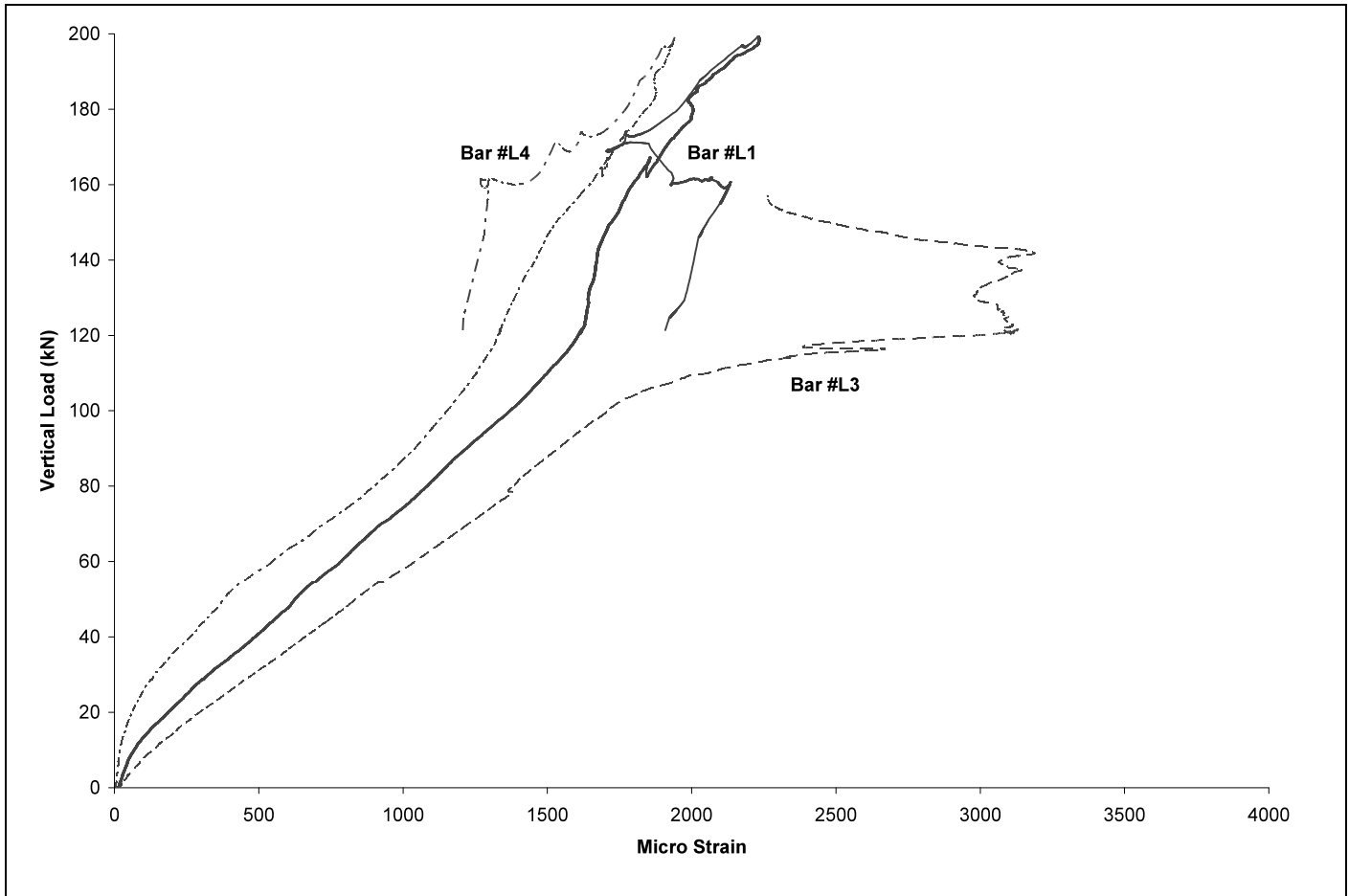
Figure A-1: Slab SN1, Strain vs. Vertical Load, L1, L3, L4
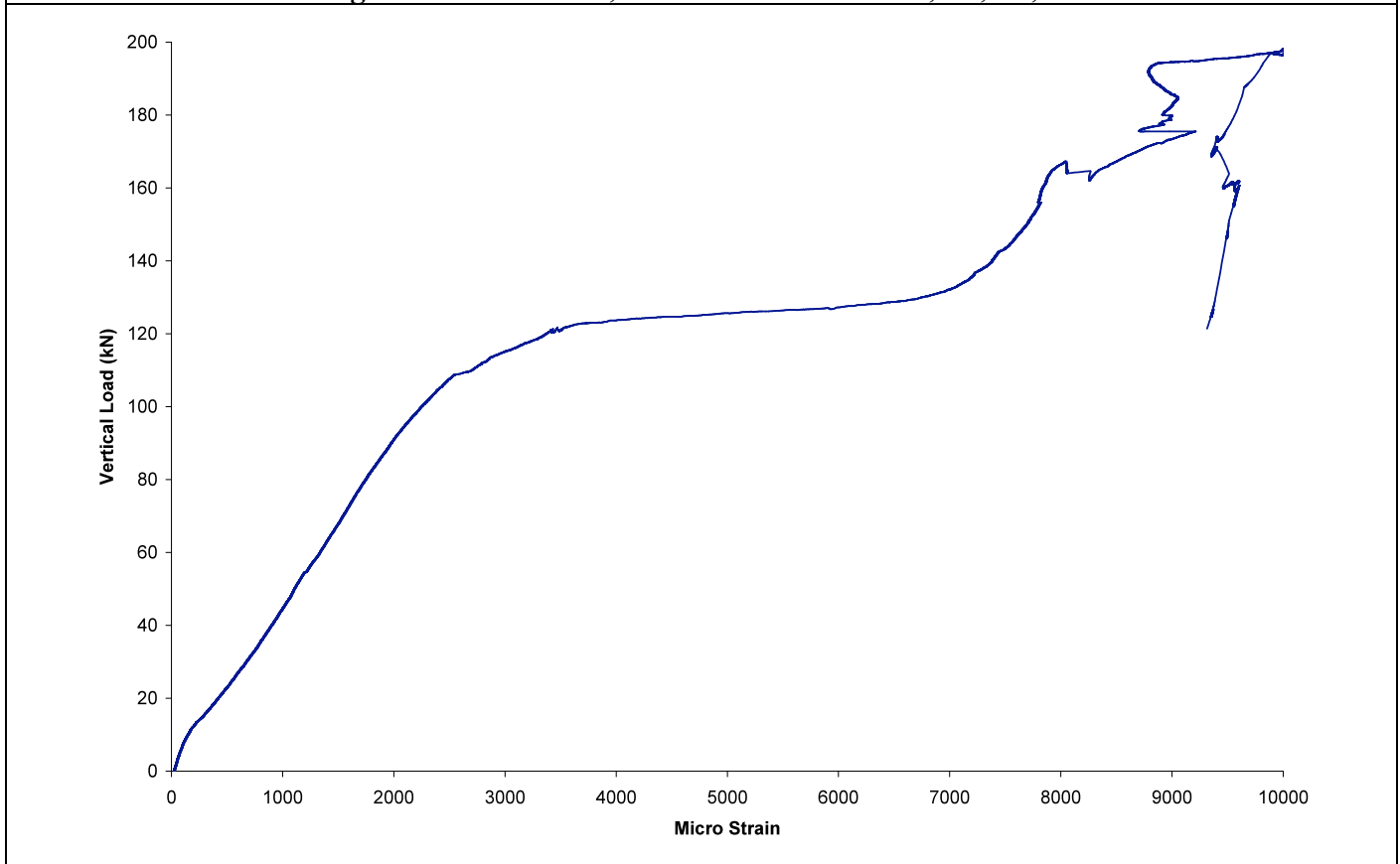
Figure A-2: Slab SN1, Strain vs. Vertical Load, L2
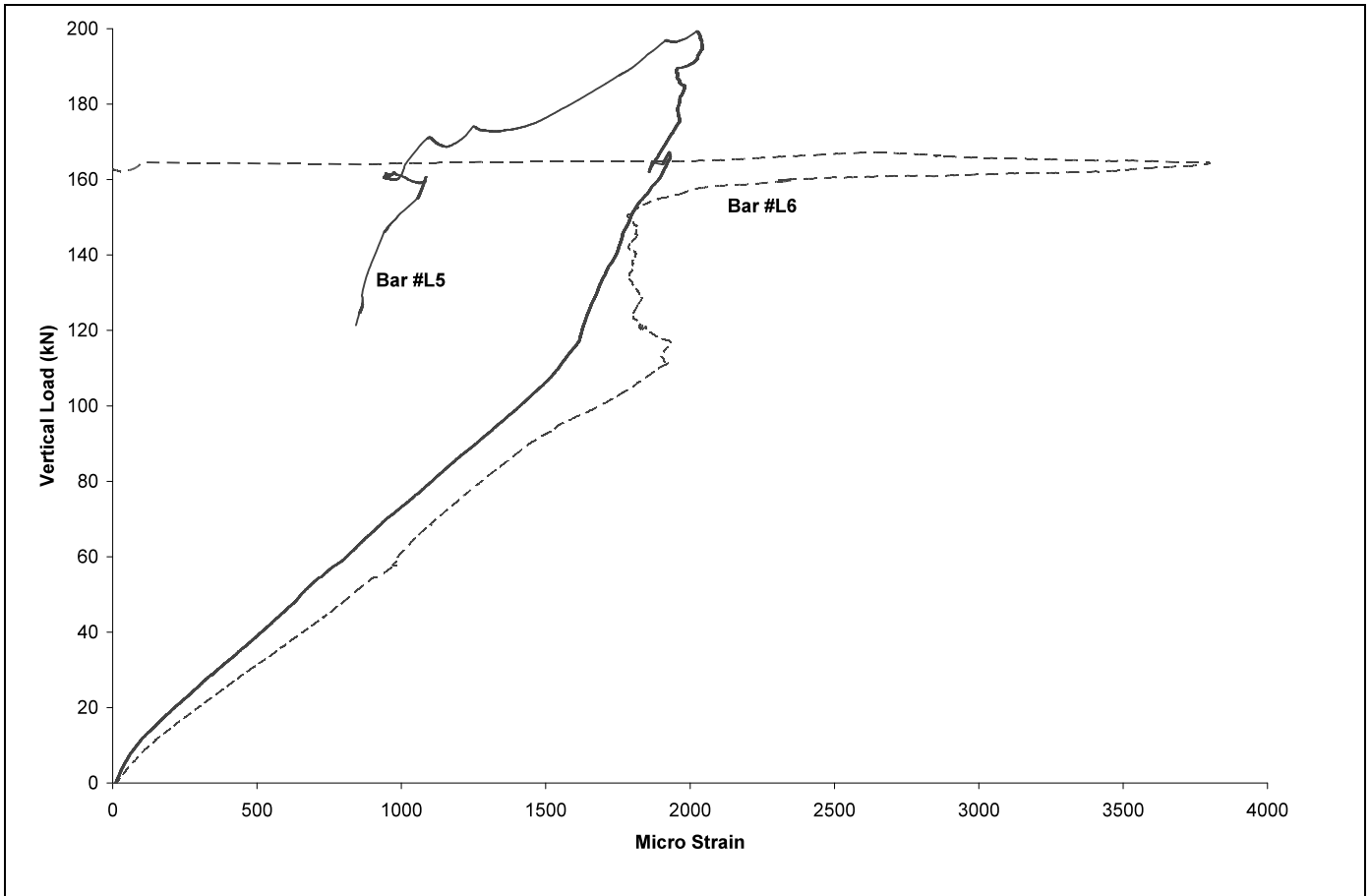
Figure A-3: Slab SN1, Strain vs. Vertical Load, L5, L6
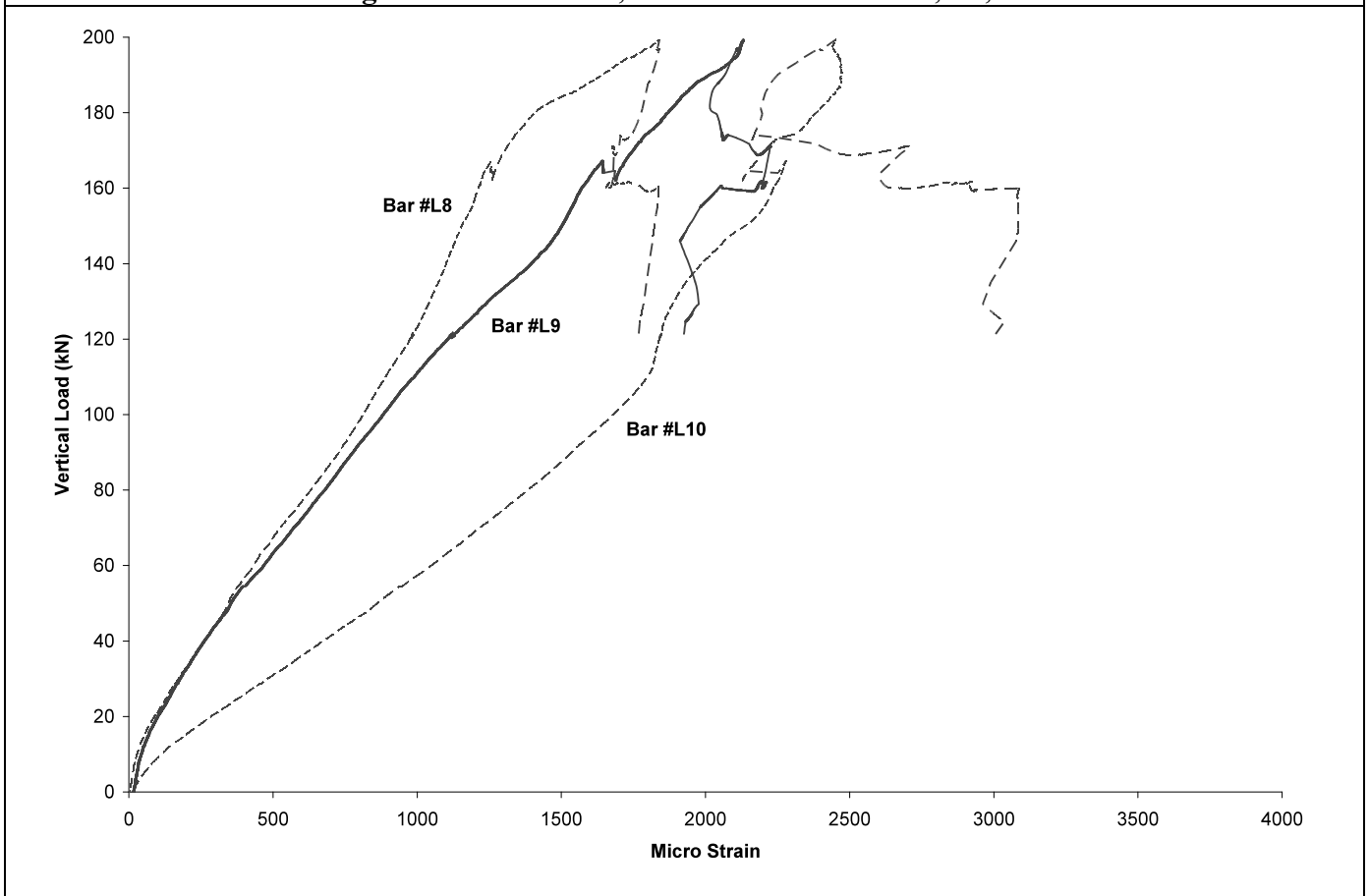
Figure A-4: Slab SN1, Strain vs. Vertical Load, L8, L9, L10
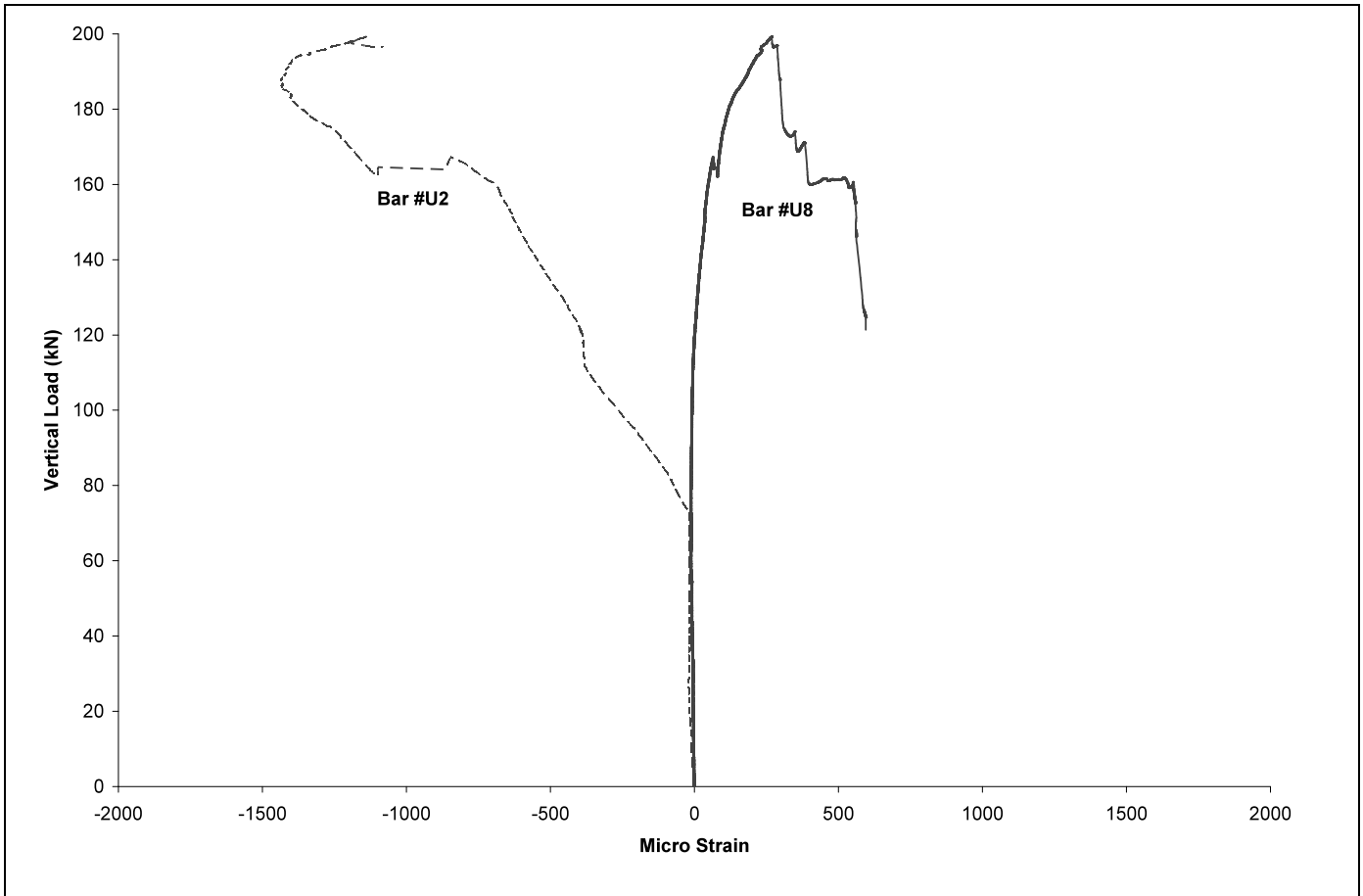
Figure A-5: Slab SN1, Strain vs. Vertical Load, U2, U8
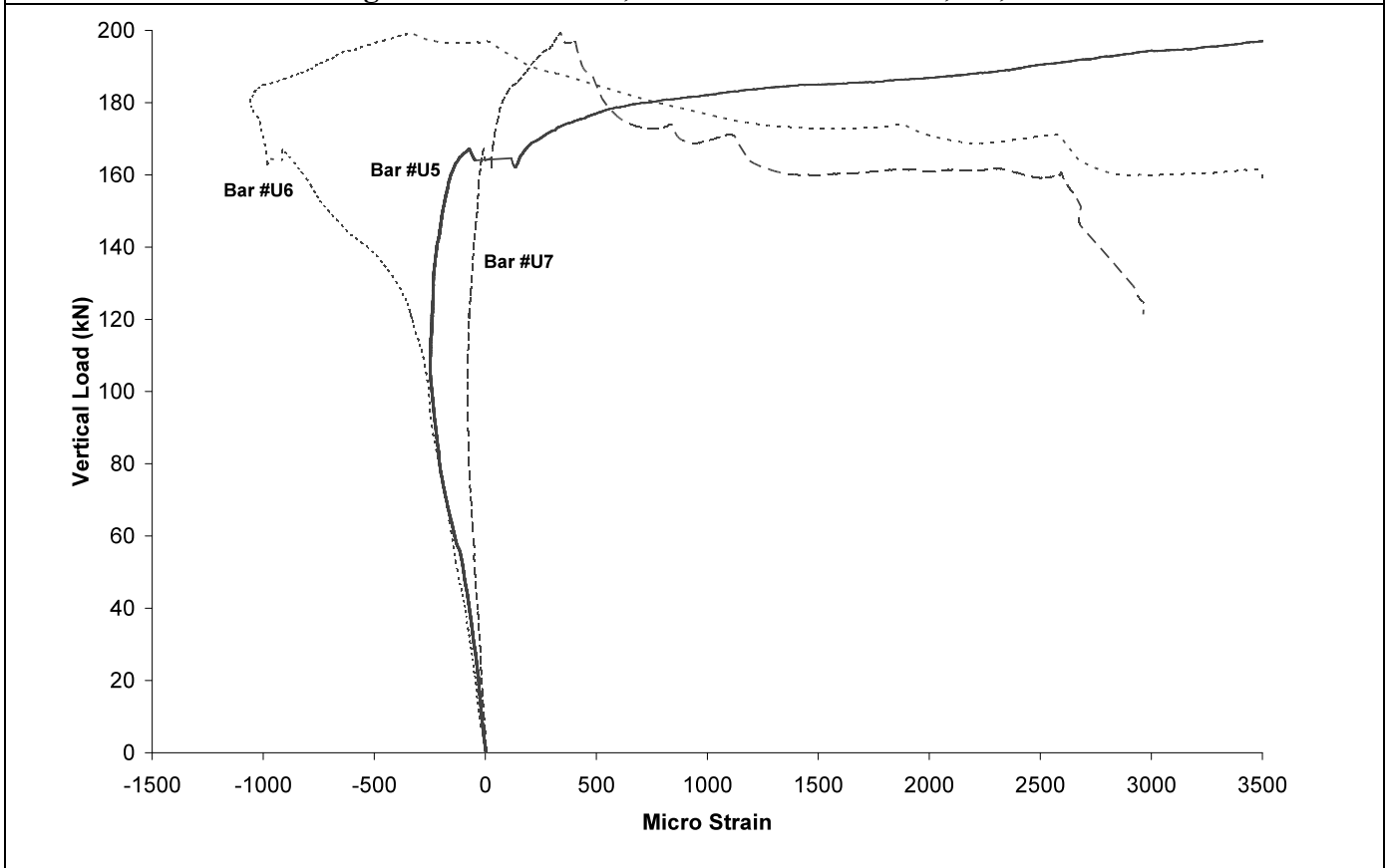
Figure A-6: Slab SN1, Strain vs. Vertical Load, U5, U6, U7

108
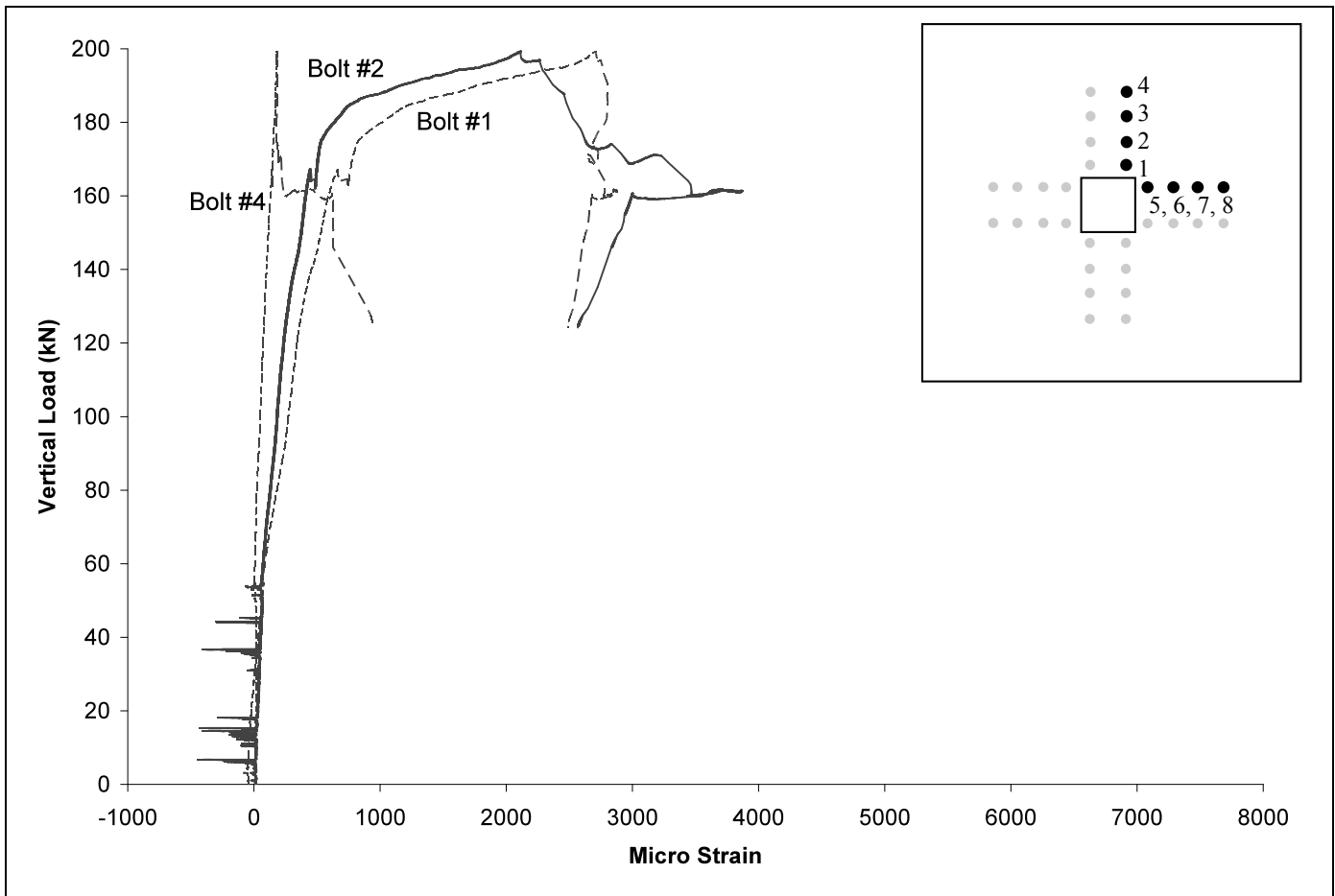
Figure A-7: Slab SN1, Strain vs. Vertical Load, Bolt #1, #2, #4
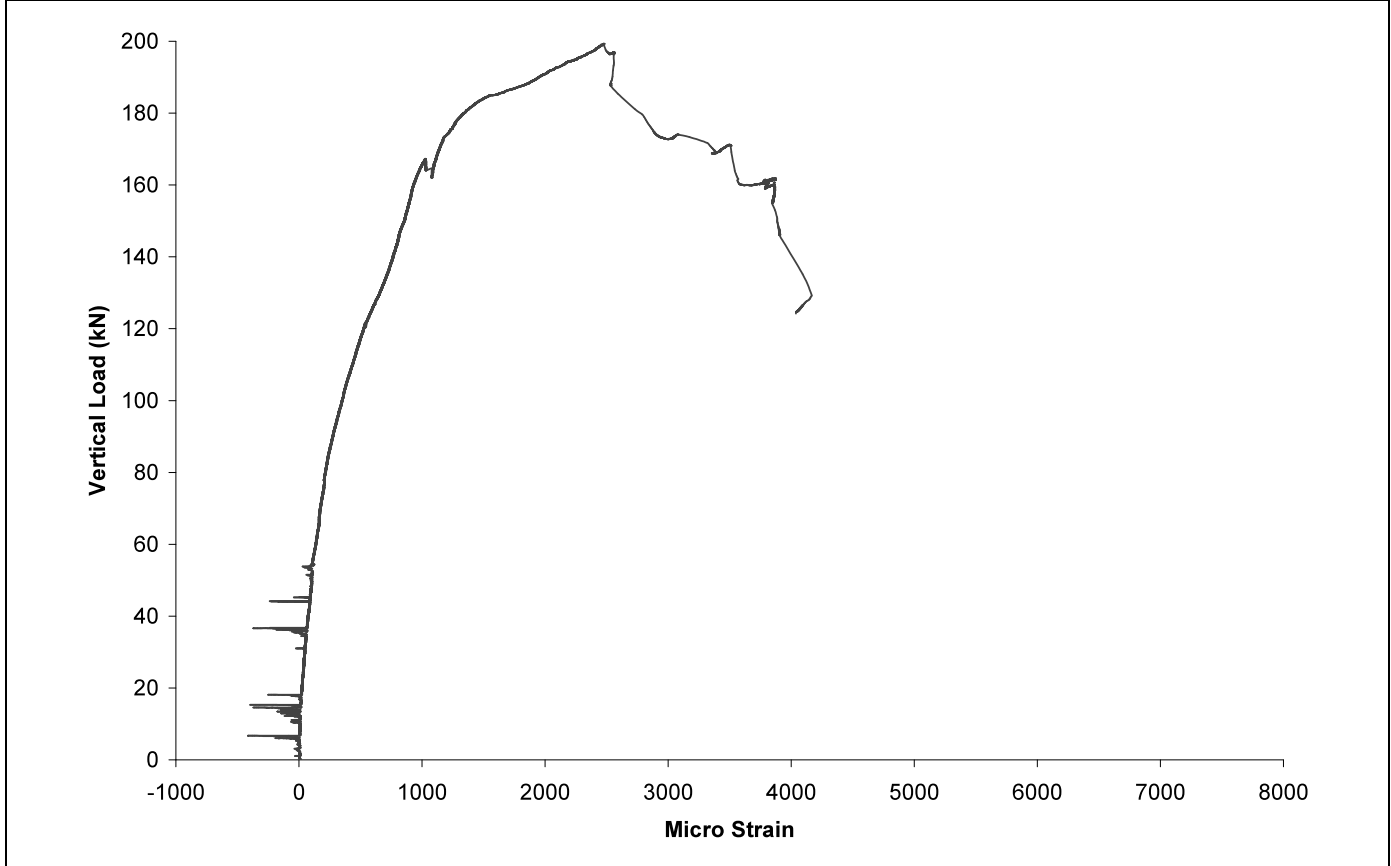
Figure A-8: Slab SN1, Strain vs. Vertical Load, Bolt #5
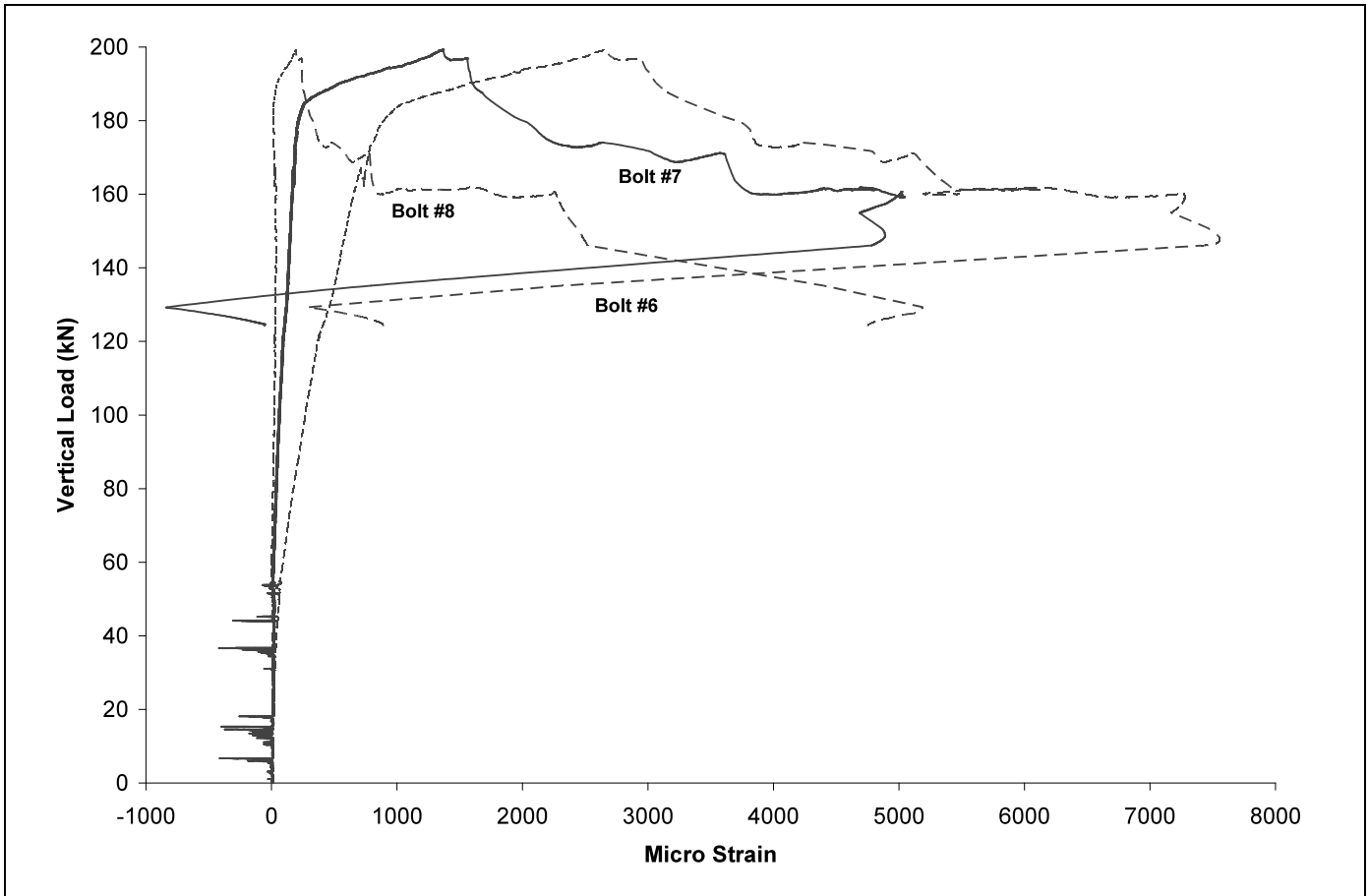
Figure A-9: Slab SN1, Strain vs. Vertical Load, Bolt #6, #7, #8
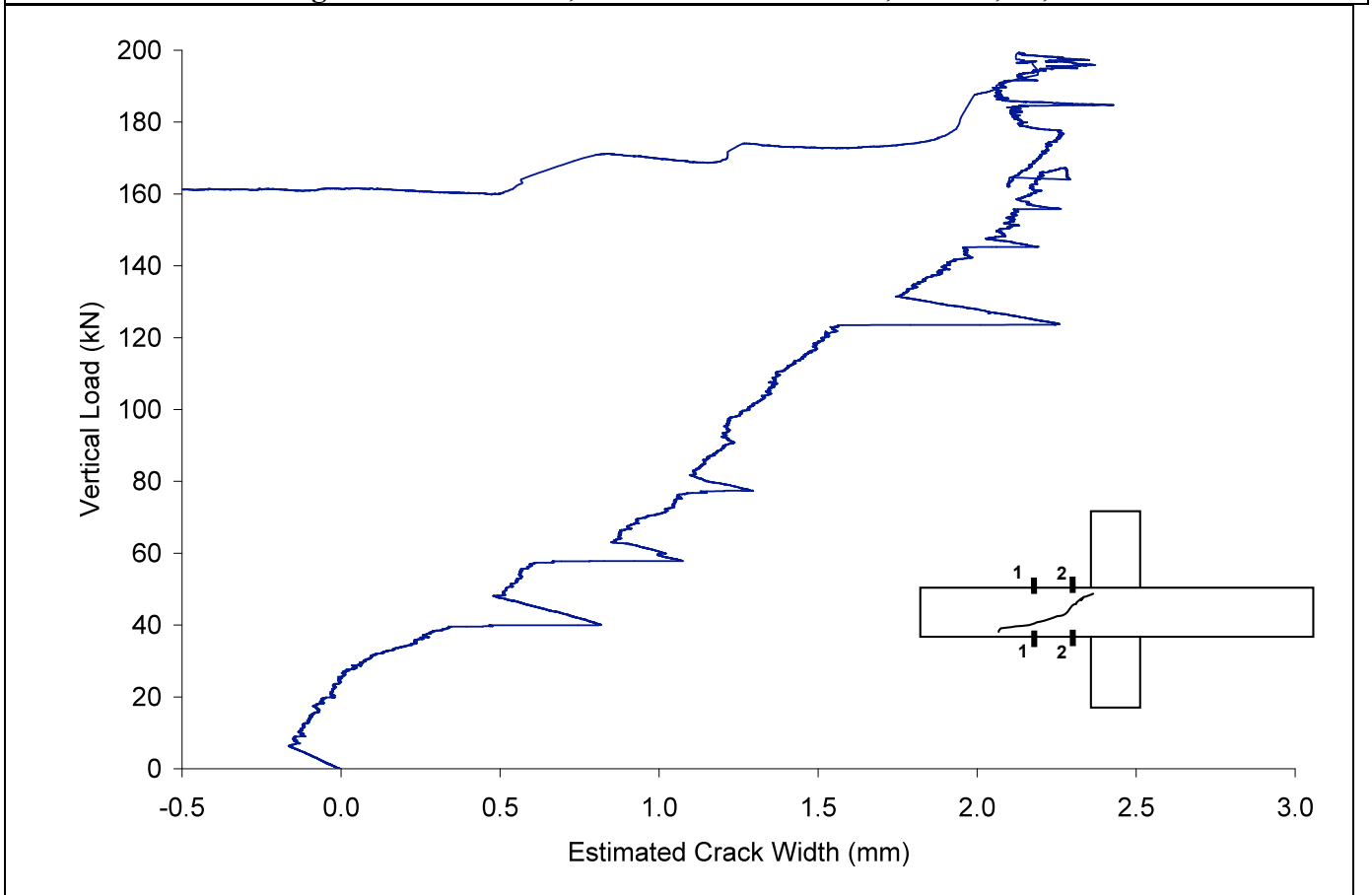
Figure A-10: Slab SN1, Estimated Crack Width vs. Vertical Load, Location 2-2
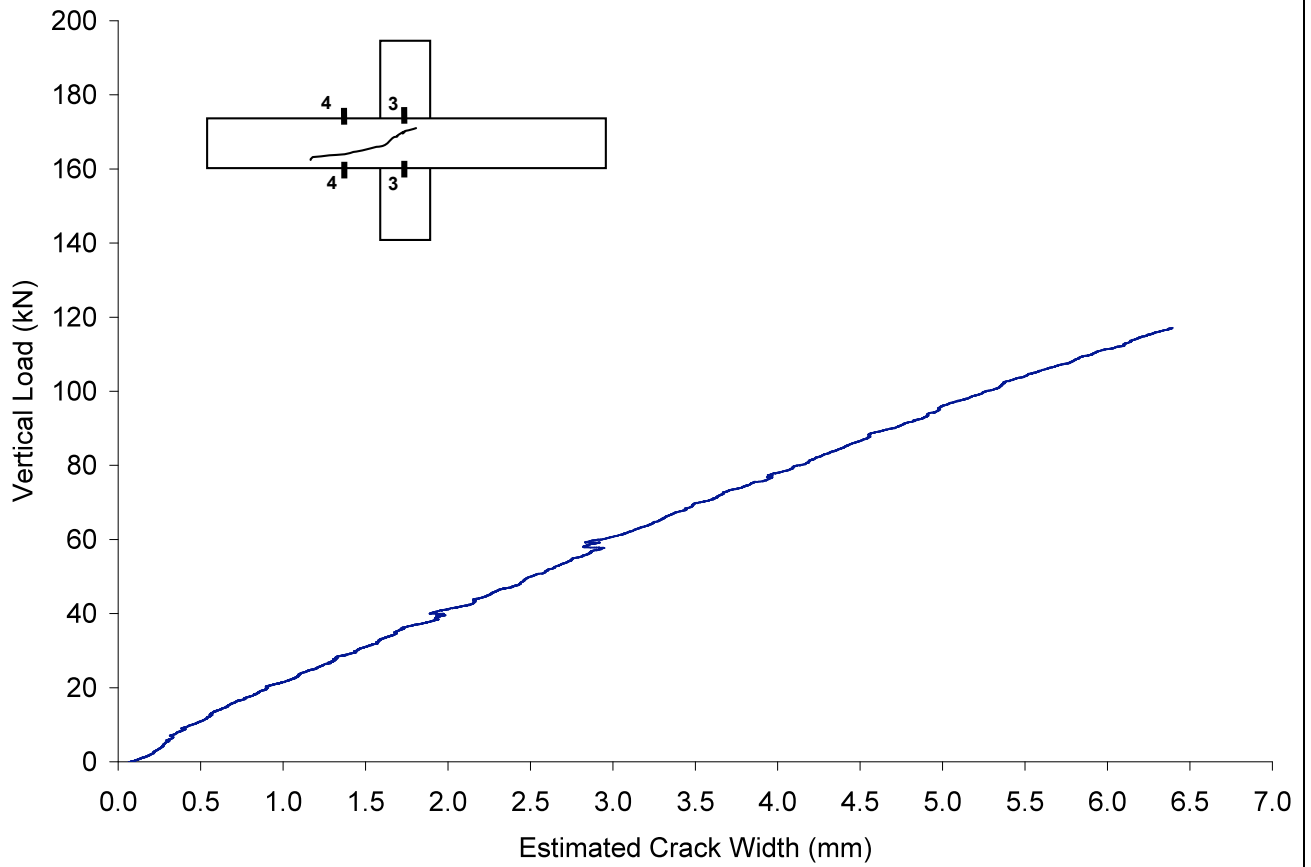
Figure A-11: Slab SN1, Estimated Crack Width vs. Vertical Load, Location 3-3
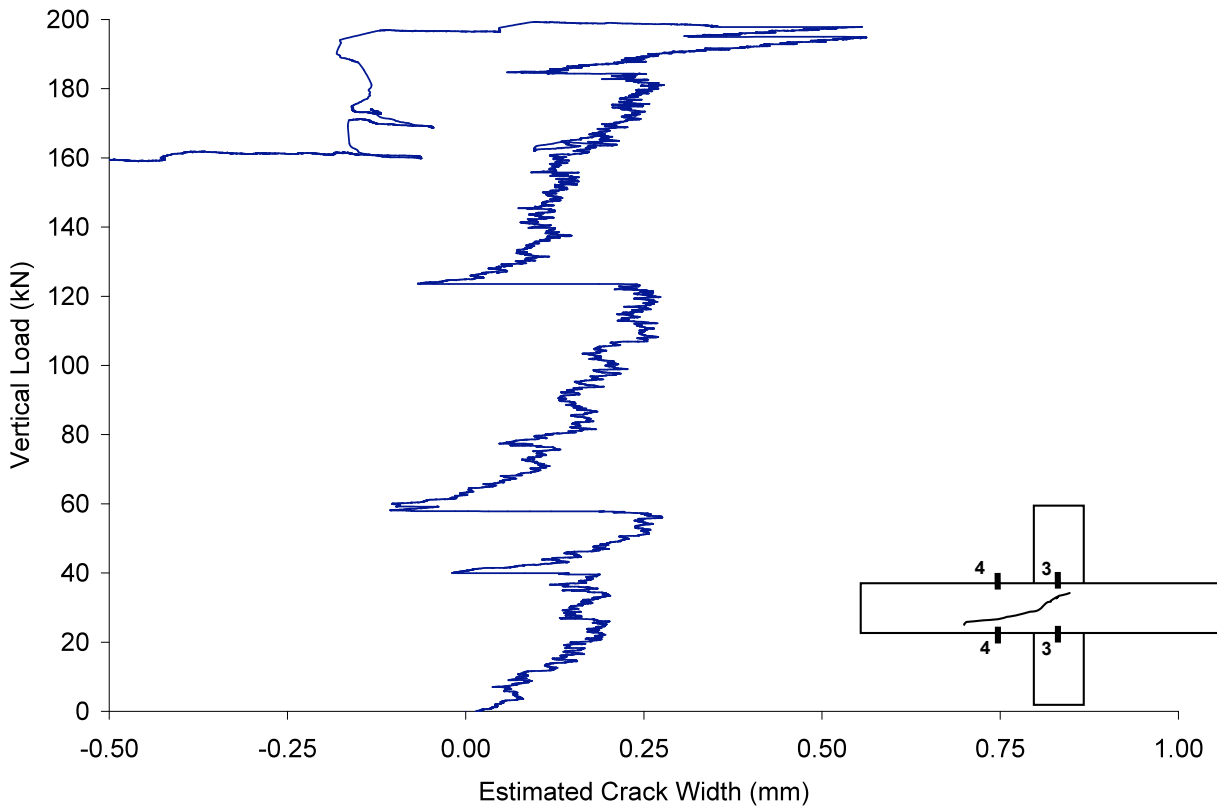
Figure A-12: Slab SN1, Estimated Crack Width vs. Vertical Load, Location 4-4

111

Appendix B – Data from SN2
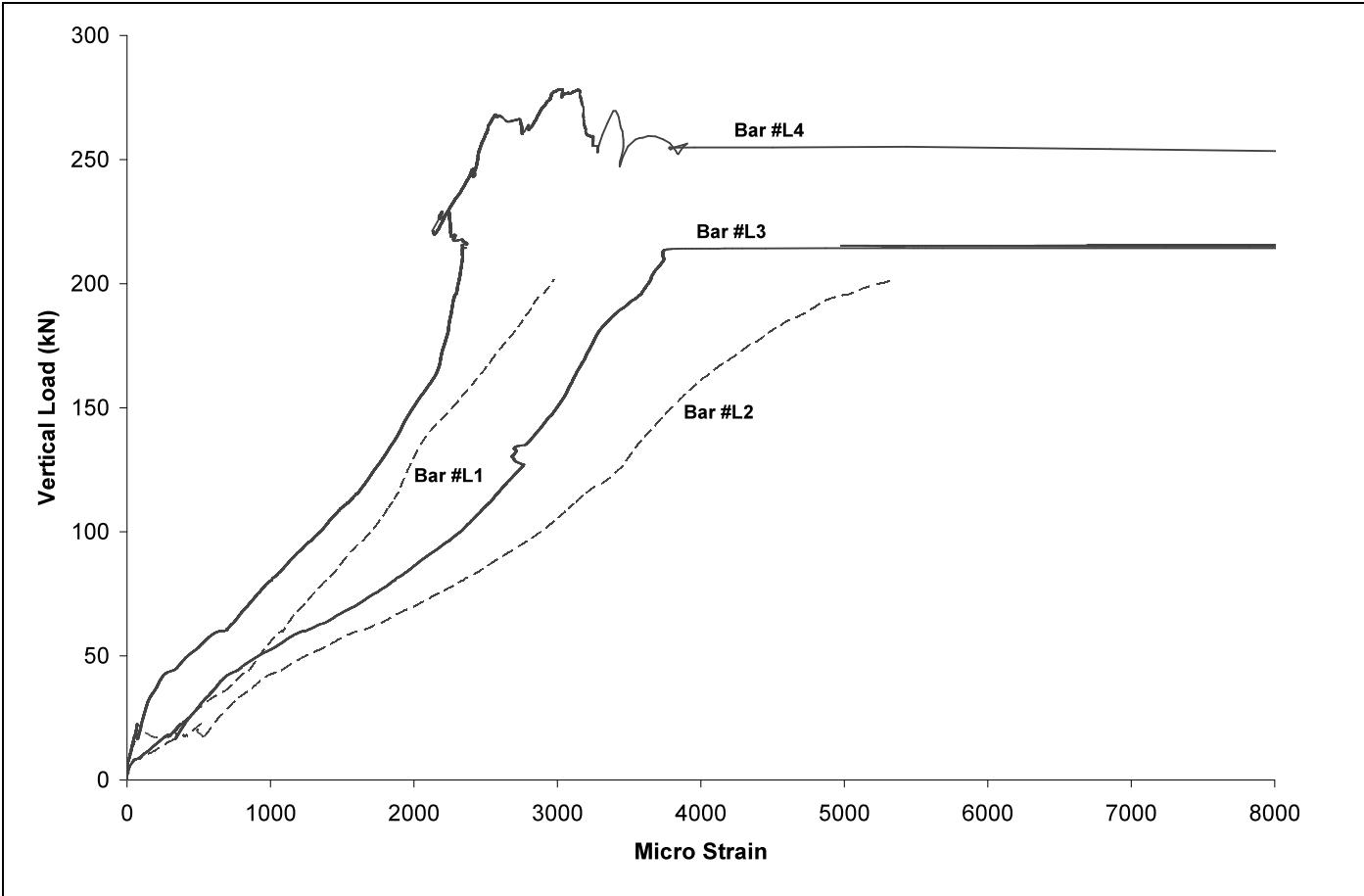
Figure B-1: Slab SN2, Strain vs. Vertical Load, L1, L2, L3, L4
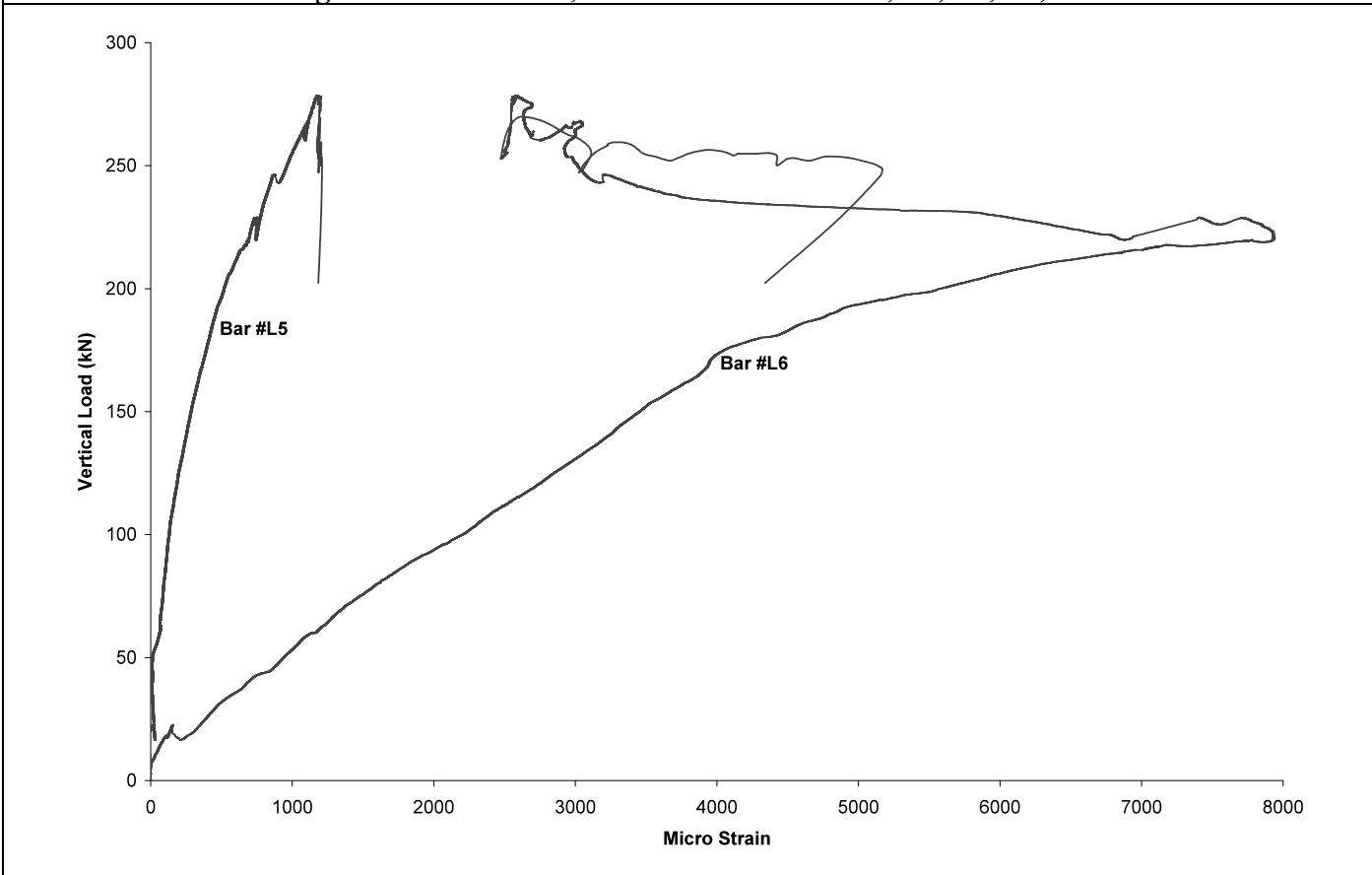
Figure B-2: Slab SN2, Strain vs. Vertical Load, L5, L6

113
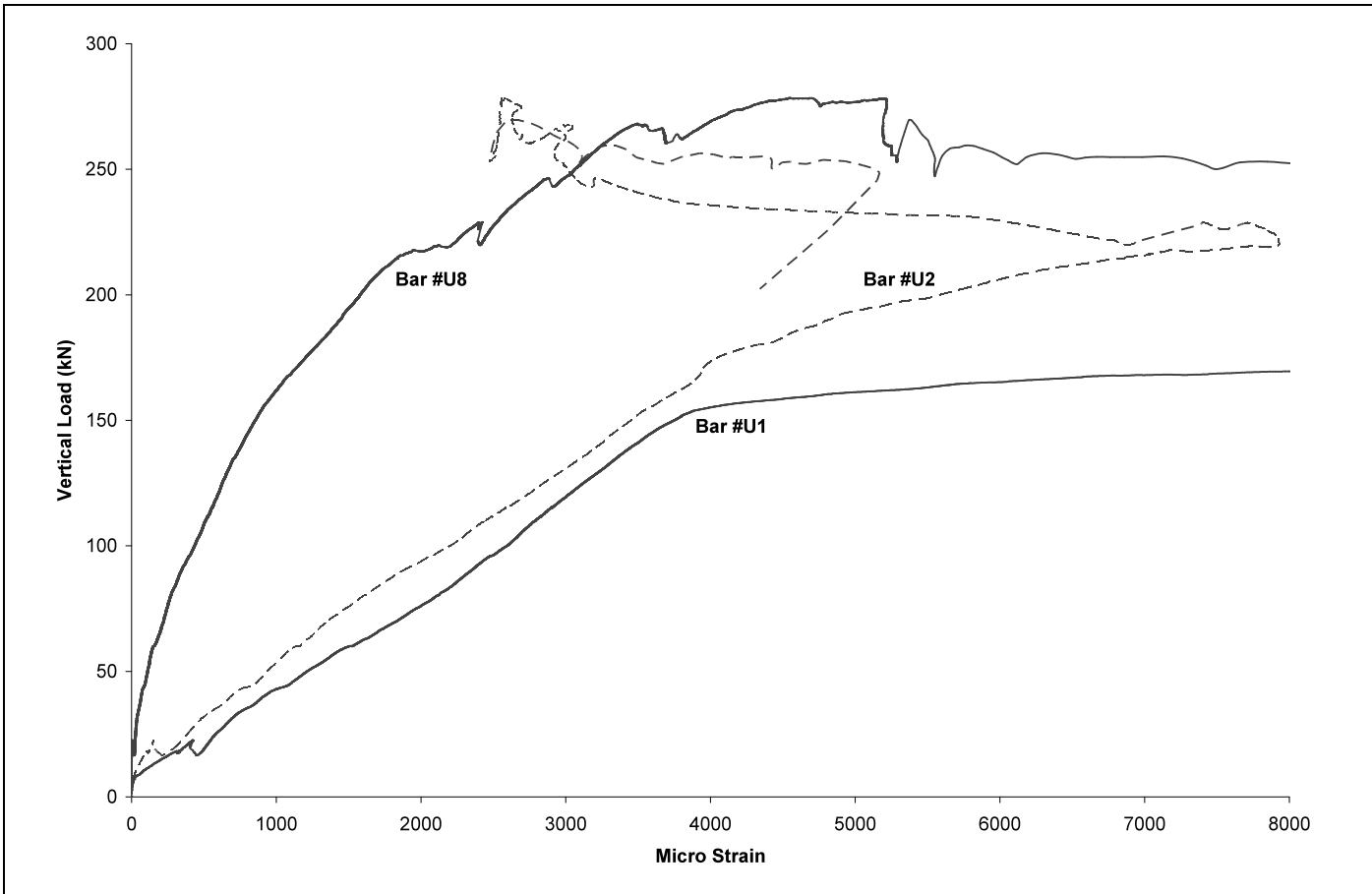
Figure B-3: Slab SN2, Strain vs. Vertical Load, U1, U2, U8
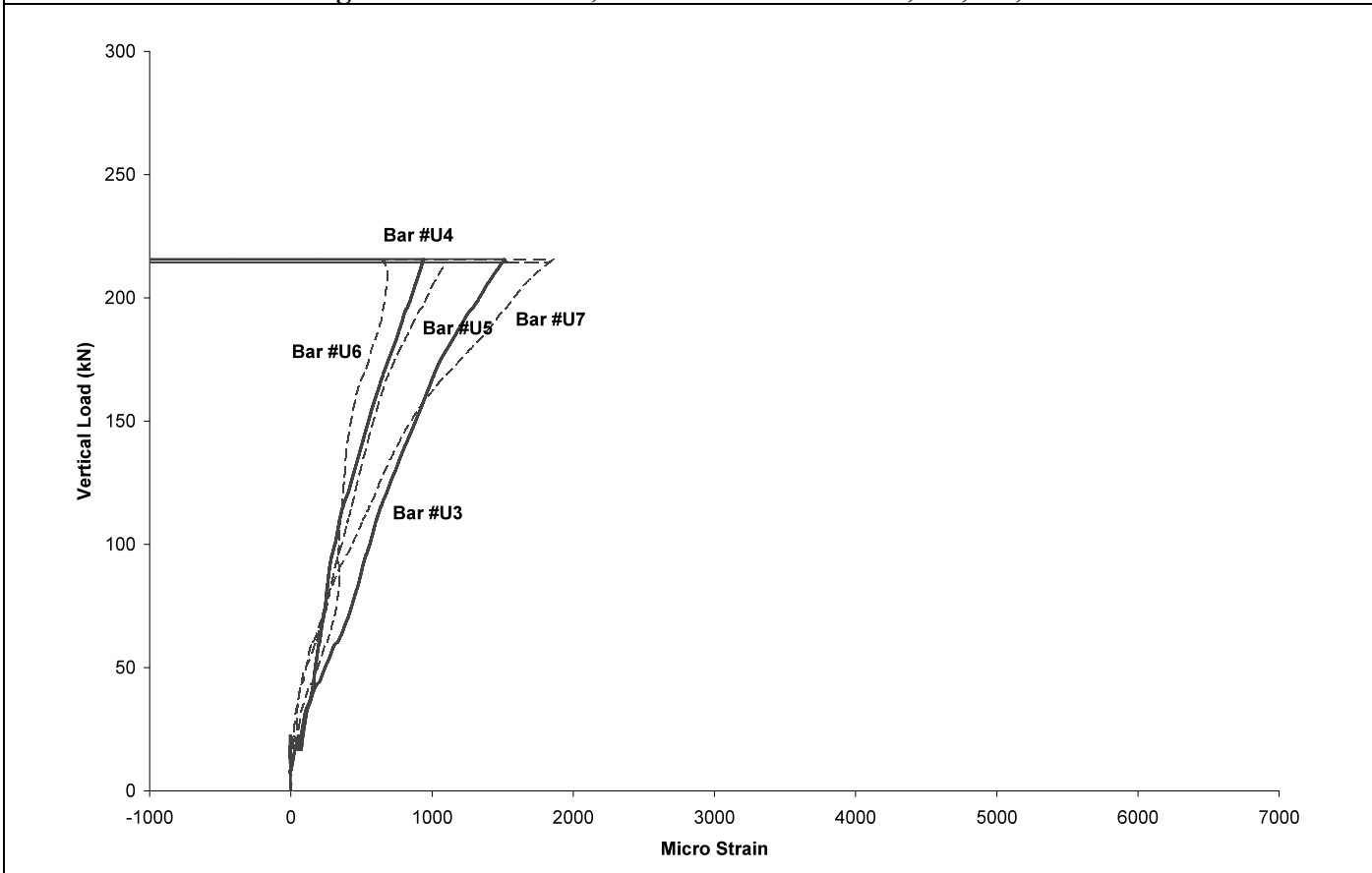
Figure B-4: Slab SN2, Strain vs. Vertical Load, U3, U4, U5, U6

114
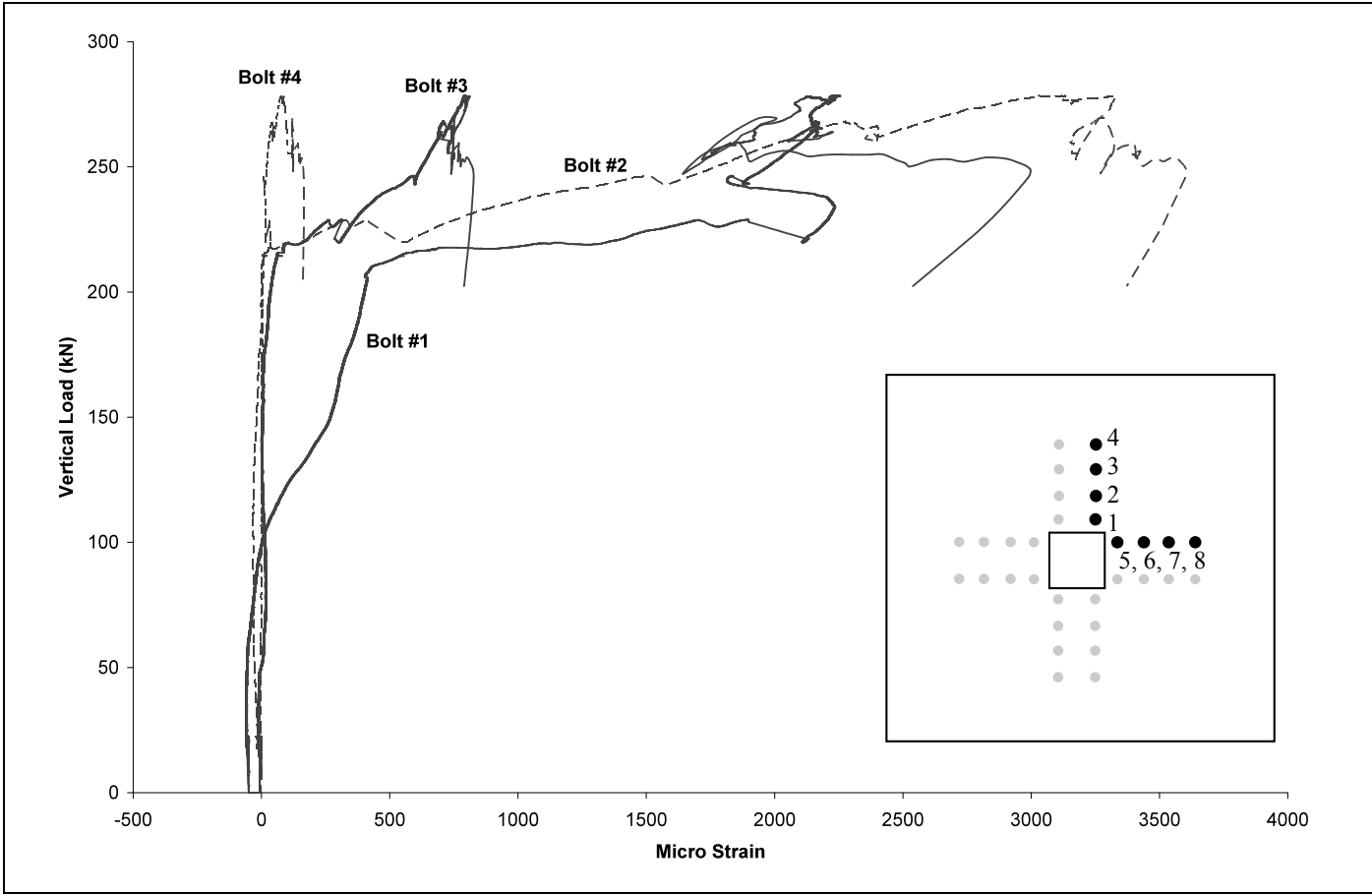
Figure B-5: Slab SN2, Strain vs. Vertical Load, Bolt #1, #2, #3, #4
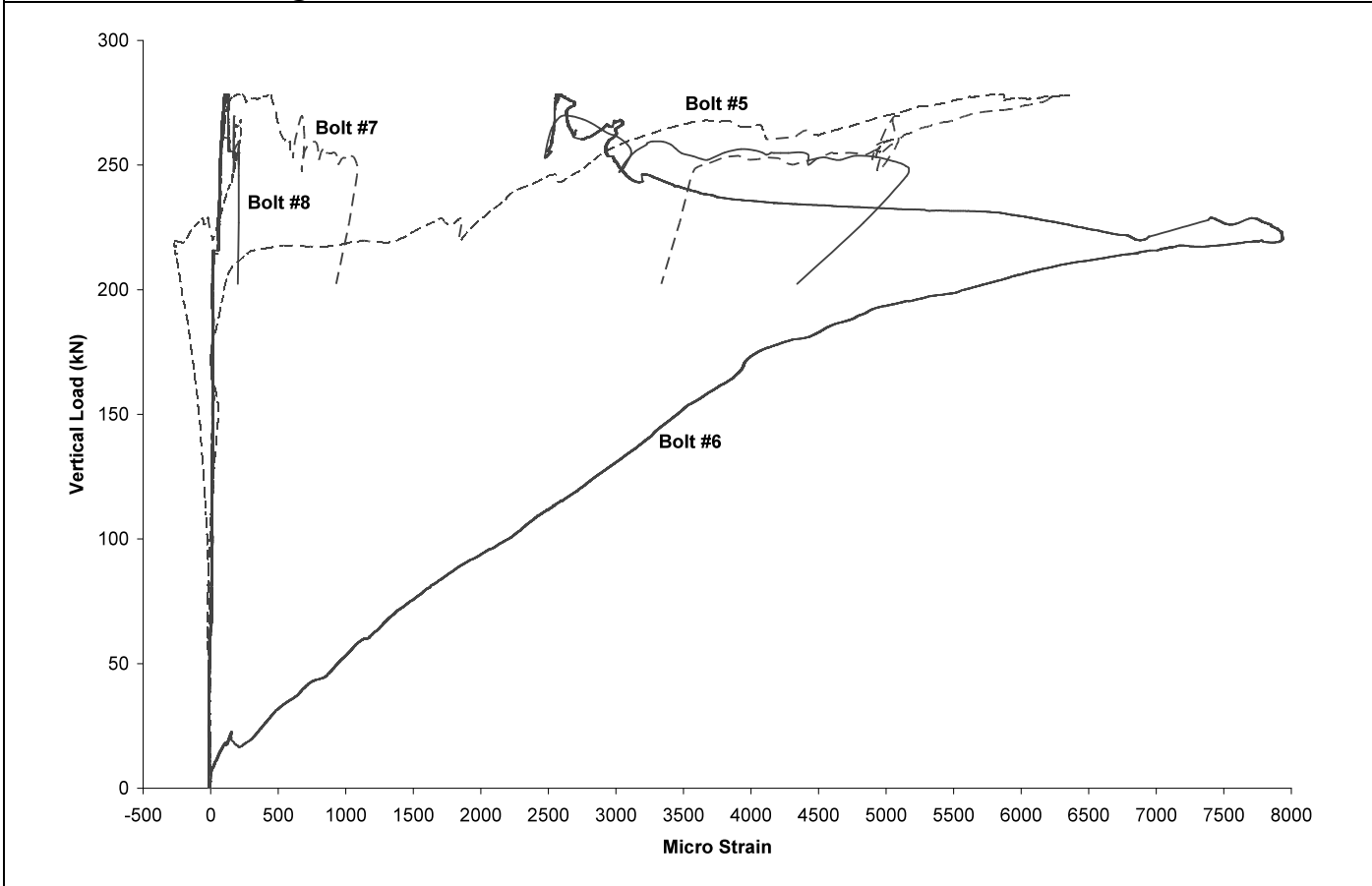
Figure B-6: Slab SN2, Strain vs. Vertical Load, Bolt #5, #6, #7, #8

115
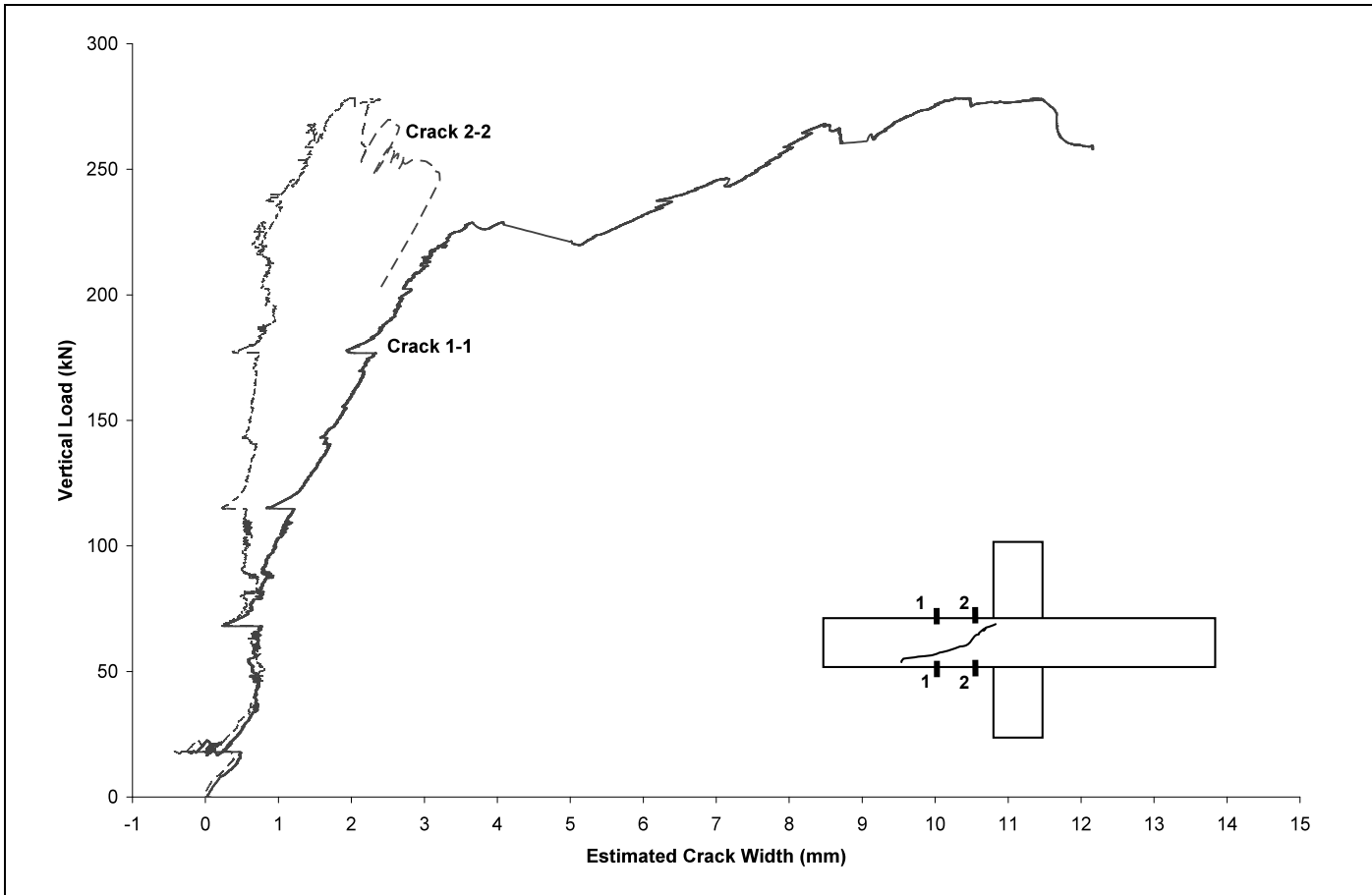
Figure B-7: Slab SN2, Estimated Crack Width vs. Vertical Load, Location 1-1, 2-2
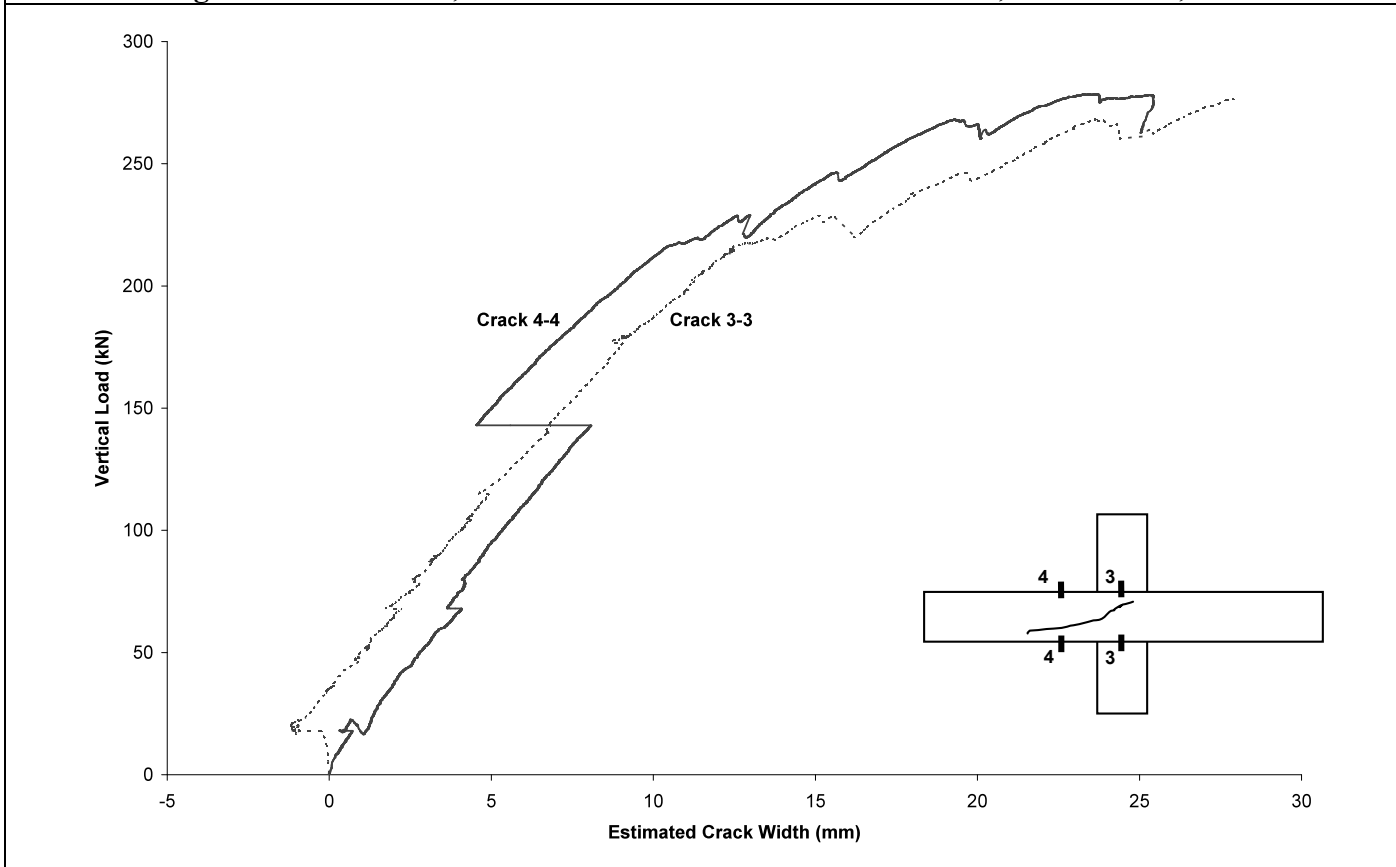
Figure B-8: Slab SN2, Estimated Crack Width vs. Vertical Load, Location 3-3, 4-4

116

Appendix C – Data from SN3
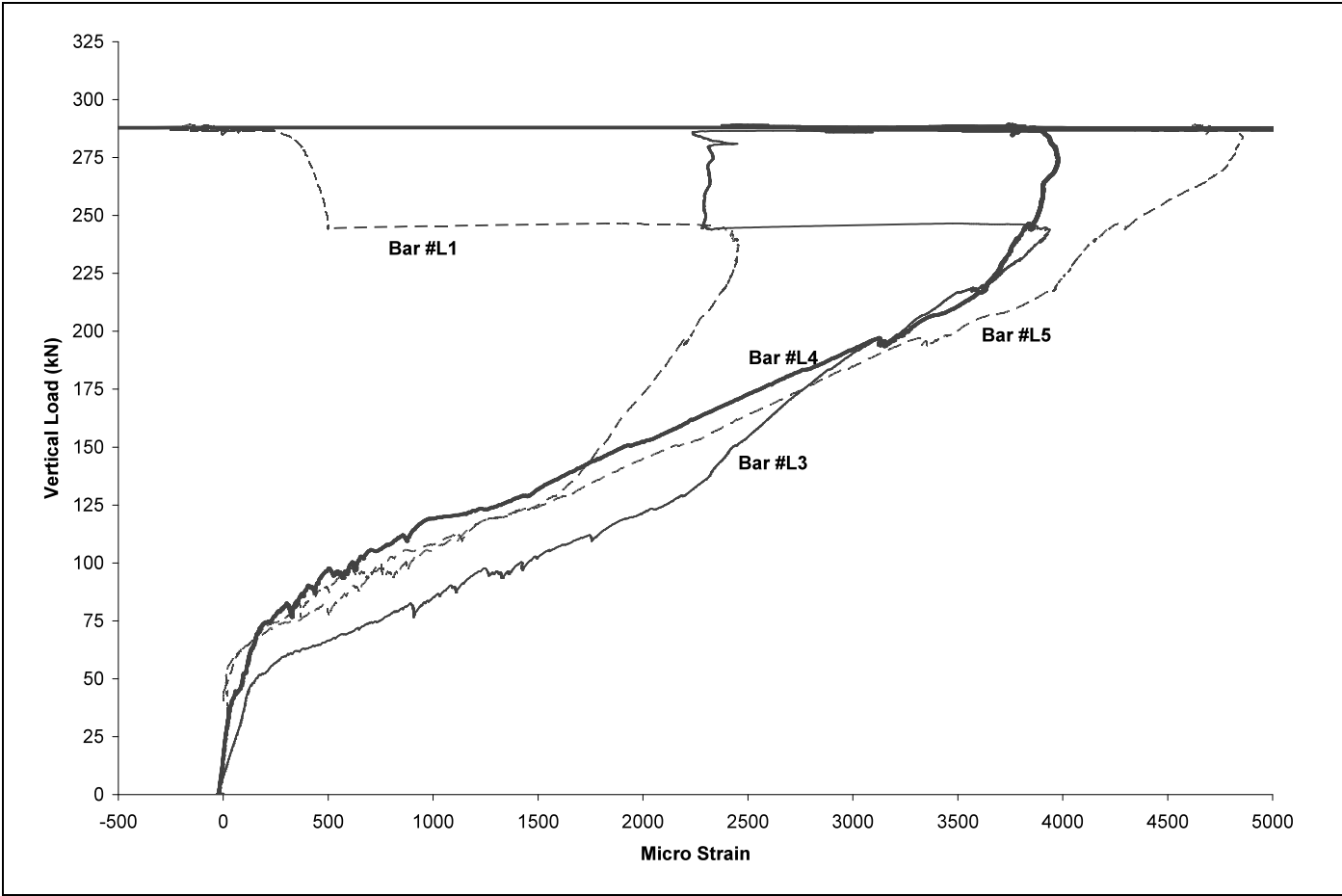
Figure C-1: Slab SN3, Strain vs. Vertical Load, L1, L3, L4, L5
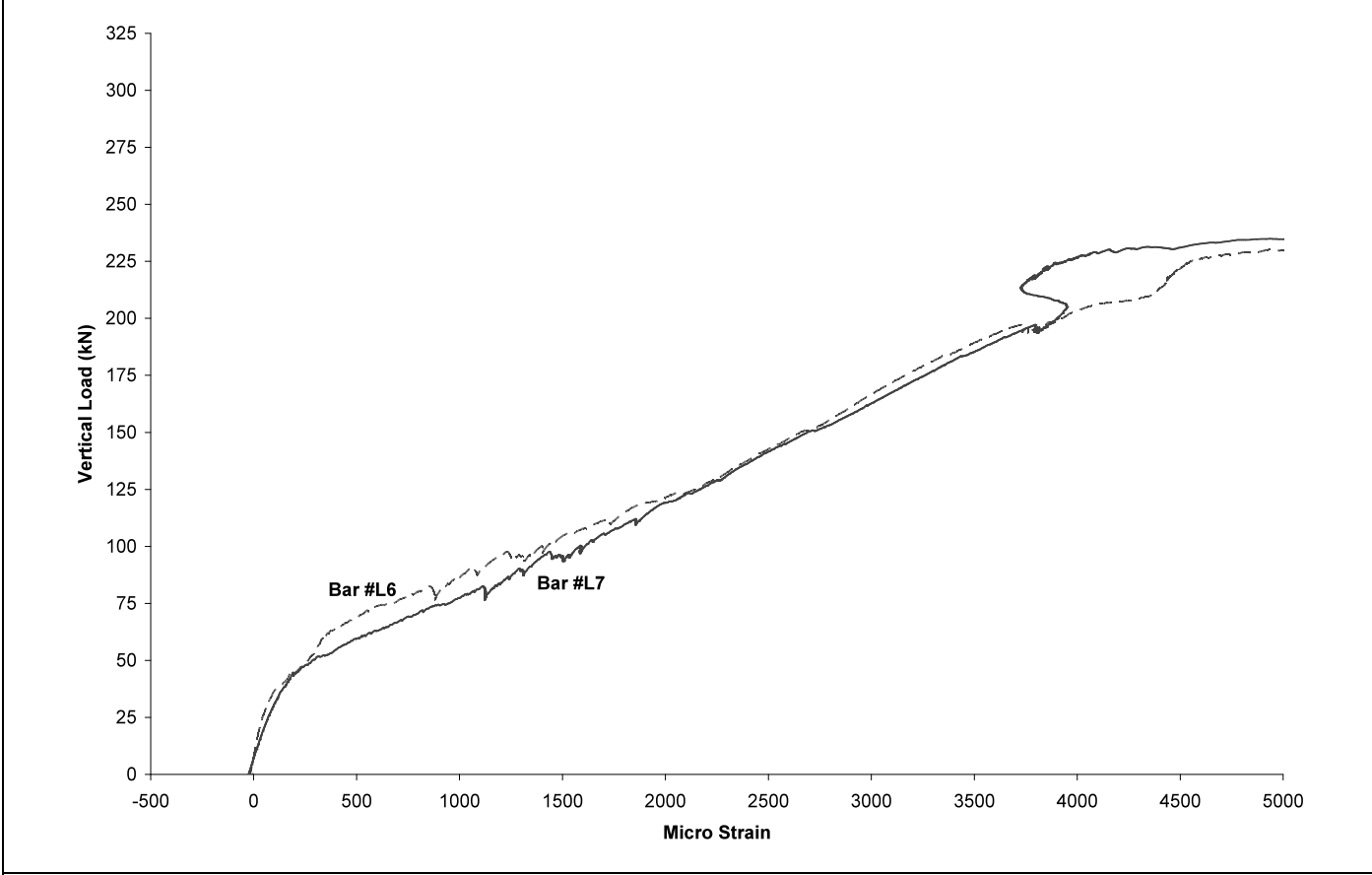
Figure C-2: Slab SN3, Strain vs. Vertical Load, L6, L7

118
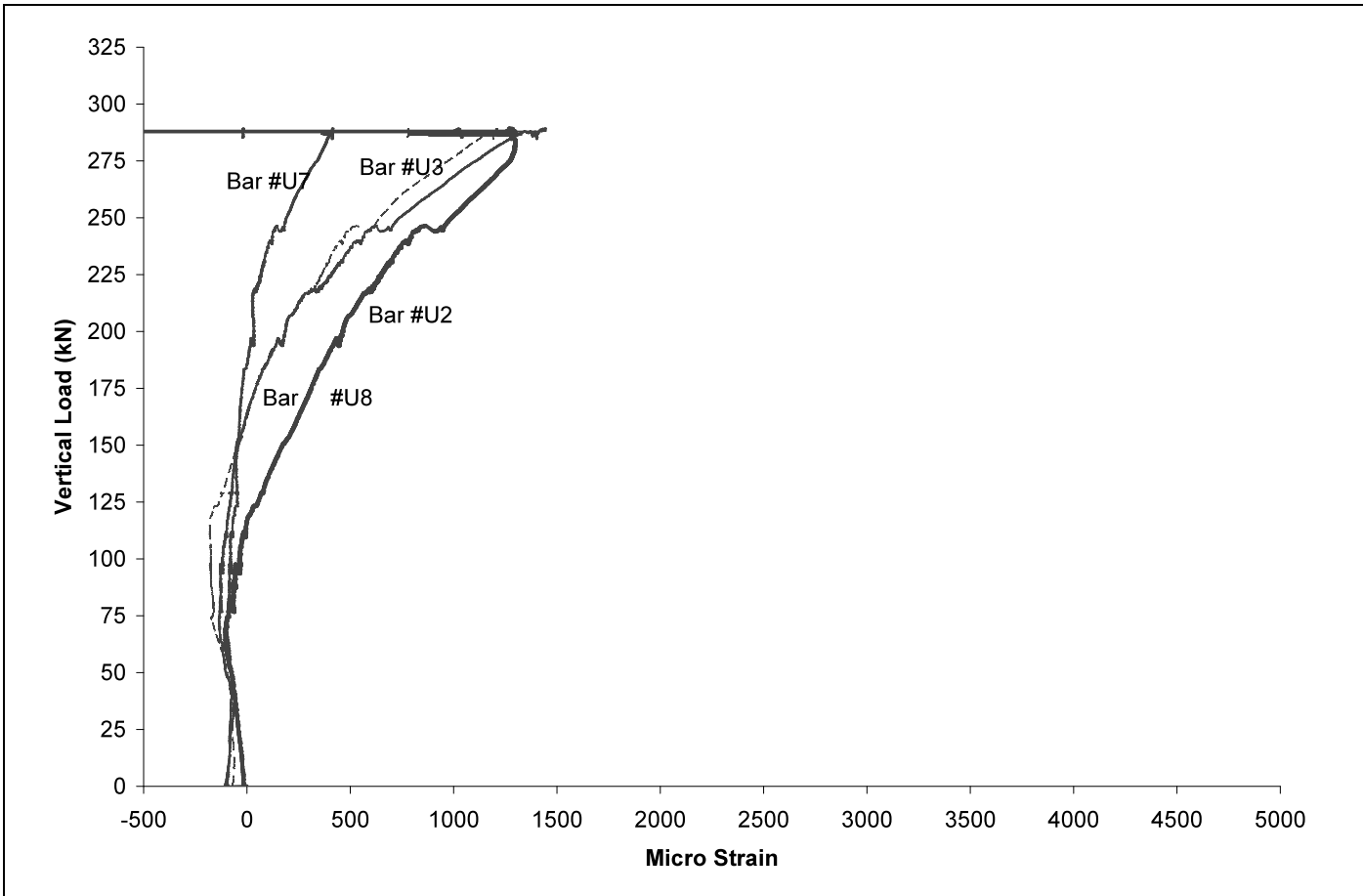
Figure C-3: Slab SN3, Strain vs. Vertical Load, U2, U3, U7, U8
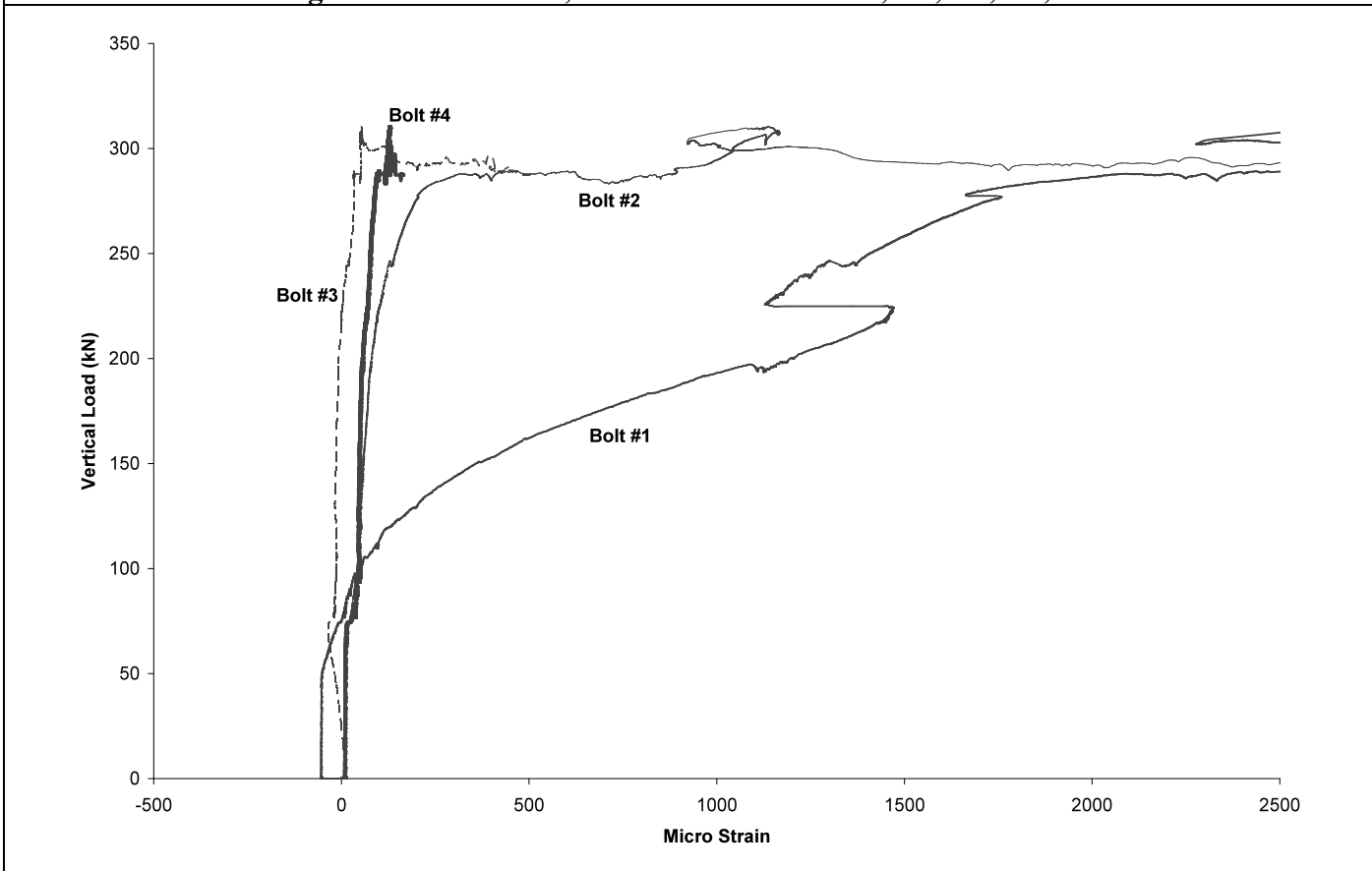
Figure C-4: Slab SN3, Strain vs. Vertical Load, Bolt #1, #2, #3, #4
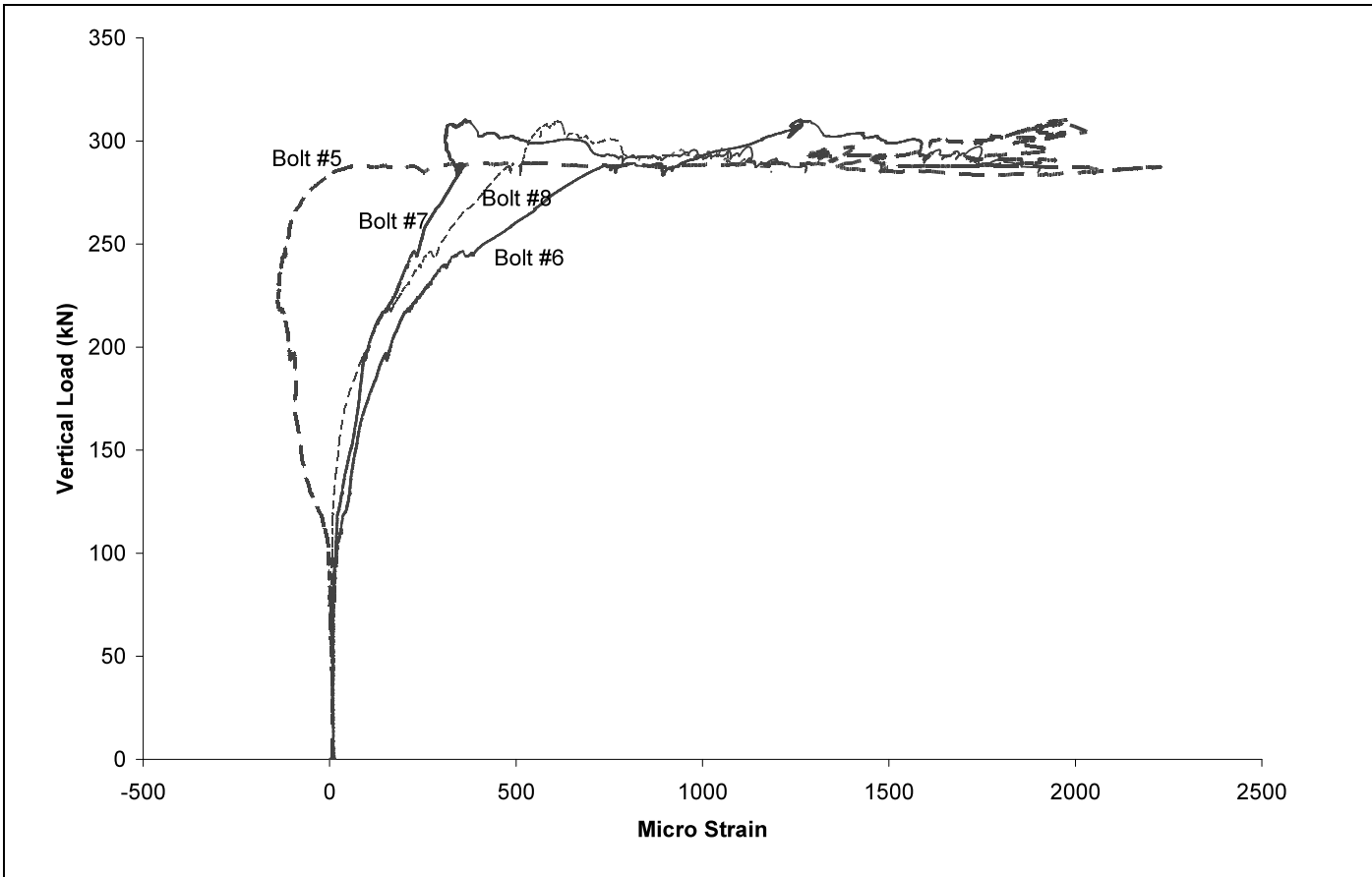
Figure C-5: Slab SN3, Strain vs. Vertical Load, Bolt #5, #6, #7, #8
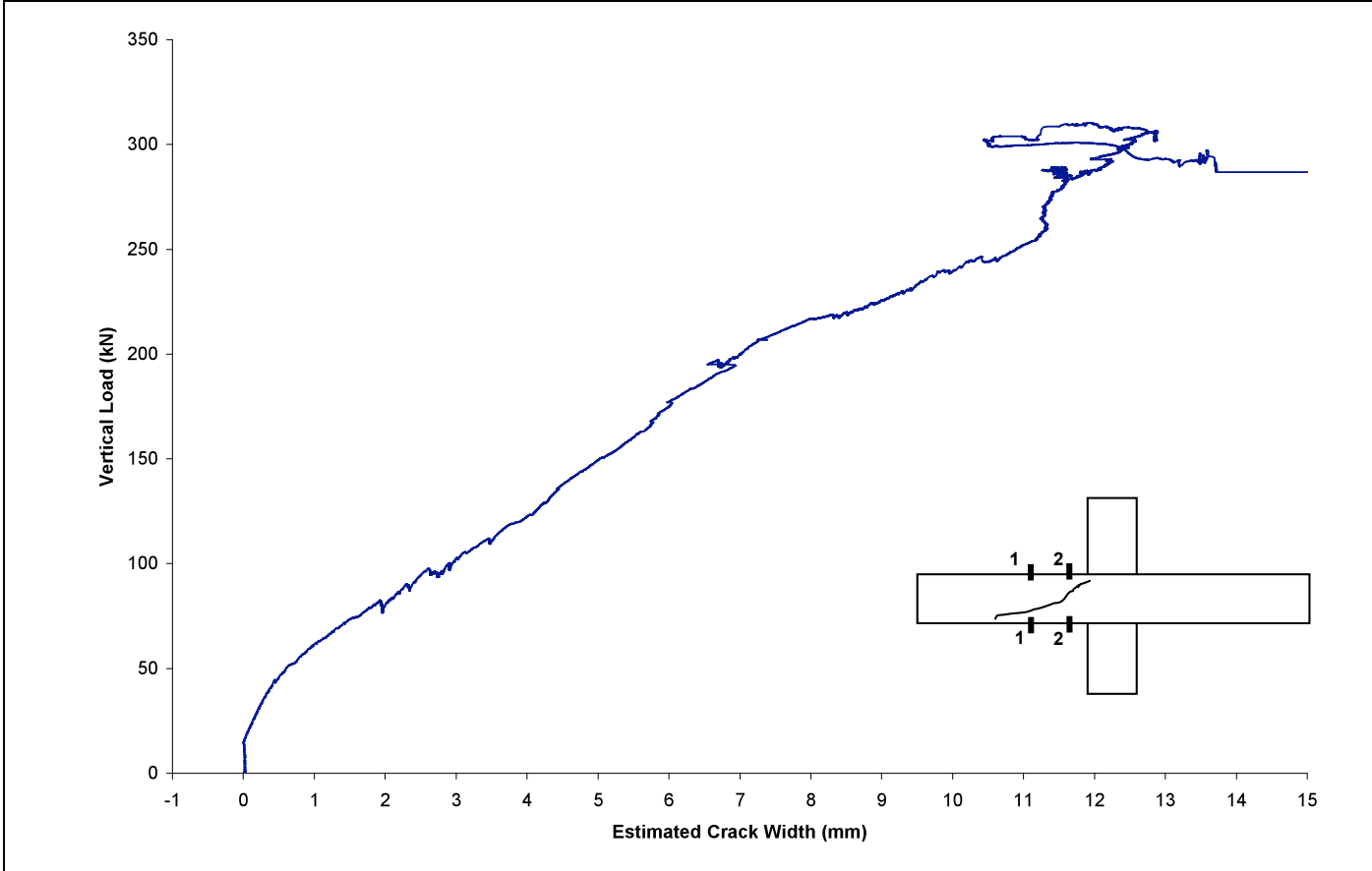
Figure C-6: Slab SN3, Estimated Crack Width vs. Vertical Load, Location 1-1
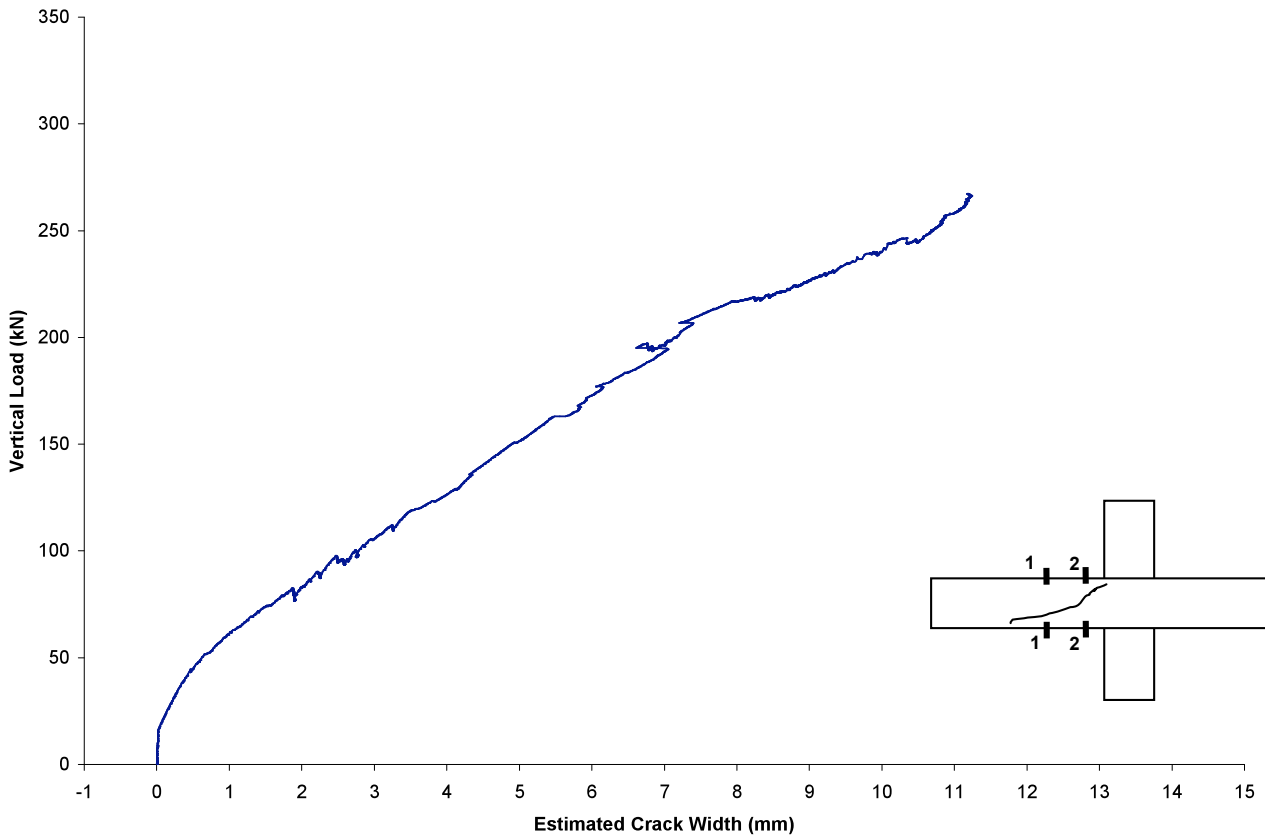
Figure C-7: Slab SN3, Estimated Crack Width vs. Vertical Load, Location 2-2
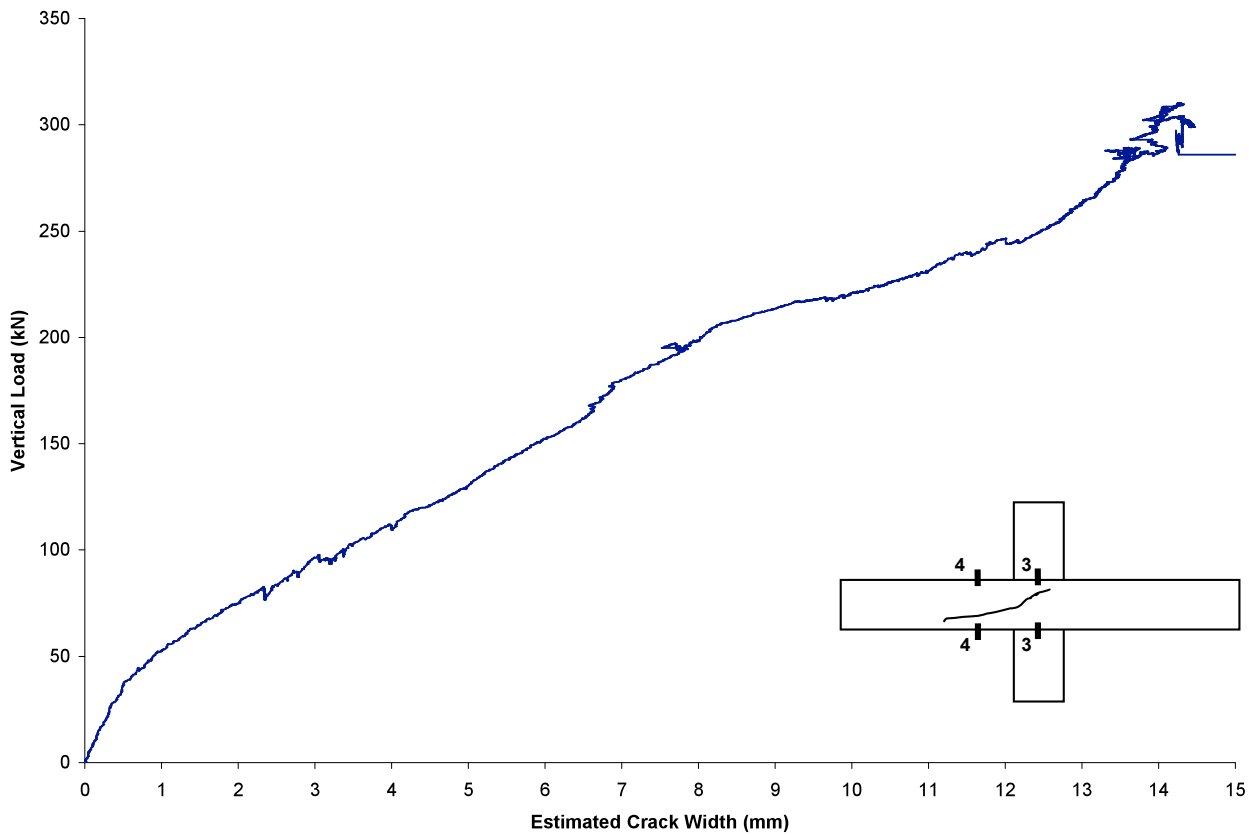
Figure C-8: Slab SN3, Estimated Crack Width vs. Vertical Load, Location 4-4

121

Appendix D – Data from SN4
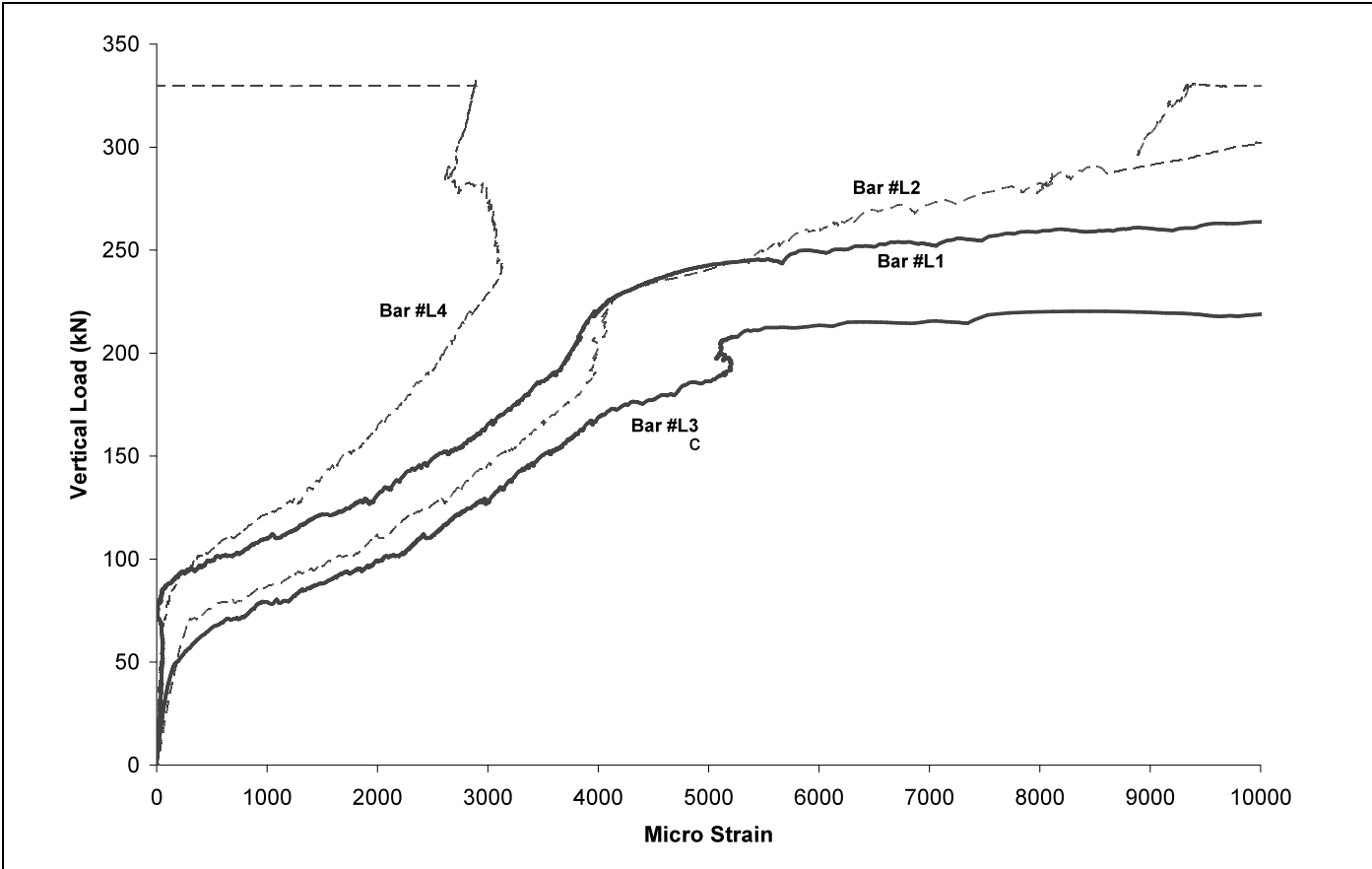
Figure D-1: Slab SN4, Strain vs. Vertical Load, L1, L2, L3, L4
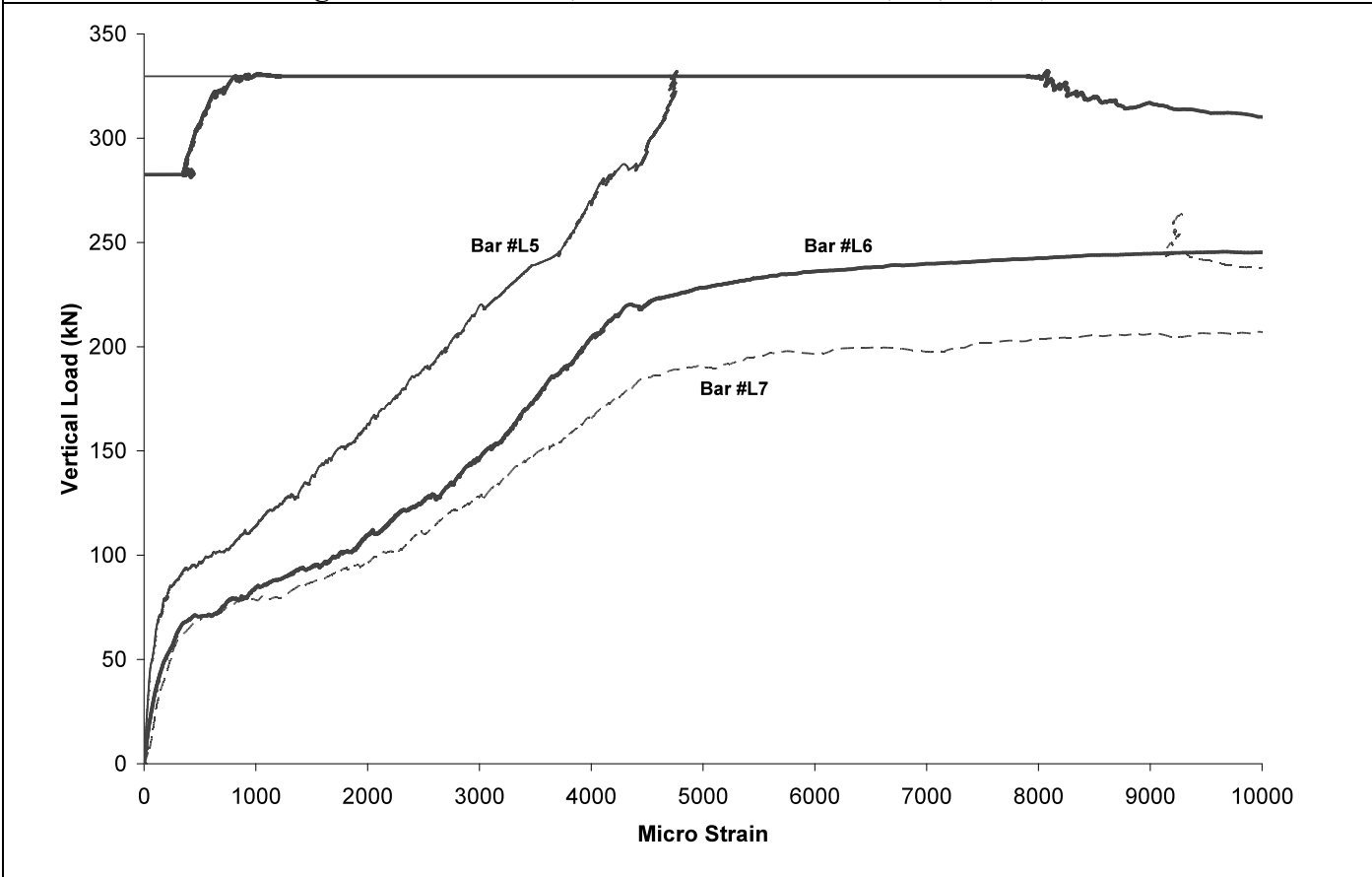
Figure D-2: Slab SN4, Strain vs. Vertical Load, L5, L6, L7

123
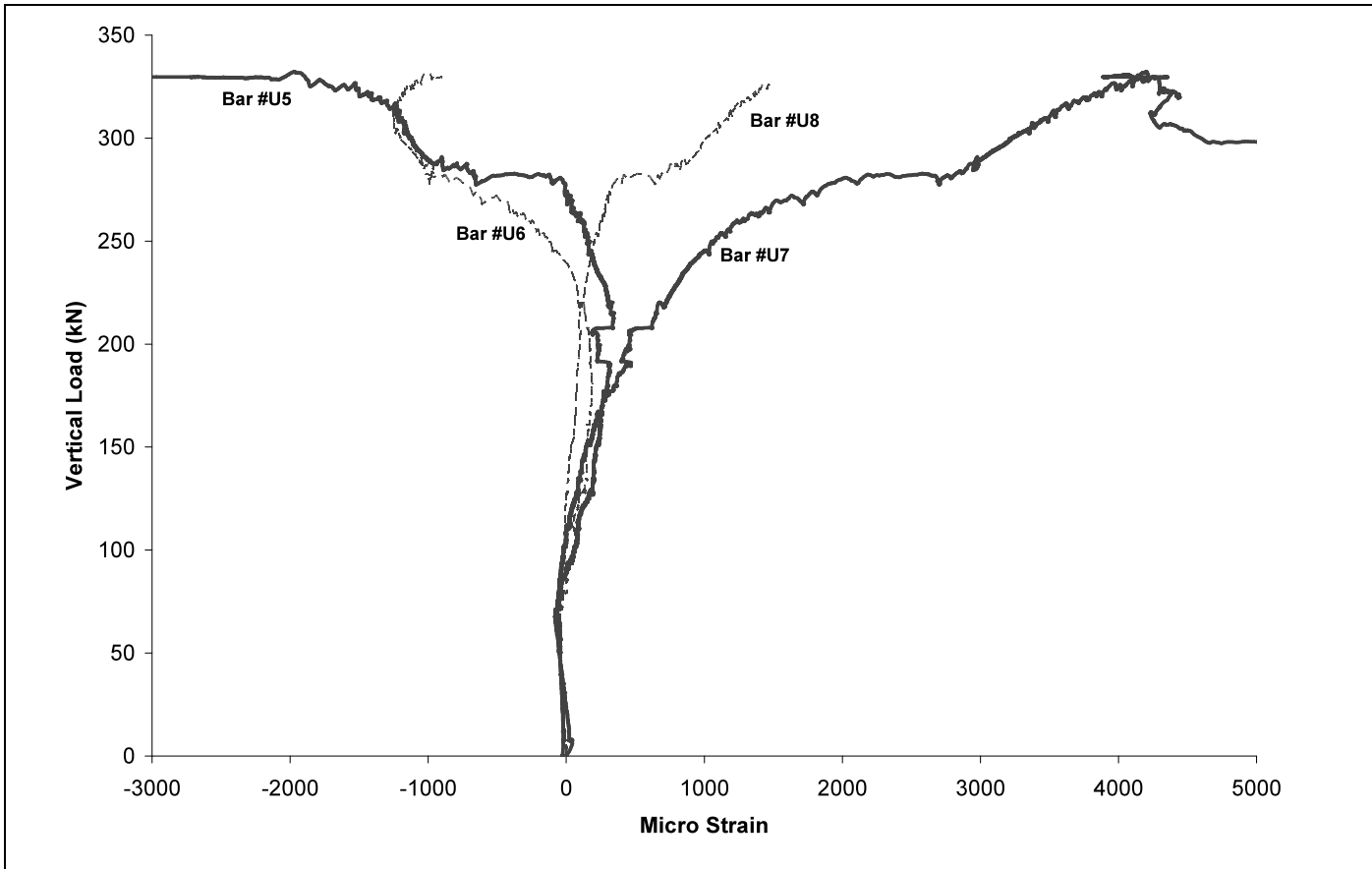
Figure D-3: Slab SN4, Strain vs. Vertical Load, U5, U6, U7, U8
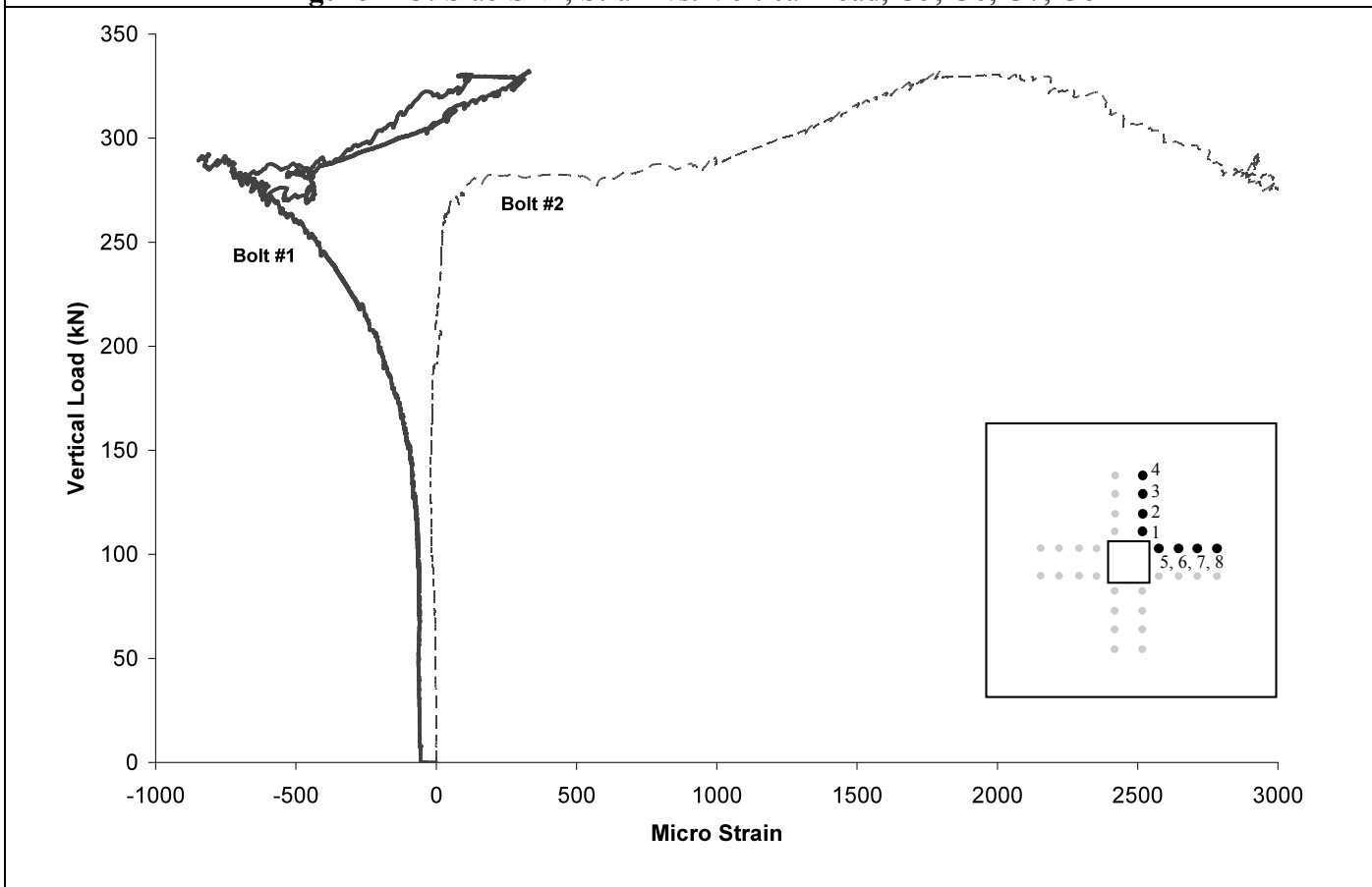
Figure D-4: Slab SN4, Strain vs. Vertical Load, Bolt #1, #2
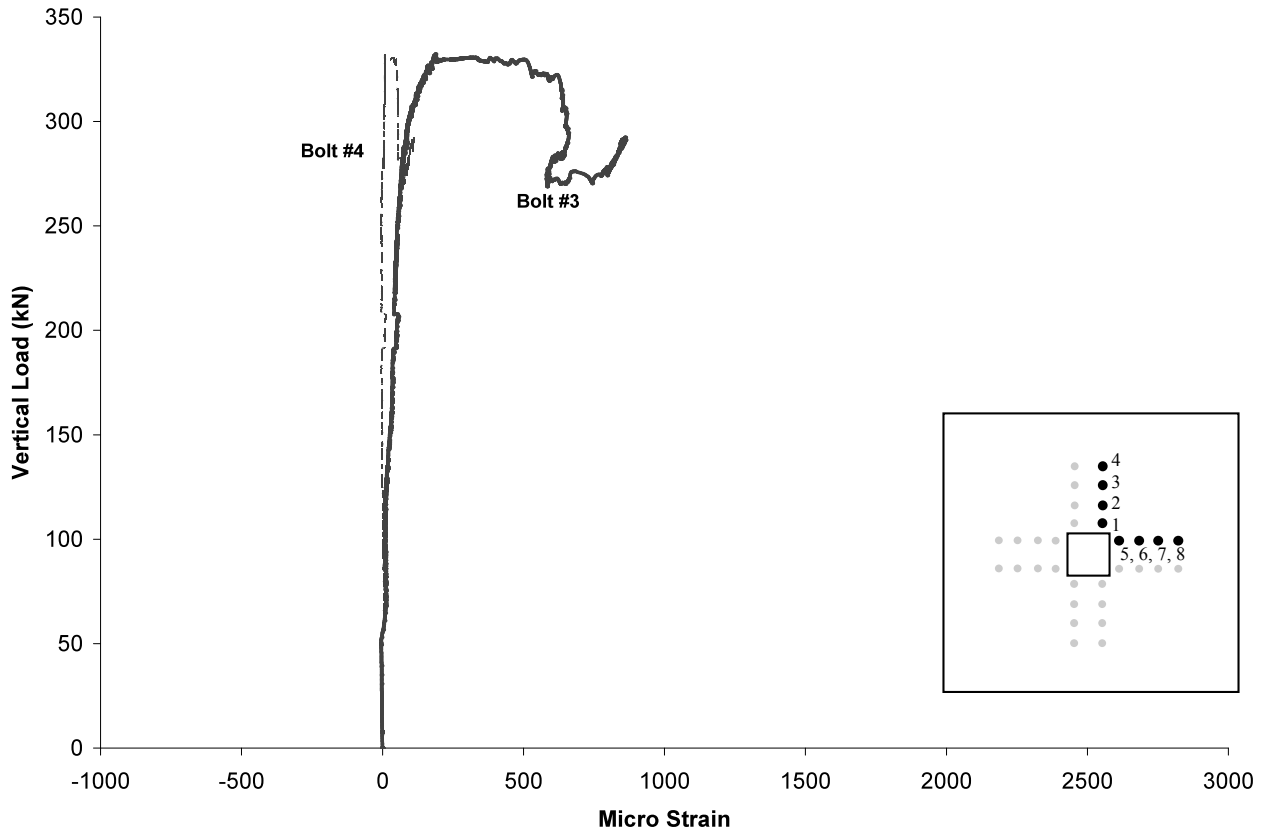
Figure D-5: Slab SN4, Strain vs. Vertical Load, Bolt #3, #4
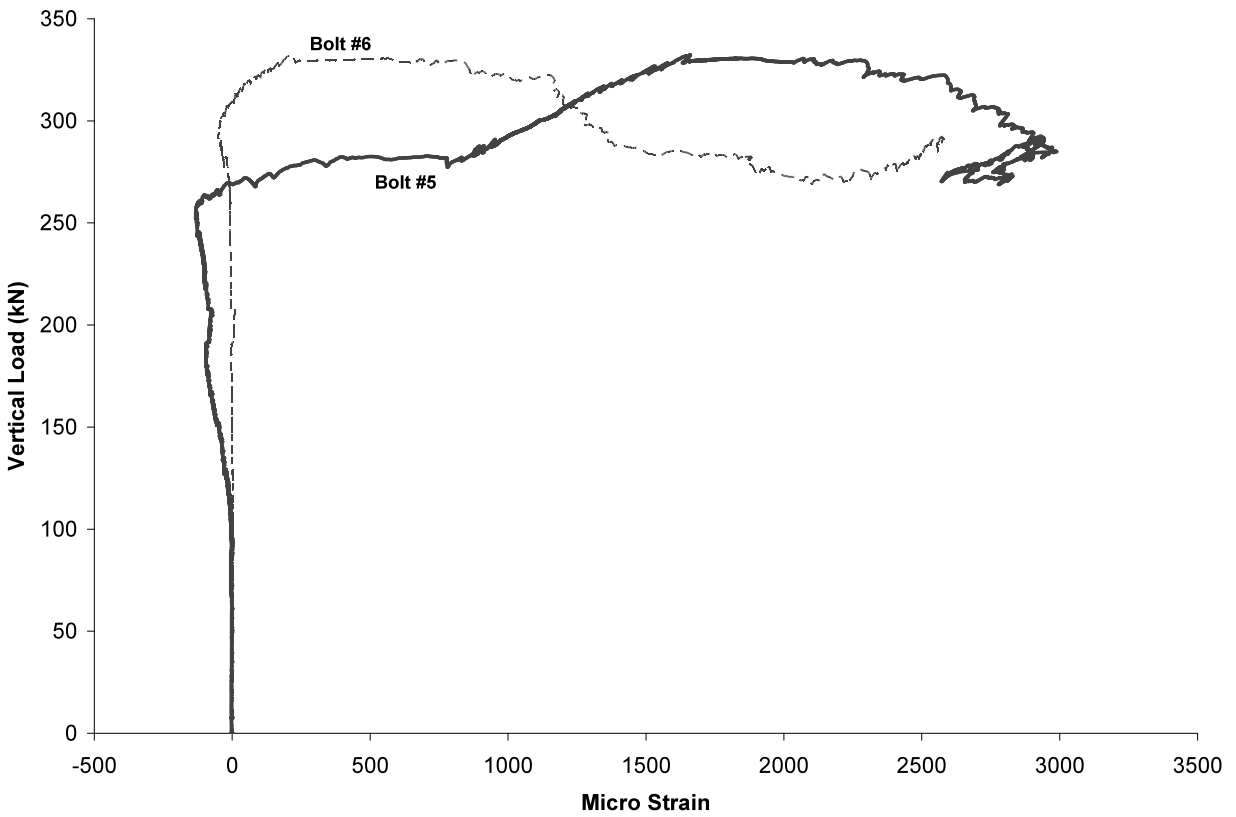
Figure D-6: Slab SN4, Strain vs. Vertical Load, Bolt #5, #6
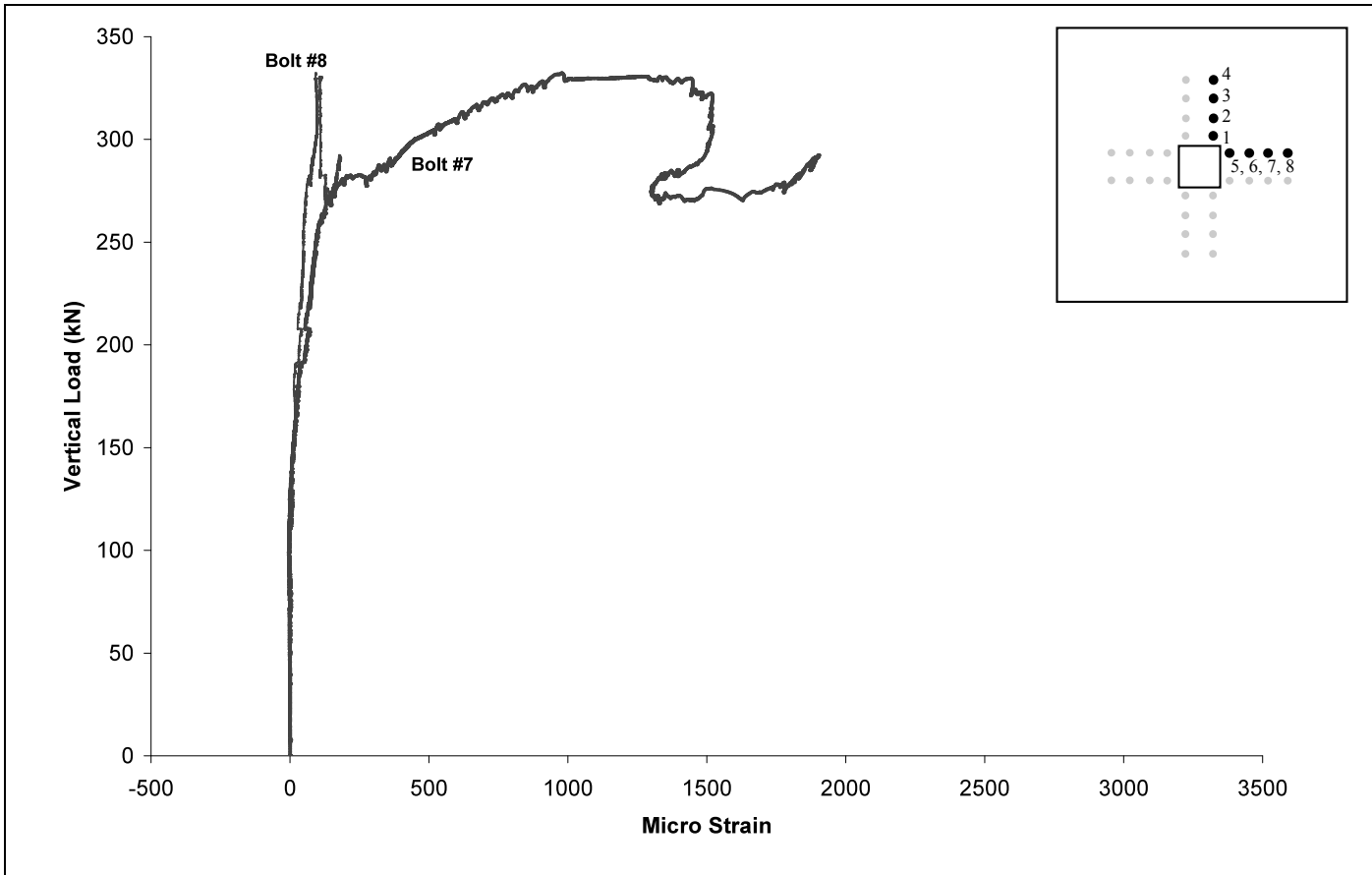
Figure D-7: Slab SN4, Strain vs. Vertical Load, Bolt #7, #8
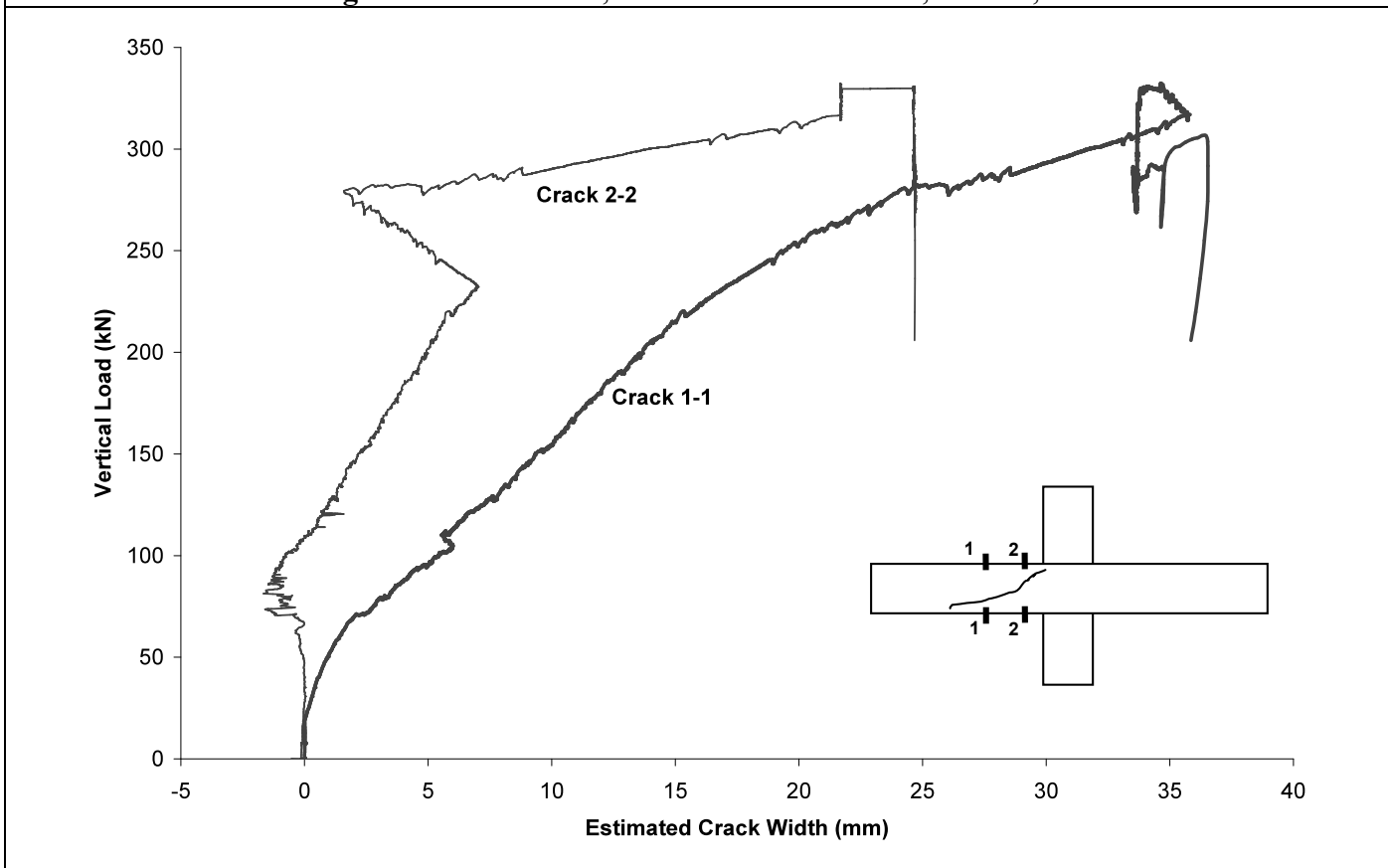
**Figure D-8:** Slab SN4, Estimated Crack Width vs. Vertical Load, Location 1-1, 2-2

Appendix E – Data from SN5
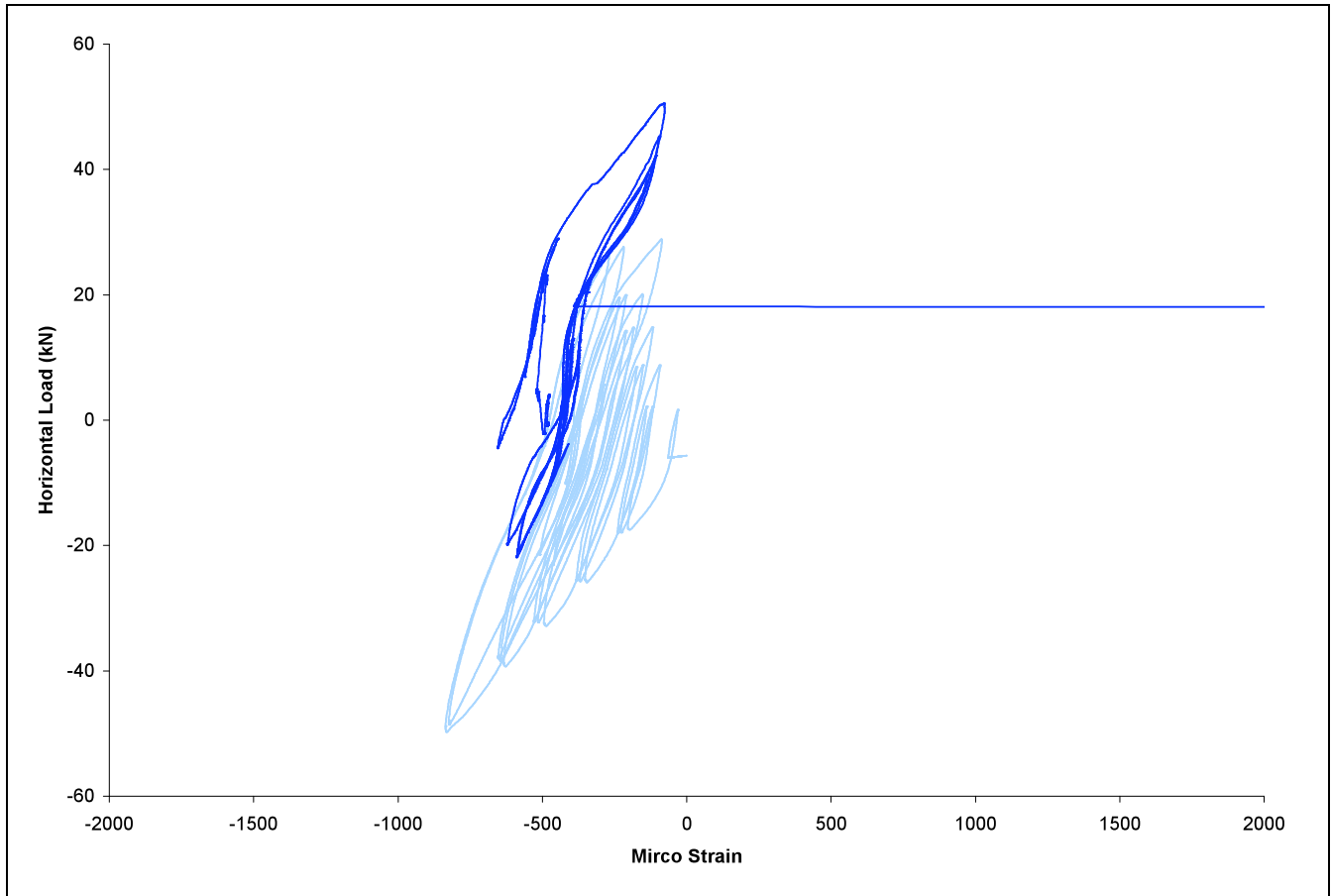
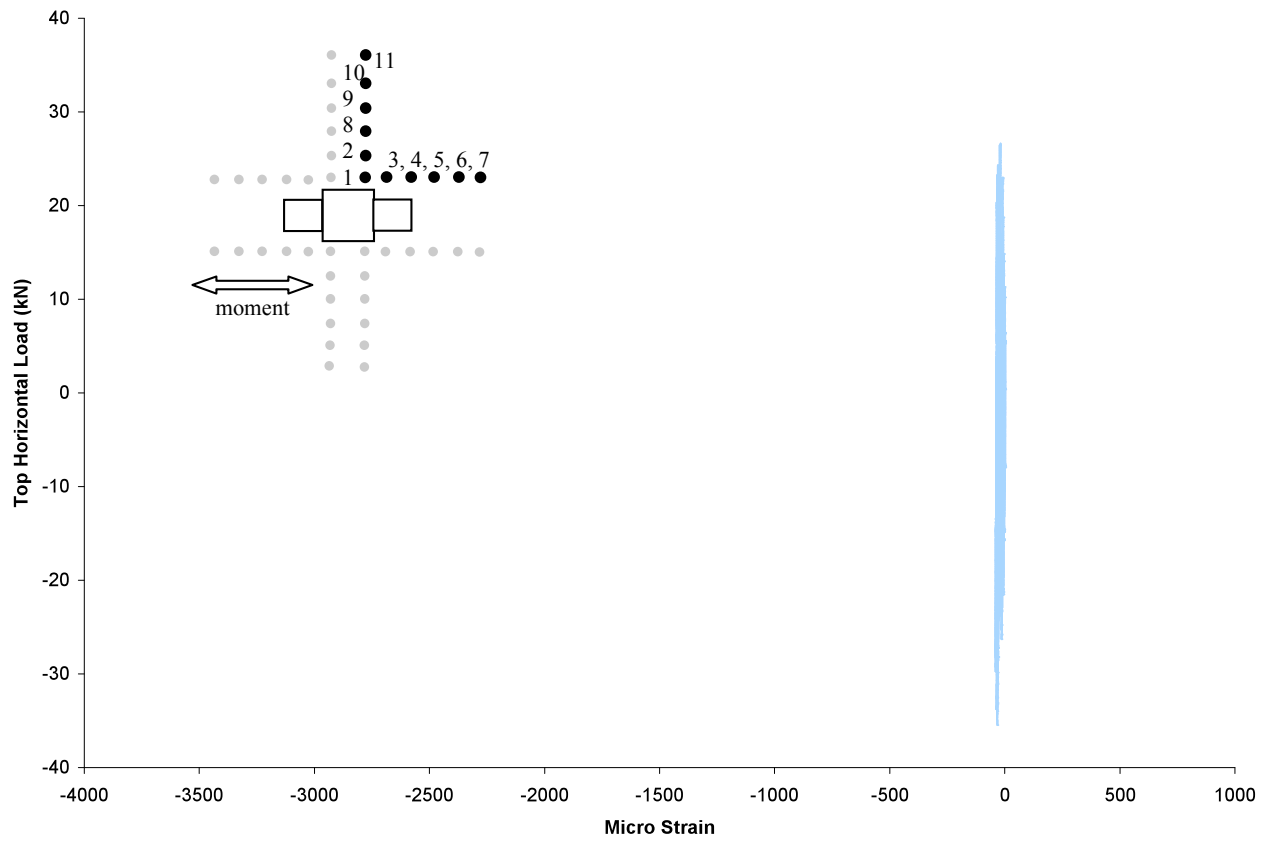**Figure E-1:** Slab SN5, Strain vs. Horizontal Load, Bar #1,2a
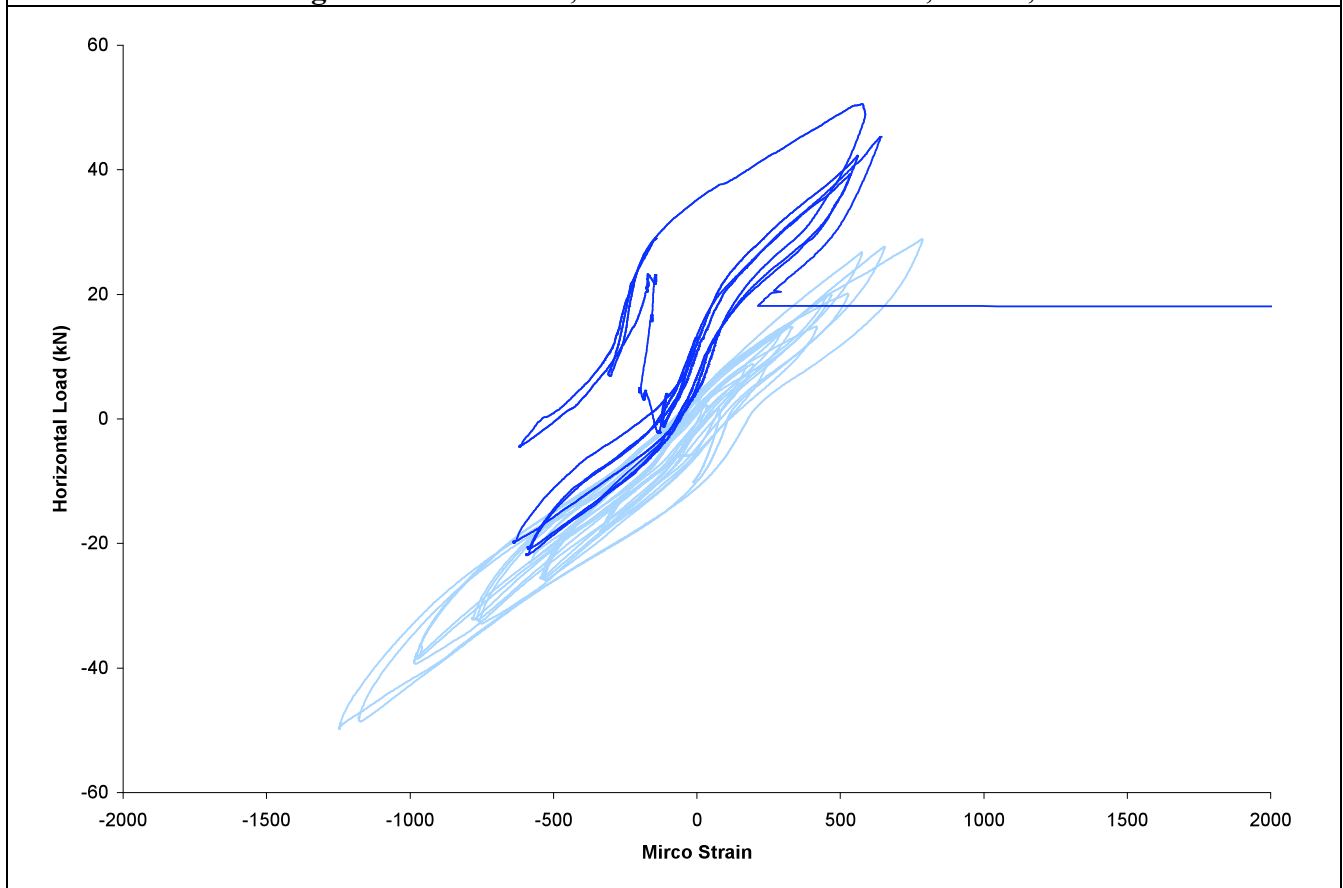
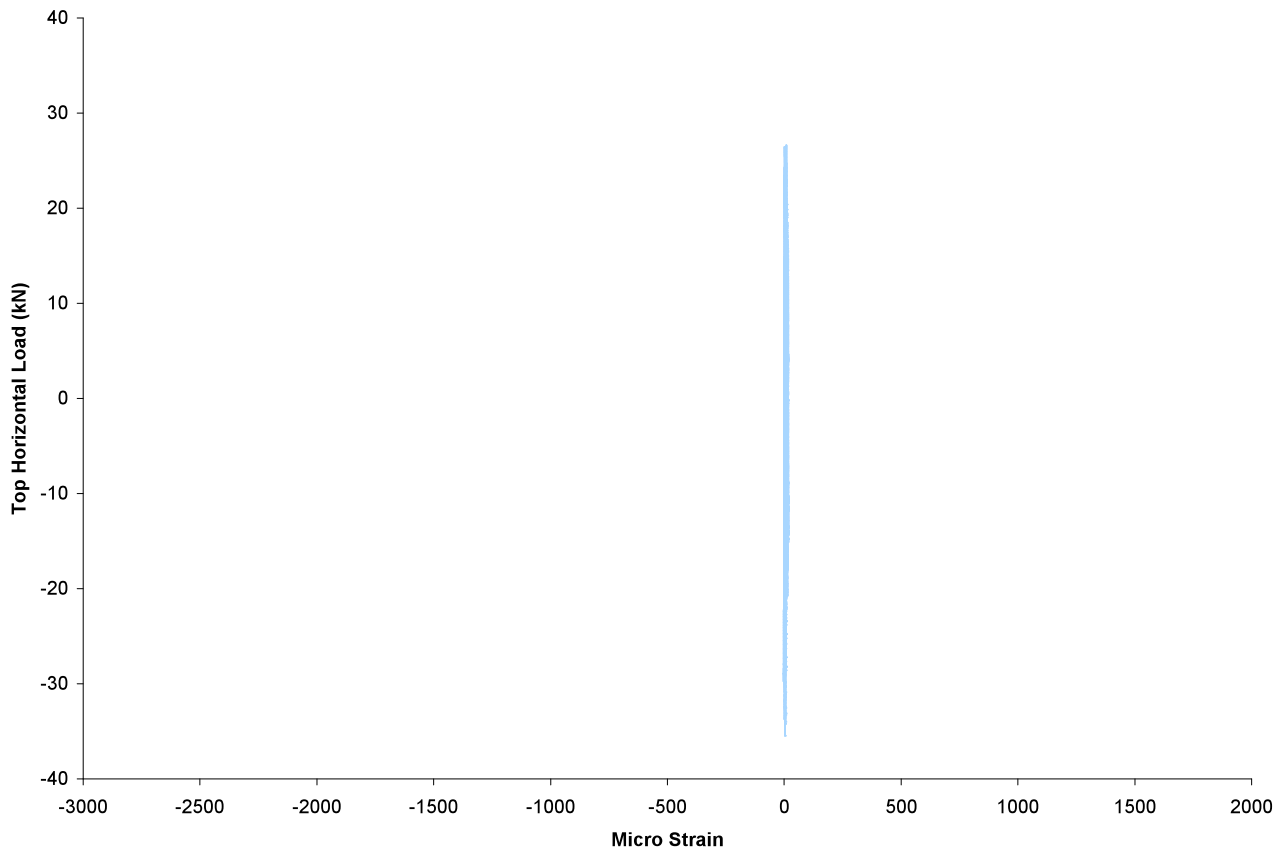**Figure E-2:** Slab SN5, Strain vs. Horizontal Load, Bar #1,2b
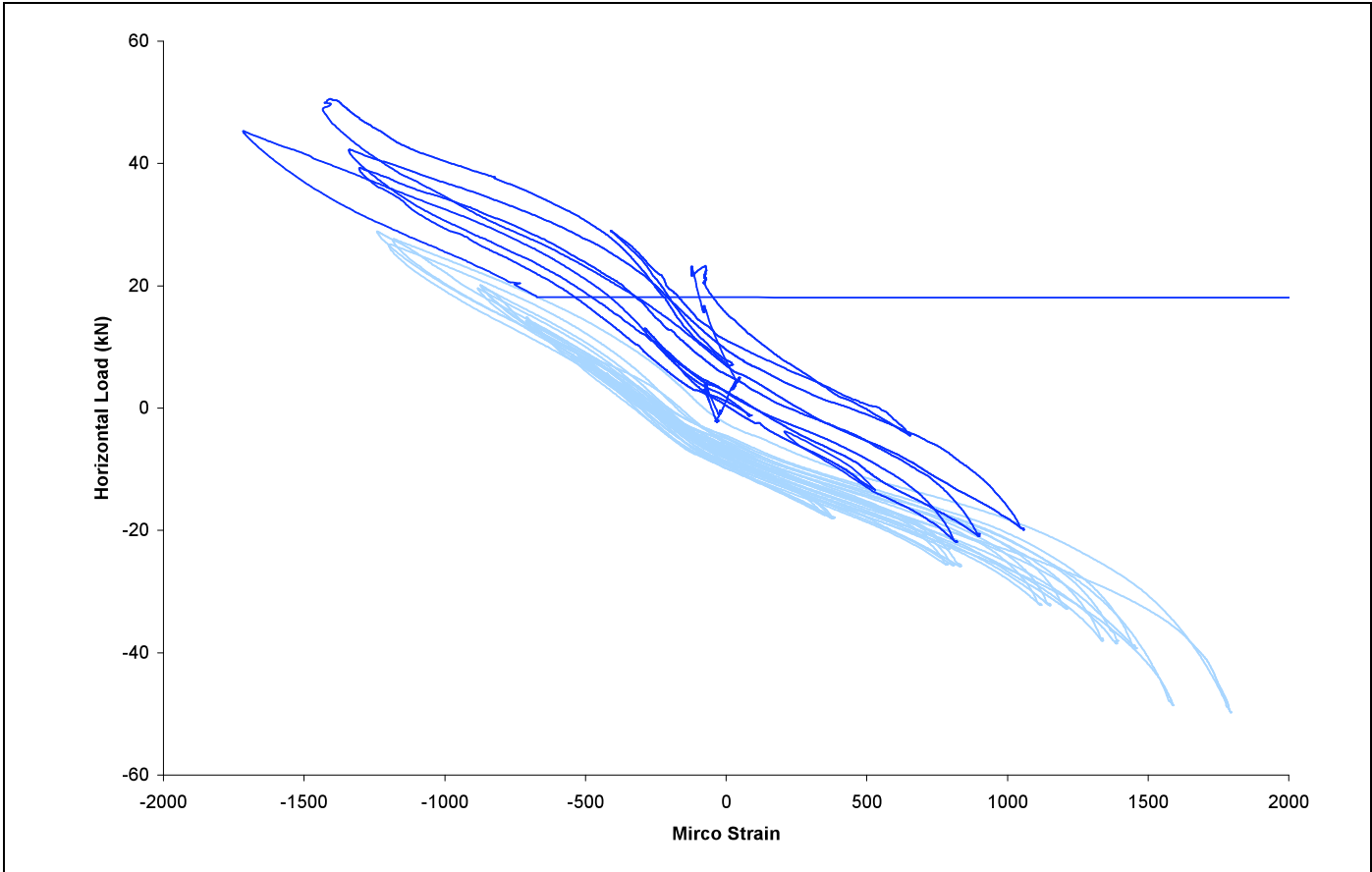
Figure E-3: Slab SN5, Strain vs. Horizontal Load, Bar #1,2c
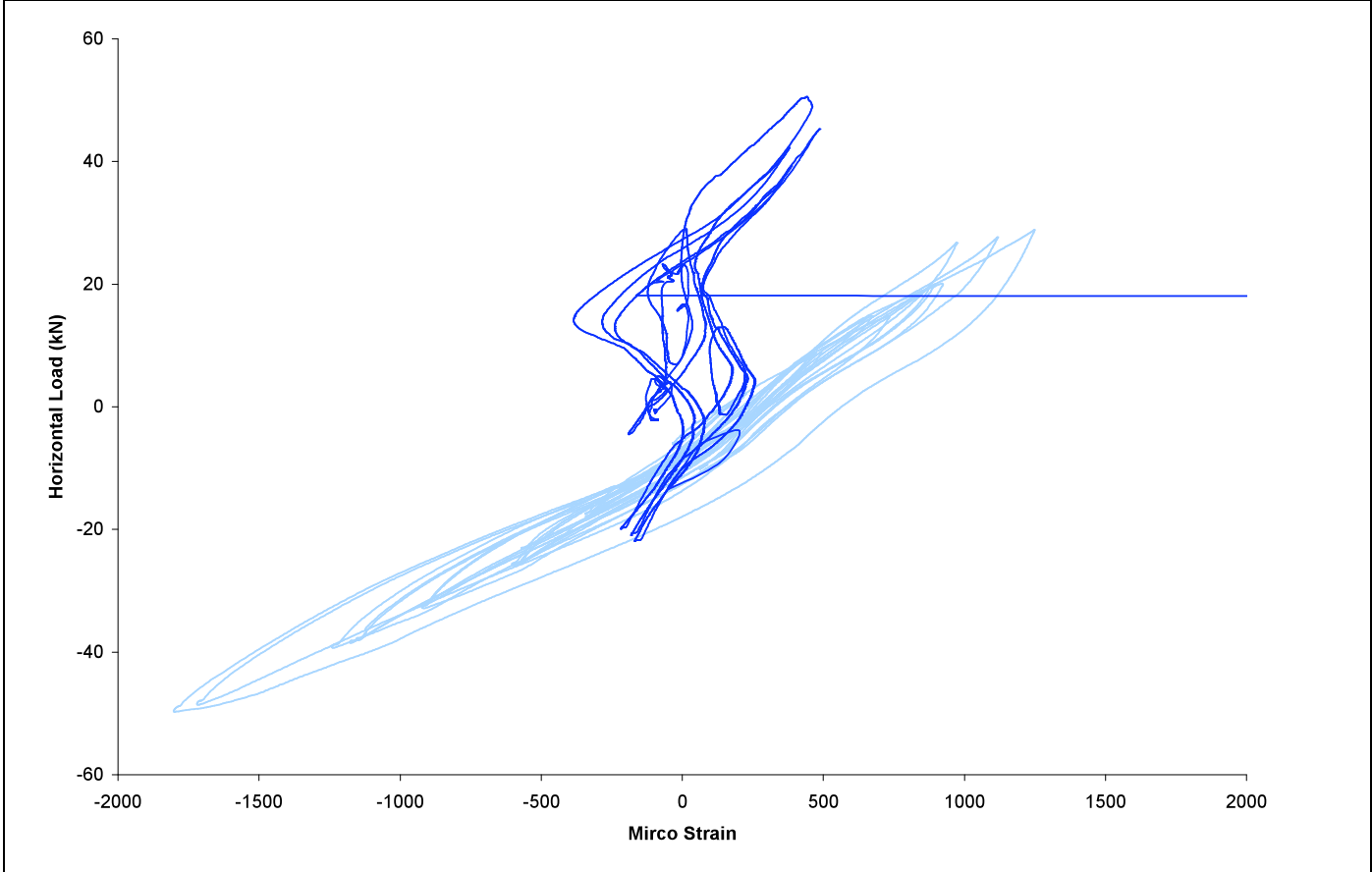
Figure E-4: Slab SN5, Strain vs. Horizontal Load, Bar #1,2d
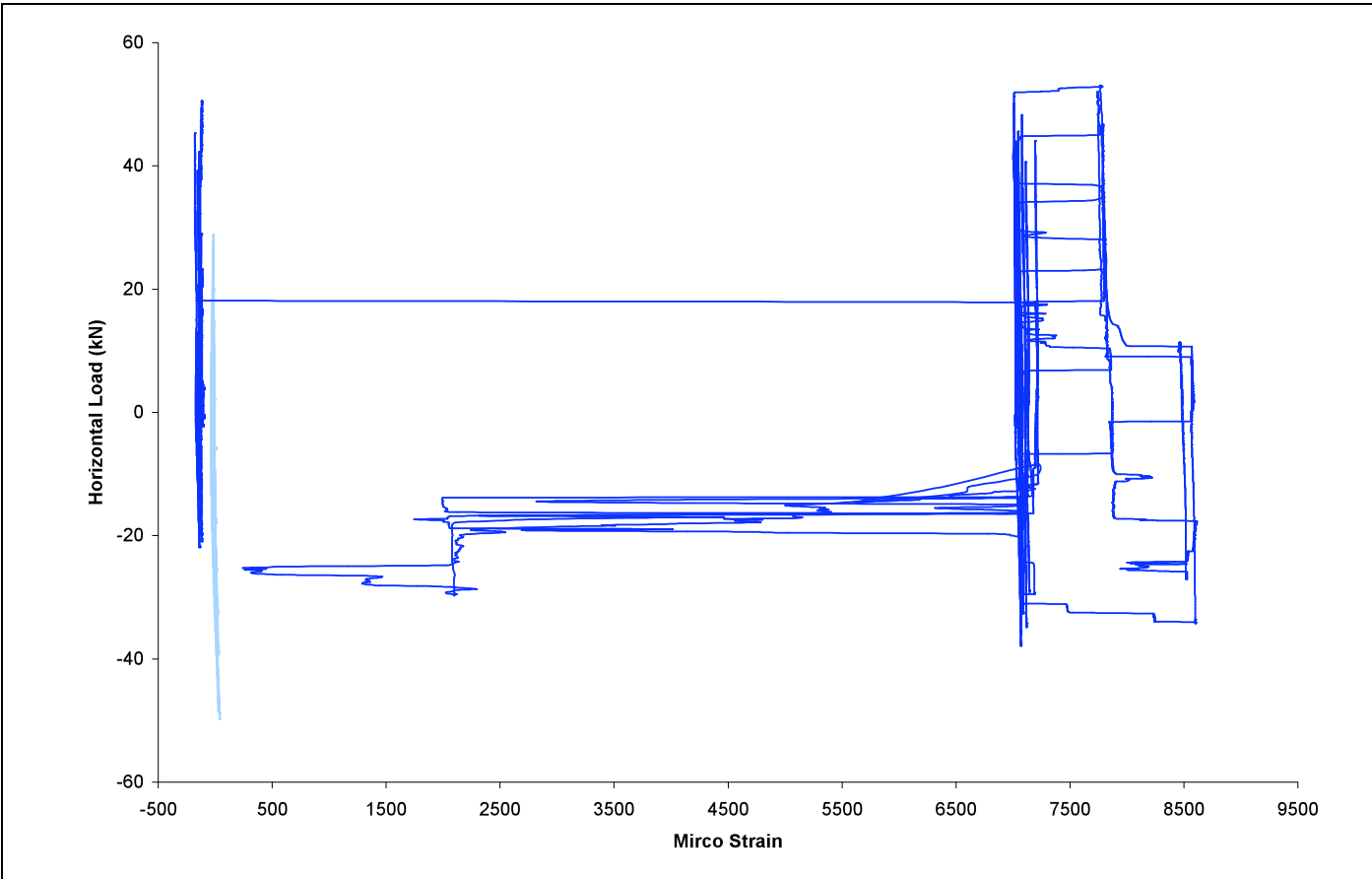
Figure E-5: Slab SN5, Strain vs. Horizontal Load, Bar #3a
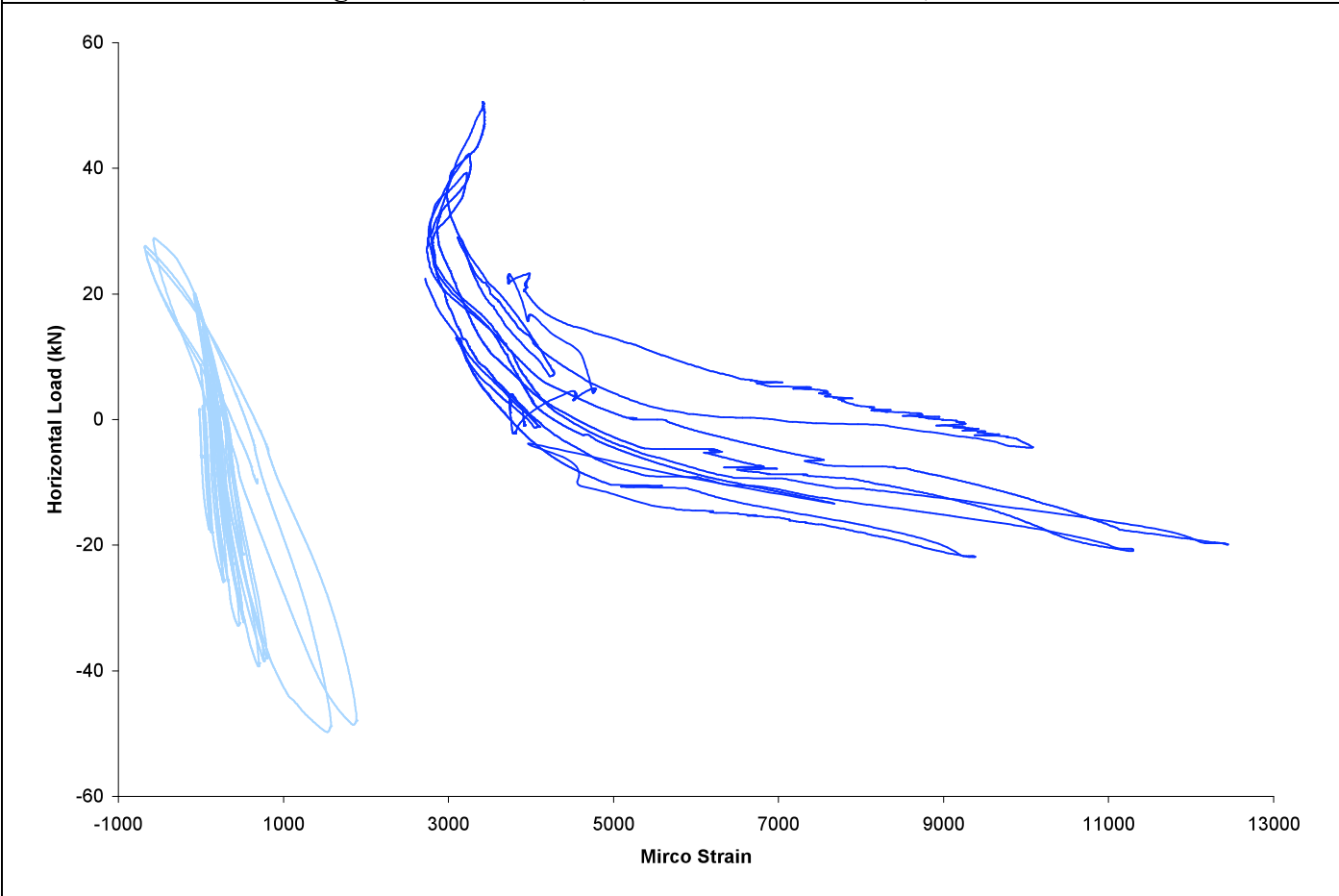
Figure E-6: Slab SN5, Strain vs. Horizontal Load, Bar #3c

130
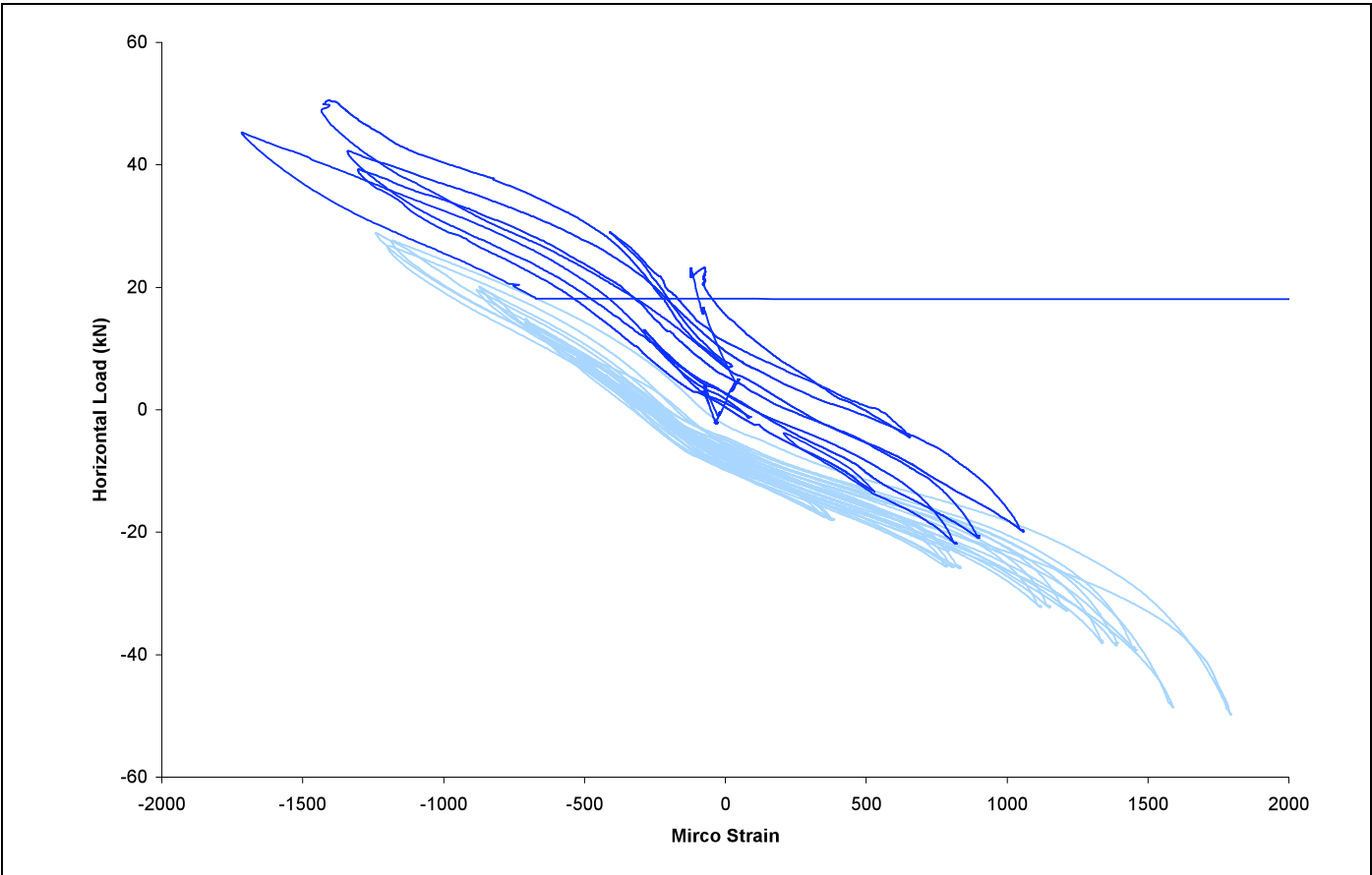
Figure E-7: Slab SN5, Strain vs. Horizontal Load, Bar #1,2c
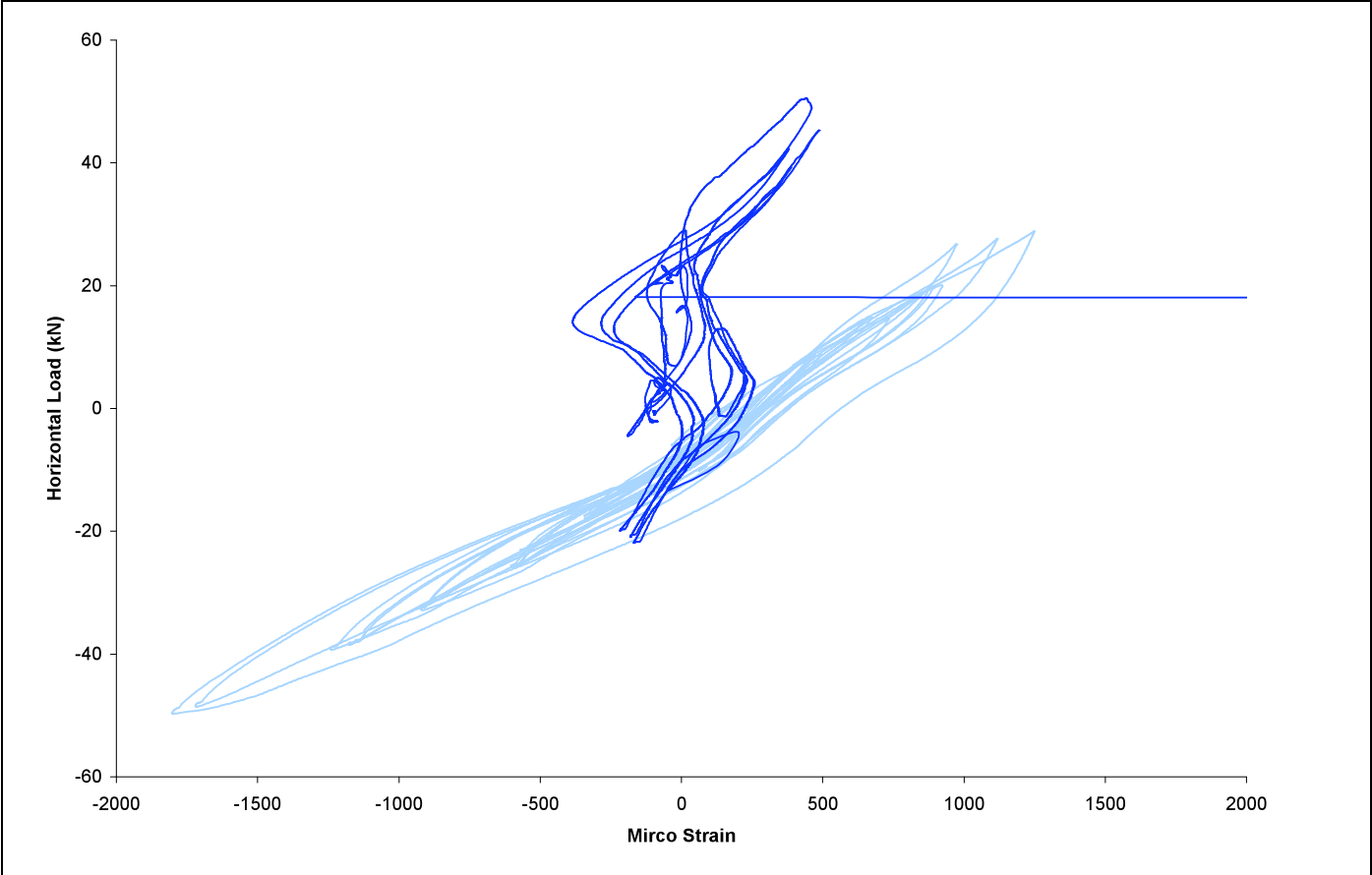
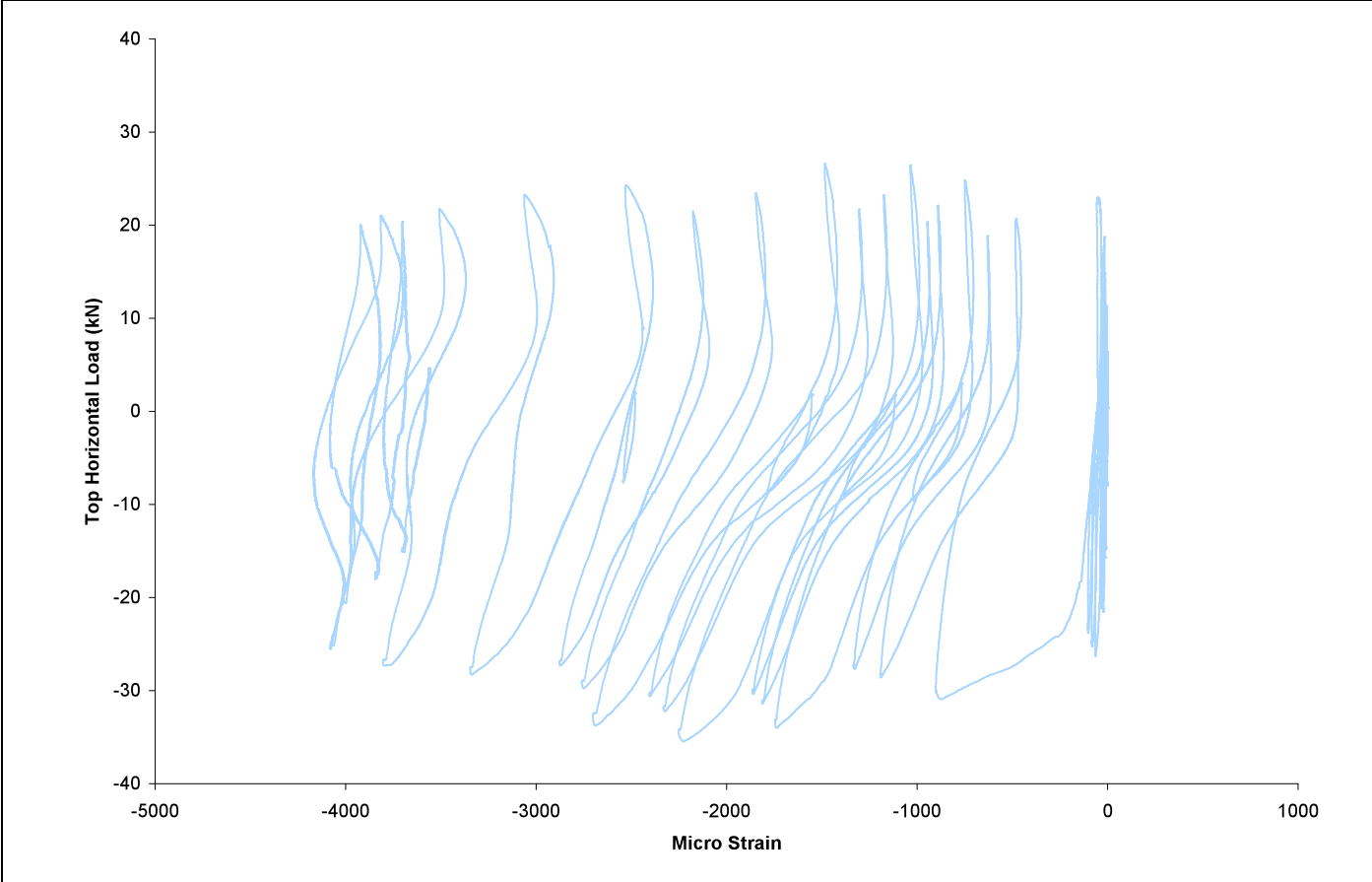**Figure E-8:** Slab SN5, Strain vs. Horizontal Load, Bar #1,2d
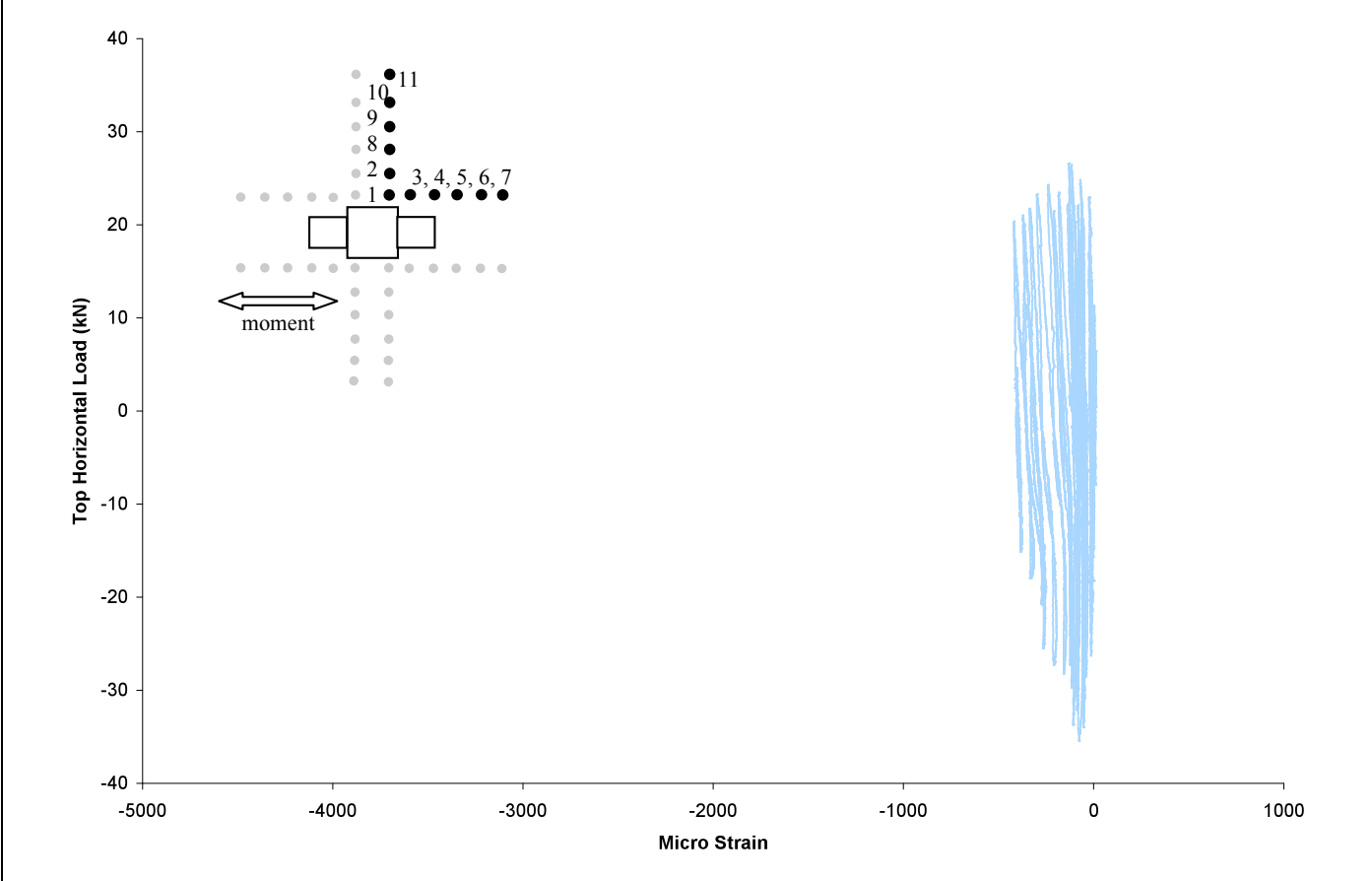
131
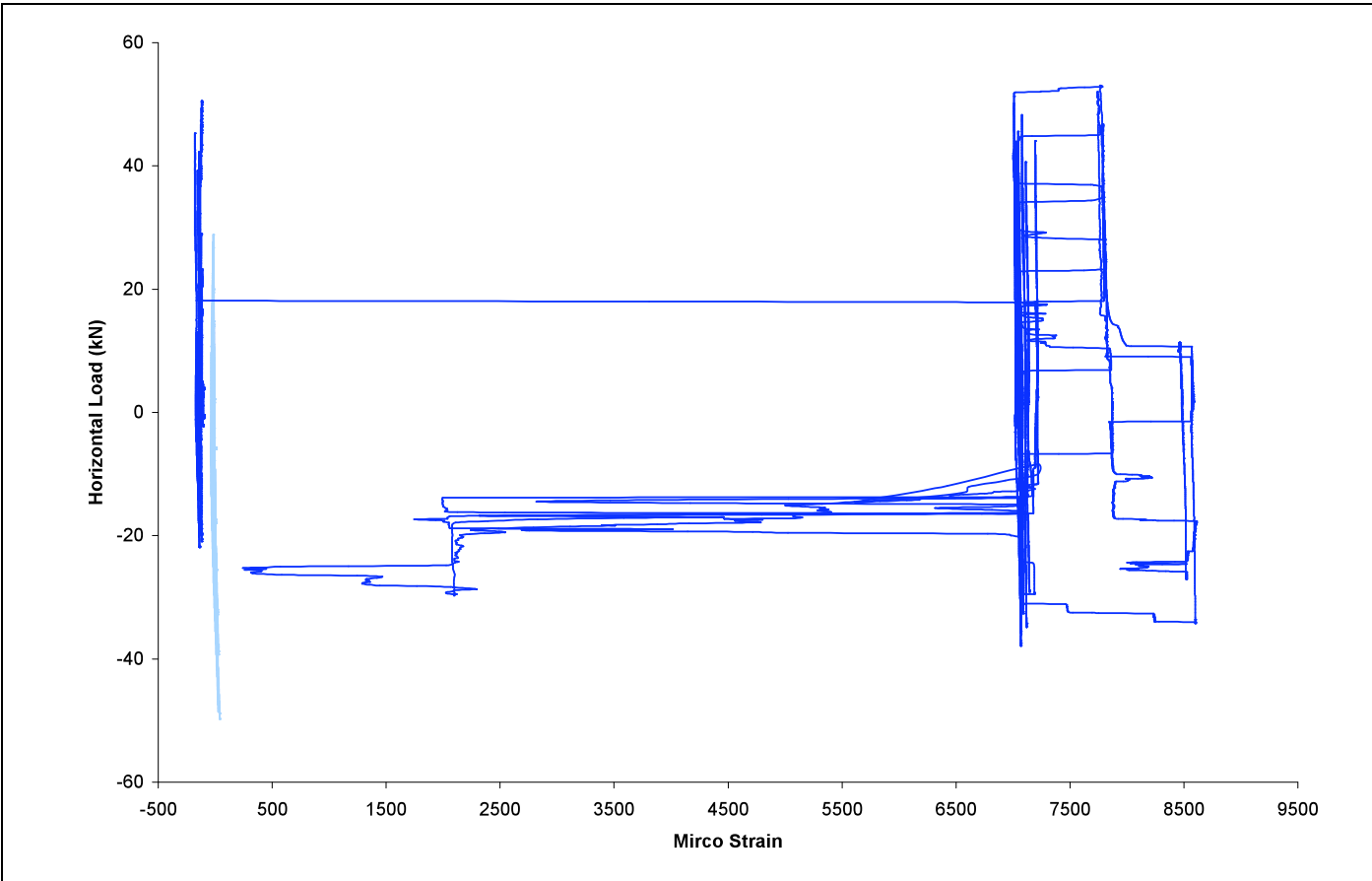
Figure E-9: Slab SN5, Strain vs. Horizontal Load, Bar #3a
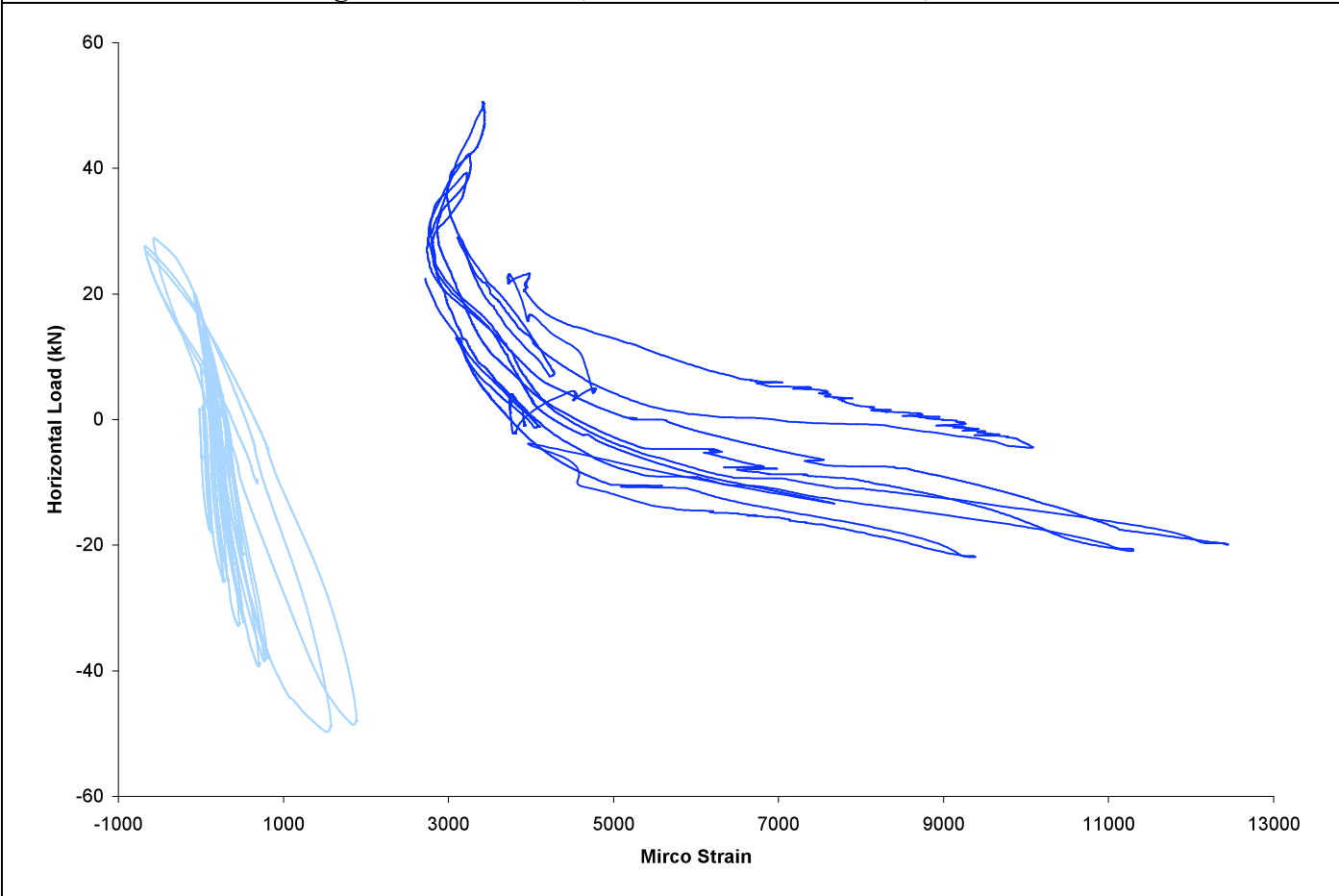
Figure E-10: Slab SN5, Strain vs. Horizontal Load, Bar #3c
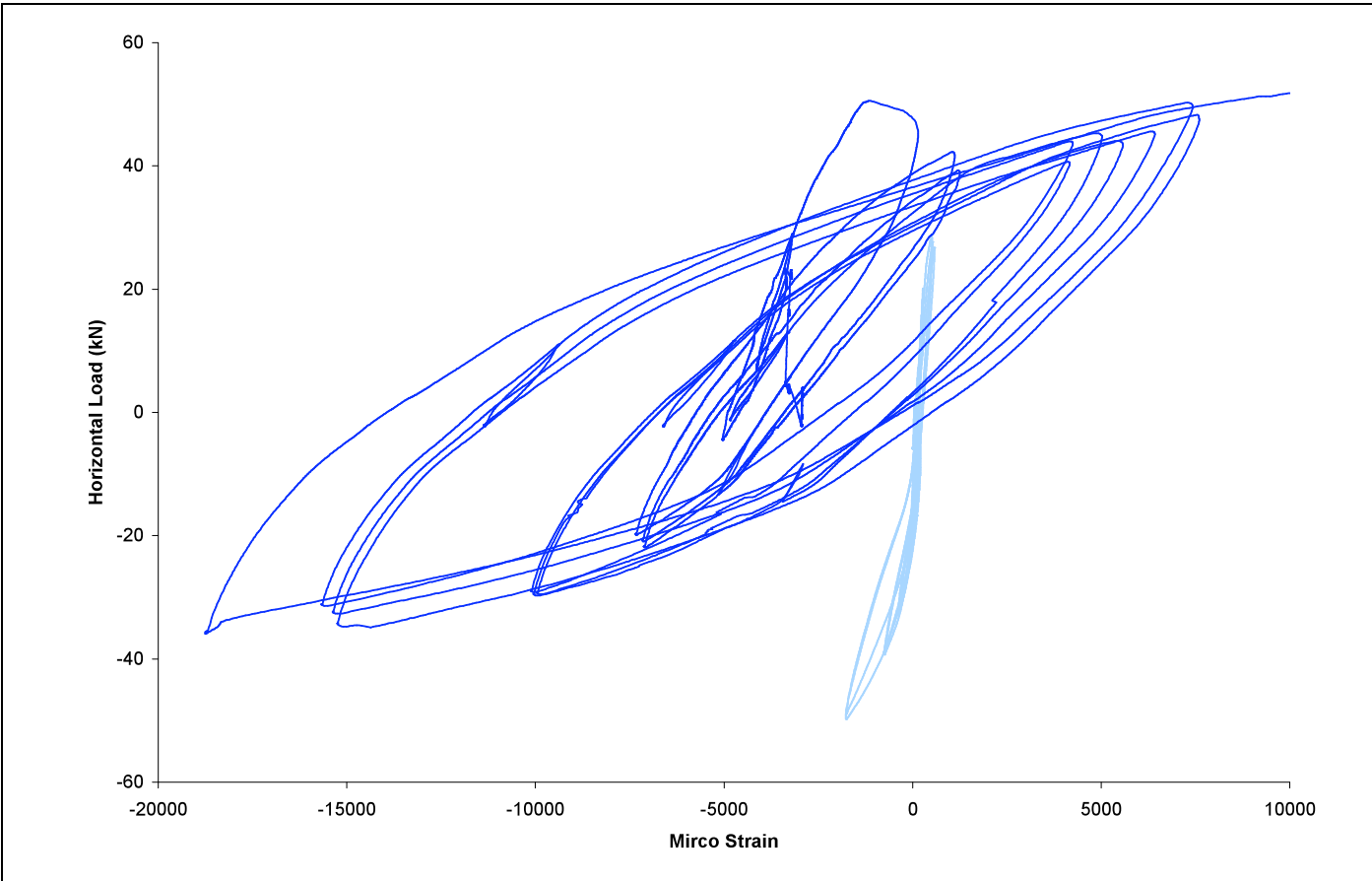
Figure E-11: Slab SN5, Strain vs. Horizontal Load, Bar #3d
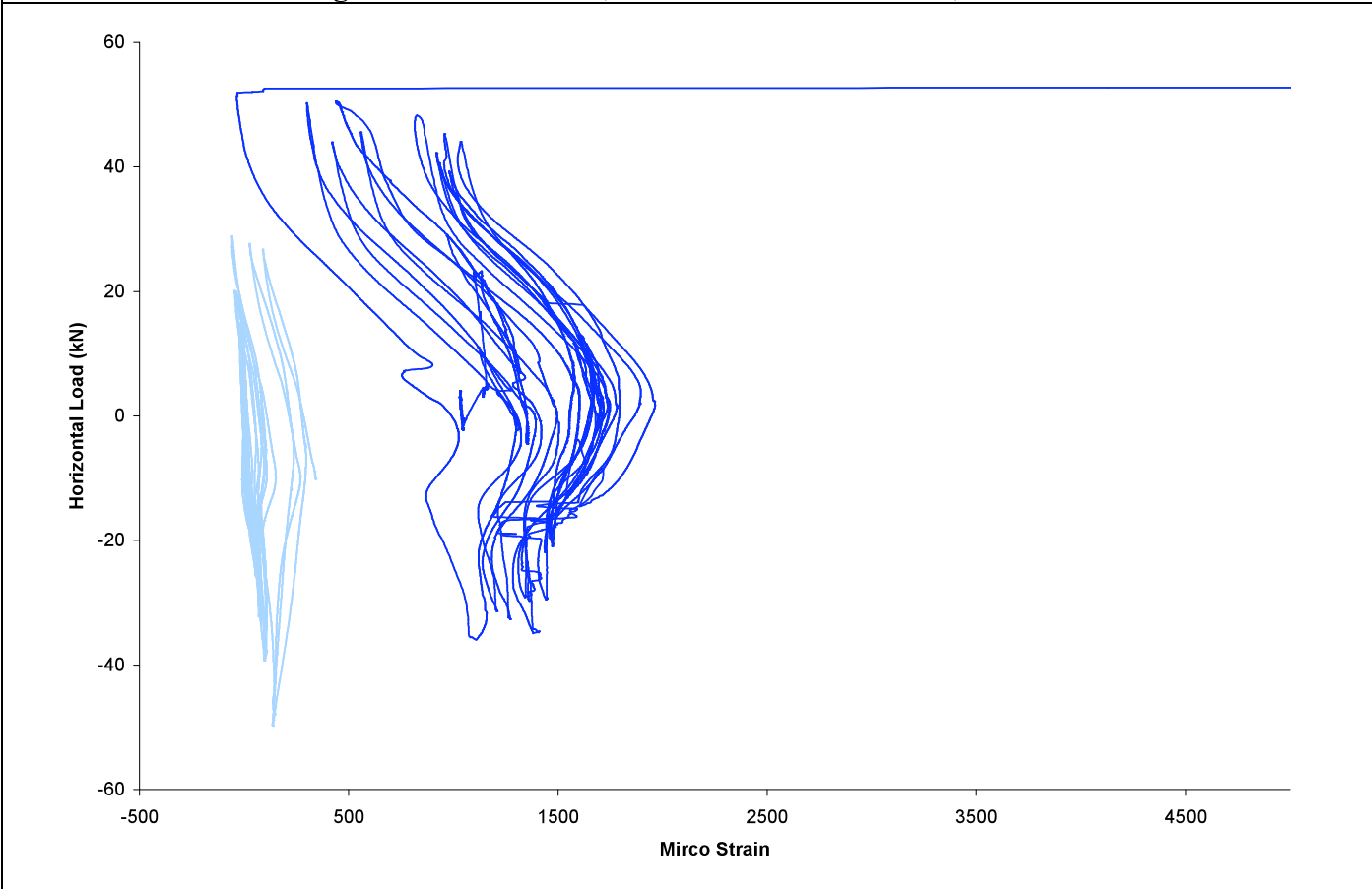
Figure E-12: Slab SN5, Strain vs. Horizontal Load, Bar #4b

133
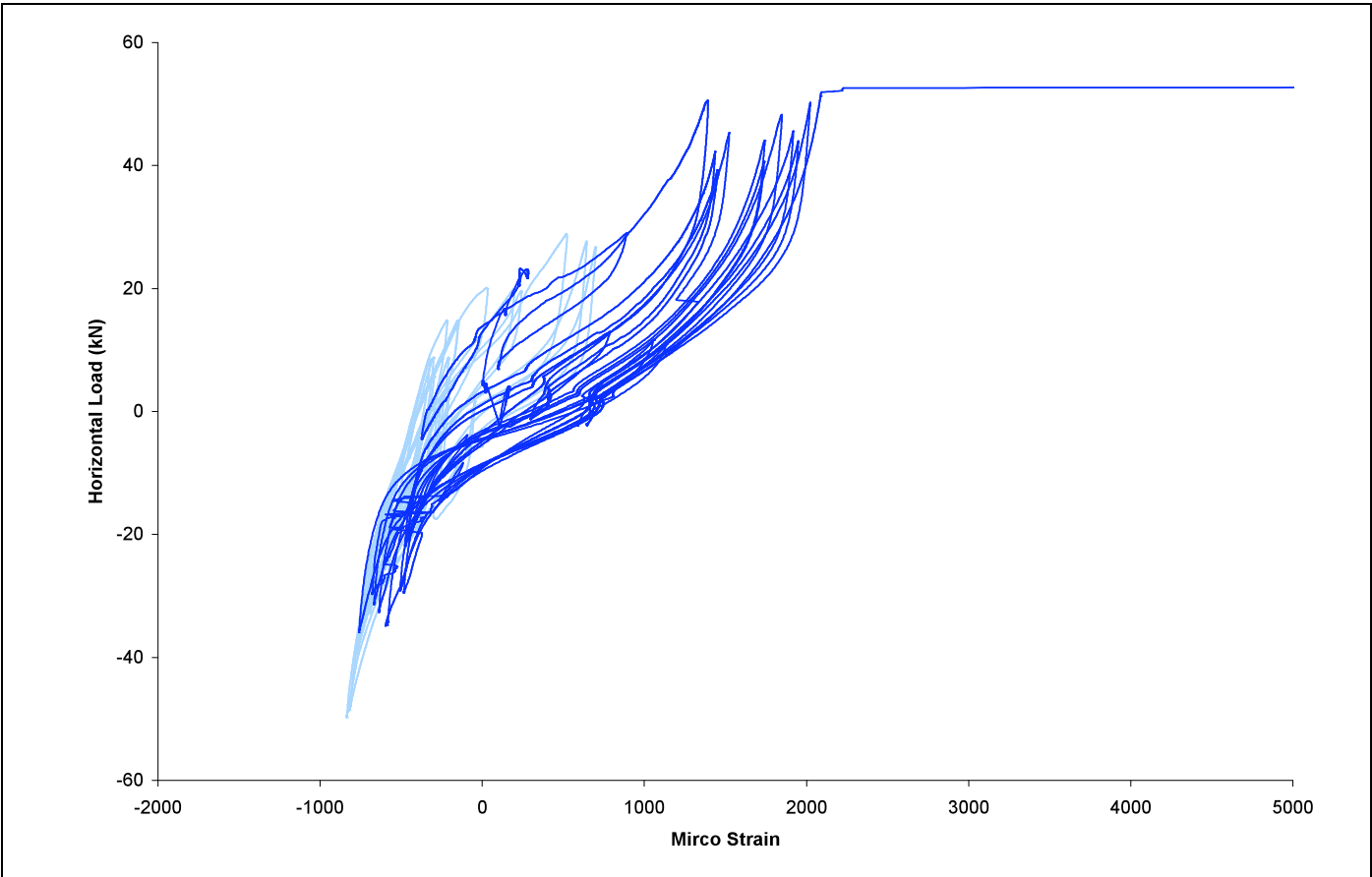
Figure E-13: Slab SN5, Strain vs. Horizontal Load, Bar #1,2a(col)
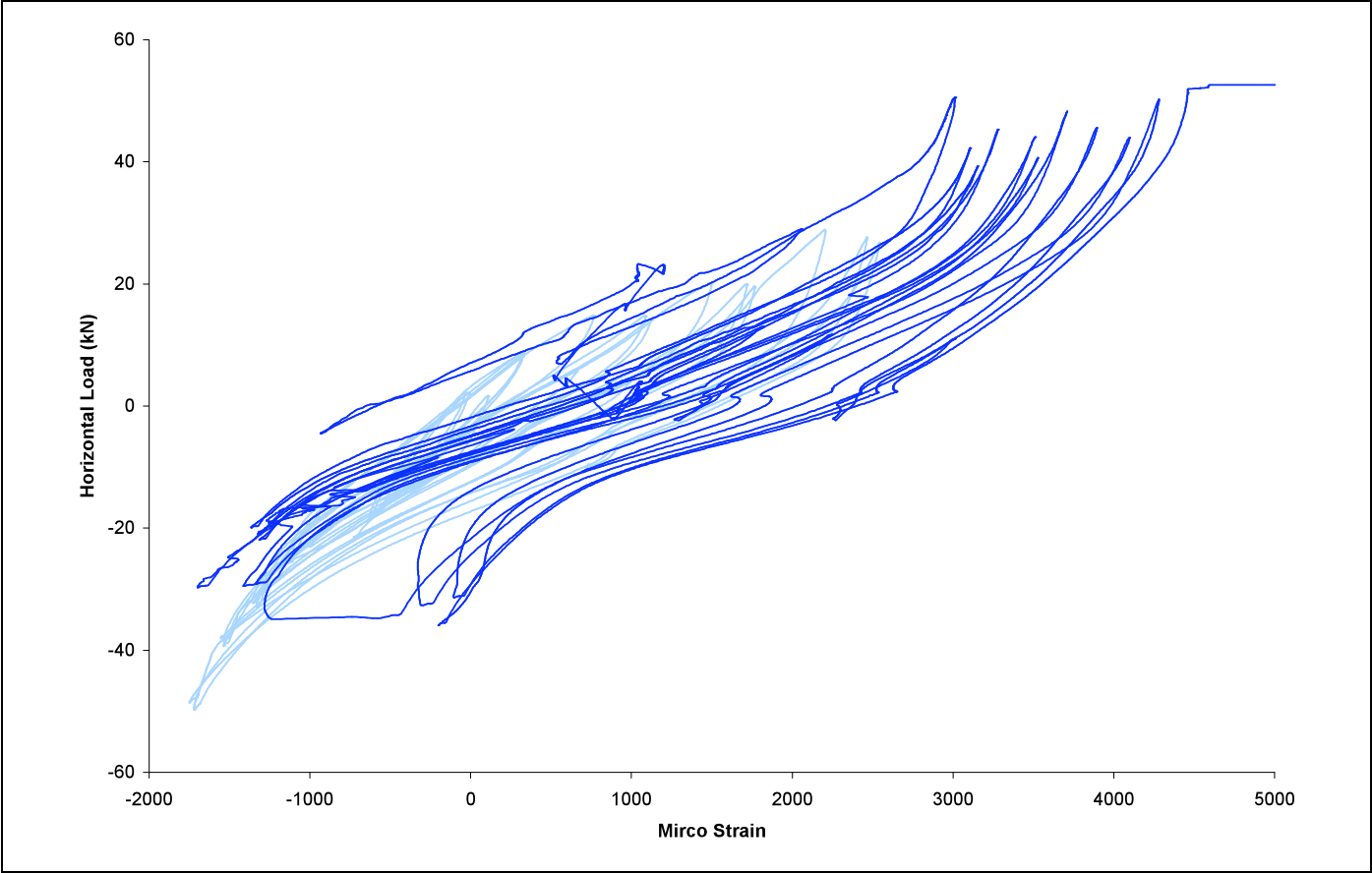
Figure E-14: Slab SN5, Strain vs. Horizontal Load, Bar #1,2b(col)
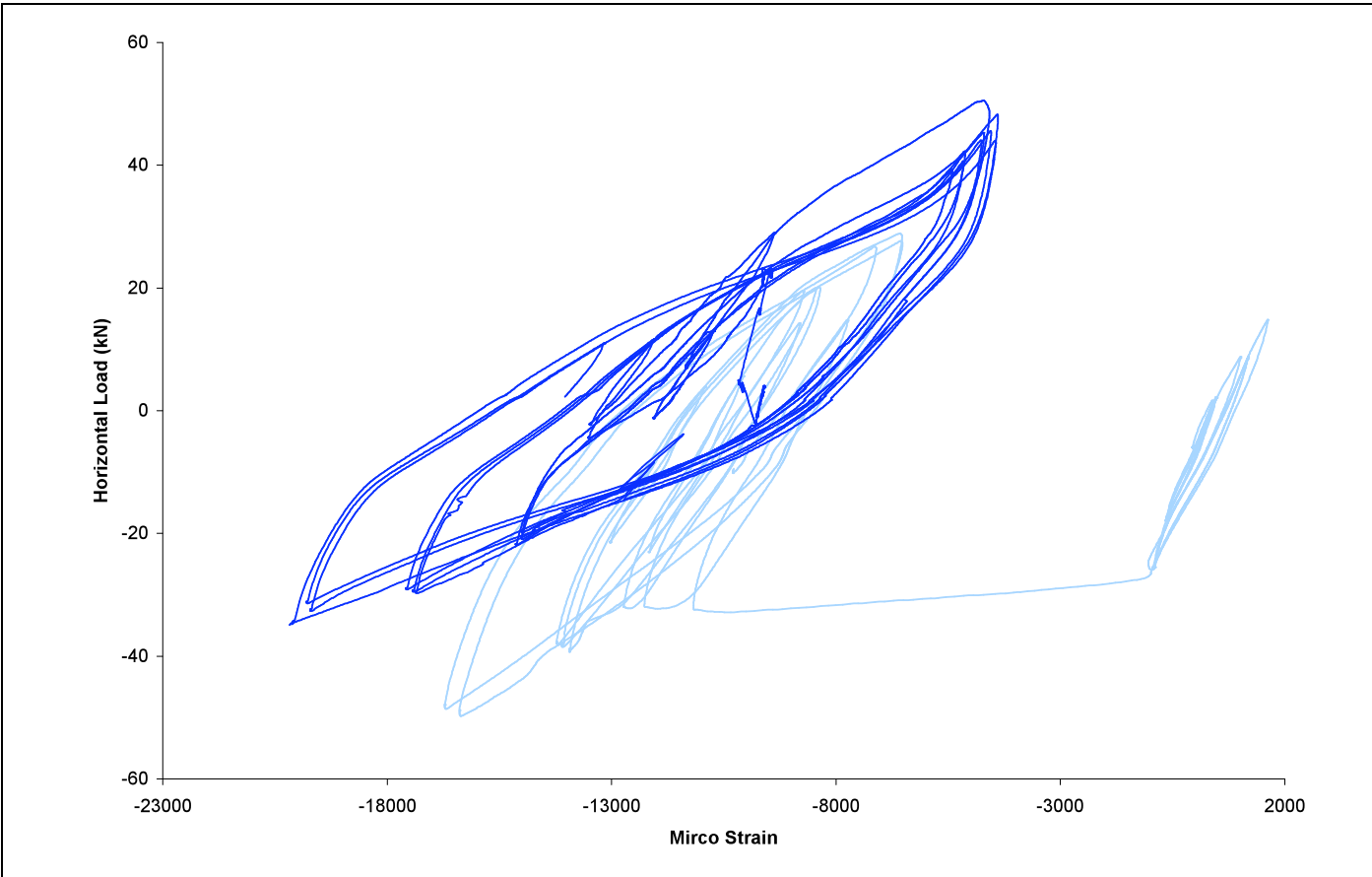
Figure E-15: Slab SN5, Strain vs. Horizontal Load, Bar #1,2c(col)
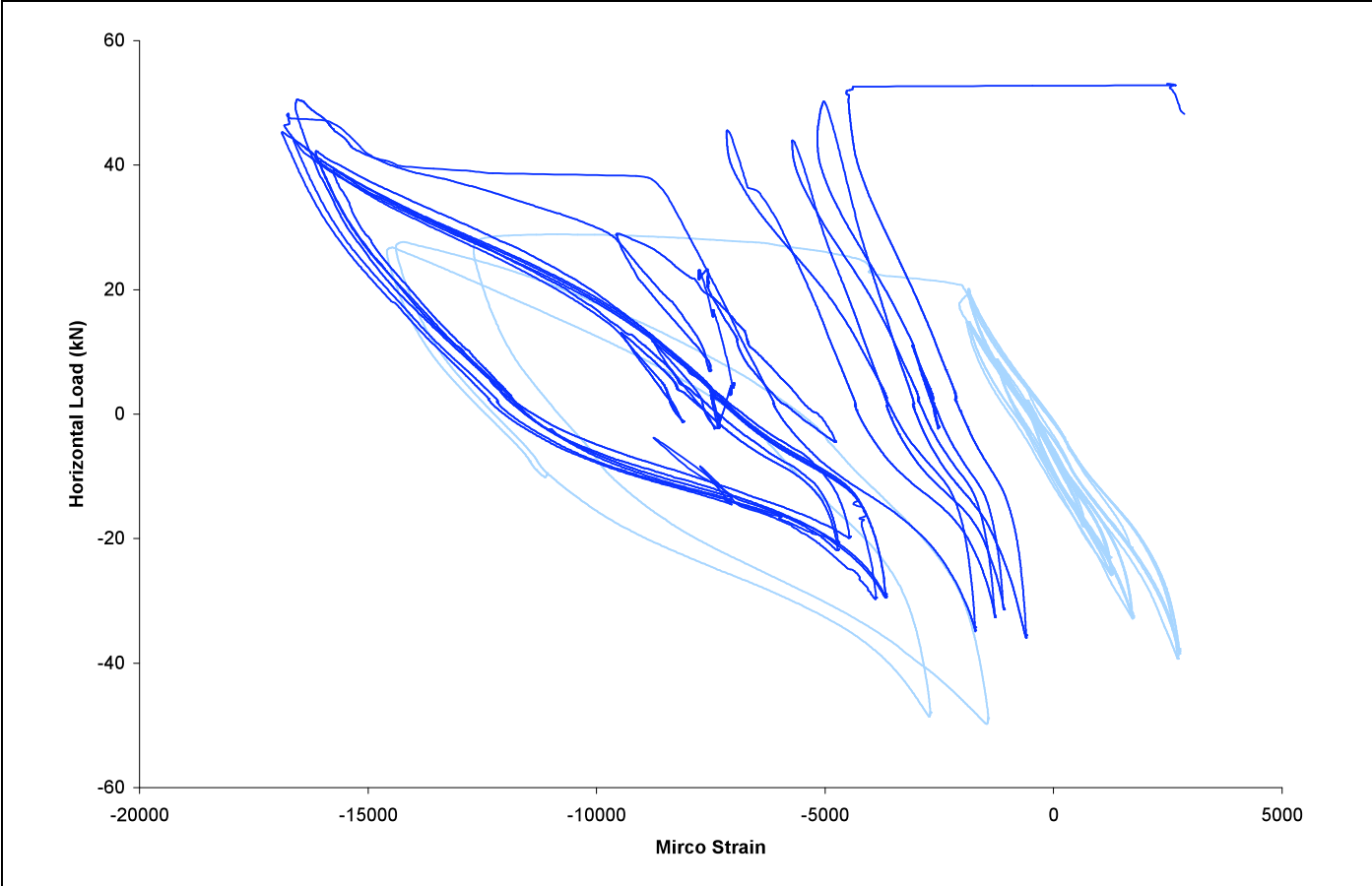
Figure E-16: Slab SN5, Strain vs. Horizontal Load, Bar #1,2d(col)
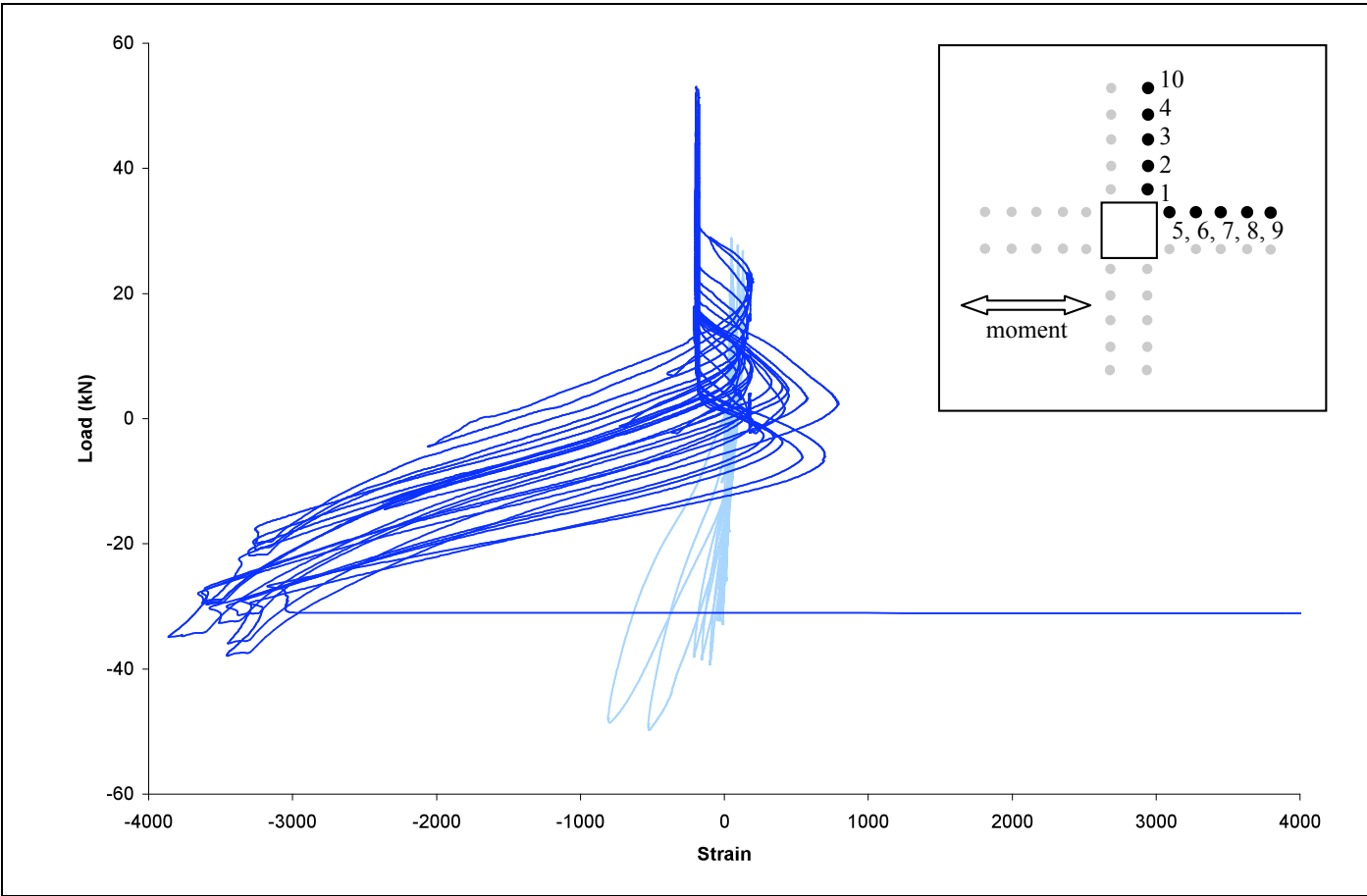
Figure E-17: Slab SN5, Strain vs. Horizontal Load, Bolt #1
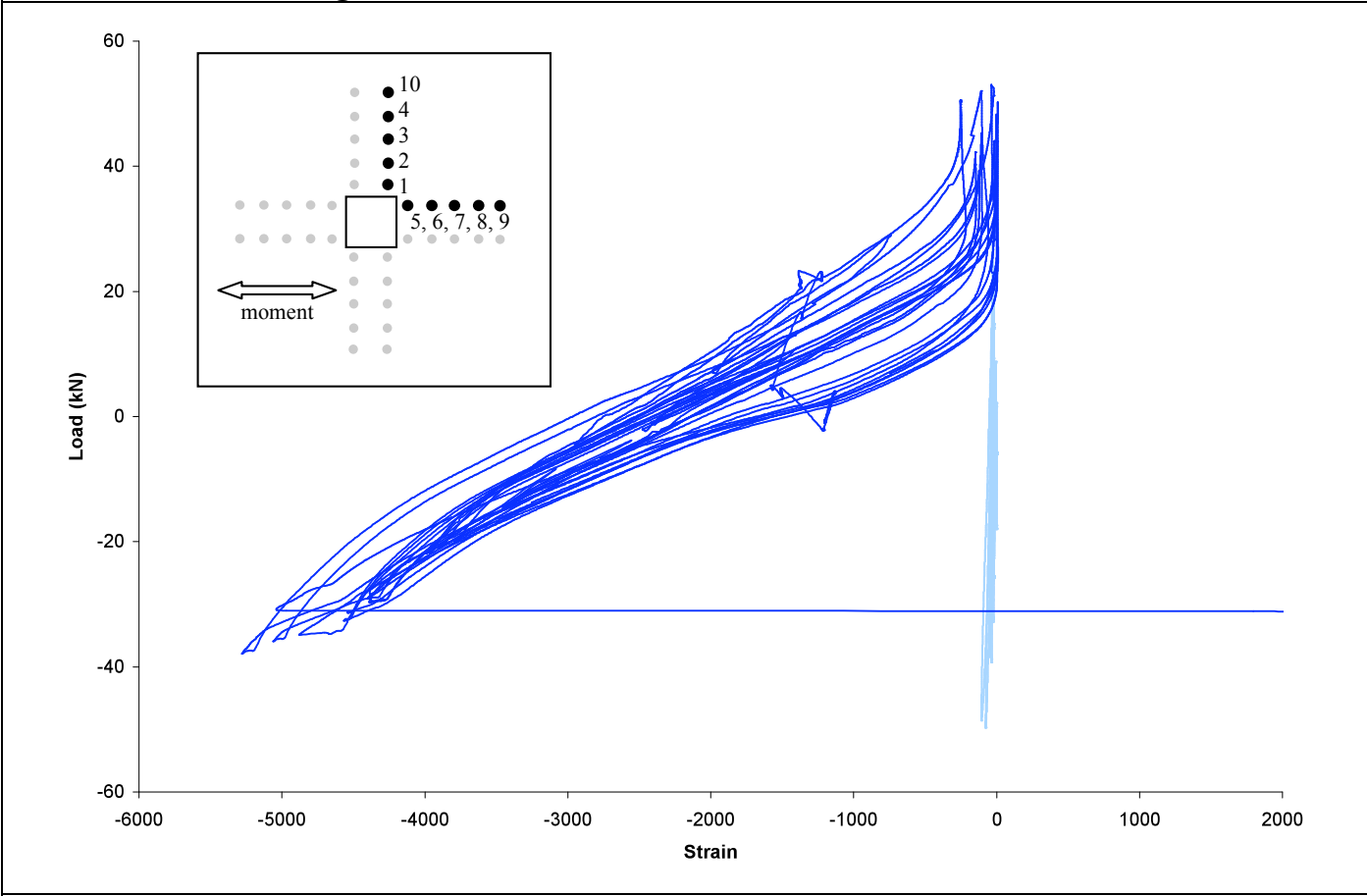
Figure E-18: Slab SN5, Strain vs. Horizontal Load, Bolt #2
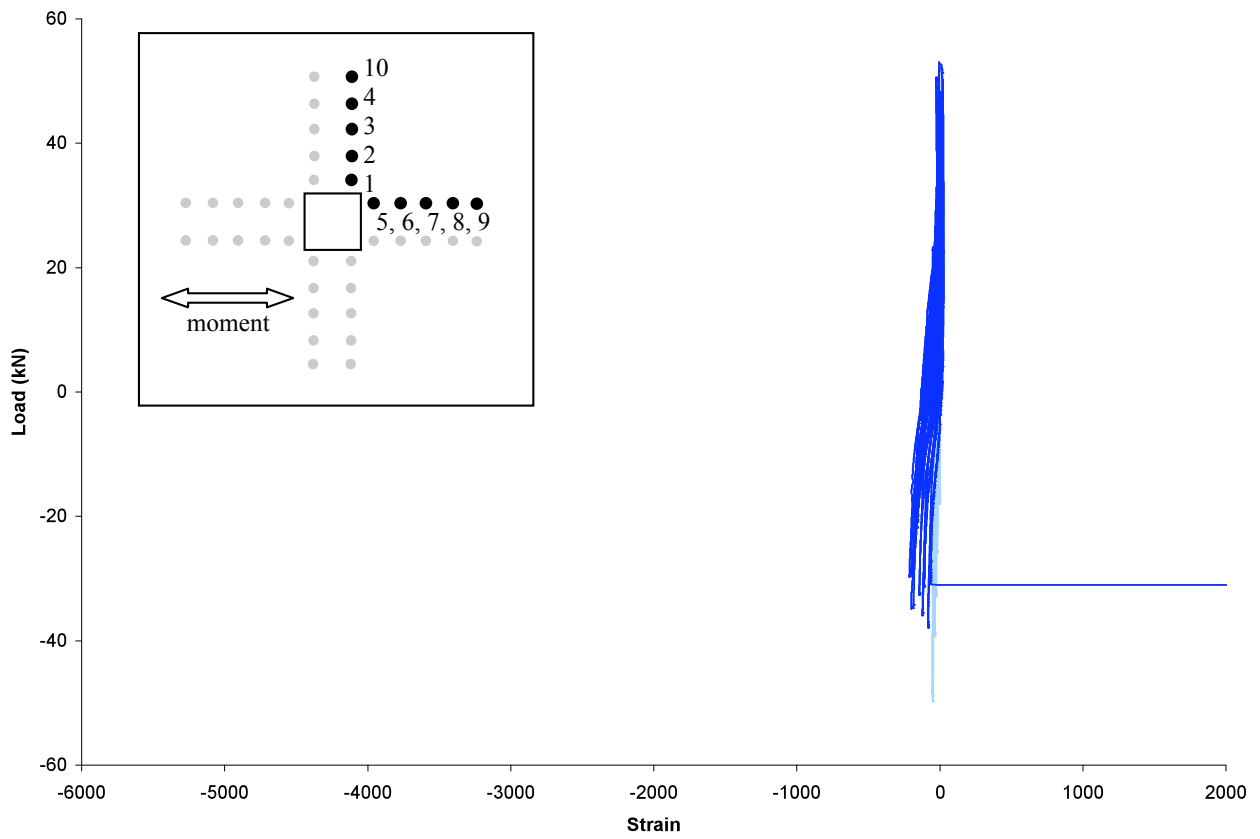
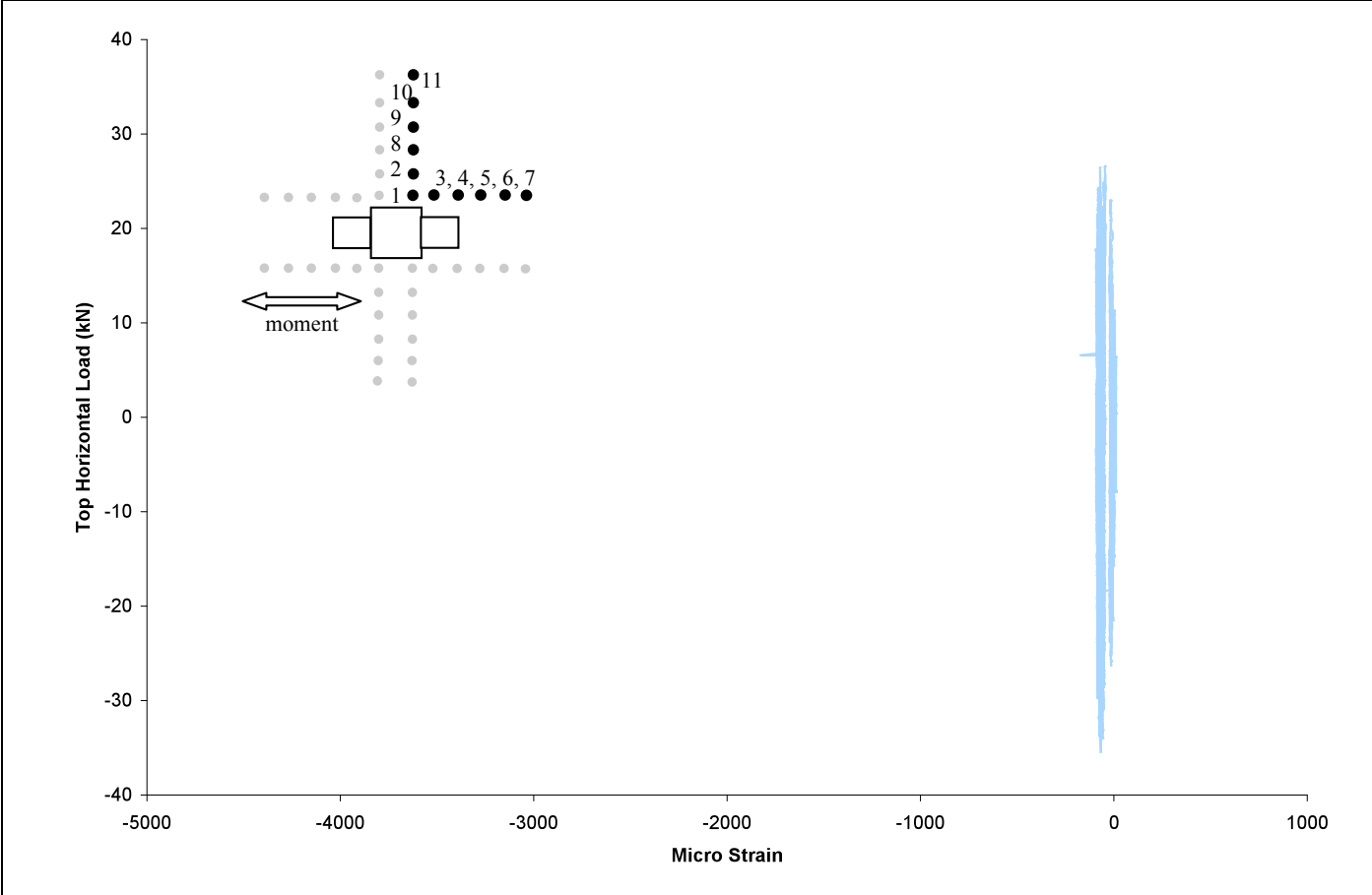**Figure E-19:** Slab SN5, Strain vs. Horizontal Load, Bolt #3
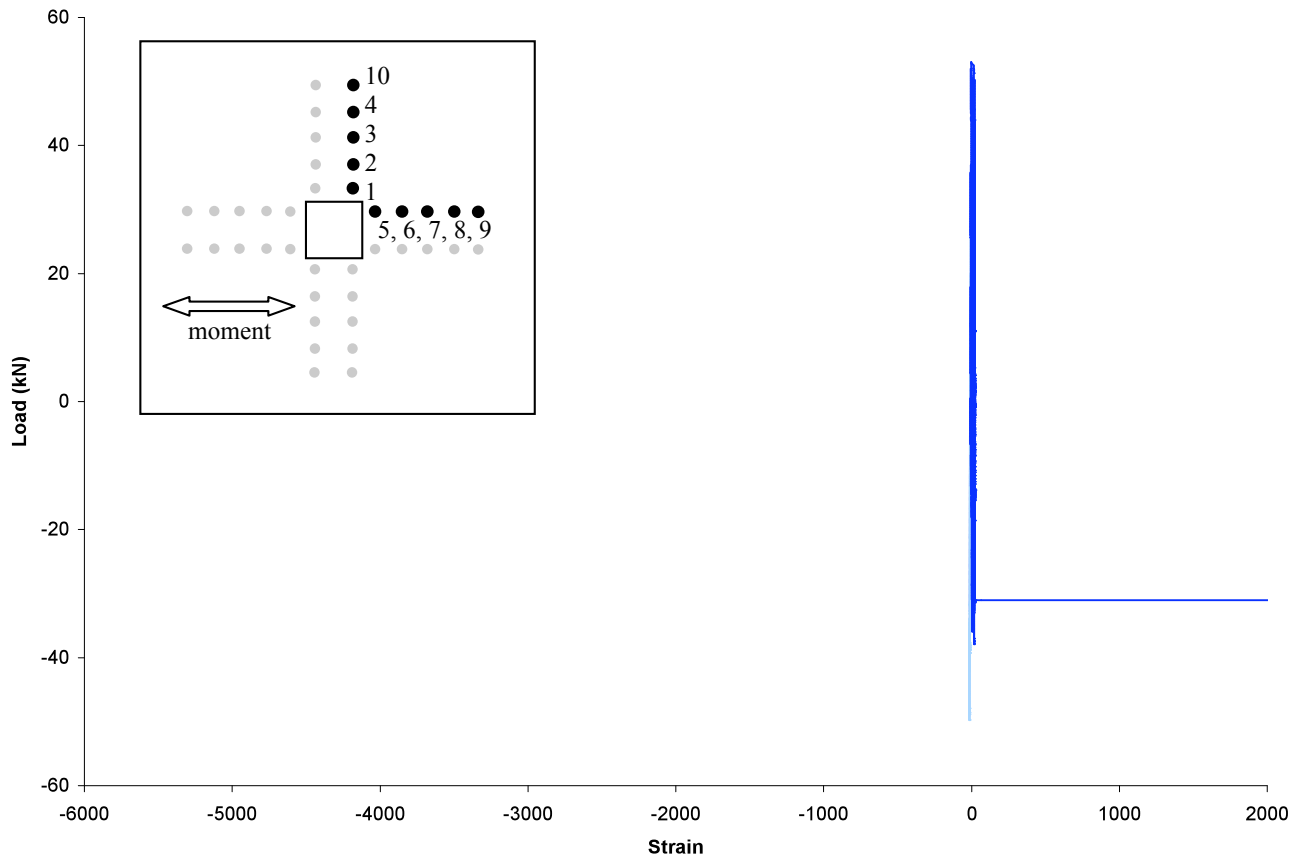
Figure E-20: Slab SN5, Strain vs. Horizontal Load, Bolt #4
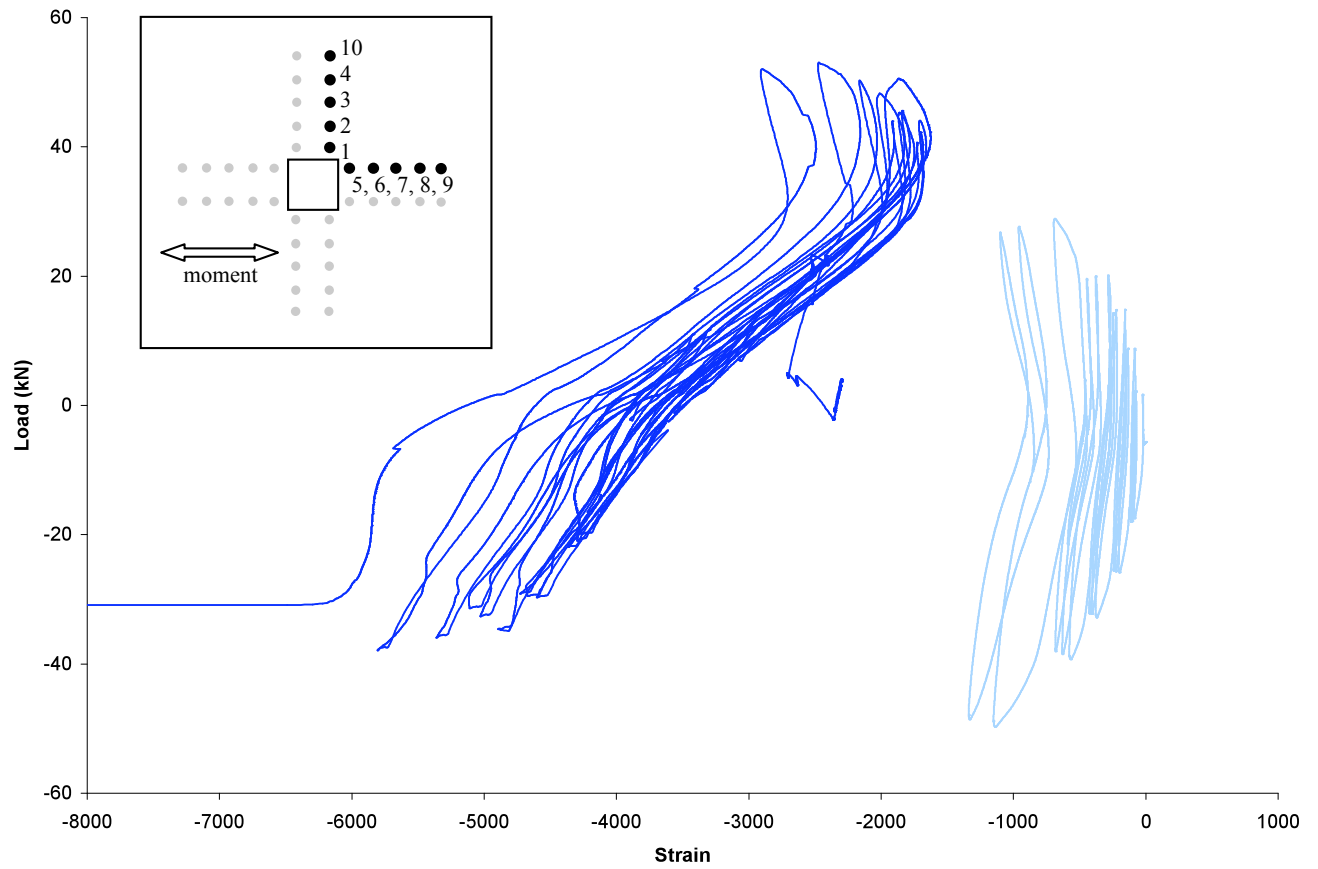
Figure E-21: Slab SN5, Strain vs. Horizontal Load, Bolt #5
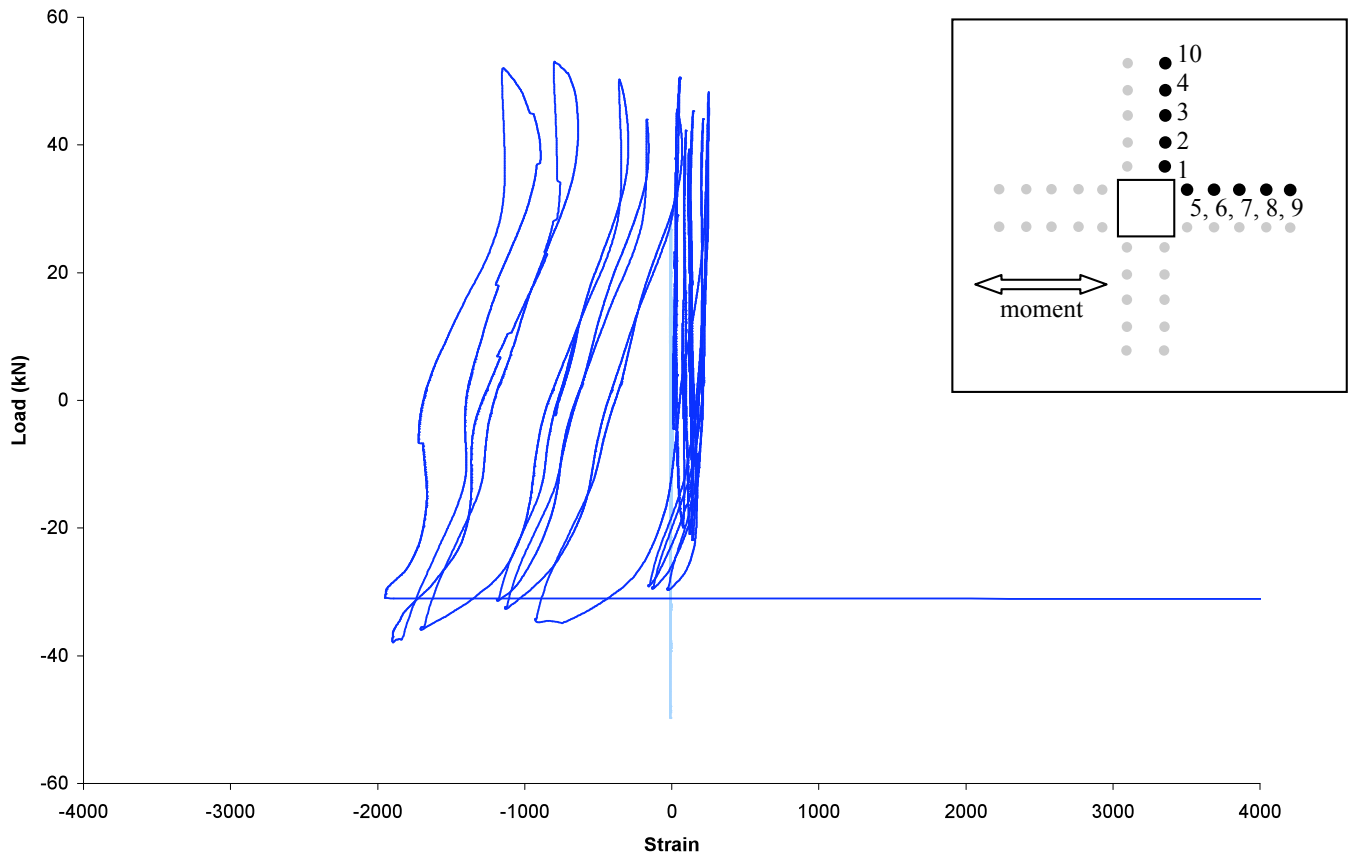
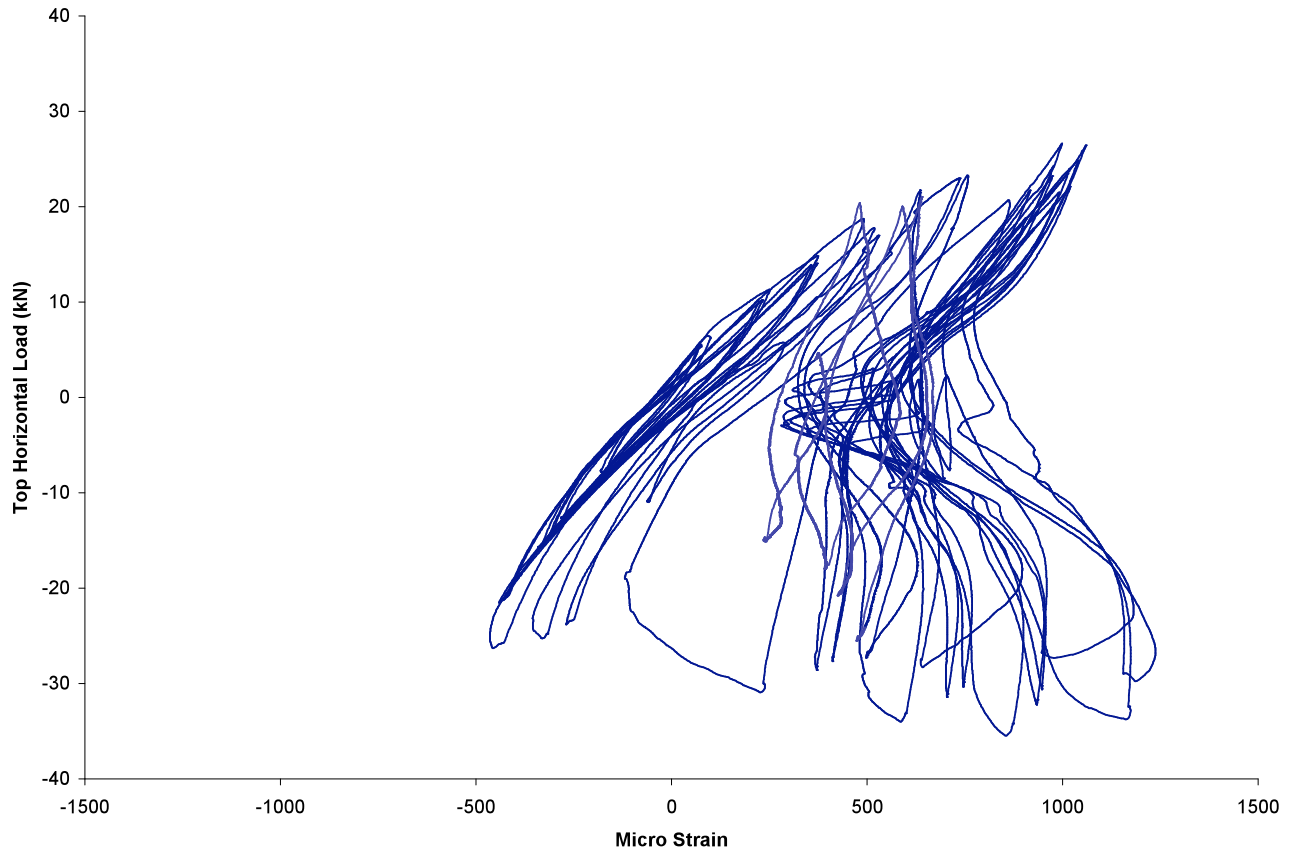**Figure E-22:** Slab SN5, Strain vs. Horizontal Load, Bolt #6

138
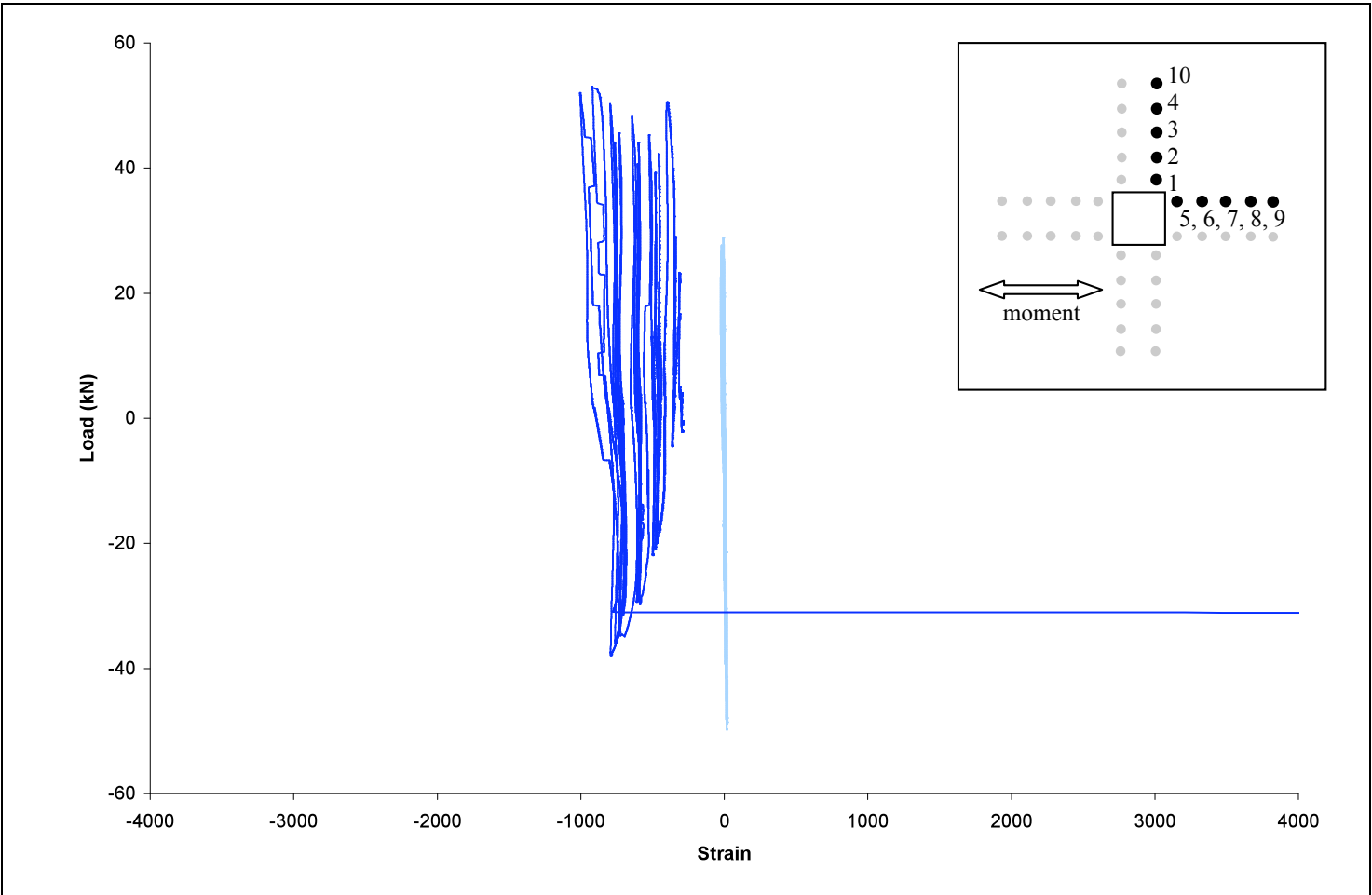
Figure E-23: Slab SN5, Strain vs. Horizontal Load, Bolt #7
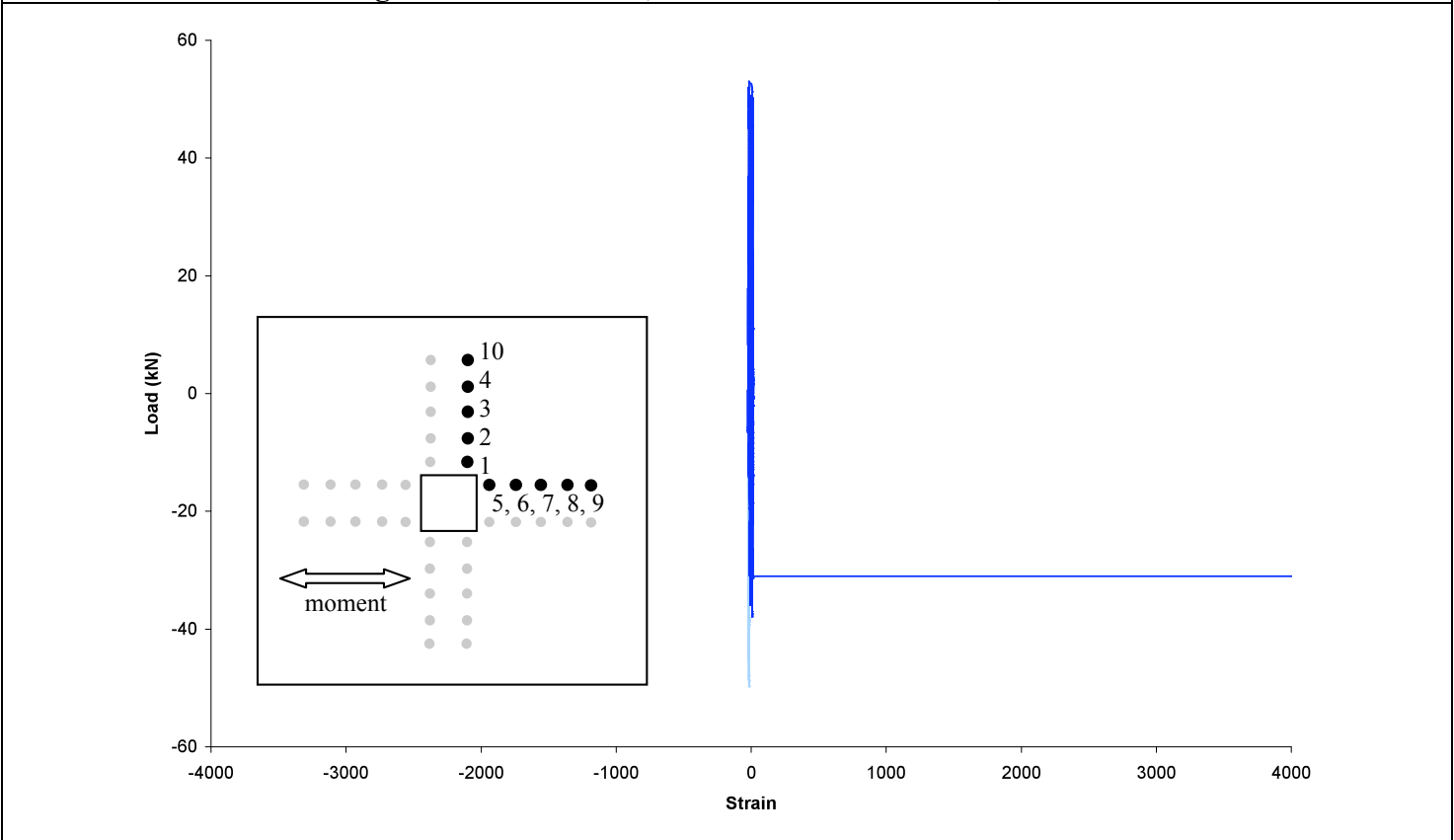
Figure E-24: Slab SN5, Strain vs. Horizontal Load, Bolt #8

139
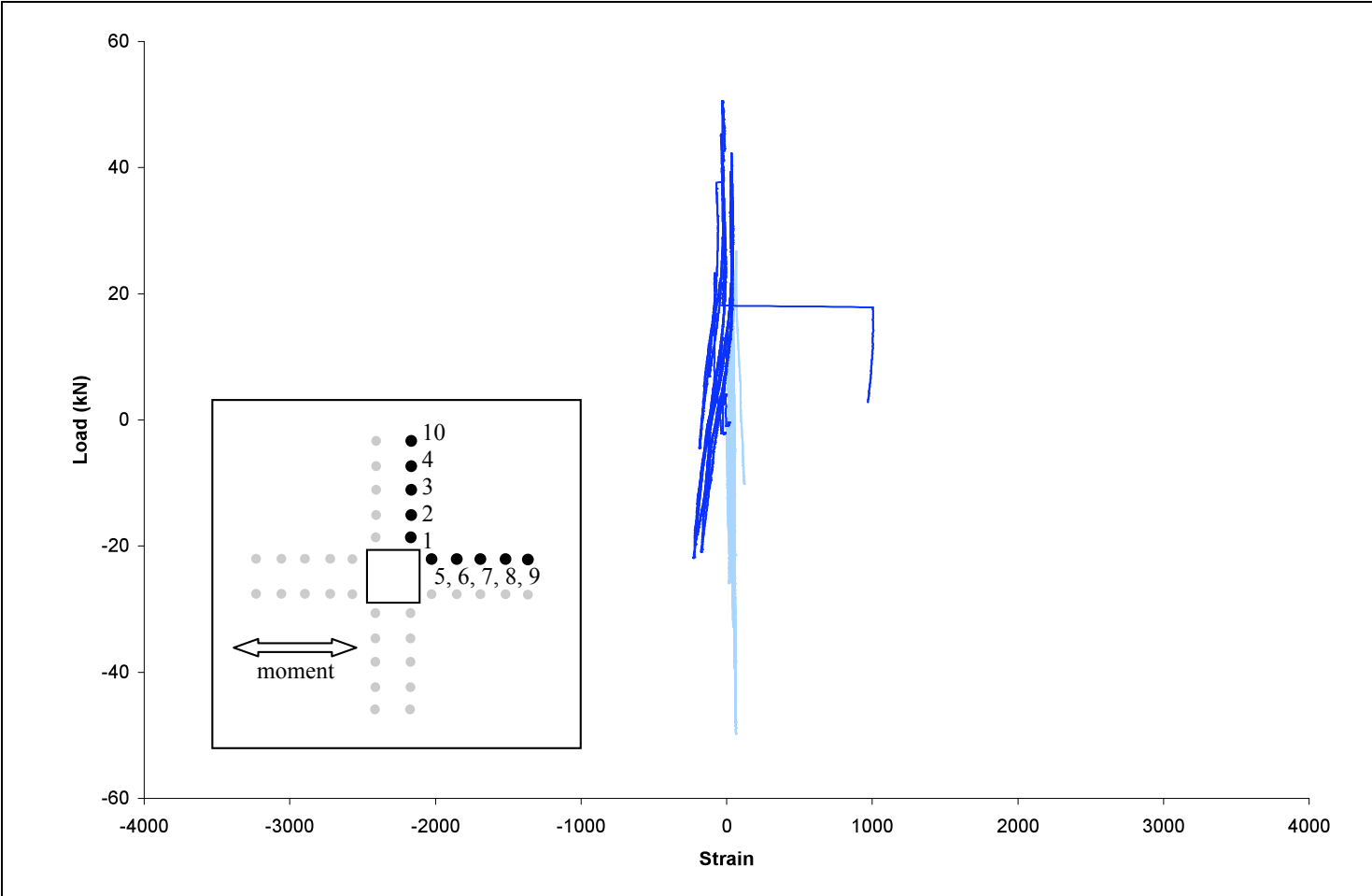
Figure E-25: Slab SN5, Strain vs. Horizontal Load, Bolt #10
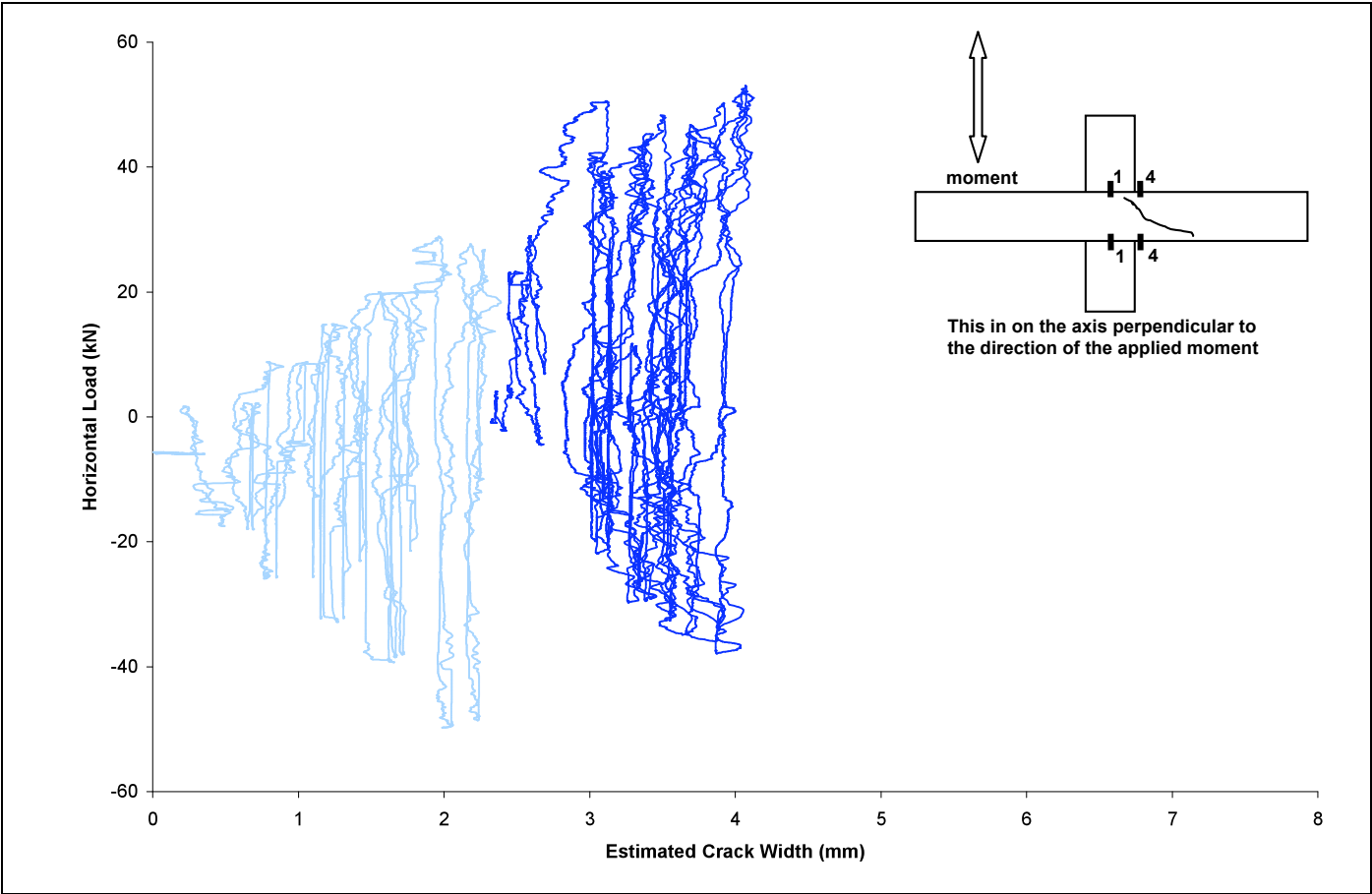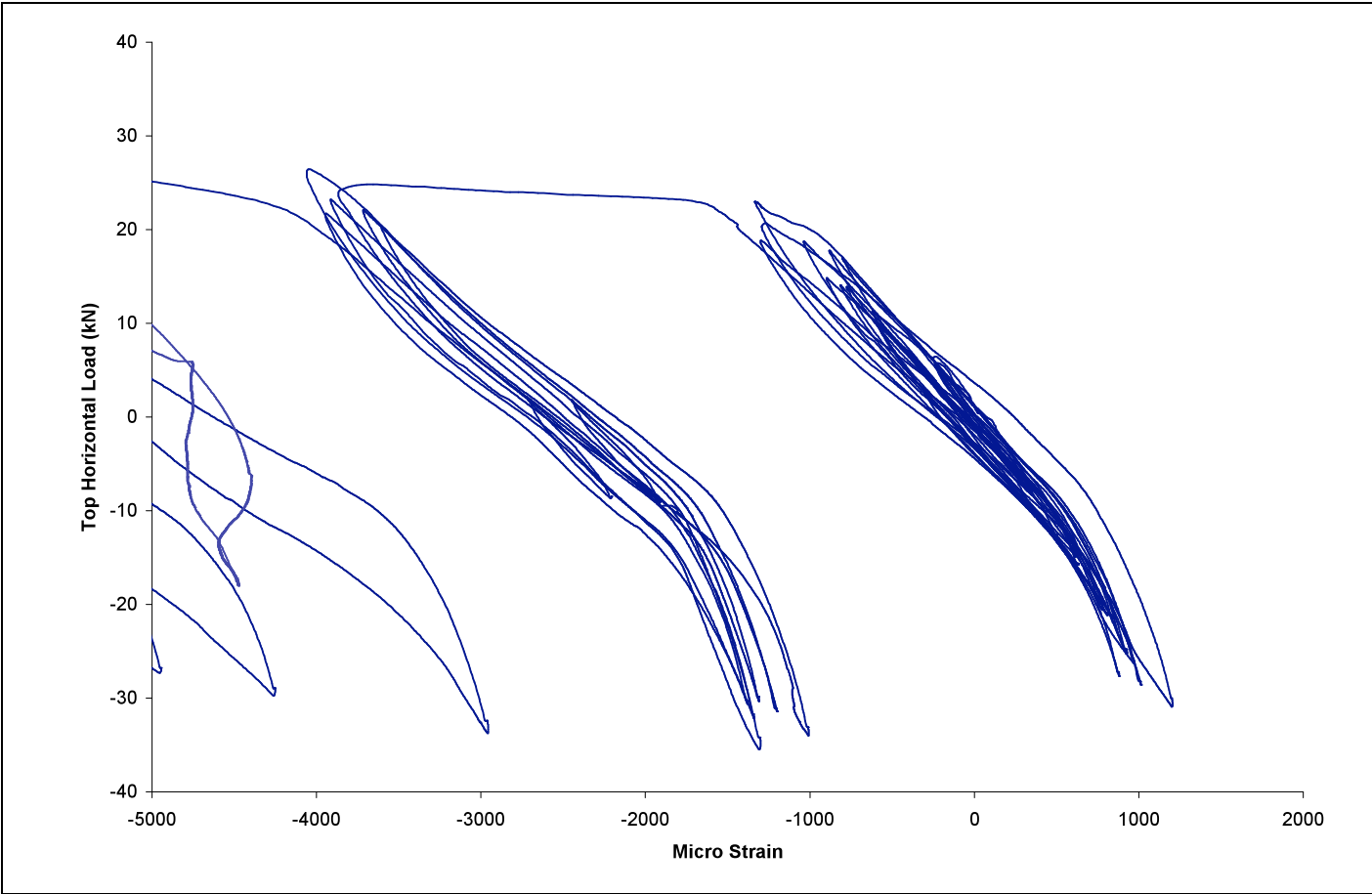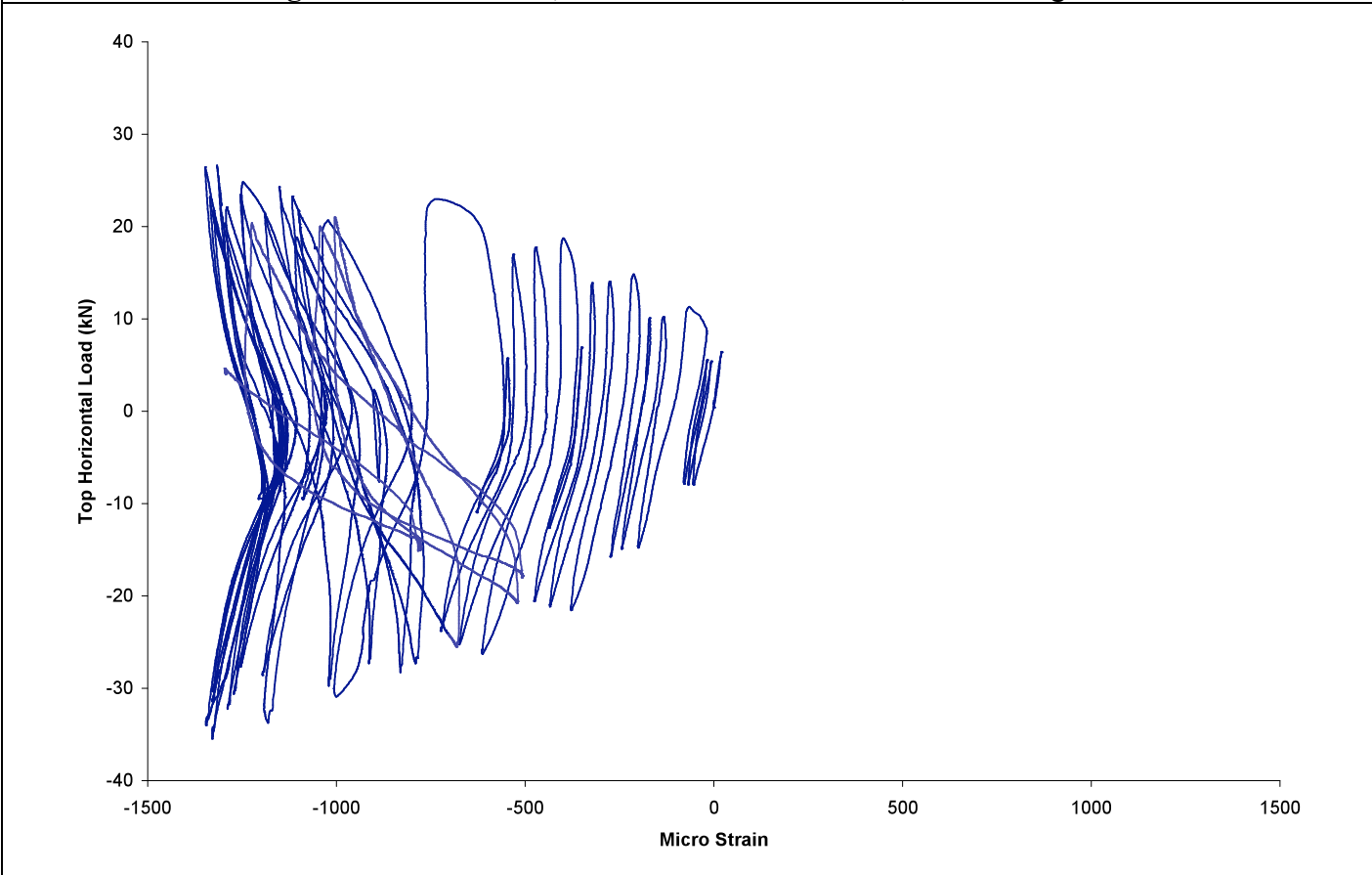
Figure E-26: Slab SN5, Estimated Crack Width vs. Horizontal Load, (4-4)
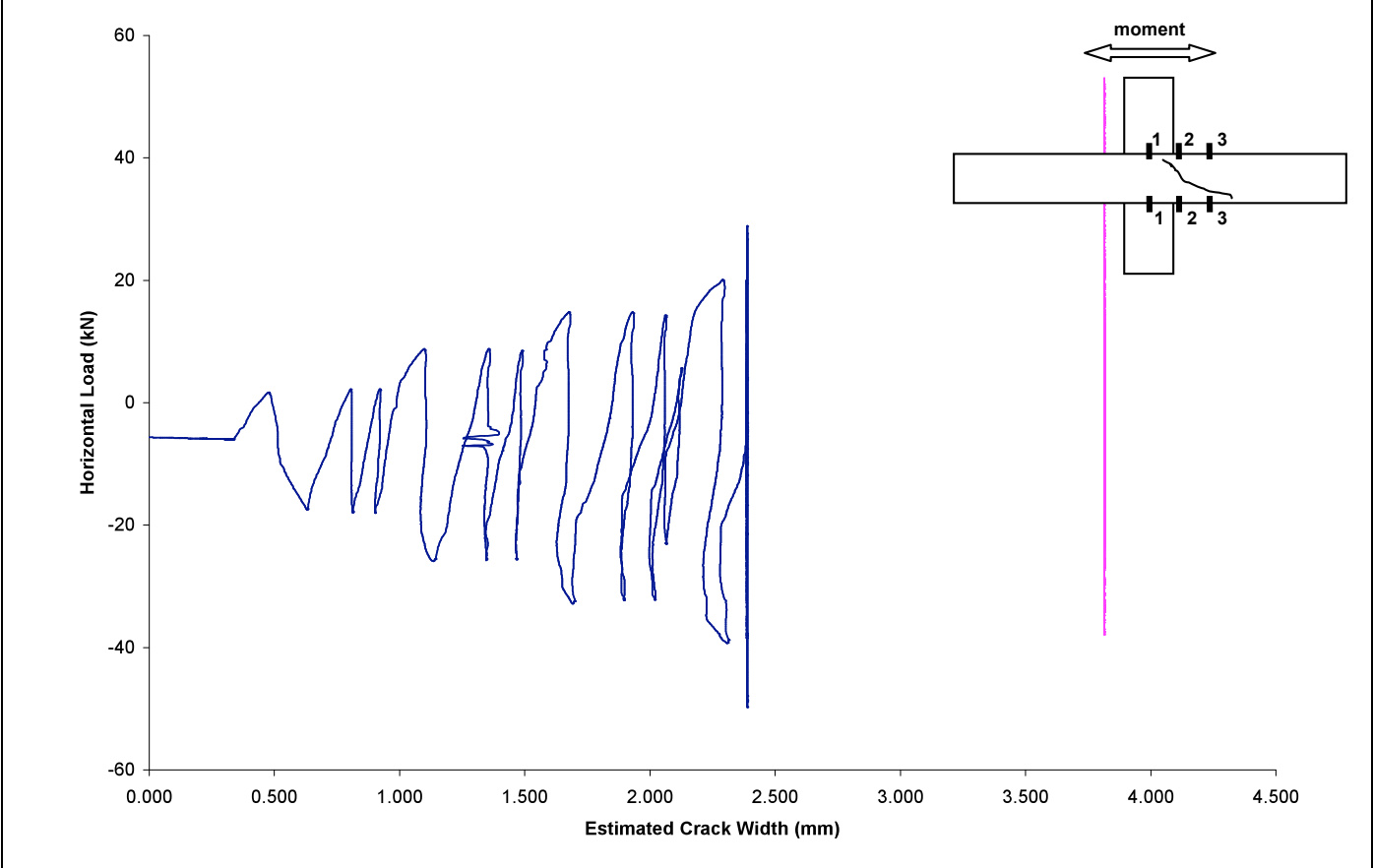
Figure E-27: Slab SN5, Estimated Crack Width vs. Horizontal Load, (1-1)

141
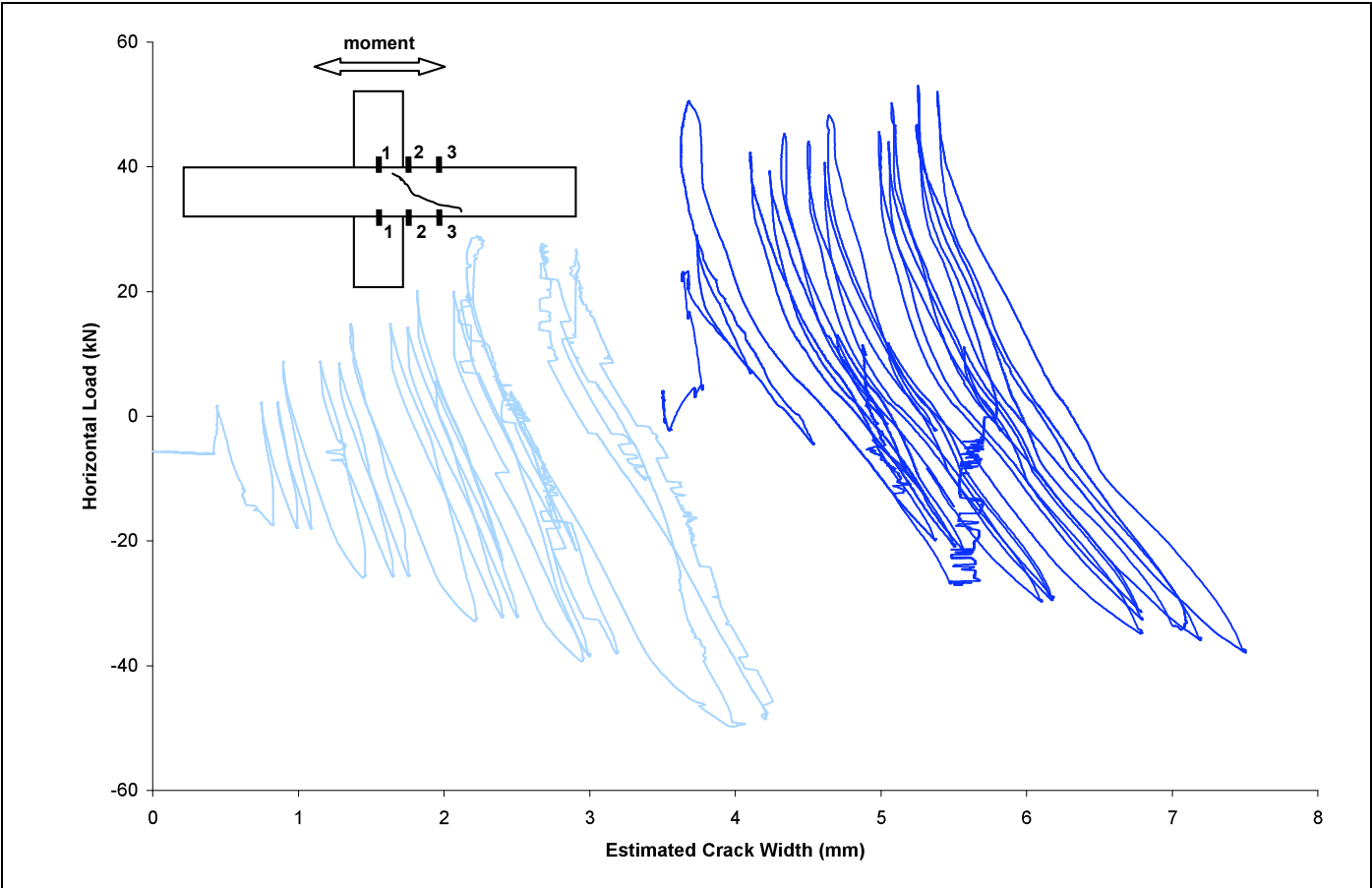
Figure E-28: Slab SN5, Estimated Crack Width vs. Horizontal Load, (2-2)
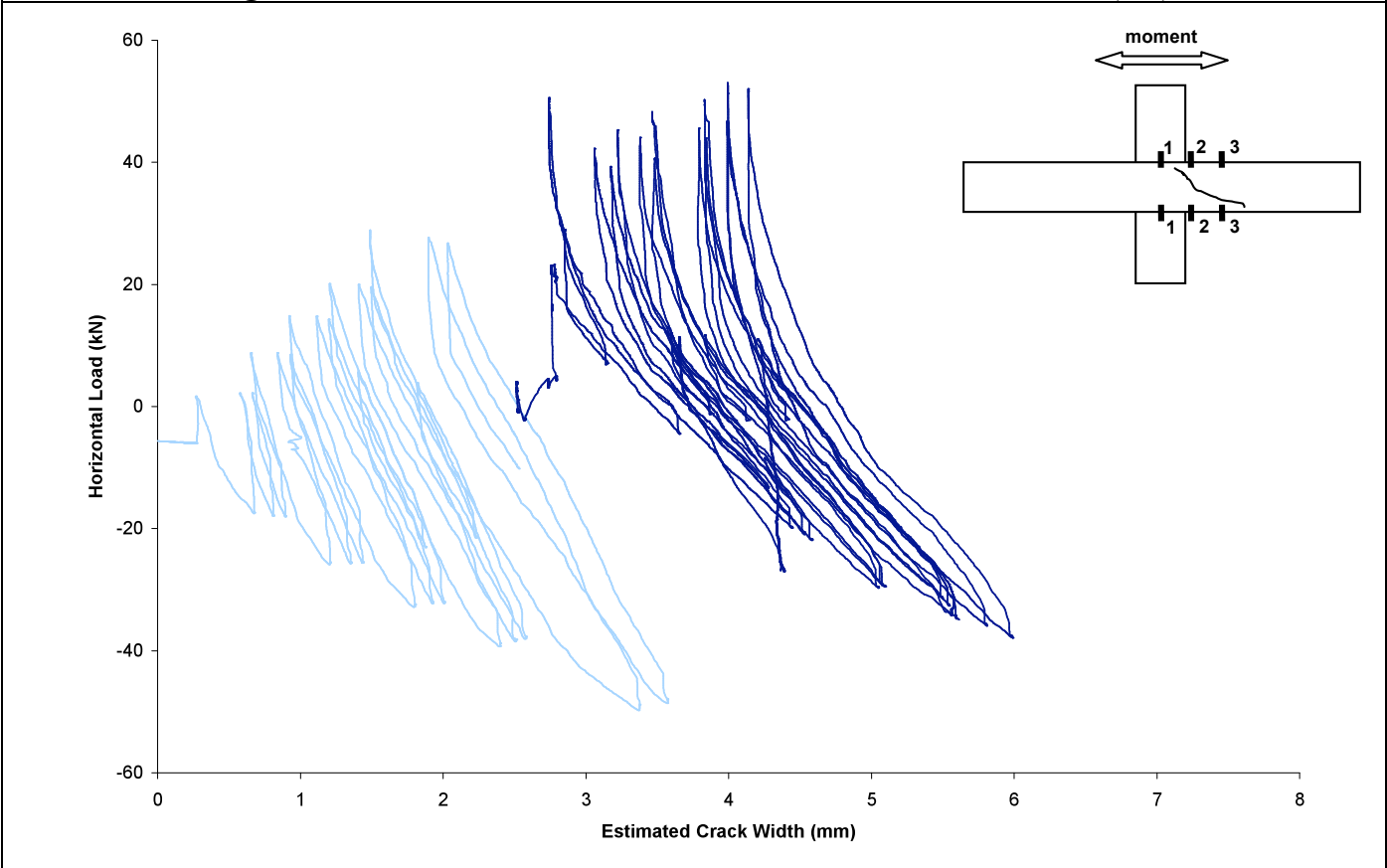
Figure E-29: Slab SN5, Estimated Crack Width vs. Horizontal Load, (3-3)

142

Appendix F – Data from SN6
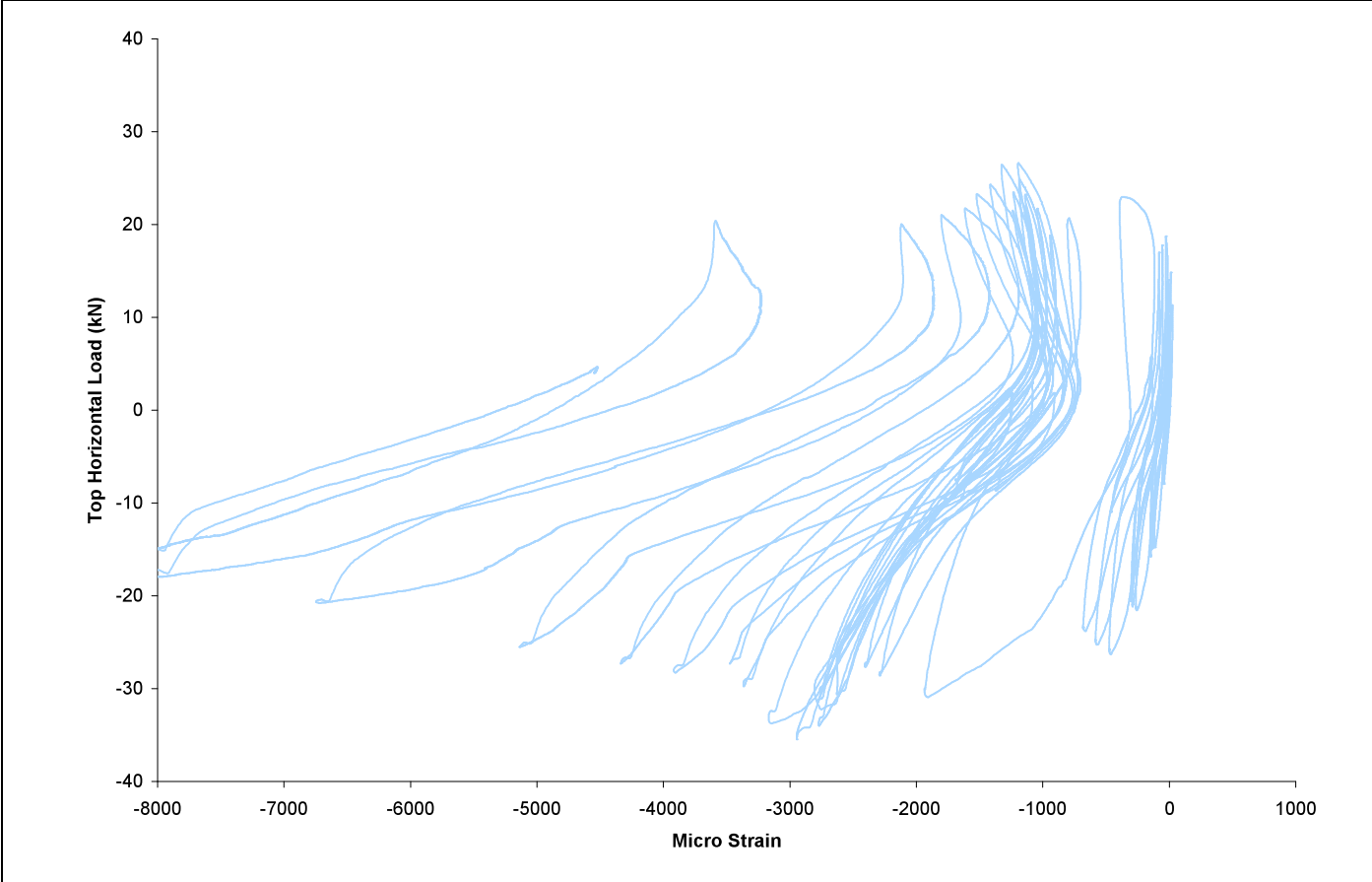
Figure F-1: Slab SN6, Strain vs. Horizontal Load, Bolt #1
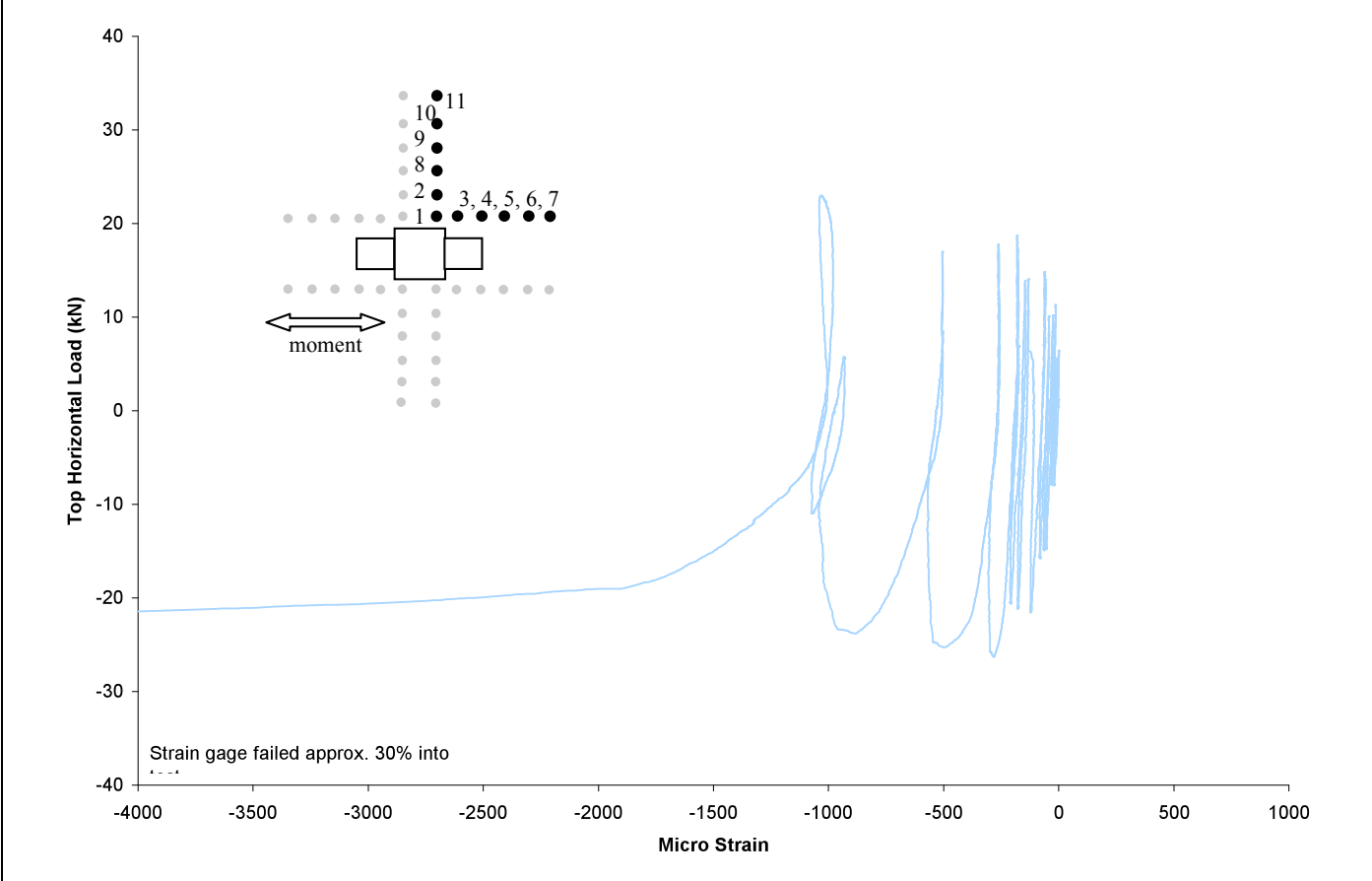
Figure F-2: Slab SN6, Strain vs. Horizontal Load, Bolt #2

144
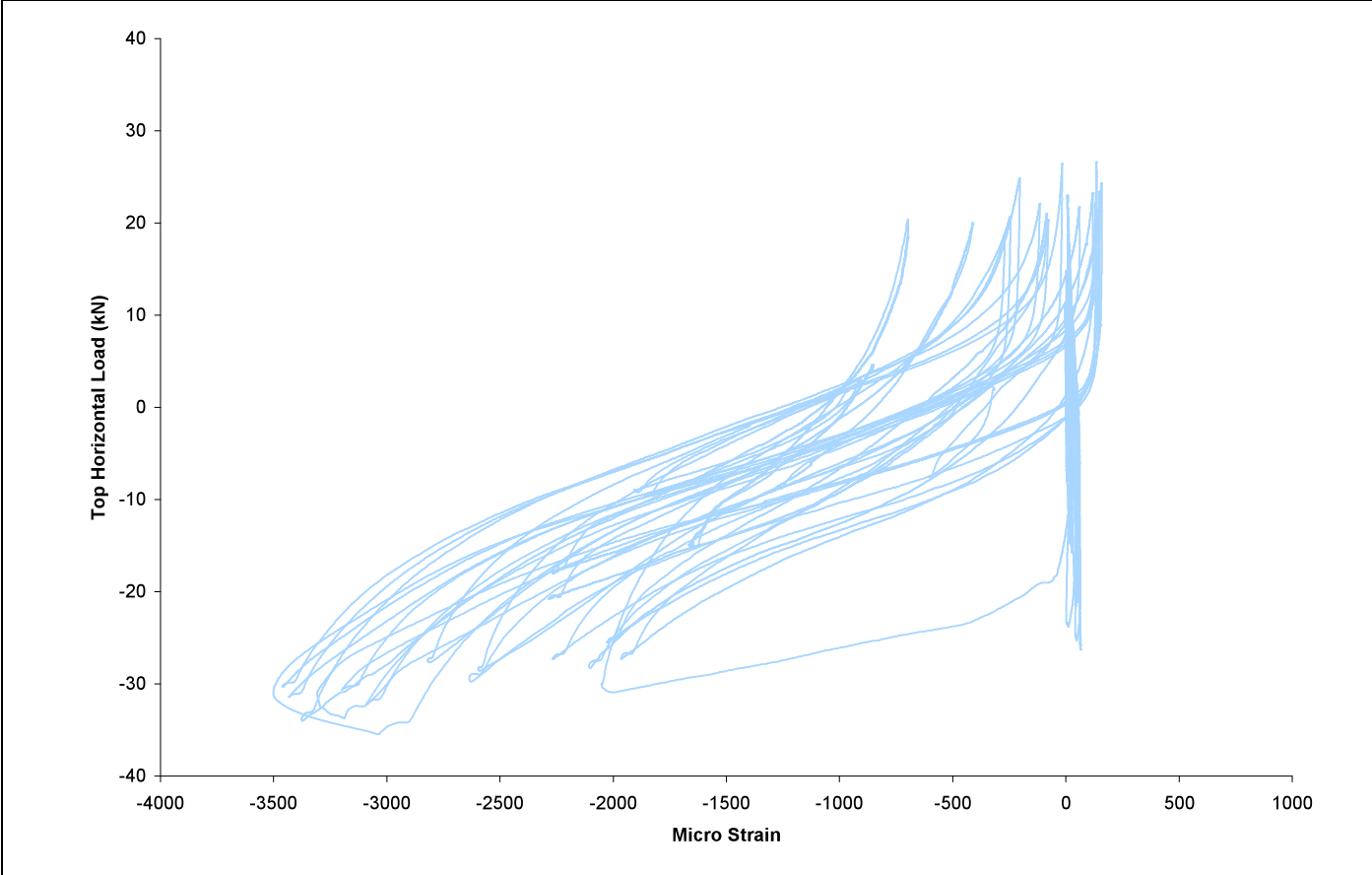
Figure F-3: Slab SN6, Strain vs. Horizontal Load, Bolt #3
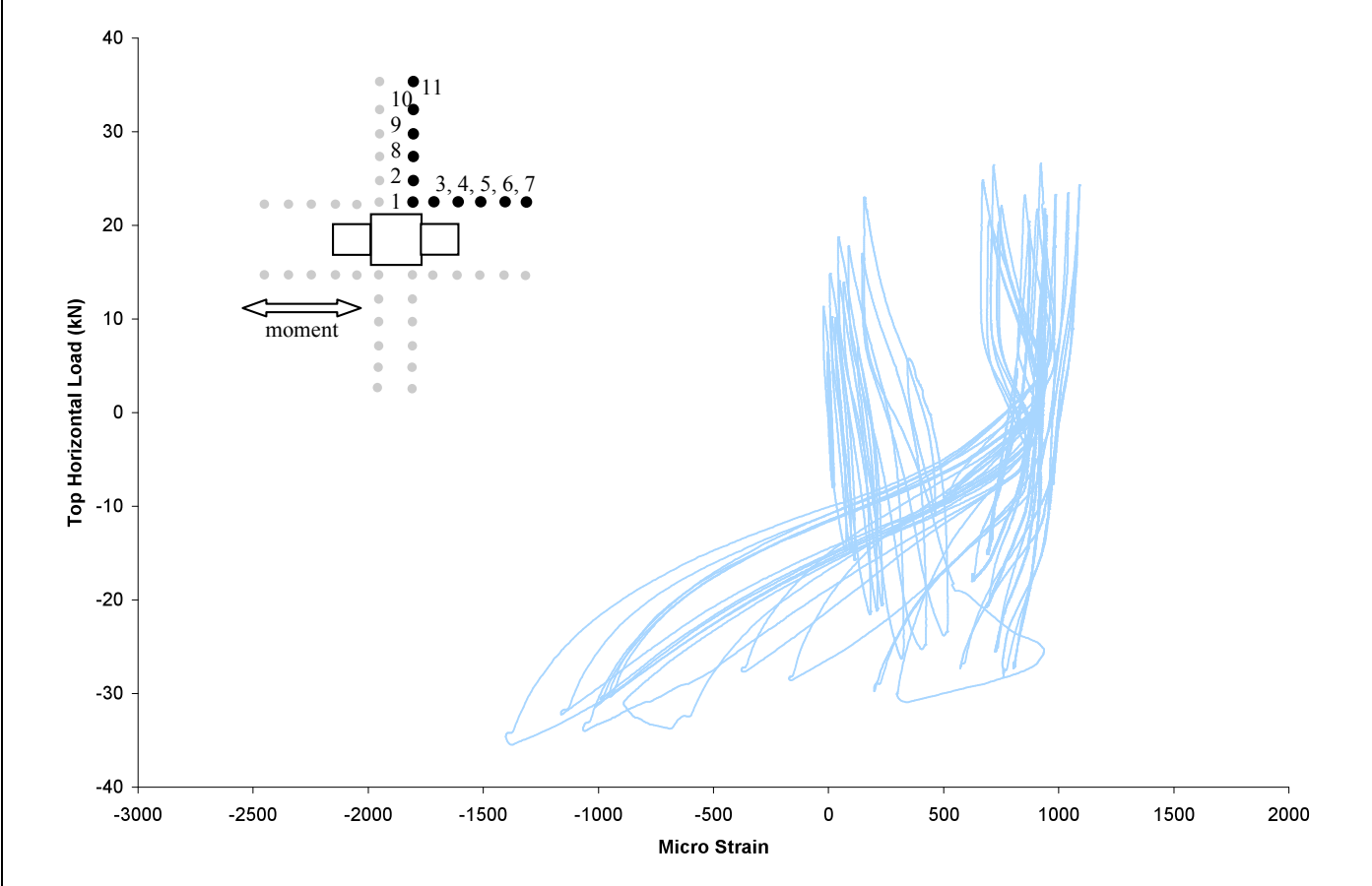
Figure F-4: Slab SN5, Strain vs. Horizontal Load, Bolt #4

145

Figure F-5: Slab SN6, Strain vs. Horizontal Load, Bolt #6

Figure F-6: Slab SN6, Strain vs. Horizontal Load, Bolt #7

146

Figure F-7: Slab SN6, Strain vs. Horizontal Load, Bolt #8

Figure F-8: Slab SN5, Strain vs. Horizontal Load, Bolt #10

Figure F-9: Slab SN6, Strain vs. Horizontal Load, Bolt #11

Figure F-10: Slab SN6, Strain vs. Horizontal Load, Rebar Gauge 6a
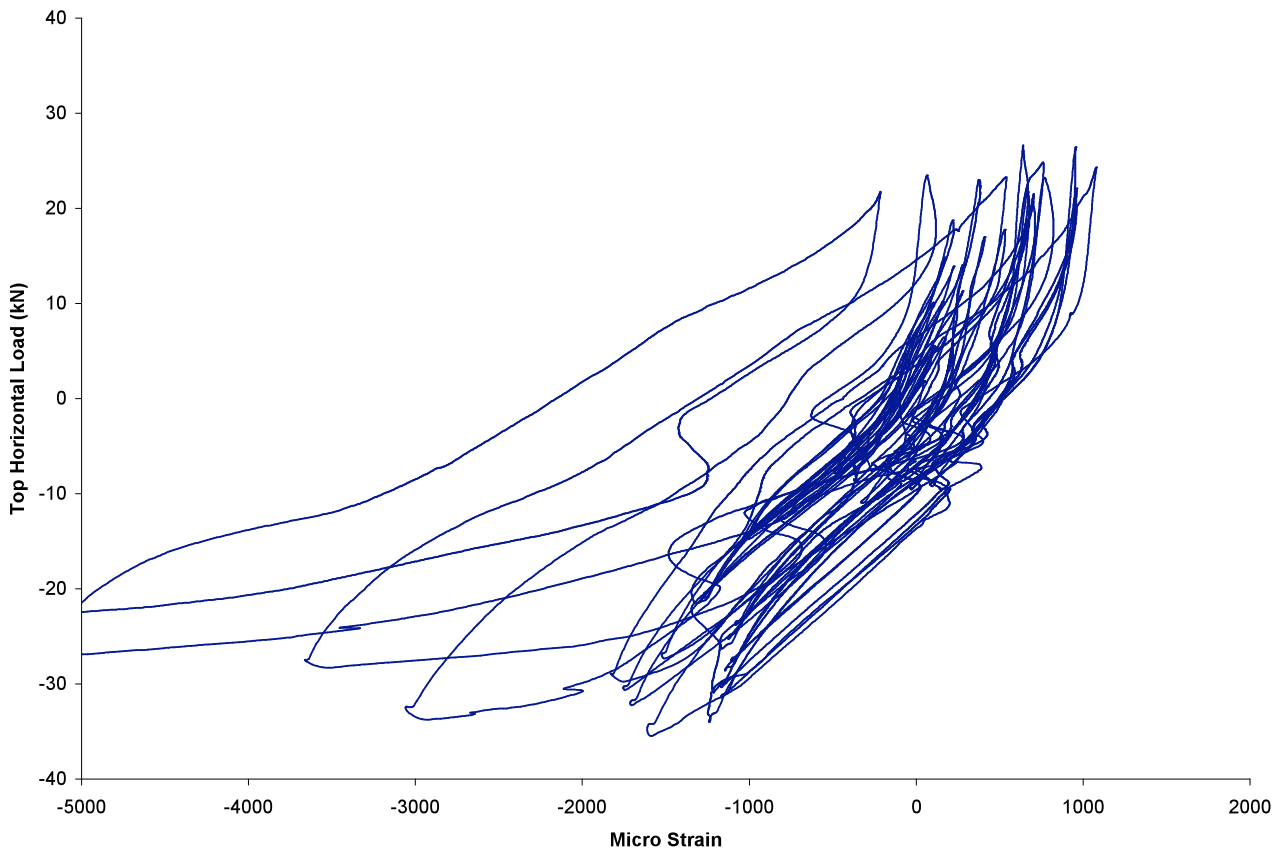
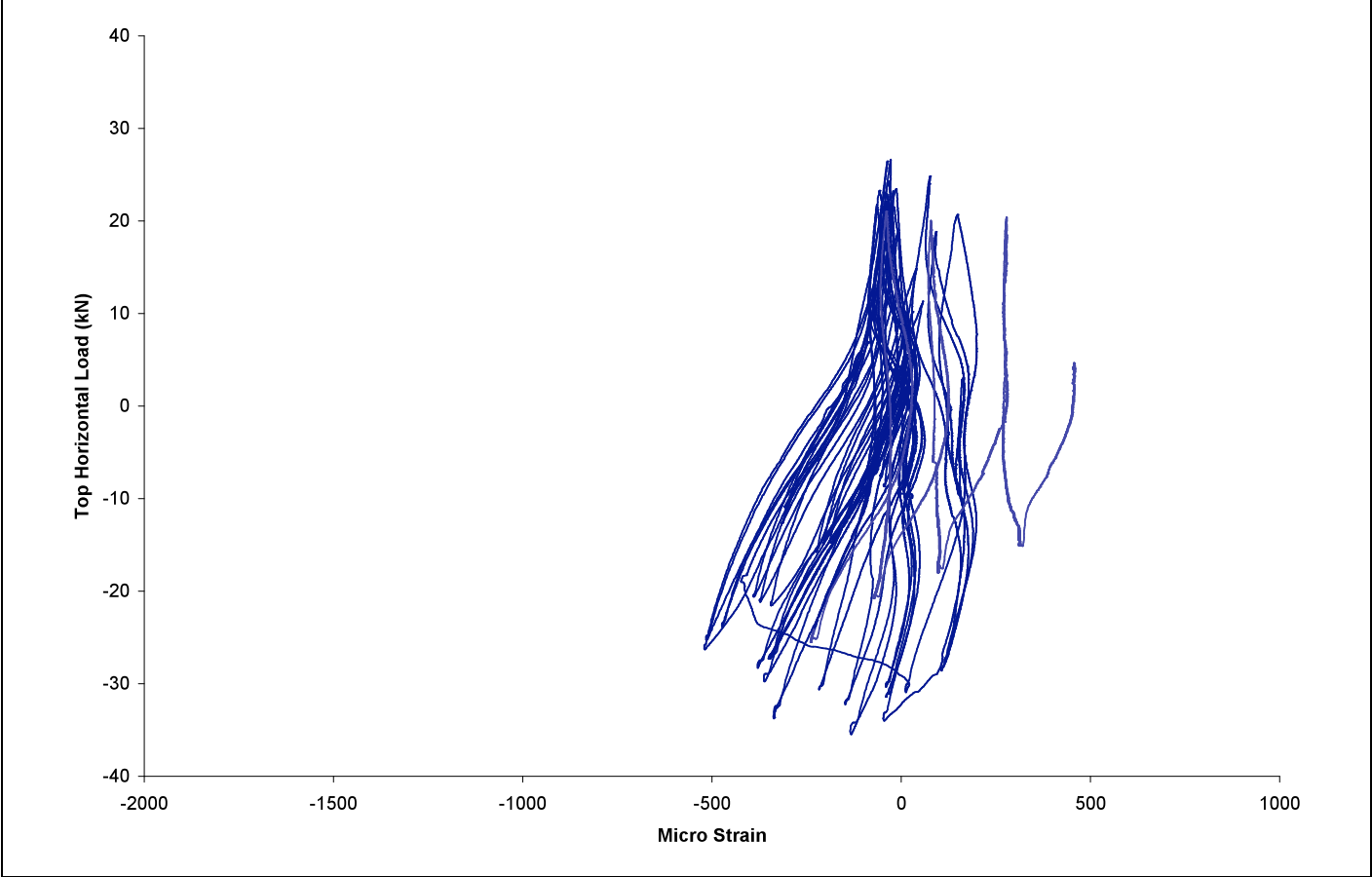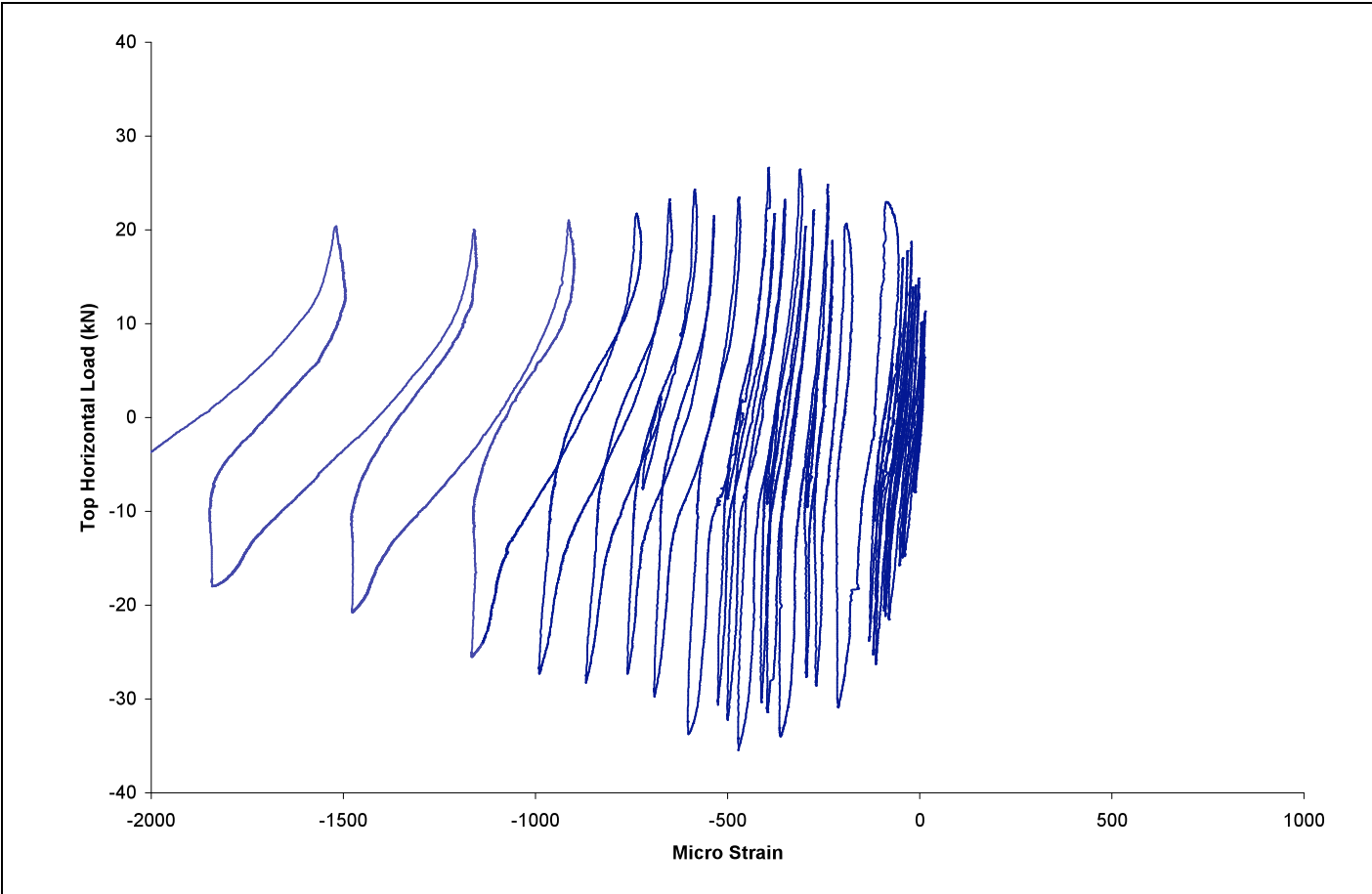**Figure F-11:** Slab SN6, Strain vs. Horizontal Load, Rebar Gauge 6b

149

Figure F-12: Slab SN6, Strain vs. Horizontal Load, Rebar Gauge 6c

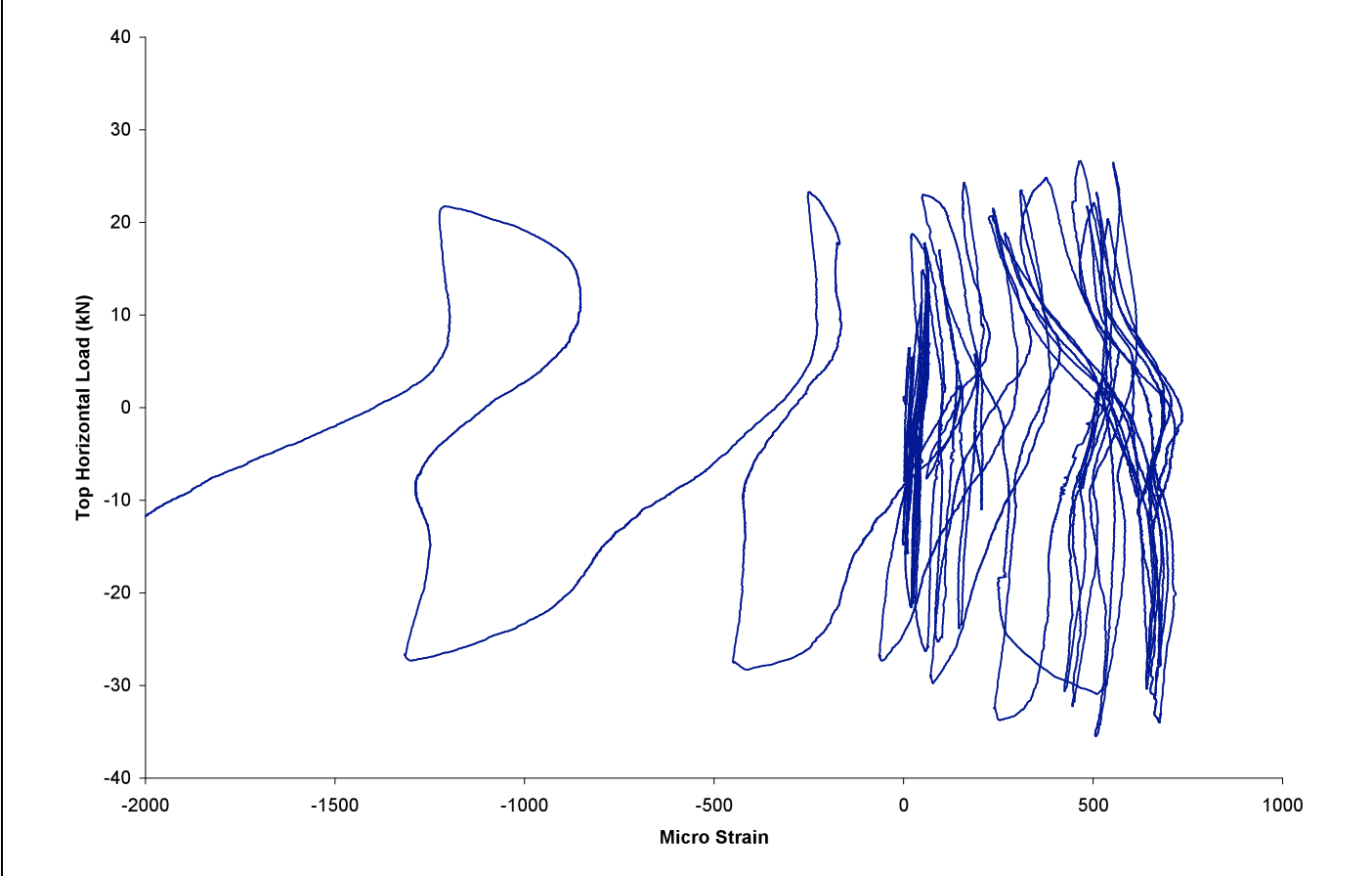**Figure F-13:** Slab SN6, Strain vs. Horizontal Load, Rebar Gauge 8a

150
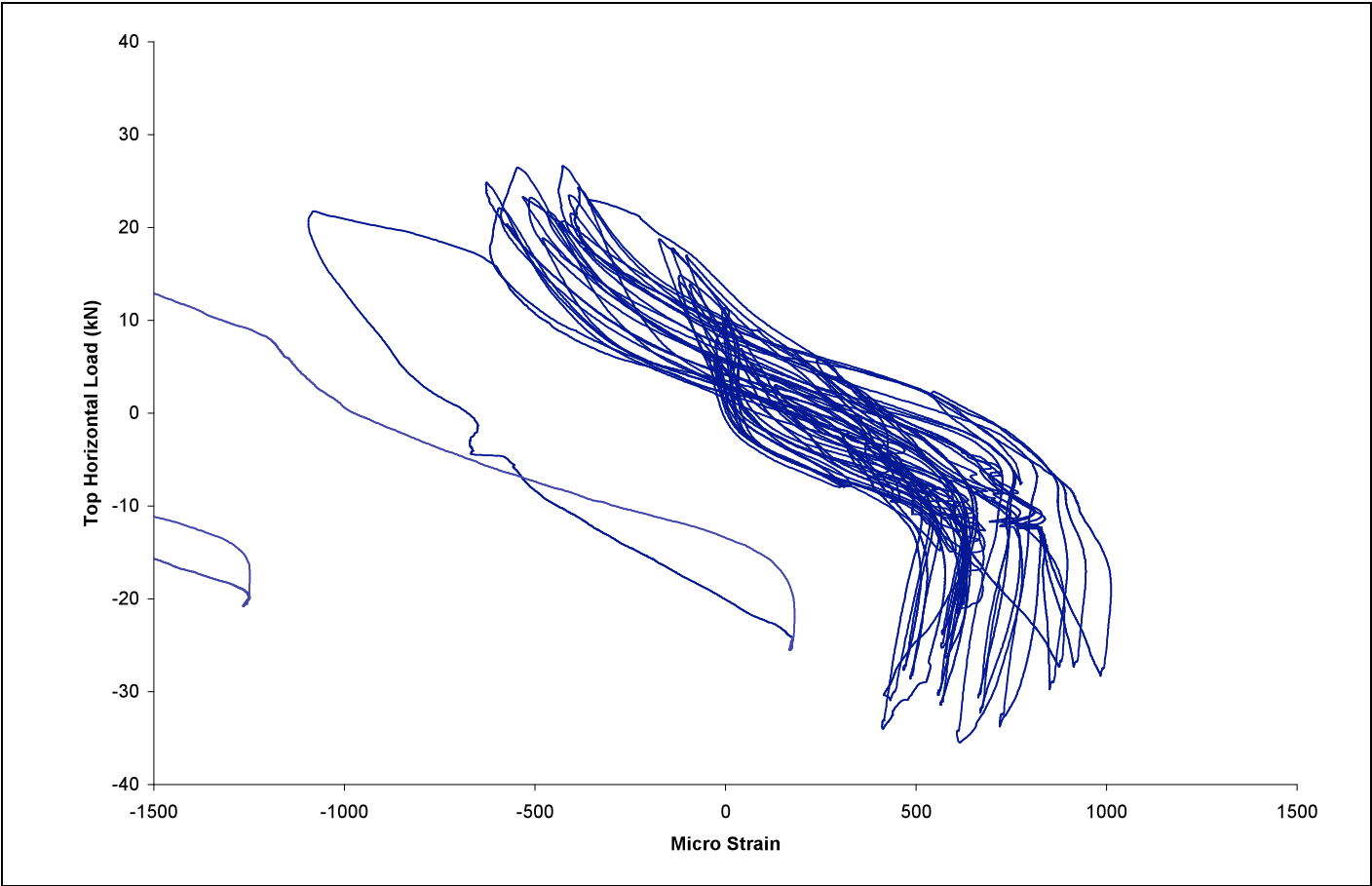
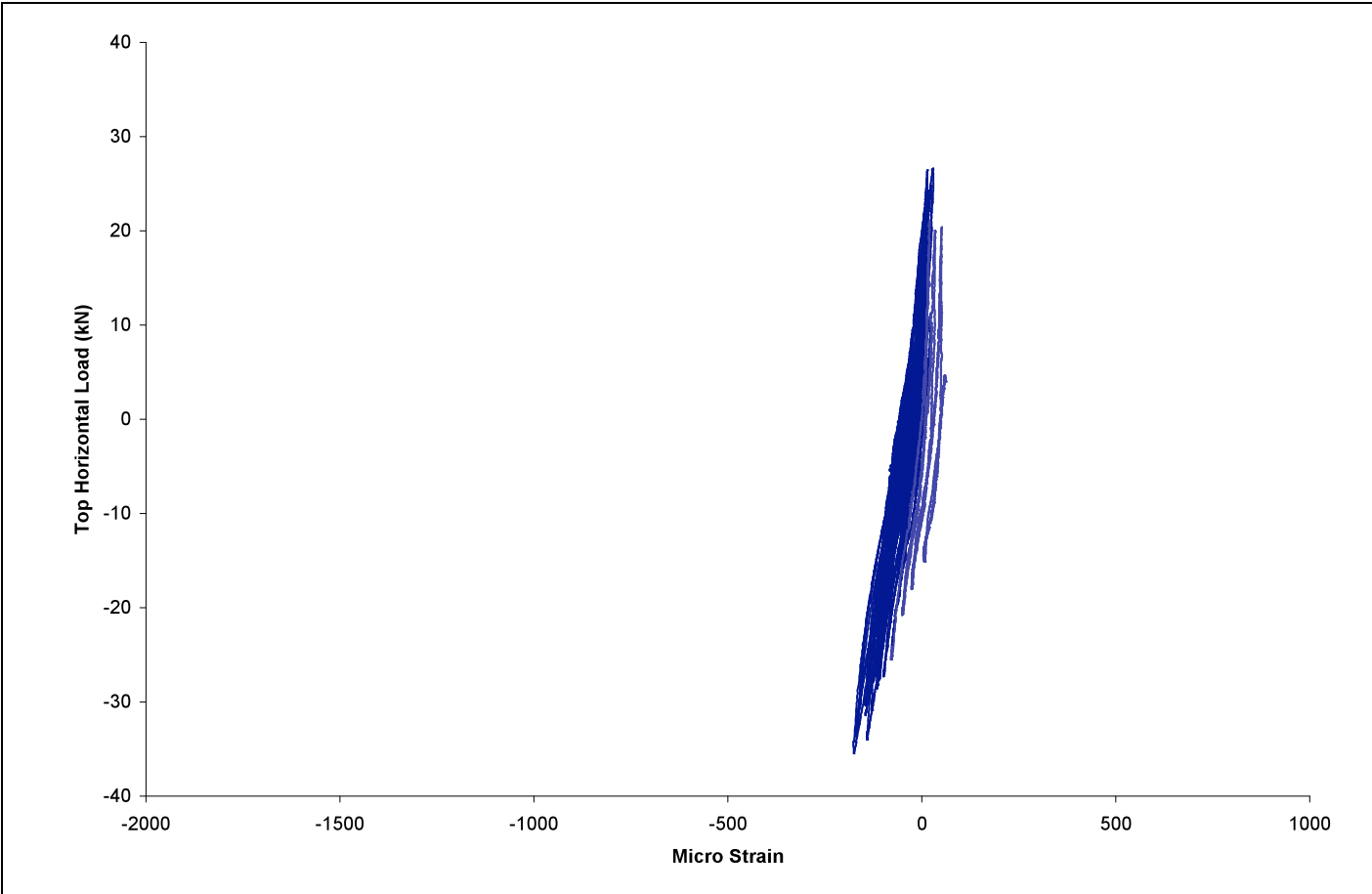**Figure F-14:** Slab SN6, Strain vs. Horizontal Load, Rebar Gauge 8b

Figure F-15: Slab SN6, Strain vs. Horizontal Load, Rebar Gauge 9b
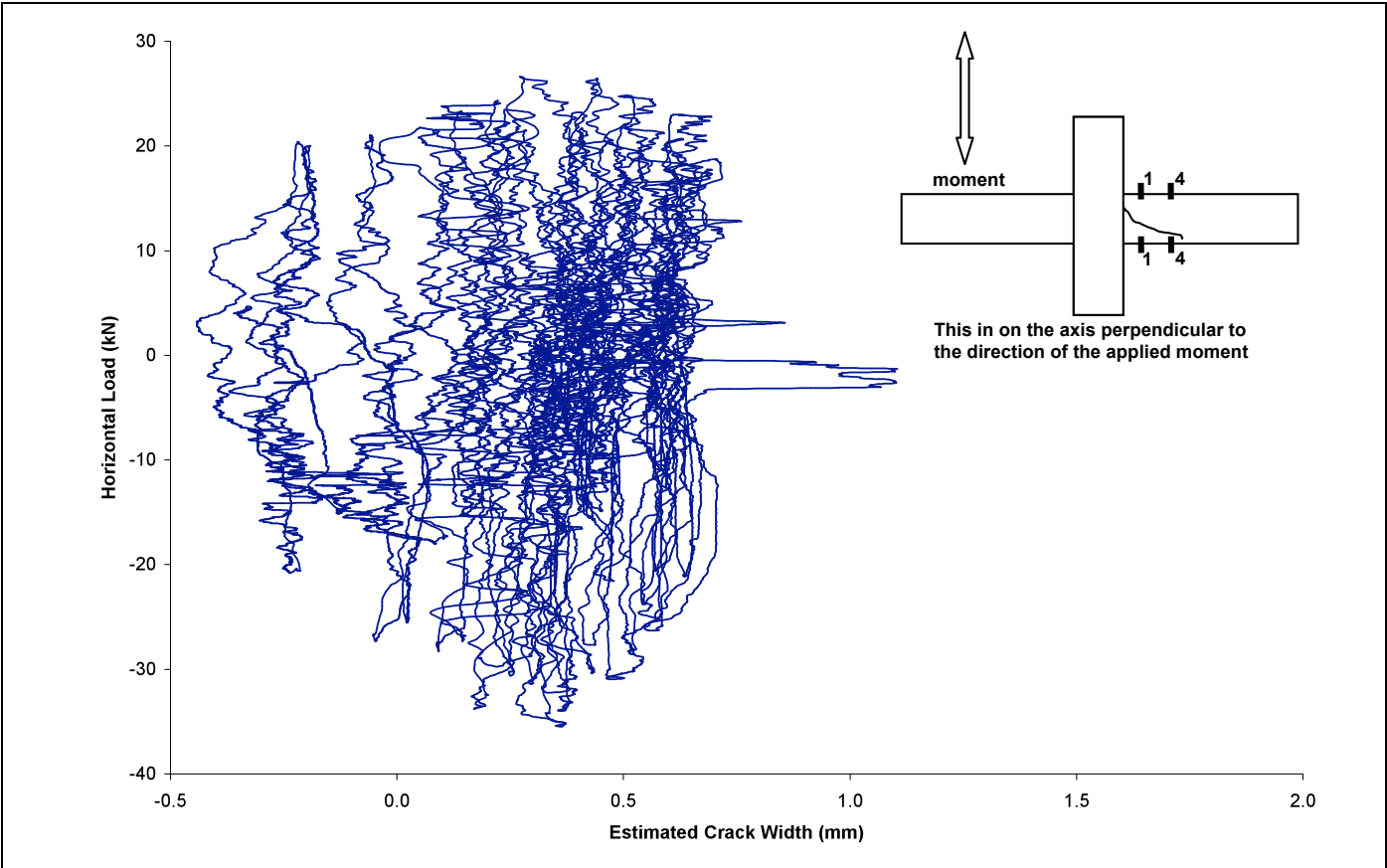
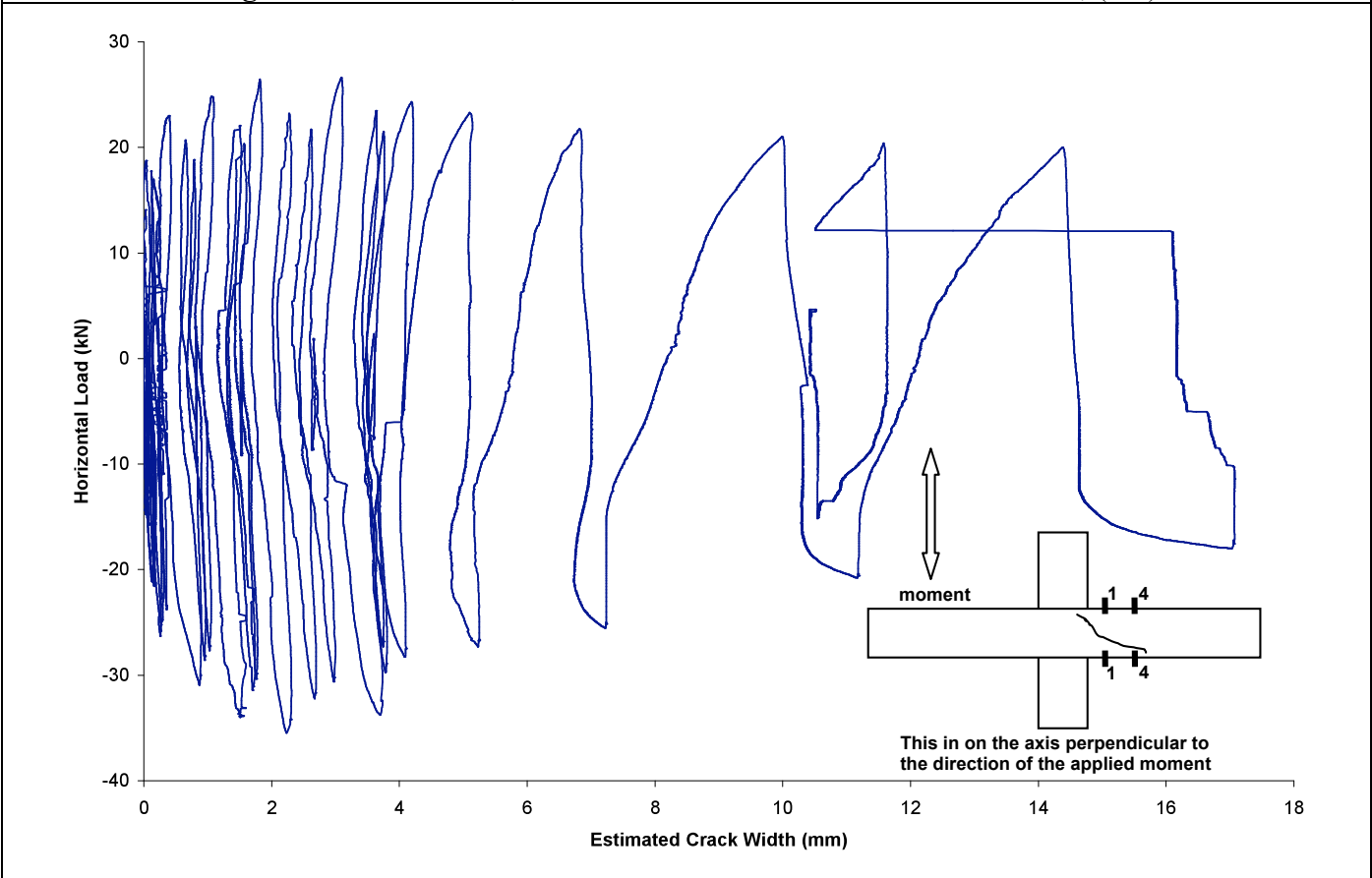**Figure F-16:** Slab SN6, Strain vs. Horizontal Load, Rebar Gauge 12a

Figure F-17: Slab SN6, Strain vs. Horizontal Load, Rebar Gauge 12b
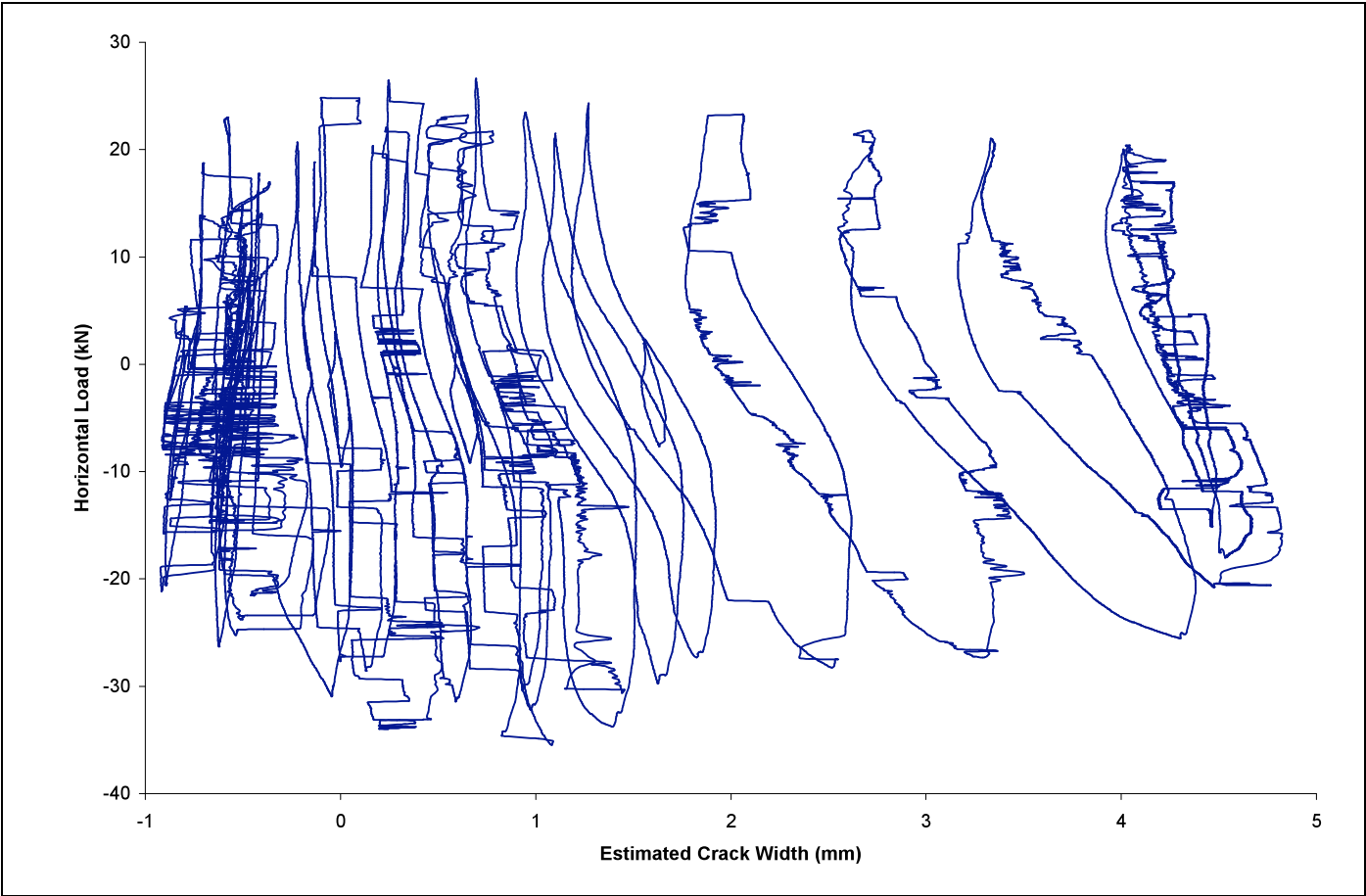
152

Figure F-18: Slab SN6, Strain vs. Horizontal Load, Rebar Gauge 13a
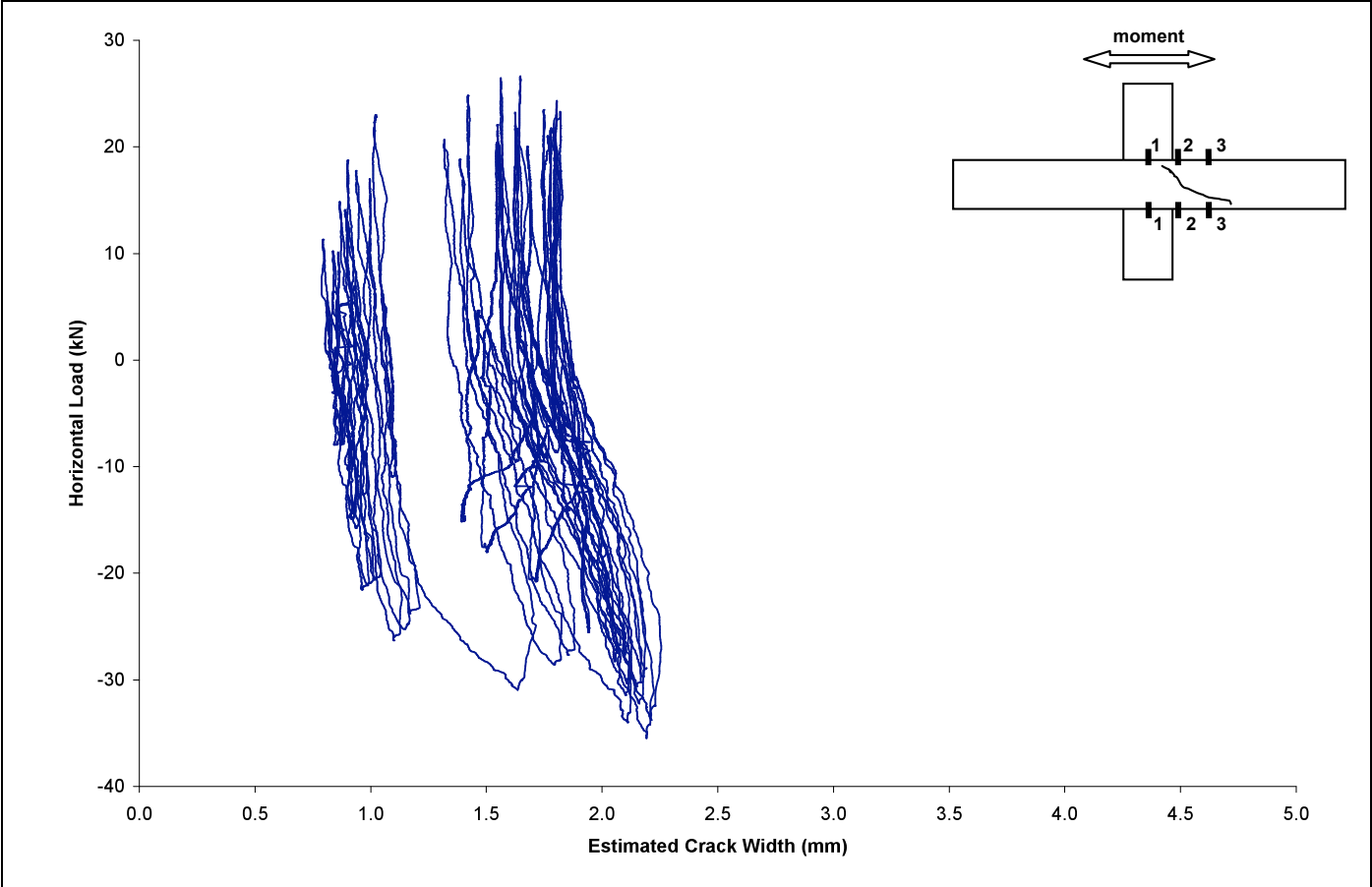
Figure F-19: Slab SN6, Estimated Crack Width vs. Horizontal Load, (4-4)

Figure F-20: Slab SN6, Estimated Crack Width vs. Horizontal Load, (1-1)

154

Figure F-21: Slab SN6, Estimated Crack Width vs. Horizontal Load, (2-2)

Figure F-22: Slab SN6, Estimated Crack Width vs. Horizontal Load, (3-3)

155

Appendix G – Product Data Sheet, Robo*REC 3610

Model REC-3610 ROBO*CRIMP™
15 Ton Battery Powered Compression Tool - 2" Jaw Opening

The REC-3610 is our 15 ton compression tool that is able to crimp splices and lugs up to 1250 MCM aluminum and 1500 MCM copper. The REC-3610 offers a wide handle opening with finger grooves, allowing easy access for gloved work.

The base of the tool is contoured for stability and incorporates finger grooves for a better grip. The tool has a latched head and its pull-out release pin cannot be entirely removed from the jaw. The jaw opens wide to accept all "P" type dies used in the industry today. The PU-15 die adapter is available for use with all 12 ton "U" type dies.

- The only 15 Ton Battery Operated Tool on the Market
- 2" Jaw Opening
- Up to 1500 MCM Cu
- Up to 1250 MCM Al
- 750/750 H-Tap
- PU-15 Die Adapter Available for All "U" Type Dies
- Flip-Top Rotating Head
- External Adjustment
- UL Classified
- Protective Rubber Boot on Head

Specifications:

Output	15 ton
Weight	24 lbs. with battery
Size	21.5"L x 10.5"H x 3.5"W
Jaw Opening	2"

Crimping Estimates:

	BP-70E
1000 MCM Cu	30

Connector Range:

Aluminum	# 8AWG-1250 MCM
Copper	# 8AWG-1500 MCM

Order Data:

Model #	Description
REC-3610	Battery Powered Compression Tool Standard Kit

To custom order a different tool kit battery and charger combination:
Add the following suffixes to the tool model number:

SM	2 BP-70EI "Smart" LED Indicator Batteries
DC	1 CH-70DCH 12 Volt DC Charger
MH	2 BP-70MH High Capacity Nickel Metal Hydride Battery with 30% more power output

Optional Accessories:

BP-70E	Replacement Battery
BP-70EI	Indicator "Smart" Battery
BP-70MH	High Capacity Battery - Nickel Metal Hydride
CH-35R	25 Minute Charger
CH-70DCH	12V DC Battery Charger

Standard ROBO* Kit includes:
1 Battery Powered Tool
1 Carrying Strap
1 Carrying Case
2 BP-70E Batteries
1 CH-35R 25 minute AC Charger

NOTE: Pricing will vary according to tool kit combination.

Huskie TOOLS
When it's on the line, you count on Huskie Tools.